STATE OF THE CLIMATE IN 2005

K. A. SHEIN,[82] ED.

Contributing Editors

A. M. WAPLE, H. J. DIAMOND, AND J. M. LEVY

AFFILIATIONS (alphabetical by author)

1. Christine Achberger, Institutionen för Geovetenskaper, Göteborgs Universitet, Göteborg, Sweden
2. Peter Ambenje, Kenya Meteorological Department, Nairobi, Kenya
3. Anthony Arguez, NOAA/NESDIS National Climatic Data Center, Asheville, North Carolina
4. Molly O. Baringer, NOAA/OAR Atlantic Oceanographic and Meteorological Laboratory, Miami, Florida
5. Gerald D. Bell, NOAA/NWS/NCEP Climate Prediction Center, Camp Springs, Maryland
6. Michael A. Bell, International Research Institute for Climate and Society, Palisades, New York
7. Mario Bidegain, University of Republic, Montevideo, Uruguay
8. Eric Blake, NOAA/NWS/NCEP National Hurricane Center, Miami, Florida
9. Mark A. Bourassa, COAPS, The Florida State University, Tallahassee, Florida
10. Jason E. Box, Byrd Polar Research Center, The Ohio State University, Columbus, Ohio
11. Olga N. Bulygina, All-Russian Research Institute of Hydrometeorological Information, Obninsk, Russia
12. Stuart M. Burgess, National Institute of Water and Atmospheric Research, Wellington, New Zealand
13. José Luis Camacho, Centro Internacional para la Investigación del Fenómeno de El Niño, Guayaquil, Ecuador
14. Suzana J. Camargo, International Research Institute for Climate and Society, Earth Institute at Columbia University, Palisades, New York
15. Muthuvel Chelliah, NOAA/NWS/NCEP Climate Prediction Center, Camp Springs, Maryland
16. Deliang Chen, Institutionen för Geovetenskaper, Göteborgs Universitet, Göteborg, Sweden
17. John C. Christy, University of Alabama at Huntsville, Huntsville, Alabama
18. Miguel Cortez Vázquez, Servicio Meteorologico Nacional, Mexico City, Mexico
19. Howard J. Diamond, NOAA/NESDIS National Climatic Data Center, Silver Spring, Maryland
20. Geoff S. Dutton, NOAA/OAR Earth Systems Research Laboratory, Boulder, Colorado
21. James W. Elkins, NOAA/OAR Earth Systems Research Laboratory, Boulder, Colorado
22. Richard A. Feely, NOAA/OAR Pacific Marine Environmental Laboratory, Seattle, Washington
23. Gao Ge, National Climate Center, China Meteorological Administration, Beijing, China
24. Ricardo F. García-Herrera, Universidad Complutense Madrid, Madrid, Spain
25. Jean-Claude Gascard, Universite Pierre et Marie Curie, Paris, France
26. Stephen Gill, NOAA National Ocean Service, Silver Spring, Maryland
27. Tracey Gill, South African Weather Service, Pretoria, South Africa
28. Karin L. Gleason, NOAA/NESDIS National Climatic Data Center, Asheville, North Carolina
29. Stanley B. Goldenberg, NOAA/OAR Atlantic Oceanographic Meteorological Laboratory, Miami, Florida
30. Gustavo Goni, NOAA/OAR Atlantic Oceanographic and Meteorological Laboratory, Miami, Florida
31. Emily K. Grover-Kopec, International Research Institute for Climate and Society, Palisades, New York
32. Michael S. Halpert, NOAA/NWS/NCEP Climate Prediction Center, Camp Springs, Maryland
33. Paul Hughes, COAPS, The Florida State University, Tallahassee, Florida
34. John E. Janowiak, NOAA/NWS Climate Prediction Center, Camp Springs, Maryland
35. Gregory C. Johnson, NOAA/OAR Pacific Marine Environmental Laboratory, Seattle, Washington
36. Khadija Kabidi, Direction de la Météorologie Nationale, Rabat, Morocco
37. Michael Karcher, Alfred Wegener Institute, Bremerhaven, Germany
38. John J. Kennedy, Hadley Centre for Climate Prediction and Research, Met Office, Exeter, United Kingdom
39. Chris Kocot, Environment Canada, Ottawa, Ontario, Canada
40. Natalia N. Korshunova, All-Russian Research Institute of Hydrometeorological Information, Obninsk, Russia
41. Mahbobeh Khoshkam, I.R. of the Iran Meteorological Organization (IRIMO), Tehran, Iran
42. K. Rupa Kumar, Indian Institute of Tropical Meteorology, Pune, India
43. Willem A. Landman, South African Weather Service, Pretoria, South Africa
44. Chris W. Landsea, NOAA/NWS/NCEP National Hurricane Center, Miami, Florida
45. Jay H. Lawrimore, NOAA/NESDIS National Climatic Data Center, Asheville, North Carolina
46. David H. Levinson, NOAA/NESDIS National Climatic Data Center, Asheville, North Carolina
47. Joel M. Levy, NOAA/OAR Climate Program Office, Silver Spring, Maryland
48. Rick Lumpkin, NOAA/OAR Atlantic Oceanographic and Meteorological Laboratory, Miami, Florida
49. John M. Lyman, NOAA/OAR Pacific Marine Environmental Laboratory, Seattle, Washington
50. José A. Marengo, CPTEC/INPE, Center for Weather Forecasts and Climate Studies, São Paulo, Brazil

51. Rodney Martínez, Centro Internacional para la Investigación del Fenómeno de El Niño, Guayaquil, Ecuador
52. Jim Maslanik, University of Colorado, Boulder, Colorado
53. Michael J. McPhaden, NOAA/OAR Pacific Marine Environmental Laboratory, Seattle, Washington
54. Christopher S. Meinen, NOAA/OAR Atlantic Oceanographic and Meteorological Laboratory, Miami, Florida
55. Matthew J. Menne, NOAA/NESDIS National Climatic Data Center, Asheville, North Carolina
56. Mark A. Merrifield, University of Hawaii at Manoa, Honolulu, Hawaii
57. Gary T. Mitchum, University of South Florida, St. Petersburg, Florida
58. Kingtse C. Mo, NOAA/NWS/NCEP Climate Prediction Center, Camp Springs, Maryland
59. A. Brett Mullan, National Institute of Water and Atmospheric Research, Ltd., Wellington, New Zealand
60. Laban A. Ogallo, IGAD Climate Prediction and Applications Centre, Nairobi, Kenya
61. Christopher Oludhe, University of Nairobi, Nairobi, Kenya
62. James E. Overland, NOAA/OAR Pacific Marine Environmental Laboratory, Seattle, Washington
63. José Daniel Pabón, Universidad Nacional de Colombia, Bogotá, Colombia
64. Daniel Paredes, Universidad Complutense Madrid, Madrid, Spain
65. Richard Pasch, NOAA/NWS/NCEP National Hurricane Center, Miami, Florida
66. Donald K. Perovich, ERDC Cold Regions Research and Engineering Laboratory, Hanover, New Hampshire
67. David Philips, Meteorological Service of Canada, Environment Canada, Ottawa, Ontario, Canada
68. Andrey Proshutinsky, Woods Hole Oceanographic Institute, Woods Hole, Massachusetts
69. Richard W. Reynolds, NOAA/NESDIS National Climatic Data Center, Asheville, North Carolina
70. Fatemeh Rahimzadeh, Atmospheric Science and Meteorological Research Center (ASMERC), Tehran, Iran
71. Madhavan Rajeevan, National Climate Centre, India Meteorological Department, Pune, India
72. Vyacheslav N. Razuvaev, All-Russian Research Institute of Hydrometeorological Information, Obninsk, Russia
73. Ren Fumin, National Climate Center, China Meteorological Administration, Beijing, China
74. Jacqueline A. Richter-Menge, ERDC Cold Regions Research and Engineering Laboratory, Hanover, New Hampshire
75. David A. Robinson, Rutgers–The State University of New Jersey, New Brunswick, New Jersey
76. Jeremy Rolph, COAPS, The Florida State University, Tallahassee, Florida
77. Vladimir E. Romanovsky, University of Alaska, Fairbanks, Fairbanks, Alaska
78. Matilde Rusticucci, Universidad de Buenos Aires, Buenos Aires, Argentina
79. Christopher L. Sabine, NOAA/OAR Pacific Marine Environmental Laboratory, Seattle, Washington
80. M. James Salinger, National Institute of Water and Atmospheric Research, Ltd., Newmarket, Auckland, New Zealand
81. Russell C. Schnell, NOAA/ESRL Global Monitoring Division, Boulder, Colorado
82. Karsten A. Shein, NOAA/NESDIS National Climatic Data Center, Asheville, North Carolina
83. Alexander I. Shiklomanov, University of New Hampshire, Durham, New Hampshire
84. Shawn R. Smith, COAPS, The Florida State University, Tallahassee, Florida
85. Wassila M. Thiaw, NOAA/NWS/NCEP Climate Prediction Center, Camp Springs, Maryland
86. Ricardo M. Trigo, CGUL, Universidade de Lisboa, Lisbon, Portugal
87. Donald Walker, University of Alaska, Fairbanks, Fairbanks, Alaska
88. Rik Wanninkhof, NOAA/OAR Atlantic Oceanographic and Meteorological Laboratory, Miami, Florida
89. Anne M. Waple, NOAA/NESDIS National Climatic Data Center (STG, Inc.), Asheville, North Carolina
90. Andrew B. Watkins, Bureau of Meteorology, Melbourne, Australia
91. Robert A. Weller, Woods Hole Oceanographic Institution, Woods Hole, Massachusetts
92. Robert Whitewood, Environment Canada, Ottawa, Ontario, Canada
93. Joshua K. Willis, NASA Jet Propulsion Laboratory, Pasadena, California
94. David B. Wuertz, NOAA/NESDIS National Climatic Data Center, Asheville, North Carolina
95. Pingping Xie, NOAA/NWS/NCEP Climate Prediction Center, Camp Springs, Maryland
96. Lisan Yu, Woods Hole Oceanographic Institution, Woods Hole, Massachusetts

CORRESPONDING AUTHOR ADDRESS: Dr. Karsten Shein, Climate Monitoring Branch, National Climatic Data Center, NOAA/NESDIS, Asheville, NC 28801
E-mail: Karsten.Shein@noaa.gov

TABLE OF CONTENTS

ABSTRACT—K. A. Shein[82]

The State of the Climate 2005 report summarizes global and regional climate conditions and places them, where possible, into the context of historical records. Descriptions and analyses of notable climatic anomalies, both global and regional, also are presented.

According to the Smith and Reynolds global land and ocean surface temperature dataset in use at the NOAA National Climatic Data Center (NCDC), the globally averaged annual mean surface temperature in 2005 was the warmest since the inception of consistent temperature observations in 1880. Unlike the previous record positive anomaly of 1998 (+0.50°C), the 2005 global anomaly of 0.53°C above the 1961–90 mean occurred in the absence of a strong El Niño signal. The record ranking of 2005 was corroborated by a dataset maintained at NASA, while United Kingdom archives placed 2005 second behind 1998. However, statistically, the 2005 global temperature anomaly could not be differentiated from either 1998 or any of the past four years. The majority of the top 10 warmest years on record have occurred in the past decade, and 2005 continues a marked upward trend in globally averaged temperature since the mid-1970s. Lower-tropospheric temperature was the second warmest on record, with northern polar regions the warmest at 1.3°C above the 1979–98 mean.

Unlike air temperatures, globally averaged precipitation was near normal relative to the 1961–90 period mean value. The global 2005 anomaly was just −0.87 mm. Over the past 25 years, only 7 years have had above-normal precipitation. Additionally, in 2005, only September–November experienced a positive anomaly. Northern Hemisphere snow cover extent was 0.9 million km^2 below the 36-year average (fifth lowest) and Arctic sea ice extent was record lowest in all months of 2005 except May, resulting in a record lowest annual average Arctic sea ice extent for the year and continuing a roughly 8% yr^{-1} decline in ice extent.

Carbon dioxide (CO_2) concentrations rose to a global average of 378.9 parts per million (ppm); about 2 ppm over the value from 2004. This record CO_2 concentration in 2005 continues a trend toward increased atmospheric CO_2 since the preindustrial era values of around 280 ppm. The globally averaged methane (CH_4) concentration in 2005 was 1774.8 parts per billion (ppb), or 2.8 ppb less than in 2004. Stratospheric ozone over Antarctica reached a minimum of 110 Dobson units (DU) on 29 September. This represented the 10th lowest minimum level in the 20 years of measurement of stratospheric ozone.

In the global ocean, sea level was above the 1993–2001 base period mean and rose at a rate of 2.9 ±0.4 mm yr^{-1}. The largest positive anomalies were in the Tropics and Southern Hemisphere. Globally averaged sea surface temperature (SST) also was above normal in 2005 (relative to the 1971–2002 mean), reflecting the general warming trend in SST observed since 1971. In the Tropics, only a weak warm phase of El Niño materialized, but dissipated by March. A relatively active Madden–Julian oscillation (MJO) resulted in the disruption of normal convective patterns in the tropical Pacific and generated several Kelvin waves in the oceanic mixed layer.

In the Atlantic Ocean basin, there was record tropical storm activity, with 27* named storms (15 hurricanes). Three became category 5 storms on the Saffir–Simpson scale, and Hurricane Wilma set a new record for the lowest pressure (882 hPa) recorded in the basin. Both Hurricanes Stan and Katrina had exceptional death tolls, and Katrina became the costliest storm on record. Below-normal tropical storm activity in several other basins resulted in near-normal conditions globally in 2005.

Regionally, annual and monthly averaged temperatures were above normal across most of the world. Australia experienced its warmest year on record, as well is its hottest April. For both Russia and Mexico 2005 was the second warmest year on record.

Intermittent and delayed monsoons in Africa and East Asia resulted in below-normal precipitation in many areas. Drought continued in much of the Greater Horn of Africa and developed in the central United States. Record severe drought occurred over both the Iberian Peninsula and western Amazonia in 2005. In the Amazon, river levels dropped by as much as 11 m between May and September. Conversely, heavy snows early in 2005 combined with a warm boreal spring to generate widespread flooding in areas of southwest Asia. Canada experienced its wettest year on record in 2005, with flooding in Alberta, Manitoba, and Ontario. In July, the South Asian monsoon delivered a record 944.2 mm of precipitation over 24 h to areas around Mumbai, India.

* Tropical cyclone counts in this report do not reflect the 10 April 2006 identification, by the NOAA National Hurricane Center, of a 28th (Subtropical) storm in the Atlantic basin. Please visit www.nhc.noaa.gov for further information.

1. INTRODUCTION—K. A. Shein[82]

This past year, 2005, was a year of weather records. Unfortunately, many of these records came with a record price. At the December 2005 United Nations Climate Change Conference [Conference of the Parties to the Convention (COP) 11 & COP/Meeting of the Party to the Protocol (MOP) 1] in Montreal, Quebec, Canada, the Munich Re Foundation (reinsurance) noted that preliminary estimates of global economic losses in which the weather was a contributing factor exceeded $200 billion U.S. Dollars (USD). This easily tops the previous record of $175 billion USD in losses in 1995, and makes 2005 the costliest weather year on record [source: Inter-Press Service and United Nations Framework Convention on Climate Change (UNFCCC)]. Of these losses, approximately $185 billion USD are attributed to windstorms (e.g., tropical cyclones), of which $125 billion were due to Hurricane Katrina, the costliest hurricane in recorded history (Munich Re 2006).

In addition, the several global temperature datasets currently used by various institutions to estimate globally averaged annual temperatures were in agreement that 2005 was one of the warmest years in the historical record. The Smith and Reynolds (2005) surface (land and ocean) temperature dataset in use at the National Oceanic and Atmospheric Administration (NOAA) National Climatic Data Center (NCDC) places 2005 as the warmest on record, although the 2005 anomaly was statistically indistinguishable from the previous record warmth of 1998. This record 2005 temperature is made even more remarkable given that it occurred in the absence of a strong El Niño anomaly.

This special supplement to *BAMS* presents a discussion and analysis of the global climate system for 2005, and discusses some of the more notable regional climatic events that had impacts on society. The purpose of the State of the Climate series of publications is to summarize the climate conditions of the past calendar year, and to put those conditions into a historical perspective, both globally and regionally.

Overall, this is the 16th annual State of the Climate report (known as the Climate Assessment until 2001) and the 10th year that the article has appeared as part of *BAMS*. However, this is the first year that the State of the Climate is appearing as a special supplement to *BAMS*. For the past six years, NOAA's NCDC has taken the lead in the document's development and production. However, this effort is truly international, with contributions from scientists from numerous institutions and organizations around the world. Special effort has been made to acknowledge all contributors, and authorship has been noted through citation by individual sections, as well as in the list of authors and the acknowledgements in the appendix. Furthermore, we acknowledge the important contribution of the World Meteorological Organization (WMO) in helping to identify and encouraging the participation of authors from regions previously underrepresented in this publication.

It should be noted that, given the complexity and variability of the global climate system, it is impossible to provide comprehensive coverage of all aspects of the observed annual climate in a document of this length. However, the authors, editors, and contributors to the State of the Climate have made every effort to address the most important aspects and events related to the climate of 2005, and have attempted to convey these to a broad audience. Additionally, data-gathering efforts, quality control, and analysis continue long after year end. Thus, although the information presented in the State of the Climate in 2005 reflects the most current data available as of early 2006, values should be considered open to update as datasets are refined.

Each year, the scope of this publication is broadened with the discussion of additional climatic variables, introduction of new or unusual topics, and expansion of coverage of regional climate summaries. Included this year is an in-depth analysis of the record Atlantic basin tropical storm season, the addition of a section on tropical convergence zones, and the improved coverage of the oceans through close collaboration with authors of the Annual Report on the State of the Oceans (NOAA OCO 2006).

The following is an executive summary that highlights many of the most important topics and statistics of the climate of 2005.

Section 2: Global climate

- Globally averaged mean annual air temperature in 2005 slightly exceeded the previous record heat of 1998, making 2005 the warmest year on record. Monthly average surface air temperatures were above normal in all 12 months.
- The globally averaged annual air temperature in 2005 was 0.62°C above the 1880–2004 mean (0.53°C above the 1961–90 mean), while 1998 was +0.59°C (+0.50°C) according to the Smith and Reynolds (2005) dataset in use at NOAA/NCDC. Comparatively, other global temperature datasets obtained slightly different values and rankings for 2005; however, no dataset was able to identify a statistically significant difference between the temperatures of the two years.

- Precipitation was, globally, at or near mean annual totals over land areas, but snow cover was below average across much of the Northern Hemisphere (NH). The NH annual snow cover extent averaged 24.7 million km^2 in 2005, 0.9 million fewer than average.
- The year was the second warmest on record for lower tropospheric temperature, with polar regions being the warmest on record. Similar warm anomalies were reported for the middle–upper troposphere. High-latitude lower-stratospheric temperatures were very cold in the NH, but were warmer than average over the Southern Hemisphere (SH).

Section 3: Global oceans

- Globally averaged sea surface temperature (SST) was above normal in 2005 (1971–2002 base), as measured by ship and buoy in situ data as well as Advanced Very High Resolution Radiometer (AVHRR) satellite remote sensing. Such positive anomalies reflect a continuance of the general warming trend seen in SST since 1971. As with 2004, high-latitude locations in the North Atlantic and North Pacific experienced the greatest positive departures. Furthermore, the areal extent of July–August SST greater than 28°C in the tropical North Atlantic increased from 2004 to 2005.
- Ocean currents were near to slightly stronger than normal in 2005, while thermohaline circulation, as measured in the Florida Straits, was near the long-term mean.
- Sea levels, based on tide gauges and satellite altimetry, were generally above average over most of the global ocean (1993–2001 base), and were consistent with long-term increases of 2.9 ±0.4 mm yr^{-1}. The highest positive anomalies were in the Tropics and SH.
- Carbon inventories may be increasing in the Pacific basin at about twice the rate of the Atlantic.

Section 4: The Tropics

- The 2004/05 El Niño did not materialize beyond a weak warm phase, which largely ended by February. Convection was suppressed across the equatorial Pacific for much of the year. Two active phases of the Madden–Julian oscillation (MJO) generated Kelvin waves that contributed to intra-annual oscillations in equatorial Pacific SST.
- The tropical cyclone season was extremely active in the North Atlantic, but was below normal in several other basins. There was an above-average number (103) of named storms globally in 2005, but the number of hurricanes/typhoons/cyclones (53) was below average. The number of major storms (28) was slightly above average. The Atlantic basin had record tropical activity, as well as several record-setting storms [e.g., lowest central pressure (Hurricane Wilma), most category 5 storms in a season (3), and most northeasterly genesis (Hurricane Vince)].

Section 5: The Poles

- In the Arctic, annually averaged surface air temperature remained above the twentieth century mean, although it was cooler than in the past two years.
- The Arctic Oscillation (AO) index was slightly negative in 2005, consistent with low index values since the mid-1990s.
- In the Arctic Ocean, the heat content of the Beaufort Gyre increased (the result of a twofold increase in Atlantic layer water temperature), and the center of freshwater shifted toward Canada and intensified.
- Record minimum NH sea ice extents were observed in every month of 2005 except May. This continues a substantial negative trend in NH sea ice extent since 1979.
- In 2005, the Arctic tundra greenness, as measured by the Normalized Difference Vegetation Index (NDVI), continued a marked trend toward greener conditions. This was coupled with a general increase in total annual discharge from large Eurasian pan-Arctic rivers, and an increase in permafrost temperatures over the past several decades.

Section 6: Regional climates

A number of significant climatic conditions affected various regions in 2005 (Fig. 1.1). This section expands upon the global coverage of previous sections by summarizing and discussing the climatic conditions and notable events that occurred in many of the world's geographic regions.

- *Africa:* Patchy and sporadic rainfall was common during the rainy seasons in the Greater Horn region, resulting in persistent drought over much of the region throughout the year. A few strong April storms generated flash floods in parts of the region. Meanwhile, western Africa experienced its second wettest rainy season since 1994, although a few areas were drier than normal. The heavy precipitation and flooding fostered a widespread cholera epidemic. Northern Africa experienced 0.25°–1.5°C above-normal average temperatures in 2005, but began the year with record cold tem-

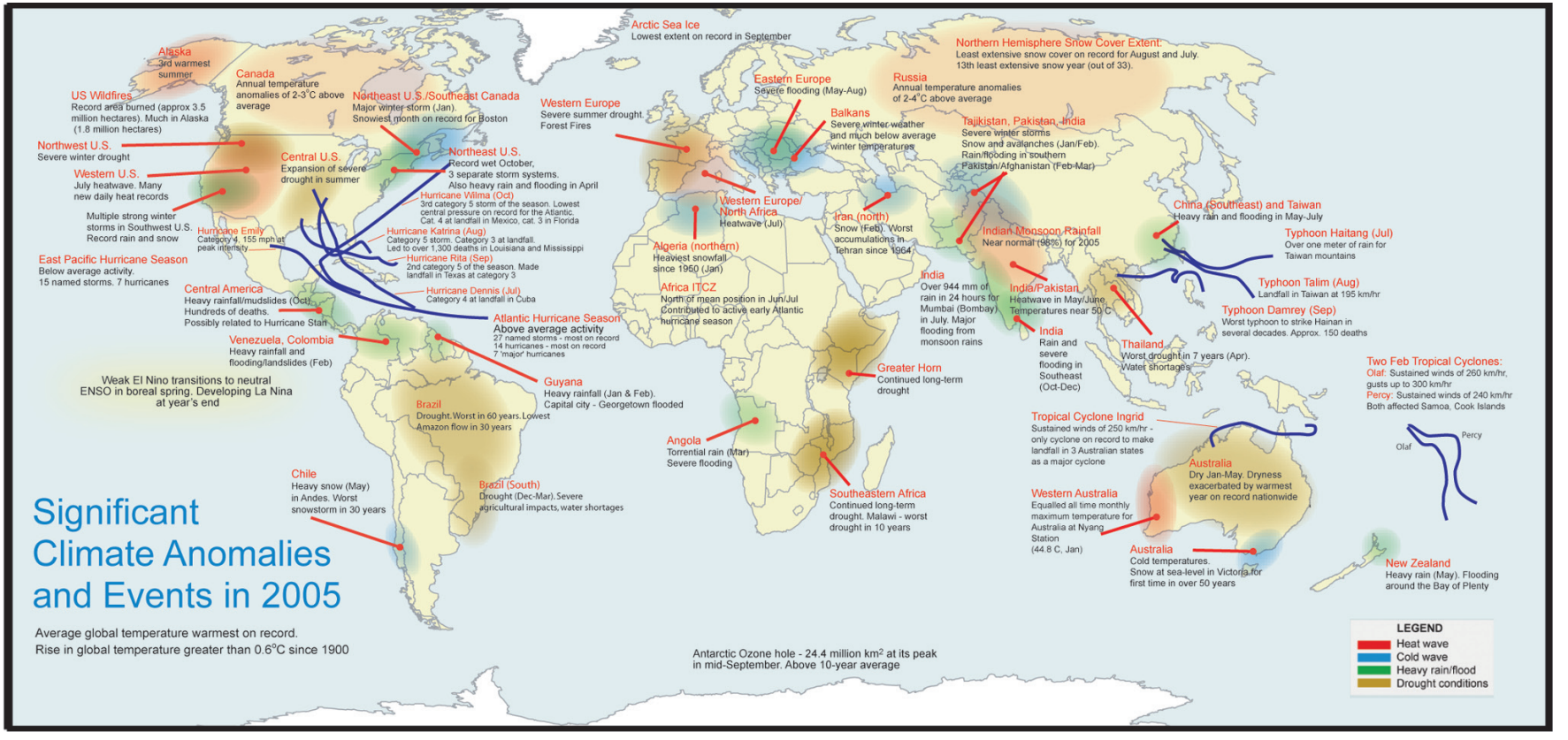

Fig. 1.1. Geographical distribution of notable climate anomalies and events occurring around the planet in 2005. [Source: NOAA/NCDC; online at www.ncdc.noaa.gov/oa/climate/research/2005/ann/ann05.html]

peratures in places. With a few exceptions, North African precipitation was generally below normal. Similarly, southern Africa also experienced warmer-than-normal annual average temperatures, but precipitation was near average after a dry start to the year.

- *North America:* In general, North America was warmer and wetter than normal in 2005. Canadian high latitudes experienced the greatest positive temperature anomalies (some near record), as well as substantially above-normal precipitation. This year was the wettest in recorded history for Canada, which included several widespread flood events in Manitoba, Alberta, and Ontario. Furthermore, Canadian Arctic sea ice extent dropped to its record lowest level, continuing the decline of roughly 8% decade^{-1} since the 1970s. The contiguous United States recorded its seventh warmest year on record, reinforcing the warming trend of the past 30 years. Unlike Canada, the United States experienced near-normal precipitation, with drought conditions in central regions and excessive precipitation in the northeast and southwest. The United States was struck by several major hurricanes, including Katrina and Rita, which resulted in losses over $125 billion USD and well over 1,000 fatalities (Munich Re 2006). A record area of the United States also was impacted by wildfires. Mexico observed above-normal precipitation, partially due to the active tropical season (e.g., Hurricanes Stan and Wilma), and had its second warmest year on record. Wilma was Mexico's most powerful landfalling hurricane on record.
- *Central America:* Annual mean temperatures were slightly above normal across Central America and the Caribbean in 2005, and conditions were generally drier than the long-term average (1979–2000). Cuban drought conditions eased, with above-normal conditions in eastern parts of the island. The region experienced heavy damage and a high death toll from the tropical storm season. Hurricane Stan brought torrential rain to Guatemala, and roughly 1,500 fatalities were reported in association with the storm.
- *South America:* Generally below-normal precipitation occurred across most of South America, except in the west and southwest. Eastern South America experienced above-normal temperatures, while western regions were below normal. Western Amazonia recorded its worst drought in 40 years.
- *Asia:* Russia observed its second warmest year on record, with some areas in northeastern Russia up to 10°C above normal in January, and Siberia had its warmest October in 65 years. In China, the annual average temperature was slightly above the 1971–2000 mean (the ninth consecutive warmer-than-normal year) and precipitation was 17.7 mm above normal. An above-normal eight tropical systems struck China in 2005, impacting millions of people and causing large economic losses. The Southeast Asian monsoon was delayed by about 10 days and was weaker than normal. As a result, precipitation in 2005 was below normal over much of continental Southeast Asia, with temperatures slightly above normal. Above-normal rainfall was experienced by many of the Southeast Asian islands. In southern Asia, severe cold started the year, but summer heat waves took their toll, and late-year winter conditions hampered relief efforts related to the 8 October earthquake in Pakistan. The region experienced a variable and delayed monsoon season, with south and west India receiving abundant rainfall while other regions were below normal. One storm deposited 944.2 mm of rainfall over 24 h on Mumbai (Bombay). In southwest Asia, well-above-normal annual average temperatures were observed, and annual precipitation was slightly below normal, although some regions experienced record snowfall or well-above-normal seasonal precipitation.
- *Europe:* Annually averaged air temperatures over Europe were slightly above normal (1961–90), except in parts of the southeast. The United Kingdom and northern Scandinavia experienced exceptional warmth. Precipitation was generally above normal in Eastern Europe and below normal in western regions. Southwest Europe had well-below-average precipitation, with severe drought across the Iberian Peninsula. Several strong extratropical cyclones affected Scandinavia, and flooding occurred in several eastern European countries.
- *Oceania:* For Australia, 2005 was the hottest year on record and temperatures were above normal across much of the region. Australia also recorded extremely dry conditions during the first half of the year, but rebounded in the second half. In general precipitation was below average for the year. New Zealand experienced above-normal temperature in 2005. Spatially variable precipitation ranged from near-record deficits to flooding rains, but on average the country observed slightly below-normal totals for the year. Over the South Pacific, temperatures also were above normal, and precipitation was spatially variable, but averaged near normal. Five strong tropical storms impacted the region, causing damage on several islands.

2. GLOBAL CLIMATE—

A. M. Waple, Ed.[89]

a. Overview

The year 2005 was notable for its global warmth, both at the surface and throughout the troposphere. Globally, surface temperature remained above average in all 12 months and reached a record high value for the year. This anomalous warmth is part of a long-term warming trend of approximately 0.7°C century^{-1} since 1900, and a rate of increase almost three times as great since 1976. This section provides a summary of tropospheric and surface global temperatures and outlines the differences between the three main surface datasets used to calculate global temperature. Also, below-average stratospheric temperatures in 2005, consistent with a stratospheric cooling trend, are discussed.

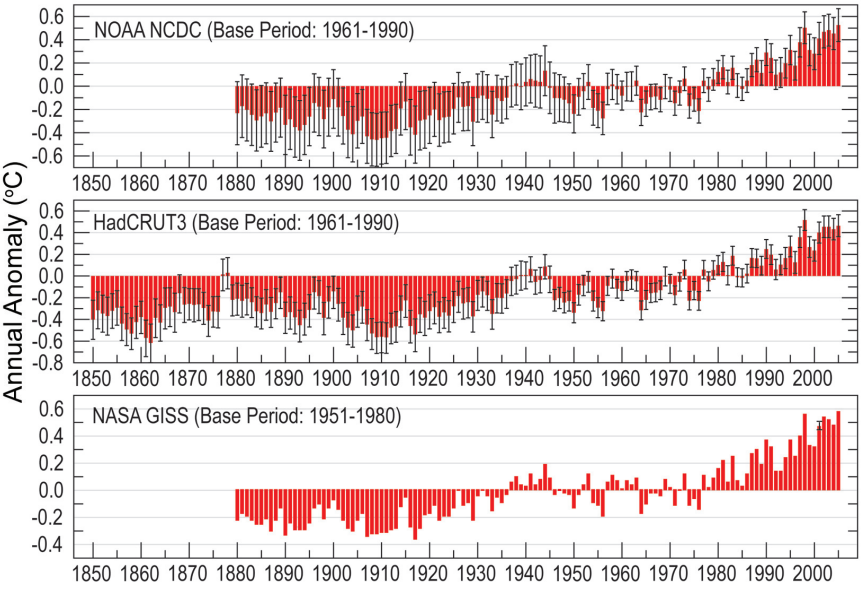

FIG. 2.1. Global annual surface temperature departures (°C) from the 1961 to 1990 average. The 95% confidence limits for the annual global estimates are shown (black error bars). [Sources: NOAA/NCDC; The Hadley Centre for Climate Prediction and Research and the Climate Research Unit of the University of East Anglia; and NASA GISS]

Global average precipitation in 2005 was near the long-term mean, with some regions wetter, and some drier than normal. Snow cover was below average across much of the Northern Hemisphere for the year, consistent with the anomalously warm surface temperatures. Global carbon dioxide (CO_2) concentration rose in 2005 by about 2 parts per million (ppm) to 378.9 ppm, which is an increase slightly above the +1.6 ppm yr^{-1} observed since 1980.

b. Global temperature

1) SURFACE TEMPERATURE—M. J. Menne[55]

The global annual average surface temperature in 2005 was at or near record high levels according to analysis conducted independently at institutions in the United Kingdom (Hadley Centre of the Met Office and the Climate Research Unit of the University of East Anglia) and in the United States [NOAA's National Climatic Data Center and the National Aeronautics and Space Administration's (NASA's) Goddard Institute for Space Studies (GISS)]. As shown in Fig. 2.1, the value for 2005 ranks as highest on record according to the NOAA and NASA analyses and second highest, behind 1998, according to the Met Office's Hadley Centre/University of East Anglia's Climate Research Unit analysis. However, when uncertainties related to estimating the global mean are considered, the two highest annual values are effectively indistinguishable from one another. Based on the NOAA/NCDC record, the rise in global surface temperatures since 1900 is 0.66°C, when calculated as a linear trend.

Record high monthly global averages were observed in April, May, June, and September 2005 (Fig. 2.2). Figure 2.2 indicates that global surface temperature values in 2005 were sustained at levels near the 1998 values, but without the influence of a

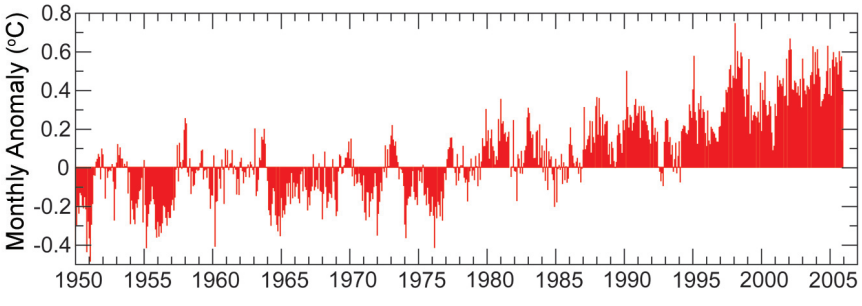

FIG. 2.2. Serial monthly surface temperature anomalies (°C) relative to a 1961–90 base period, based on Quayle et al. (1999). [Source: NOAA/NCDC]

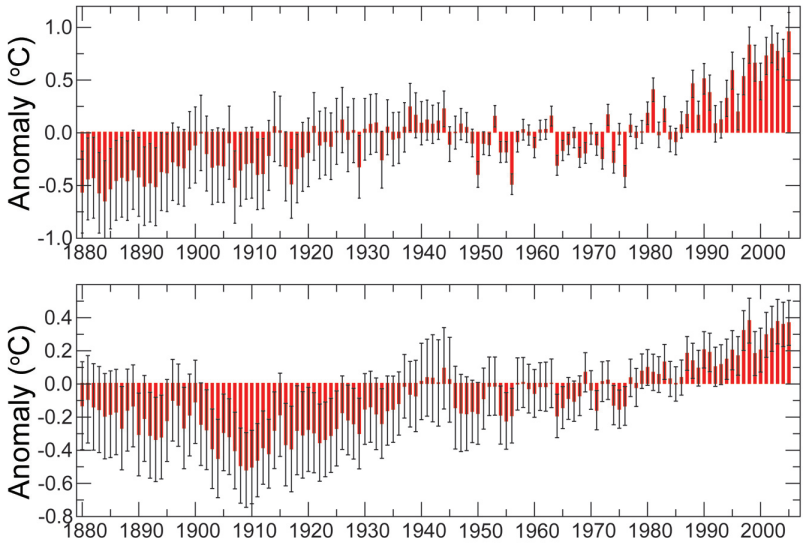

Fig. 2.3. Sea surface and land surface temperature anomalies (°C) with respect to the 1961–90 mean. [Source: NOAA/NCDC]

strong El Niño–Southern Oscillation (ENSO) warm event like that which occurred in 1997/98.

Global land surface temperatures ranked highest on record according to the NOAA/NCDC record, while sea surface temperatures ranked third highest (Fig. 2.3), behind 1998 and 2003. Many regions across the globe recorded temperatures well in excess of the 1961–90 mean (Fig. 2.4). In some areas, most notably throughout much of the North Atlantic basin, the average for 2005 exceeded the 90th or 98th percentiles of the mean annual temperature distribution (Fig. 2.5) estimated using 1961–90 observations (Horton et al. 2001). These anomalies are discussed in more detail in the tropical cyclones section (see section 4c). Averaged separately by hemisphere, 2005 surface temperatures rank as second highest in the NH and as sixth highest in the SH according to the NOAA/NCDC archive.

Regionally, 2005 temperatures were highest on record in Australia. High average temperatures were also observed across much of Canada and Siberia. An intense heat wave occurred across India, Pakistan, and Bangladesh in May and June. Conversely, cold conditions were experienced across much of Europe and North Africa in February. These events are discussed in detail in the regional climate sections (see section 6).

ii) Upper-air tropospheric temperatures—J. C. Christy[17]

The temperature variations of three broad atmospheric layers, the low to middle troposphere (LT: surface–300 hPa), the middle troposphere to lower stratosphere (MT: surface–70 hPa), and the upper troposphere to lower stratosphere (LS: 150–20 hPa) are presented. Products from two radiosonde-based datasets—Radiosonde Atmospheric Temperature Products for Analysis of Climate (RATPAC; Free et al. 2005) based on 85 stations, and Hadley Atmospheric Temperatures (HadAT2; Thorne et al. 2005) based on about 650 stations—are included in the data. Satellite products are of the LT, MT, and LS from the University of Alabama in Huntsville (UAH; Christy et al. 2003) and of the MT and LS from Remote Sensing Systems (RSS; Mears et al. 2003).

The annual LT temperature anomaly for 2005 was second warmest (tied for second in UAH) since either radiosonde (1958) or satellite (1979) records began (Fig. 2.6). The warmest calendar year remains 1998[1]. The anomaly correlations are extremely high

[1] Note that global and tropical tropospheric temperatures tend to lag surface temperatures by about 6 months, meaning the phase of the ENSO warmth was shifted further into 1998 for upper air relative to that which was measured at the surface.

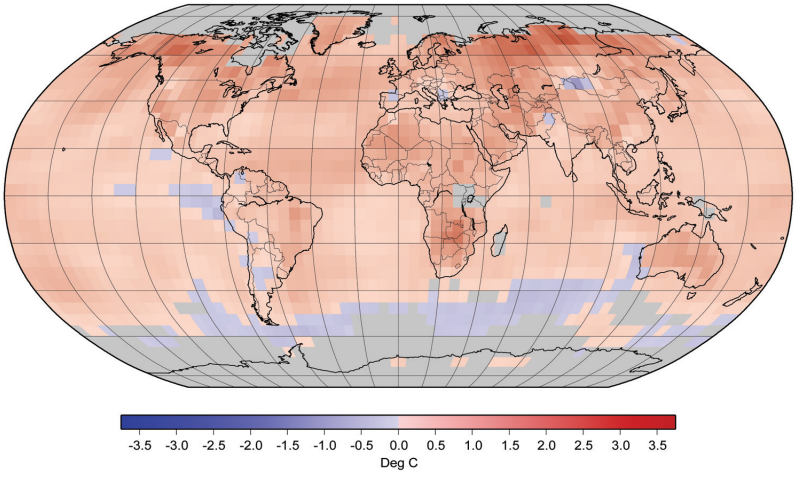

Fig. 2.4. Geographic distribution of surface air temperature anomalies (°C) in 2005 relative to the 1961–90 mean. [Source: NOAA/NCDC]

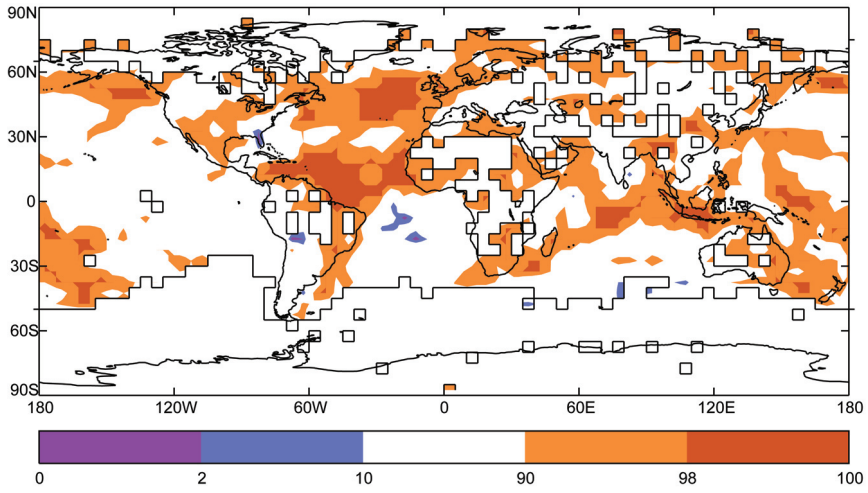

FIG. 2.5. Land surface temperature anomalies (°C) based on HadCRUT3 expressed as percentiles of modified two-parameter gamma distributions fit to annual data for 1961–90 according to Horton et al. (2001). [Source: Hadley Centre for Climate Prediction and Research]

among the datasets, but the linear trend reveals slight differences since 1979 (Table 2.1). The largest trends in all datasets are found in the northern third of the globe. A visual interpretation of long-term change suggests a relatively strong increase in global temperatures around 1978 and another shift to warmer temperatures associated with the 1997/98 ENSO. The base period for the plot is 1979–98, and since 1977, no seasonal anomaly has dipped below –0.4°C. Since 1998, only one dataset has dipped below –0.1°C.

The northern polar region (60°–85°N) experienced its warmest annual reading in the period of record (+1.3°C). No large-scale region had an annual mean negative anomaly relative to the 1979–98 base period, although smaller areas did.

The MT layer (Fig. 2.7), which includes some stratospheric influence, presents a similar picture. However, while 2005 was the second warmest globally for the two radiosonde datasets, it was fourth and fifth warmest in the RSS and UAH satellite datasets, respectively. Linear trends in MT are more negative than LT, because the cooling stratosphere exerts an influence on MT (Table 2.1).

The quasi-biennial oscillation (QBO) was in the easterly phase in 2005 and contributed to a tropical (20°N–20°S) anomaly that was the coldest on record in the stratosphere. The 2005 global annual anomaly was near those of 1995, 1996, and 2000 in the satellite records (Fig. 2.8), but was not the coldest. Linear trends are more variable among the datasets, but all indicate significant cooling over the period (Table 2.1). However, since about 1995, global trends have been near zero (Fig. 2.8).

High-latitude LS anomalies were exceptionally cold in a broad area centered over Greenland, but were warmer than average over eastern Antarctica. The coldest large-scale monthly anomalies occurred over the NH polar region in January and February (-6°C, 60°–85°N), while the warmest monthly

TABLE 2.1. Linear trends (°C decade^{-1}) from 1979 to 2005 of global and tropical (20°S–20°N) anomalies for the three temperature products. 1958–2005 trends in parentheses.

	RATPAC	HadAT2	UAH	RSS
Global LT	+0.15 (+0.15)	+0.17 (+0.15)	+0.13*	
Tropical LT	+0.11 (+0.13)	+0.09 (+0.13)	+0.07	
Global MT	+0.04 (+0.08)	+0.06 (+0.09)	+0.05	+0.14
Tropical MT	+0.02 (+0.08)	+0.01 (+0.09)	+0.06	+0.15
Global LS	–0.71 (–0.42)	–0.57 (–0.36)	–0.45	–0.32
Tropical LS	–0.75 (–0.45)	–0.60 (–0.34)	–0.41	–0.29

* When subsampled at 50°–85°N to more closely represent the geographical extent of HadAT2, UAH LT "global" trend is +0.15°C decade^{-1}.

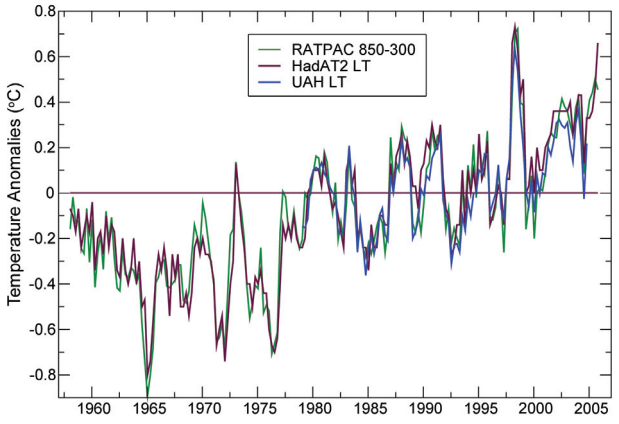

Fig. 2.6. Seasonal anomalies (°C) of global average lower-tropospheric layer temperature. HadAT2, UAH, and RSS depict the temperature of layers representing the microwave brightness temperature weighting functions (roughly surface to 300 hPa, peaking around 700 hPa), while RATPAC depicts the 850–300-hPa layer mean temperature.

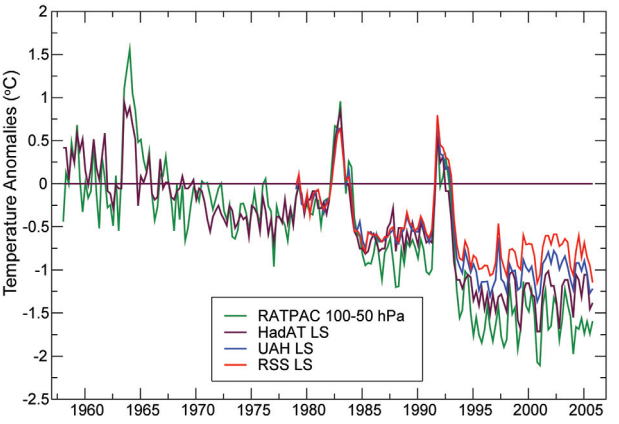

Fig. 2.8. Seasonal anomalies (°C) of global lower-stratospheric temperature. This layer begins around 120 hPa and diminishes above 20 hPa. RATPAC data depict anomalies of the 100–50-hPa layer.

anomalies (+2°C) appeared over the SH polar region in October and November. This marks the fourth year in a row where anomalies of the SH polar region were above average (1979–98) for austral spring in satellite records (see section 5c).

c. Hydrologic cycle

1) Global precipitation

(i) Land—D. H. Levinson,[46] J. H. Lawrimore,[45] and D. B. Wuertz[94]

Global precipitation anomalies determined from land-based gauges were analyzed on both an annual and a seasonal basis using data from the Global Historical Climatology Network (GHCN; Peterson and Vose 1997). Anomalies over the period of 1901–2005 were determined from the GHCN dataset with respect to the 1961–90 mean using those stations with a minimum of 20 years of data during the base period (Peterson and Vose 1997; Vose et al. 1992). Global precipitation was average in 2005, with an annual anomaly less than 1 mm (−0.87 mm) below the 1961–90 mean (Fig. 2.9a).

Over the past two-and-a-half decades, global precipitation has been generally below the long-term mean, with above-average precipitation anomalies in only 7 of the last 25 years. This multidecadal period of below-normal precipitation and anomalously dry conditions began during the early 1980s, and has continued through the 1990s into the present decade. The peak in this dry period appears to have occurred in 1992, corresponding with a multiyear El Niño event. Previous studies (i.e., Ropelewski and Halpert 1987) have shown that variability associated with ENSO influences large-scale precipitation patterns in the Tropics and midlatitudes, both of which contribute to generally drier conditions at high latitudes.

Regardless of the potential causes of the multidecadal dry period, much of the observed signal in global precipitation anomalies appears to be seasonally dependent (Figs. 2.9b–e). In 2005, negative anomalies were observed in three of the four seasons, with only the boreal autumn [September–November (SON)] having above-average precipitation for the year. During this extended dry period, below-normal precipitation occurred primarily during two seasons [March–May (MAM) and June–August (JJA)], with the boreal summer having the longest continuous

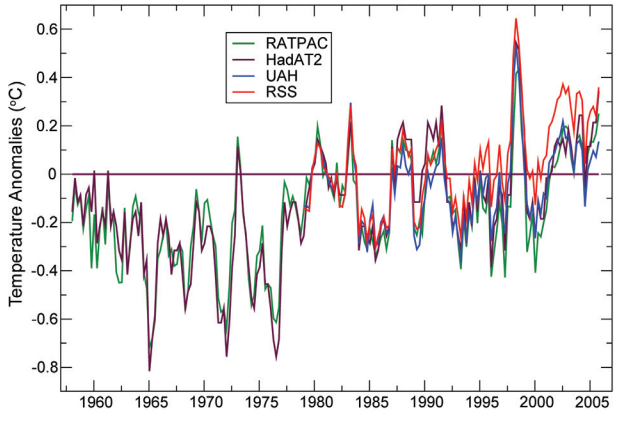

Fig. 2.7. Seasonal anomalies (°C) of global average tropospheric temperature. This layer includes a portion of the lower stratosphere, representing a microwave brightness temperature weighting function that starts at the surface, peaks in the midtroposphere, and diminishes rapidly above 100 hPa.

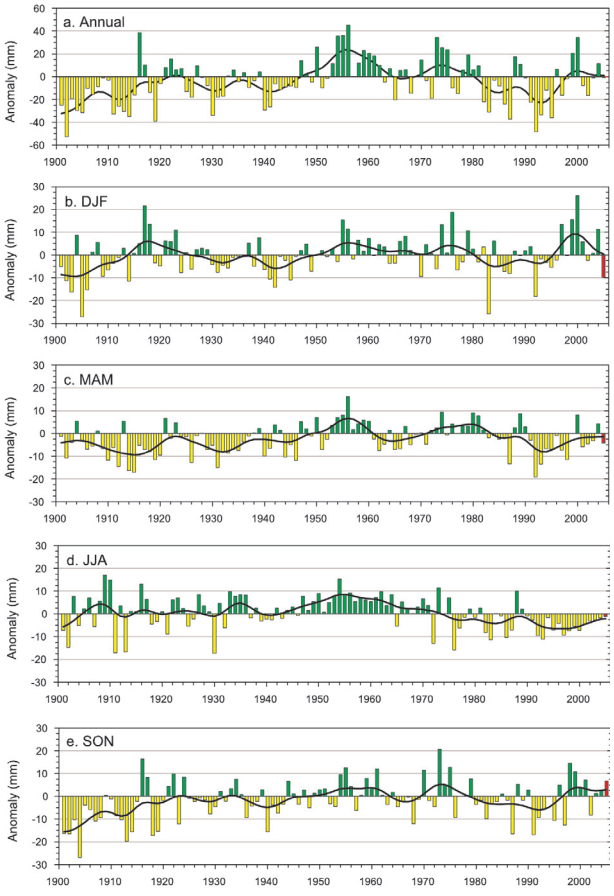

Fig. 2.9. Time series of annual and seasonal global precipitation anomalies over the period 1901–2005, with observations from the GHCN dataset: a) annual, b) December–February (DJF), c) MAM, d) JJA, and d) SON. The precipitation anomalies were calculated in mm with respect to the 1961–90 base period mean: green bars = positive anomalies, yellow bars = negative anomalies, and red bar = 2005 anomaly. In addition, the black line in each time series denotes the smoothed annual or seasonal values using a 13-point binomial filter.

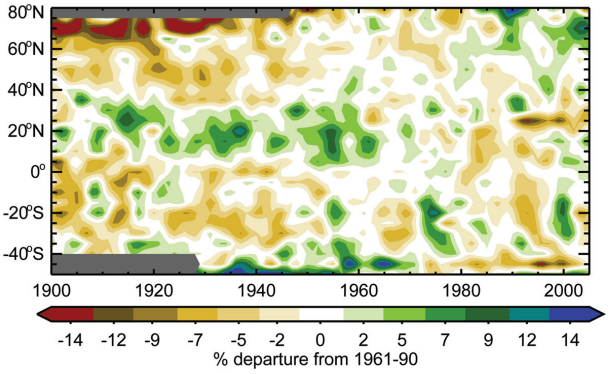

Fig. 2.10. Hovmoeller plot of the percentage departure from 1961 to 1990 means of GHCN global annual precipitation, with zonal means determined over 5° latitude bands and covering the period 1900–2005. A 13-point binomial filter was applied to each zonal time series, with green and blue shades corresponding to wet anomalies and red and brown shades corresponding to dry anomalies. Gray shading in the early twentieth century is due to a lack of data in high-latitude regions.

period of drier-than-normal conditions, extending from the late 1980s through 2005.

For the first half of the twentieth century, and extending into the 1960s, much of the Tropics in the NH were dominated by wet precipitation anomalies, while midlatitude regions in both hemispheres were drier than normal (Fig. 2.10). It is likely that the period of dry anomalies in the northern high-latitudes during 1900–40 was due to a lack of precipitation data, as well as a systematic undercatch of snow and solid precipitation. Since the 1960s, there has been an extended period of dry anomalies in the Tropics, particularly in the NH. In recent years, including 2005, high-latitude regions of the NH have been wetter than normal, with a multiyear wet period north of 60°N.

Significant precipitation anomalies were observed at many long-term monitoring locations over the past year (Fig. 2.11), but several regions stand out as being either significantly wetter or drier than normal. Of special note were the large dry anomalies in parts of East Asia, particularly across southern Japan, eastern China, and the Korean Peninsula, in part due to below-normal number of landfalling tropical cyclones (see section 4c). Other regions with significant dry anomalies included much of Australia, South Africa and coastal areas of the Gulf of Guinea, the Iberian Peninsula and France, and a large portion of the central United States, extending from the Gulf of Mexico to the Great Lakes. Locations significantly

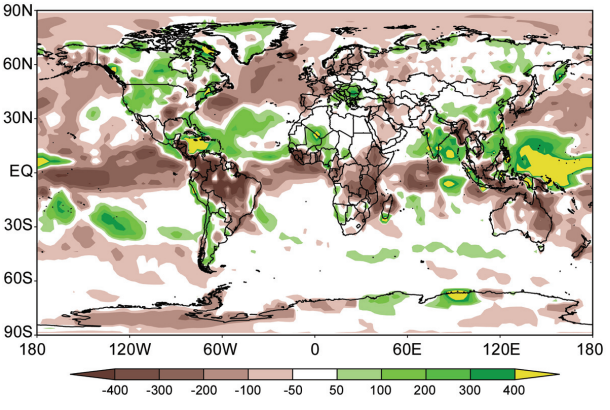

Fig. 2.11. Precipitation anomalies (mm) relative to a 1970–2000 base period from the gauge–satellite merged CAMS–OPI precipitation dataset (Janowiak and Xie 1999).

wetter than average in 2005 included most of Scandinavia, Senegal and the Atlantic coast of West Africa, Venezuela and Columbia, and a large portion of the Caribbean basin. Further details on these and other regional precipitation anomalies can be found in section 6.

(ii) Oceans—P. Xie[95] and J. E. Janowiak[34]

Real-time monitoring of global oceanic precipitation is routinely conducted at NOAA's Climate Prediction Center (CPC) with the use of the gauge–satellite merged Climate Anomaly Monitoring System (CAMS)–outgoing longwave radiation (OLR) Precipitation Index (OPI) dataset (Janowiak and Xie 1999). By combining the gauge observations of precipitation collected and archived by CPC via CAMS (Ropelewski et al. 1985) with the satellite-based OPI (Xie and Arkin 1998), CAMS–OPI provides monthly precipitation estimates over global land and ocean on a real-time basis.

Global oceanic precipitation during 2005 is characterized by rainbands associated with the intertropical convergence zone (ITCZ), South Pacific convergence zone (SPCZ), and the midlatitude oceanic storm tracks (Fig. 2.12). Mean precipitation over the entire global ocean during 2005 was 2.840 mm day^{-1}, equivalent to a freshwater influx of 1036.6 kg m^{-2}. Maximum annual precipitation rates of over 10 mm day^{-1} were observed during the year over the tropical western Pacific where the ITCZ merges with the SPCZ (see section 4d). Meanwhile, relatively light precipitation occurred over several oceanic dry zones of the southeast Pacific, northeast Pacific off the coast of the southwest United States, southeast Atlantic, tropical North Atlantic near western Africa, and the eastern Indian Ocean.

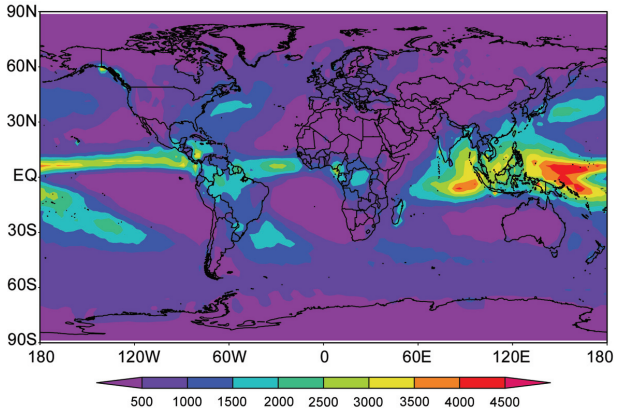

Fig. 2.12. Precipitation totals (mm) for 2005 from the gauge–satellite merged CAMS–OPI precipitation dataset (Janowiak and Xie 1999).

The distribution of precipitation anomalies during 2005 indicates a dipole pattern of wet and dry anomalies over the western and eastern tropical Pacific, respectively (Fig. 2.11). Although weak El Niño conditions prevailed over the tropical Pacific in the second half of 2004 and continued into early 2005 (Lyon and Barnston 2005; see also section 4b), enhanced precipitation was limited mostly to the tropical Pacific west of the date line. This pattern is different from that typical of a medium or strong El Niño event when large positive precipitation anomalies occur over the central and eastern Pacific (Ropelewski and Halpert 1989; Xie and Arkin 1997).

Enhanced convection, and attendant above-normal precipitation, was first observed in late 2004 over the tropical western Pacific north of Indonesia (Fig. 2.13). The positive precipitation anomaly intensified as it moved eastward, and reached its maximum intensity during January–March of 2005. Such large intraseasonal variations present in Fig. 2.13 are associated with the strong MJO (Madden and Julian

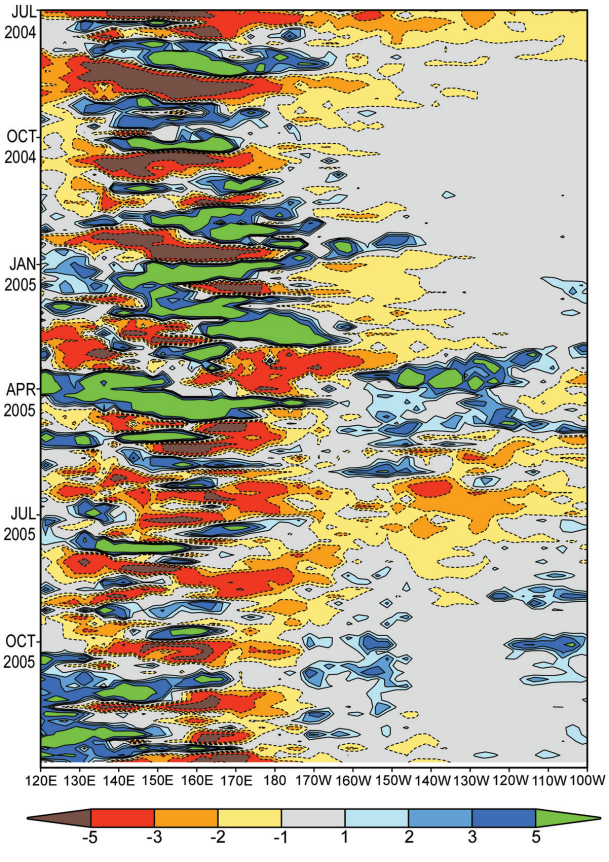

Fig. 2.13. Time–longitude section of precipitation anomaly (mm; 1979–95 base period) averaged over the tropical Pacific (5°S–5°N) as observed by the Global Precipitation Climatology Project (GPCP) pentad precipitation dataset (Xie et al. 2003).

1971) activity that was observed during that period (Climate Prediction Center 2005). The positive precipitation anomaly over the tropical western Pacific gradually shifted westward during the second half of 2005 as the coupled ocean–atmosphere system evolved toward a weak La Niña.

A substantial positive precipitation anomaly was observed over regions of strong hurricane activity in the Atlantic basin, especially the Caribbean Sea (see section 4c). The Atlantic ITCZ was located slightly north of its climatological latitude, which is reflected by two parallel bands of positive and negative precipitation anomalies over the tropical Atlantic (Fig. 2.11).

Substantially depressed precipitation over the northwestern Atlantic during 2005 also was noticeable. Examination of monthly precipitation and atmospheric circulation fields suggest that the bulk of the negative precipitation anomaly over the region was the result of below-normal winter storm activity in the oceanic storm track, which is a climatological feature over the western North Atlantic during the cool season. This reduced storminess was associated with strong anticyclonic blocking activity over the high latitudes that was observed during the winter season.

ii) Snow—D. A. Robinson[75]

Annual snow cover extent (SCE) over NH lands averaged 24.7 million km^2 in 2005. This is 0.9 million km^2 less than the 36-yr average and ranks 2005 as having the 32nd most extensive cover of record (Table 2.2). This evaluation includes snow over the continents, including the Greenland Ice Sheet. The SCE in 2005 ranged from 47.6 million km^2 in February to 2.3 million km^2 in August. Monthly snow extent values are calculated at the Rutgers Global Snow Laboratory from weekly SCE maps produced by NOAA meteorologists, who rely primarily on daily visible satellite imagery to construct the maps.

Hemispheric SCE was only above the long-term mean in February, March, and December; thus, the 12-month running means of NH extent were below the long-term average throughout the year (Fig. 2.14). This has almost exclusively been the situation since the late 1980s. Eurasian SCE was somewhat below the long-term average in 2005 and ranked as the 25th most extensive cover of the satellite era. North American SCE was much below average, ranking 35th (Figs. 2.15 and 2.16).

As is common, 2005 SCE showed significant spatial and temporal variability. For instance, hemi-

Table 2.2. Monthly and annual climatological information for NH and continental snow extent between November 1966 and December 2005. Included are the numbers of years with data used in the calculations, means, standard deviations, 2005 values, and rankings. Areas are in millions of km^2. 1968, 1969, and 1971 have 1, 5, and 3 missing months, respectively, and thus are not included in the annual (Ann) calculations. North America includes Greenland.

	Yrs	Mean	Std dev	2005	2005 NH rank	Eurasia rank	North American rank
Jan	39	46.9	1.5	46.7	21	27	15
Feb	39	45.9	1.9	47.6	9	3	33
Mar	39	41.0	1.9	41.3	18	12	25
Apr	39	31.4	1.7	29.9	31	20	38
May	39	20.5	1.9	17.6	38	36	38
Jun	38	11.0	2.1	9.0	31	31	30
Jul	36	4.9	1.4	3.0	36	33	35
Aug	37	3.5	1.0	2.3	37	33	37
Sep	37	5.7	1.0	4.8	31	33	21
Oct	38	18.3	2.6	16.9	31	24	34
Nov	40	34.1	2.1	32.2	32	30	31
Dec	40	43.5	1.8	44.5	10	11	13
Ann	36	25.6	1.0	24.7	32	25	35

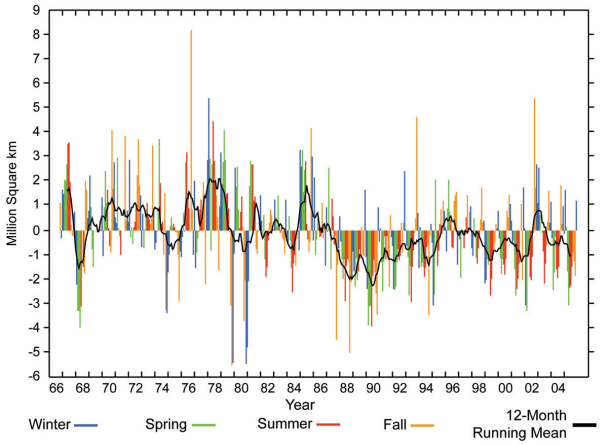

Fig. 2.14. Anomalies of monthly snow cover extent over Northern Hemisphere lands (including Greenland) between Nov 1966 and Dec 2005, calculated from NOAA snow maps. Also shown are 12-month running mean anomalies of hemispheric snow extent, plotted on the seventh month of a given interval. Mean hemispheric snow extent is 25.6 million km^2 for the full period of record. Monthly means for the period of record are used for nine missing months between 1968 and 1971 in order to create a continuous series of running means. Missing months fall between June and October; no winter months are missing.

spheric SCE ranked in the top 10 in February and December, while totals ranked in the lowest 10 from April through November. February's NH anomaly was positive due to the Eurasian extent being the third largest on record, despite North America ranking 33rd. December's high ranking was the result of extensive cover over both continents; this followed November, when both ranked quite low. Spring snow cover continues to be less extensive in the second half of the satellite record than in the first half. Lower-than-average North American SCE was first noted in February, while well-below-average Eurasian cover did not occur until May.

Over the contiguous United States, end-of-winter SCE was very low after February, while in Alaska, May SCE was at a record low. Both regions began the boreal fall snow season slowly, especially in Alaska, where SCE was at a record low in September and only increased to second lowest in October and third lowest in November, resulting in a very long snow-free season for 2005 in Alaska.

Maps depicting daily, weekly, and monthly conditions, daily and monthly anomalies, and monthly climatologies for the entire period of record may be viewed at the Rutgers Global Snow Laboratory Web site (available online at http://climate.rutgers.edu/snowcover).

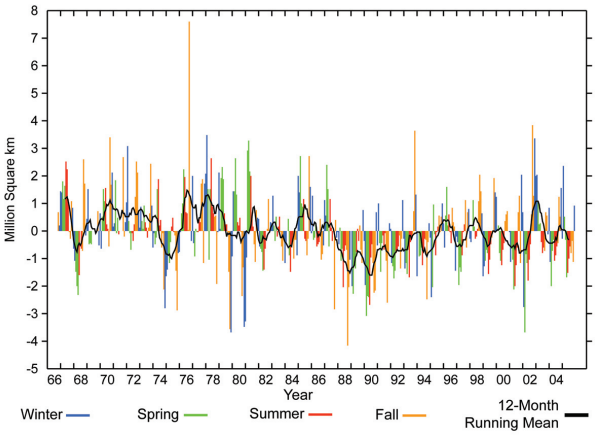

Fig. 2.15. Same as Fig. 2.14, except for Eurasia.

d. Trace gases

1) Carbon dioxide—R. C. Schnell[81]

Carbon dioxide emitted from natural and anthropogenic (i.e., fossil fuel combustion) sources is partitioned into three mobile reservoirs: atmosphere, oceans, and the terrestrial biosphere. The result of increased fossil fuel combustion has been that atmospheric CO_2 has increased from about 280 ppm (parts in 10^6 by dry-air mole fraction) at the start of the industrial revolution to about 380 ppm today (Fig. 2.17a). Roughly half the emitted CO_2 remains in the atmosphere and the remainder has gone into two "sinks"–oceans and the land biosphere (which includes plants and soil carbon).

The present rate of anthropogenic carbon emission to the atmosphere is nearly 7 Pg yr^{-1} (Pg = 10^{15} g). During the 1990s, net uptake by the oceans was estimated at 1.7 ±0.5 Pg yr^{-1}, and by the land biosphere

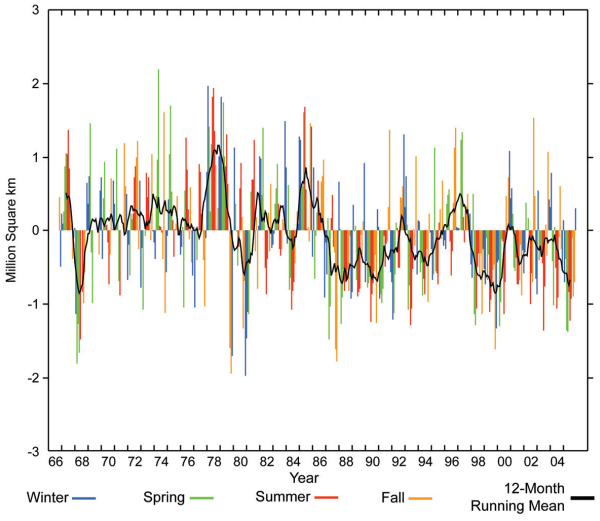

Fig. 2.16. Same as Fig. 2.14, except for North America (including Greenland).

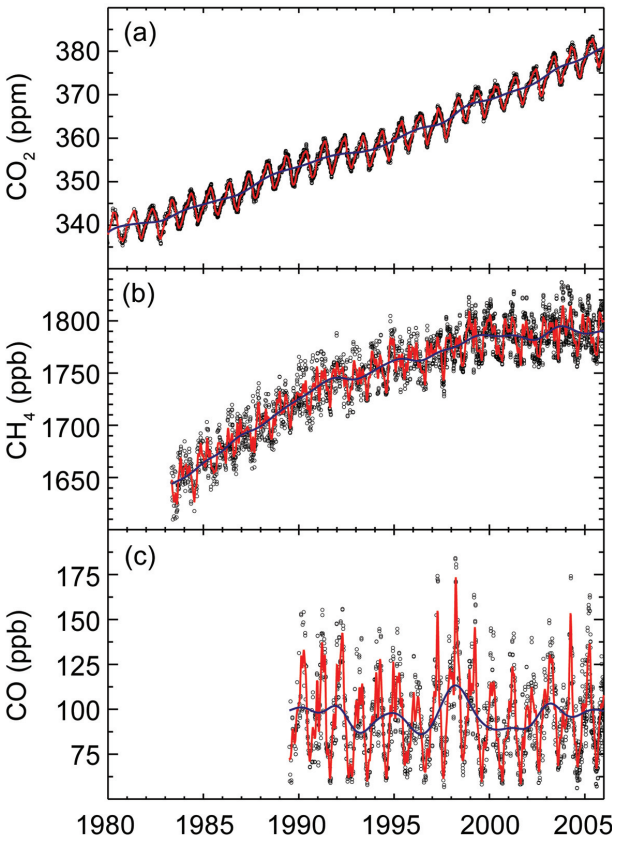

FIG. 2.17. Trace gas mole fractions (black symbols) determined from samples collected at the NOAA ESRL Mauna Loa Observatory (MLO) for (a) CO_2 (courtesy: T. J. Conway, NOAA). Current trends at MLO and globally averaged are available online at www.cmdl.noaa.gov/ccgg/trends/. (b) CH_4 (courtesy: E. J. Dlugokencky, NOAA), and (c) CO (courtesy: P. C. Novelli, NOAA). In all panels, the solid blue line is the deseasonalized trend and the red line is a smooth curve fitted to the black symbols. More plots can be found online at www.cmdl.noaa.gov/ccgg.

as 1.4 ±0.7 Pg yr^{-1} (Prentice et al. 2001). The gross atmosphere–ocean and atmosphere–terrestrial biosphere (i.e., photosynthesis and respiration) fluxes are on the order of 100 Pg yr^{-1}. Interannual variations in the atmospheric increase of CO_2 (Fig. 2.17a; based on Conway et al. 1994) are not attributed to variations in fossil fuel emissions, but rather to small changes in these net fluxes. Most attempts to explain the interannual variability of the atmospheric CO_2 increase have focused on short-term climate fluctuations (e.g., ENSO and post–Mt. Pinatubo cooling), but the mechanisms, especially the role of the terrestrial biosphere, are poorly understood. To date, about 5% of conventional fossil fuels have been combusted. If combustion were stopped today, it is estimated that after a few hundred years, 15% of the total carbon emitted would remain in the atmosphere, and the remainder would be in the oceans.

In 2005, the globally averaged atmospheric CO_2 mole fraction was 378.9 ppm, just over a 2 ppm increase from 2004. This continues the steady upward trend in this abundant and long-lasting greenhouse gas. Since 1900, atmospheric CO_2 has increased 84 ppm (22%), with an average annual increase of 1.6 ppm since 1980.

In calculating the global mean mole fractions of CO_2 and other trace gases, the number of stations varies through time and may be different for each gas at any point in the period of record. Each record is temporally smoothed, with evenly spaced values selected from these temporal fits to generate new fits as a function of latitude (ϕ). Values extracted from the latitude fit at a spacing of $\sin(\phi) = 0.05$ (i.e., at equal atmospheric volumes) define a matrix of species value as a function of time and latitude. These are then used to calculate global averages at weekly and annual time resolution (Conway et al. 1994).

ii) Methane—R. C. Schnell[81]

Methane's (CH_4) contribution to anthropogenic radiative forcing, including direct and indirect effects, is about 0.7 W m^{-2}, or roughly half that of CO_2. Also, changes in the burden of CH_4 feed back into atmospheric chemistry, affecting the concentrations of hydroxyl (OH) and ozone (O_3). The increase in CH_4 since the preindustrial era is responsible for about half of the estimated increase in background tropospheric O_3 during that time. Changes in OH concentration affect the lifetimes of other greenhouse gases such as hydrochlorofluorocarbons (HCFCs) and hydrofluorocarbons (HFCs).

High-precision measurements of atmospheric CH_4 provide climate modelers with current and past rates of CH_4 increase, and they are also useful in constraining the CH_4 budget. During 20 years of measurements, CH_4 has increased, but the rate of increase has slowed in recent years (Fig. 2.17b). A large increase in 1998 was likely the result of climatic conditions that resulted in increased emissions from wetlands and biomass burning. Measurements of CH_4 at Mauna Loa, Hawaii, remained nearly constant from 1999 to 2002 (Dlugokencky et al. 2003). In 2003, CH_4 increased by about 5 ppb (parts in 10^9 by dry-air mole fraction), primarily due to increases in the Northern Hemisphere. This was followed by a small decrease in 2004, and little change from those levels in 2005. Globally averaged CH_4 in 2005 was 1774.8 ppb, which represented a decrease of 2.8 ppb from 2004.

iii) Carbon monoxide—R. C. Schnell[81]

Unlike CO_2 and CH_4, carbon monoxide (CO) does not strongly absorb terrestrial infrared radiation, but does impact climate through its chemistry. The chemistry of CO affects OH (which influences the lifetimes of CH_4 and HFCs) and tropospheric O_3 (itself a greenhouse gas), so emissions of CO can be considered equivalent to emissions of CH_4 (Prather 1996). Current emissions of CO may contribute more to radiative forcing over decadal time scales than emissions of anthropogenic nitrous oxide (N_2O; Daniel and Solomon 1998).

Carbon monoxide mole fractions from Mauna Loa (Fig. 2.17c, symbols) show little trend over the measurement period (updated from Novelli et al. 2003). Superimposed on the flat trend is a significant increase during 1997 and 1998, which was likely the result of tropical (Langenfelds et al. 2002) and boreal biomass burning (Kasischke et al. 2000). Because the lifetime of CO is relatively short (a few months), the anomaly quickly disappeared and CO quickly returned to pre-1997 levels. Carbon monoxide levels in 2005 were comparable to those found in the early 2000s. The globally averaged CO mole fraction in 2005 was 83.5 ppb, very near the average of the past five years. Since 1991, little trend in globally averaged CO has been observed.

iv) Nitrous oxide and sulfur hexaflouride—J. W. Elkins[21] and G. S. Dutton[20]

Atmospheric N_2O and sulfur hexafluoride (SF_6) are present in lower concentrations than CO_2, but the radiative forcing of each is far greater. Nitrous oxide is the third strongest greenhouse gas, while each SF_6 molecule is 22,200 times more effective as an infrared absorber than one CO_2 molecule, and has an atmospheric lifetime of between 500 and 3200 years. The concentration of both species has grown at a linear rate, N_2O at 0.76 ppb yr^{-1} (0.25% yr^{-1}) since 1978 (Fig. 2.18a) and SF_6 at a rate of 0.22 ppt (parts in 10^{12} by dry-air mole fraction) yr^{-1} (~5% yr^{-1}) since 1996 (Fig. 2.18b).

The concentration of 320 ppb N_2O in 2005 has added a radiative forcing of around 0.17 W m^{-2} over the preindustrial N_2O concentration of around 270 ppb (Fig. 2.18a). Atmospheric N_2O is also a major source of stratospheric nitric oxide (NO), a compound that helps to catalytically destroy stratospheric O_3.

The atmospheric concentration of SF_6 has grown due to its use as an electrical insulator for power transmission throughout the world. Its global mean concentration was 5.75 ppt at the end of 2005 (Fig. 2.18b). While total radiative forcing of SF_6 from preindustrial times to the present is relatively small (0.003 W m^{-2}), its long atmospheric lifetime, high atmospheric growth rate, and high global warming potential are a concern for the future.

v) Halocarbons—R. C. Schnell[81]

Concern over stratospheric ozone depletion has restricted or eliminated production of many halocarbons. The phase out of human-produced halocarbons was the result of the 1987 Montreal Protocol on Substances that Deplete the Ozone Layer. As a result of these efforts, mixing ratios of many ozone-depleting gases have been declining at Earth's surface in recent years; this decline continued in 2005 (Fig. 2.19). NOAA/Earth System Research Laboratory (ESRL)/Global Monitoring Division (GMD) measurements from around the globe show that tropospheric mixing ratios of CFC-12, the longest lived and most abundant human-made ozone-depleting gas in the atmosphere, peaked within the last few years (Fig. 2.19a).

Those data also show that mixing ratios of some halogenated gases continue to increase globally (Figs. 2.19a–d). The most rapid increases are in HCFCs and HFCs, which are chemicals commonly used as replacements for chlorofluorocarbons (CFCs), halons, and other ozone-depleting gases. Although HCFCs contain chlorine (Cl) and deplete O_3 with a reduced efficiency compared to CFCs, HFCs do not participate in O_3-destroying reactions.

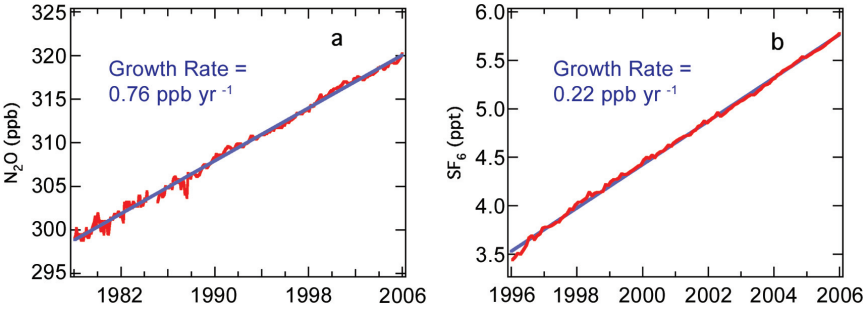

Fig. 2.18. (a) Global atmospheric N_2O from the NOAA/ESRL in situ and flask network (red) has increased with a linear growth rate (blue) of 0.76 ppb yr^{-1} from 1978 to the end of 2005. (b) Global atmospheric SF_6 from the NOAA/ESRL in situ and flask network (red) has increased at a linear rate (blue) of 0.22 ppt yr^{-1} from 1996 to the end of 2005.

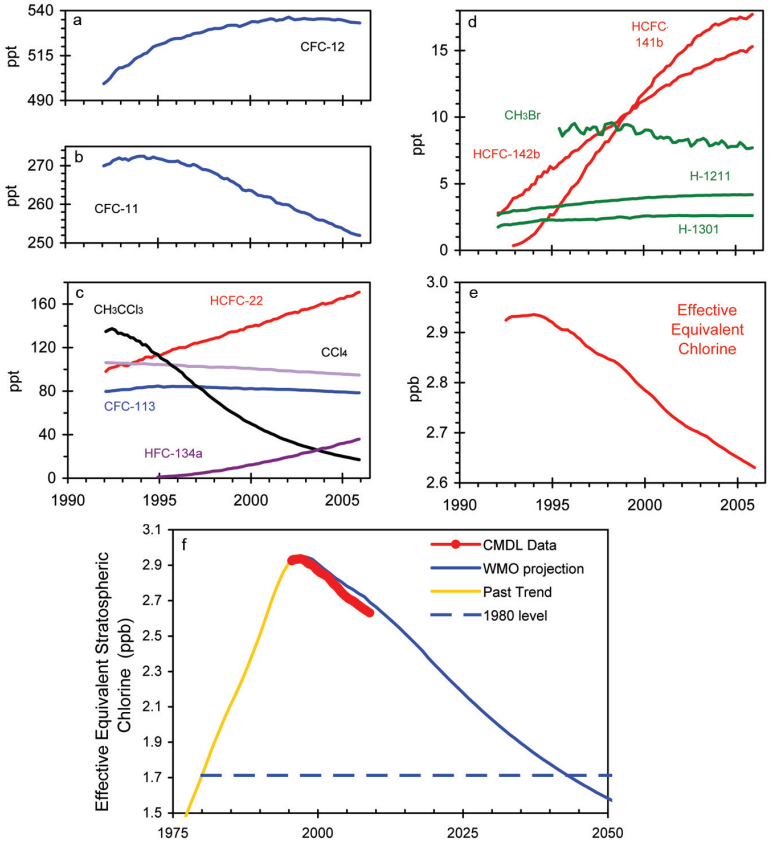

FIG. 2.19. (a)–(d) Changes in global mean tropospheric mixing ratios (ppt) of the most abundant CFCs, HCFCs, HFCs, chlorinated solvents, and brominated gases, calculated from atmospheric measurements made at remote sites in both the NH and SH. [Source: NOAA/ESRL/GMD cooperative air sampling network] (e) Secular changes in atmospheric equivalent chlorine (EECl; ppb). (f) Recent changes in effective equivalent stratospheric chlorine (EESC) observed by the NOAA/GMD global network relative to the secular changes observed in the past. EESC is derived from EECl by adding 3 yr to represent the lag associated with mixing air from the troposphere to the middle stratosphere (updated from Montzka et al. 2003a,b). [Courtesy: S. A. Montzka, J. H. Butler, T. Thompson, D. Mondeel, and J. W. Elkins, NOAA/CMDL]

Increases in HCFCs have slowed notably in recent years. By mid-2005, the Cl in the three most abundant HCFCs amounted to 217 ppt, or 8.0% of all Cl carried by long-lived halocarbons. Mixing ratios of HFC-134a, the most abundant HFC in the global background atmosphere, increased nonlinearly in the 1990s. From 2001 through 2005, however, it has increased in the global troposphere at a fairly constant linear rate of 4.2 ppt yr^{-1}. Concern over increases in HFCs is largely due to their efficiency as absorbers of infrared radiation.

The influence of these disparate trends on future levels of stratospheric ozone can be gauged roughly from a sum of Cl and bromine (Br) in long-lived halocarbons, provided the enhanced efficiency for Br to destroy ozone is considered. This sum is expressed as effective equivalent chlorine (EECl; Fig. 2.19e), and is derived from surface-based measurements. EECl provides an estimate of the O_3-depleting power of the atmosphere a few years in the future, when air at Earth's surface will have become mixed into the stratosphere.

Observations indicate that the EECl content of the lower atmosphere has declined at a mean rate of 26 ppt yr^{-1} since its peak in 1994. Scenarios projecting future halocarbon mixing ratios have been derived elsewhere based upon full compliance with the fully amended and revised Montreal Protocol and our understanding of atmospheric lifetimes of these gases (Montzka et al. 2003b). These analyses suggest that it will take 40–50 years for EECl to decline to the levels present in 1980, before O_3 depletion was first observed. This 1980 level is notable, given that one might expect nearly full recovery of stratospheric ozone once the atmospheric EECl returns to this level. The time frame for O_3 recovery will depend upon other factors as well, such as stratospheric temperatures and atmospheric aerosol loading. Nonetheless, the declines in EECl from 1994 to the present time represent a significant drop in the atmospheric EECl burden. As of 2005, EECl had declined 20% of the way back to the 1980 level (Fig. 2.19f).

Changes in the direct radiative influence of long-lived halocarbons can be estimated from observed changes in atmospheric mixing ratios with knowledge of trace-gas radiative efficiencies. Such an analysis suggests that the direct radiative forcing of these gases was still increasing in 2005, though at a much slower rate than observed from 1970 to 1990.

3. GLOBAL OCEANS—J. M. Levy[47] and K. A. Shein[82], Eds.

a. Overview—K. A. Shein[82]

Recent decades have seen a marked increase in our knowledge of the coupled ocean–atmosphere system, although as is discussed, it is only through a number of relatively new or planned ocean-monitoring ac-

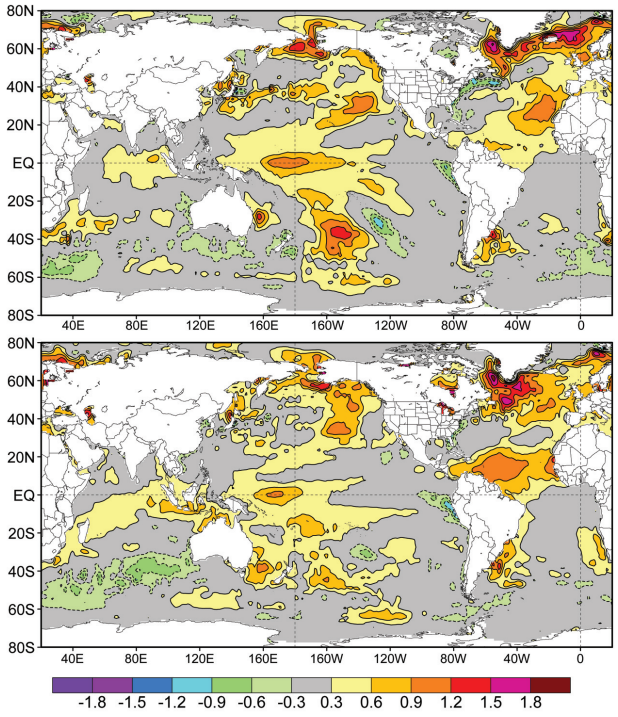

Fig. 3.1. Annual SST anomalies (°C) for (top) 2004 and (bottom) 2005, computed relative to a 1971–2000 base period.

tivities that our understanding of these interactions, such as the role of the oceans in the anomalously active 2005 Atlantic tropical storm season, can be improved. Notable characteristics of the oceans in 2005 included above-normal sea surface temperatures, and heat losses that were generally below normal over the global basins. Globally, ocean circulation was near to slightly stronger than normal in 2005, and average sea levels continued their rise for another year. Also, there is preliminary information that anthropogenic carbon inventories may be increasing in the Pacific at about twice the rate of the Atlantic.

b. Temperature

1) SSTs—R. W. Reynolds[69]

Annually averaged SSTs for both 2004 and 2005 (Fig. 3.1) are derived from monthly fields interpolated from the Reynolds et al. (2002) weekly optimum interpolation (OI) analyses. The analysis uses ship and buoy in situ SST data as well as satellite SST retrievals from the infrared (IR) AVHRR and anomalies are departures from the 1971–2002 base period mean (Xue et al. 2003).

The impression is that the anomalies are primarily positive, and are part of the overall warming trend of global SSTs since 1971. Comparisons of the two years show two important changes: the first in middle latitudes (40°–66°N) and the second in the tropical North Atlantic (0°–30°N). In the midlatitude regions, there is a tendency for the positive anomalies to increase from 2004 to 2005 in the eastern Pacific and western Atlantic. Both regions show an overall warm anomaly for the period of 1995–2005, although variability in the Pacific is less than the Atlantic. There is also evidence of regular summer warming in the Pacific region from 2000 to 2005. This signal is only clearly evident in the Atlantic region in 2003, and is the oceanic response to that summer's European heat wave.

During 2005, there was a record number of strong Atlantic hurricanes. There has been discussion regarding whether changes in SSTs can imply statistically significant changes in hurricanes (Webster et al. 2005) or not (Trenberth 2005), but all of the reports state that SSTs are not the only variable affecting hurricanes. Because of the changes in the northern tropical Atlantic SSTs from 2004 to 2005, time series are shown for the North Atlantic (10°–30°N) and Gulf of Mexico (Fig. 3.2). The tropical Atlantic region shows overall warm anomalies with irregular variability on 2- to 5-yr periods, which does not strongly correlate with the seasonal cycle or ENSO. However, a relatively strong maximum anomaly occurs in the summer of 2005. The time series from the Gulf of Mexico appears to be noisier without any noticeable signal. Goldenberg et al. (2001) state that local SSTs greater than 26.5°C are needed to generate

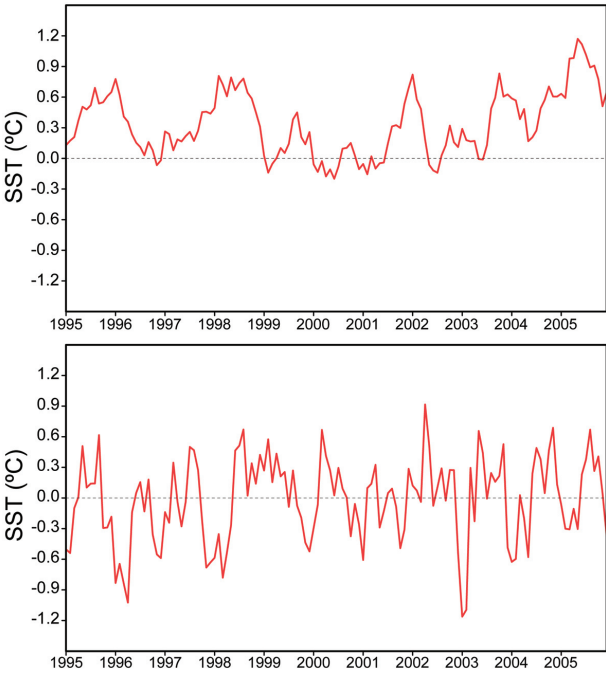

Fig. 3.2. Time series (January 1995–December 2005) of monthly SST anomalies (°C) for the (top) tropical North Atlantic and (bottom) the Gulf of Mexico.

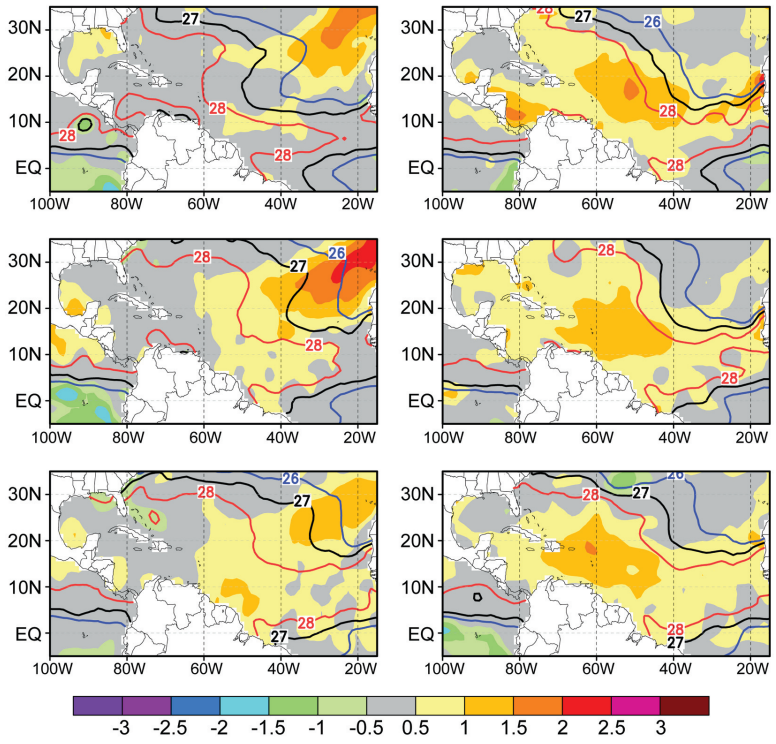

FIG. 3.3. Tropical monthly SST anomalies (°C) for July, August, and September (left) 2004 and (right) 2005. Contours show the corresponding monthly total (anomaly + climatology) SST isotherms for 26°, 27°, and 28°C.

hurricanes. A closer examination of the 2004 and 2005 tropical Atlantic anomalies shows that areas exceeding 26.5°C are similar in the corresponding months for 2004 and 2005 (Fig. 3.3). However, the areal extent of SST greater than 28°C is larger in July and August 2005 than in July and August 2004.

II) HEAT CONTENT—G. C. Johnson,[35] J. M. Lyman,[49] and J. K. Willis[93]

Ocean storage and transport of heat and freshwater, and their variations, are intrinsict to many aspects of climate, including El Niño, the North Atlantic Oscillation (NAO), the global water cycle, hurricane seasons, and global change (e.g., Levitus et al. 2005; Hansen et al. 2005). Regional studies of decadal freshwater variability are possible in well-sampled regions like the North Atlantic (e.g., Curry and Mauritzen 2005), but in situ ocean salinity data are too sparse and their reporting is too delayed for a global 2005 perspective of ocean freshwater storage. However, the rapidly maturing Argo Project array of profiling floats measuring temperature and salinity (Roemmich et al. 2004) is remedying this situation.

Here we discuss an estimate of the upper-ocean (0–750 m) heat content anomaly (OHCA) for 2005 produced by combining in situ ocean temperature data and real-time satellite altimetry data collected from 1 January to 31 October 2005 following the techniques of Willis et al. (2004). The 2005 combined OHCA map when compared to a 1993–2002 baseline (Fig. 3.4, top) shows eddy and meander variability down to 100-km mapping scales. There is a great deal of small-scale spatial variability associated with the western boundary currents in every gyre, as well as the Antarctic Circumpolar Current.

Large-scale patterns are also evident in the OHCA. The combined OHCA map for 2005 is high in the subpolar North Atlantic and low in the subtropical North Atlantic, consistent with a decreased strength of the North Atlantic Current. This pattern is probably related to decadal changes in the NAO index (e.g., Curry and McCartney 2001). The NAO index was lower in 2005 than during the baseline period, and has generally trended lower from 1993 through 2005. For the most part, the Tropics in 2005 have only slightly higher OHCA than average, reflecting the lack of a pronounced El Niño or La Niña in 2005. In 2005, OHCA is high throughout the South Pacific and South Atlantic Oceans in a belt located north of the Antarctic Circumpolar Current. This change may be related to changes in the wind-stress field associated with an increase in the Antarctic Oscillation.

The difference in combined OHCA maps between 2005 and 2004 (Fig. 3.4, bottom) illustrates the large year-to-year variability in ocean heat storage, with changes reaching or exceeding the equivalent of an 80 W m^{-2} surface flux. Ocean advection likely plays a large role in many of these changes. Such differences between the two years clearly show the influence of eddies and meanders, but there are also contributions from some of the aforementioned larger-scale patterns in the subtropics and subpolar regions. The decrease of OHCA in the central equatorial Pacific between 2005 and 2004 probably reflects the transition from weak El Niño to more normal conditions. Finally, given the strong 2005 hurricane season and the potential link between hurricane intensity and warm ocean waters (e.g., Emanuel 2005), the large increases in OHCA around Florida and the Gulf of Mexico are also of interest.

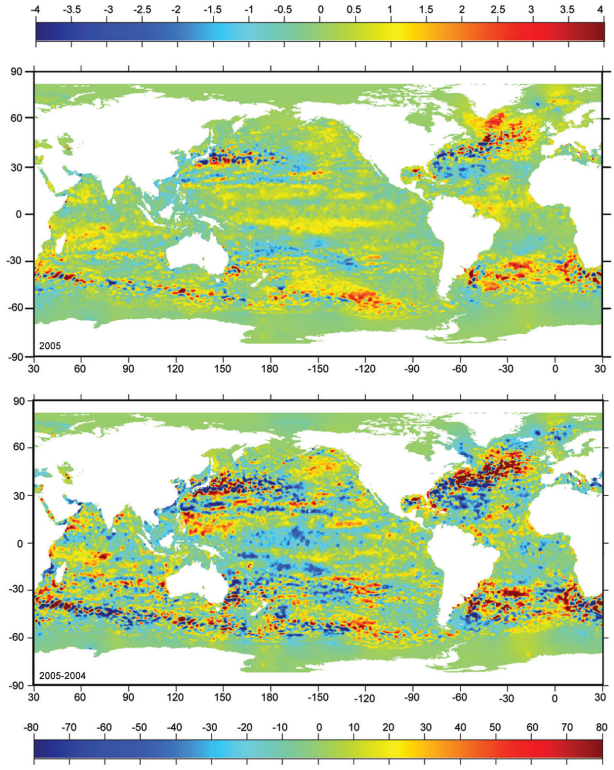

Fig. 3.4. Combined satellite altimeter and in situ ocean temperature data upper-ocean (0–750 m) heat content anomaly (OHCA) (J m^{-2}) map for (top) 2005 relative to a 1993–2002 base period, following Willis et al. (2004), and (bottom) the difference between 2005 and 2004 OHCA maps expressed as a surface heat flux equivalent (W m^{-2}).

iii) Heat fluxes—L. Yu[96] and R. A. Weller[91]

The oceanic latent heat flux (LHF) is heat energy extracted from the ocean by the evaporation of surface water, and sensible heat flux (SHF) is heat energy transferred by conduction and convection at the air–sea interface. These two fluxes vary with near–sea surface circulation, humidity, and temperature, and influence weather and climate processes. The global change of the two fluxes in 2005 is examined here using daily analyzed fields produced by the Objectively Analyzed Air–Sea Fluxes (OAFlux) project. The resulting flux fields were validated against more than 100 flux buoy measurements acquired by the Woods Hole Oceanographic Institution (WHOI) Upper Ocean Processes group (Moyer and Weller 1997) and by the Pilot Research Moored Array in the Tropical Atlantic (PIRATA) and Tropical Atmosphere Ocean/Triangle Trans-Ocean Buoy Network (TAO/TRITON) moored buoy arrays in the tropical Atlantic and the equatorial Pacific Oceans (Yu et al. 2004).

The 2005 annual mean field of LHF plus SHF over the global oceans (Fig.3.5, top) shows that large oceanic latent and sensible heat losses occurred over the regions associated with three major Western Boundary Currents (WBCs): the Kuroshio, Gulf Stream, and African Agulhas Currents. In these regions near-surface vertical gradients of humidity and temperature are largest and the wind speeds are greatest in the respective hemisphere's fall and winter seasons, and the cold season variability of LHF plus SHF dominates the annual mean pattern. On a year-to-year basis, variability of the oceanic heat losses in the three WBC regions is also largest, with magnitudes reaching or exceeding 40 W m^{-2}. This is clearly shown from the difference map of the 2004 and 2005 annual mean LHF plus SHF (Fig. 3.5, bottom). Interestingly, the signs of the anomalies associated with different WBC systems are different. For example, the total oceanic heat loss was enhanced (large positive anomalies) from 2004 to 2005 over the Kuroshio region, but reduced (large negative anomalies) over the Gulf Stream region.

Influence of eddy-scale structures is evident in the 2-yr difference map (Fig. 3.4, bottom). Nevertheless, the change in the LHF plus SHF field from 2004 to 2005 is large scale—the anomalies are primarily negative over the global basins, suggesting that the oceanic heat loss was overall reduced in 2005 (Fig. 3.6, top). A persistent, long-term increase in the globally averaged annual mean LHF plus SHF is particularly notable, although that trend appears to have decreased in recent years. It is not clear yet

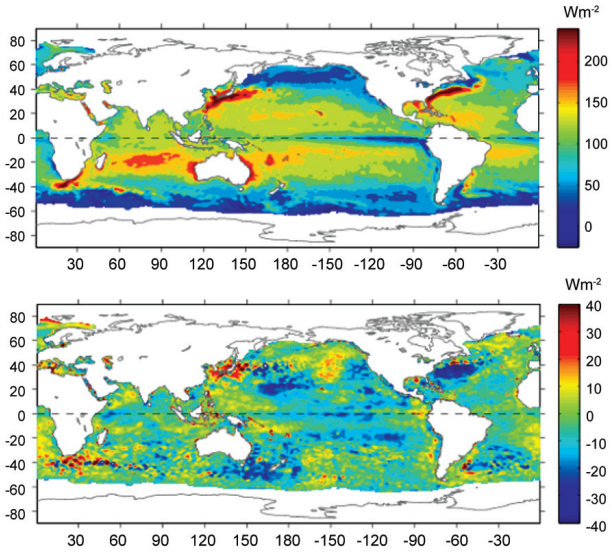

Fig. 3.5. (top) Annual mean latent plus sensible heat fluxes (W m^{-2}) in 2005. Sign is defined as upward (downward) positive (negative). (bottom) Differences between 2004 and 2005 annual mean latent plus sensible heat fluxes.

whether or not the reduction in oceanic heat loss for 2005 is a trend change, or merely a short-term anomaly. Additionally, the globally averaged LHF plus SHF has increased by about 10 W m^{-2} in the past 20 yr, and the magnitude of the variability is dominated by that of the LHF. The mean SHF value is about one order smaller than that of LHF, and the change in SHF is also small (< 2 W m^{-2}) over the entire analysis period.

Areal averages of LHF plus SHF variability in the Kuroshio and Gulf Stream regions clearly show a large upward trend in both (Fig. 3.6, bottom). However, unlike the global averages, the regional averages show strong interannual fluctuations. Whereas the upward trend in global averages begins in 1981 (start of the analysis record) and has flattened in recent years, the boundary current regional averages show a trend toward larger values only starting in the early 1990s but remaining positive to the present. Furthermore, the slope of the trend in these two regions is twice as great as that of the global averages. Overall, the regional oceanic heat loss has been enhanced by about 20 W m^{-2} over the past two decades.

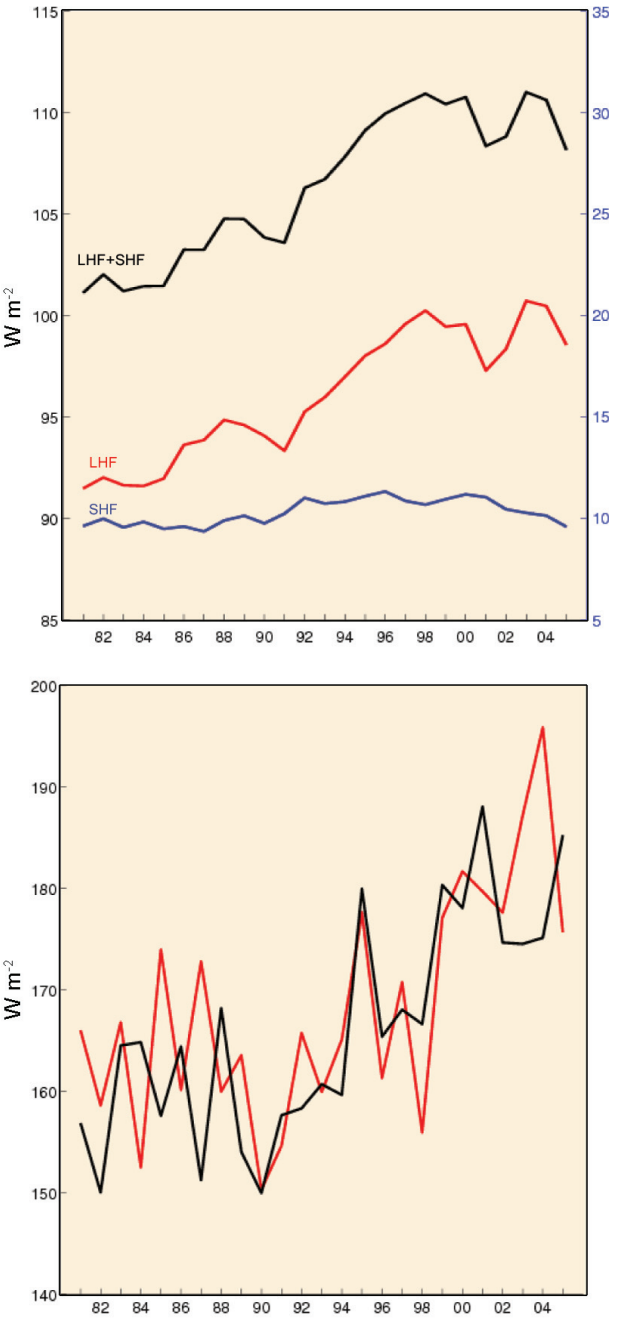

Fig. 3.6. (top) Year-to-year variations of globally averaged annual mean latent heat flux (red), sensible heat flux (blue), and latent plus sensible heat flux (black). (bottom) Year-to-year variations of the annual mean latent heat plus sensible heat fluxes averaged over the regions of the Gulf Stream [(25°–45°N, 85°–50°W), red] and Kuroshio [(20°–40°N, 120°–150°E), black].

c. *Circulation*

1) Surface currents—R. Lumpkin[48] and G. Goni[30]

Near-surface currents are measured in situ by satellite-tracked drifting buoys and by acoustic point-measuring meters on the Autonomous Temperature Line Acquisition System (ATLAS) moorings. In 2005, the drifter array reached its target goal of 1250 drifters worldwide, becoming the first fully realized component of the Global Ocean Observing System. During 2005, surface currents were well sampled globally, except in the far northern Pacific, the southwest Pacific between 20° and 40°S, 150°E to the date line, the Arabian Basin of the Indian Ocean, and the extreme Southern Ocean south of 55°S.

A climatology of monthly mean currents was computed from all available drifter observations from 1994 to 2004, using the methodology of Lumpkin and Garraffo (2005). Anomalous currents were calculated with respect to this climatology (Fig. 3.7).

(i) Indo-Pacific basins

Annual mean anomalies were most prominent in the tropical Pacific Ocean (Fig. 3.7). Westward anomalies of nearly 20 cm s^{-1} were observed on the equator between 120°W and the date line. Weaker anomalies of 5–10 cm s^{-1} were seen in the North Equatorial Current (NEC) region (10°–20°N). Drifter observations did not indicate anomalously strong eastward currents in the Kuroshio Extension or North Pacific Current, conflicting with the simple hypothesis of a more-intense-than-average wind-driven gyre.

The strongest intraseasonal anomalies were observed in early 2005 in the western and central tropical Pacific, associated with Kelvin wave activity driven by

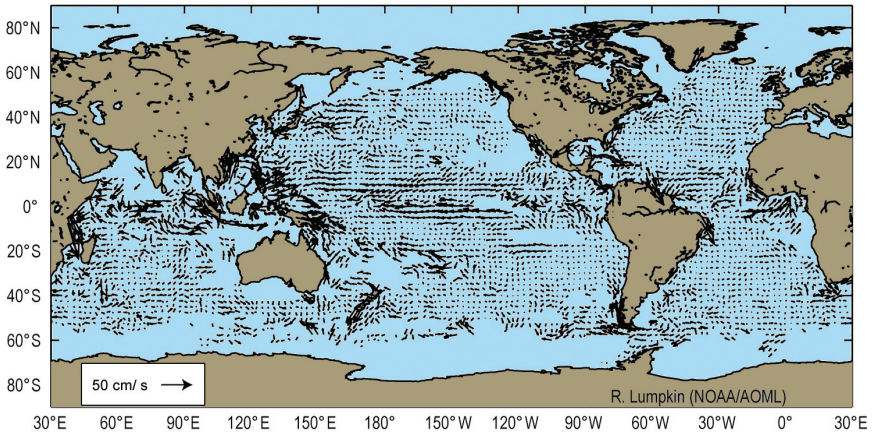

Fig. 3.7. 2005 mean anomalies (cm s^{-1}) from 1994–2004 surface current climatology.

intraseasonal (MJO) wind fluctuations (cf. Eisenman et al. 2005). In January (Fig. 3.8), very strong westward anomalies were measured in the northern branch of the South Equatorial Current (nSEC). The nSEC at 0°–5°S, 160°W–170°E was 80–100 cm s^{-1} westward, compared to a mean January speed of 40–60 cm s^{-1}. During February, a dramatic reversal was seen at 6°–12°S, 155°W–180° where several drifters moved eastward at 50–100 cm s^{-1}. Drifters suggested the passage of a second Kelvin wave in March and April, when strong westward, then eastward, anomalies were seen west of the date line (Fig. 3.8). This was corroborated by observations at the TAO mooring at 0°, 170°W. The previously noted NEC anomalies were first observed in February. Westward anomalies in the South Equatorial Current (SEC) at 0°–6°S appeared in April. Both the NEC and SEC continued to flow anomalously quickly through the remainder of the year.

(ii) Atlantic Basin

The North Atlantic subtropical gyre, benchmarked by transport through the the Florida Straits and Yucatan Channel, was close to its decadal mean strength during 2005. The Western Boundary Current transport through the Florida Straits, measured by cable voltage, averaged 31.4 ±1.2 Sv (1 Sv is 10^6 m^3 s^{-1}) during 2005 (C. Meinen 2006, personal communication), not significantly different from the 1982–2005 mean of 32.1 Sv. Transport through the Yucatan Channel, estimated from altimetric sea level anomaly variations calibrated by in situ transects, indicated a transport within 1 Sv of the long-term mean. In the North Equatorial Current region (5°–15°N, 30°–50°W), westward anomalies of 10 cm s^{-1} were observed. Drifter deployments during recent French research cruises seeded the Gulf of Guinea region heavily for the first time, and anomalies here were large, but may reflect a poorly defined climatology for the period of 1994–2004. Thus, it is difficult to tell from these data what role anomalous advection may have played in the development of the unusually large cold tongue during 2005.

(iii) Southern Ocean

Drifters did not reveal large-scale anomalies in the strength of the Antarctic Circumpolar Current (Fig. 3.7). From August to December, 18 drifters passed south of Cape Horn. These drifters indicated that the flow entering the Drake Passage was 8 ±9 cm s^{-1}, much weaker than the mean speed of 23 ±11 cm s^{-1} here. This anomaly was most prominent during August–September. Four drifters passed through the region during February–May, measuring speeds of 27 ±14 cm s^{-1}

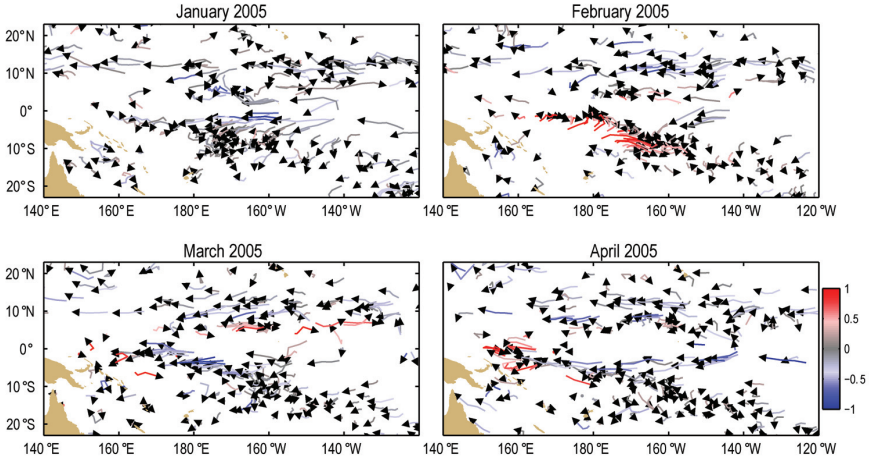

Fig. 3.8. January–April 2005 drifter trajectories in the tropical Pacific. Arrowheads indicate direction; color indicates zonal speed anomaly (m s^{-1}, positive eastward).

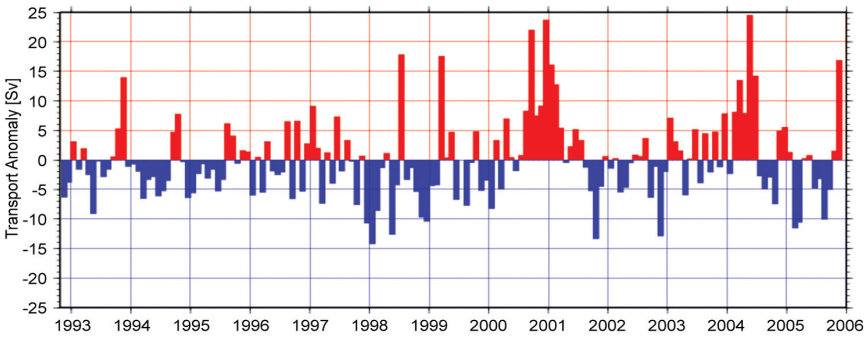

FIG. 3.9. Monthly geostrophic transport anomalies (Sv) of the Agulhas Current at 28°W derived from satellite altimetry observations.

(very close to normal). Altimetric estimates of geostrophic transports suggest that the 2005 annual mean of the geostrophic transport remained slightly lower than its historical value, and significantly lower (5–10 Sv) than during 2004 (Fig. 3.9).

ii) THERMOHALINE CIRCULATION—M. O. Baringer[4] and C. S. Meinen[54]

The component of the ocean circulation associated most with variability in heat redistribution is the meridional overturning circulation (MOC), also called the thermohaline circulation. The MOC is a global circulation cell wherein high-latitude surface waters are cooled and become denser, and in certain locations this dense water sinks and flows toward the Tropics. In tropical and subtropical regions around the world these waters warm, become less dense, and return to the surface to flow back toward higher latitudes, while transporting a significant amount of heat. The primary locations where deep convection occurs are in the northern North Atlantic and in the subpolar ocean around Antarctica, while the upwelling of new surface waters is spread broadly around the globe.

Variations in the strength of the overturning circulations are directly related to variations in net poleward heat transport. Current best estimates for the steady-state global mass and heat transport can be found in the analyses of Ganachaud and Wunsch (2003; see also Talley 2003). For example, the North Pacific overturning cell carries about 0.5 PW northward, but most of this heat transport is associated with water mass transformations in the upper layers of the ocean, while the North Atlantic carries a much larger transport of 1.2 PW northward, most of which is carried in the top-to-bottom MOC system. Typically, it is this deep circulation cell that is described as the MOC, although other oceans and water masses are important for the redistribution of heat.

The Florida Current contains most of the upper limb of the MOC as it flows through the Florida Straits in the North Atlantic, with a smaller contribution being carried by the Antilles Current east of the Bahamas. Fluctuations in the Florida Current have shown a clear negative correlation with the atmospheric phenomenon known as the NAO, however while the NAO has been trending toward its negative extreme over the past 20 yr, the Florida Current transport shows no such long-term trend through 2005 (Fig. 3.10). The annual mean transport observed in 2005 (31.4 Sv) falls just within the lowest quartile of historical annual mean transports from the cable. However, this transport is well within 1 std dev of the long-term mean of 32.1 Sv, and given the statistical standard error (1 Sv) of the mean for the year, 2005 cannot be considered anomalous in terms of the Florida Current transport.

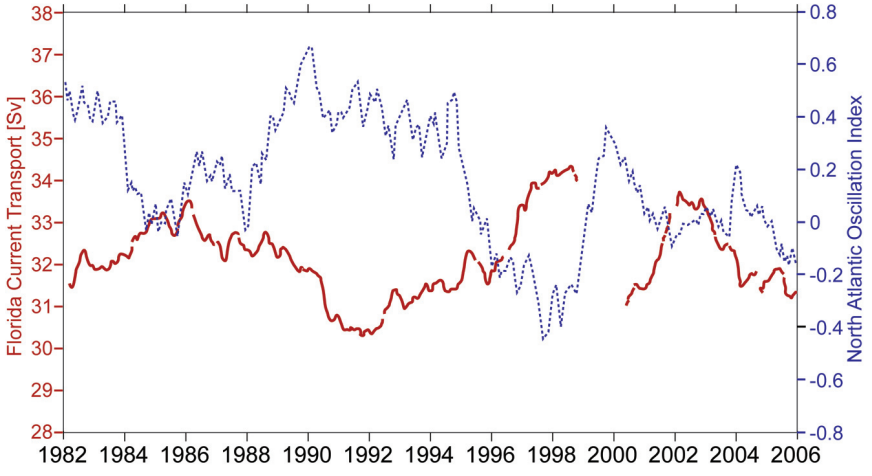

FIG. 3.10. Florida Current transport (Sv; red solid) as measured by the NOAA-funded submarine cable across the Florida Straits, along with the NAO index (blue dashed) produced by NOAA/NCEP.

In the near future, a new NOAA-funded system for monitoring the Deep Western Boundary Current coupled with a new international program for monitoring the basin-wide circulation [Meridional Overturning Circulation Heat-Transport and Heat Flux Array (MOCHA)] will allow for a greater degree of certainty in statements regarding variations in the integrated, basin-wide MOC circulations and the time scales on which they vary. Bryden et al. (2005), postulated a 30% reduction in the MOC transport between the 1950s and the present day; however, that analysis was based on a very limited dataset. Other data over the past few decades, such as the moored observations of the Deep Western Boundary Current at the southeast Newfoundland Rise in the early 1990s and early 2000s showed no indication of such a significant trend in the MOC (F. Schott 2005, personal communication). In contrast, Koltermann et al. (1999) showed the large variability of the MOC that they concluded was related to the strength of Labrador Sea Water production with larger (smaller) MOC transport corresponding to less (more) Labrador Sea Water export. More recently, these data have been reanalyzed to formally test the hypothesis that the MOC circulation was steady. Lumpkin et al. (2006, manuscript submitted to *J. Mar. Res.*) found that a steady MOC over the same time period could not be ruled out, based on the uncertainty in determining the barotropic circulation. Also, if Bryden et al. (2005) are correct in that the thermohaline circulation has been reduced over the past 50 yr by 30%, this represents a much higher rate of change than that predicted in coupled climate model simulations (e.g., Schmittner et al. 2005).

Changes in heat transport on the order of 30%, such as that postulated by Bryden et al. (2005), could have substantial impacts on climate, and time series observations are clearly necessary in order to put one-time hydrographic sections in temporal context. The programs in place in 2005 are an excellent first step toward the development of an integrated measurement system, including repeated hydrographic sections and moored observations that can play a significant role in measuring and monitoring the MOC system over a broader range of locations than would be feasible with moored instrumentation alone. However, much work remains before it will be possible to state that the Atlantic MOC system, much less the global overturning circulation system, is truly being monitored.

d. Sea level—M. A. Merrifield,[56] S. Gill,[26] and G. T. Mitchum[57]

Data on sea level were obtained from both tide gauges and satellite altimetry [Ocean Topography Experiment (TOPEX)/Poseidon/Jason]. Tide gauges have long observed sea level, and these instruments still provide the long-term context for understanding climate variations. Since 1992, however, satellite altimetry has provided global views of the sea surface height field. Sea level anomalies in 2005 were computed relative to 1993–2001 mean values (Fig. 3.11). Coastal and island sea level deviations, as measured by tide gauges, were generally consistent with the deep ocean patterns measured by satellite altimeters. A notable exception was the east coast of North America, where coastal tide gauge sea levels were higher than normal, whereas nearby ocean values from altimetry were lower than normal.

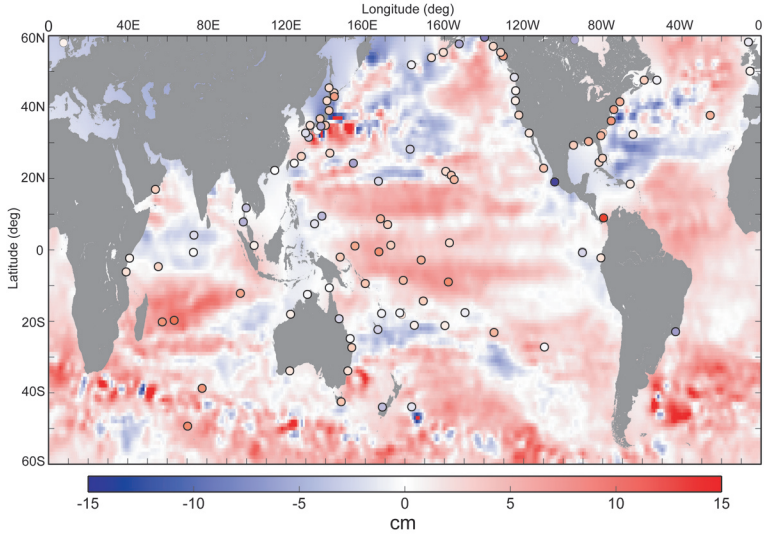

Fig. 3.11. Deviation of 2005 annual average sea level (cm) from 1993 to 2001 mean, as measured by (colored shading) satellite altimeter and (filled circles) tide gauges. [Source: University of Hawaii Sea Level Center]

The deviations shown in Fig. 3.11 were above average over most of the global ocean. Since at least 1993 (the time span of TOPEX/Poseidon/Jason altimeter measurements) global sea levels have been rising at a linear rate of 2.9 ± 0.4 mm yr^{-1} (Leuliette et al. 2004; Cazenave and Nerem 2004; see also information online at http://sealevel.colorado.edu/). The general increase in globally averaged sea level during 2005 was consistent with this longer trend. At any particular point, however, the rate of sea level change can be very different from the globally aver-

aged rate. A notable example is along the coasts of North America, where sea level has fallen in recent years. In the North Pacific, this is presumably associated with a trend in equatorward winds near the coast, which favor upwelling. Recent sea level trends appear to be determined by the polarity of the Pacific Decadal Oscillation (Mantua et al. 1997; Cummins et al. 2005; see information online at http://tao.atmos.washington.edu/pdo/), and it seems likely that the North Pacific sea level trend pattern will reverse sign, resulting in rising sea levels near the North American coast.

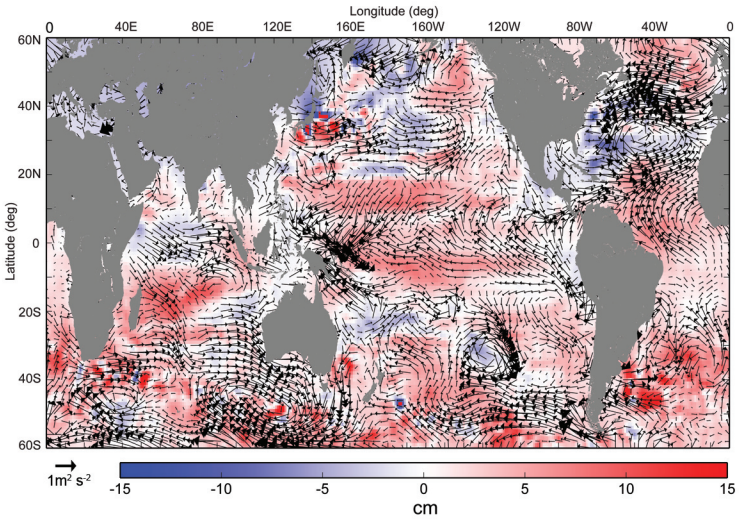

Fig. 3.12. Same as Fig. 3.11, excluding tide gauge deviations, and including the 2005 deviation of surface winds (m^2 s^{-2}). [Source:NCEP]

Other regional patterns also are evident. In general, levels were higher than average in the Tropics and the Southern Hemisphere. Regions of lower-than-average sea level occurred in the midlatitude North Atlantic, the North Pacific, the tropical Indian Ocean, and off the east and west coasts of Australia. In many instances, the sea level deviations can be linked directly to anomalous surface winds (Fig. 3.12). A striking example is a cyclonic wind anomaly centered over the North Atlantic. This anomaly corresponds to a weakening of the Bermuda high, and possibly to a corresponding weakening of the subtropical oceanic gyre. This would account for the aforementioned lowered sea level in the open ocean, and the higher-than-average tide gauge sea levels along the North American coast.

Relative to the previous year, 2005 saw a noticeable increase in sea level in the region of the western tropical Pacific north of the equator and east of the Philippines. This pattern developed in response to the increased local anticyclonic wind forcing in 2005 relative to 2004. Otherwise, sea level changes in the tropical oceans were generally weak, consistent with the relatively weak ENSO variability experienced in 2005 (see section 4b).

In addition to these large-scale, low-frequency patterns, extreme sea levels were also examined. NOAA has developed a new exceedance probability product from long-term tide station records using a generalized extreme value analysis approach (Zervas et al. 2005). The remarkably active hurricane season of 2005, in terms of number and severity of storms, produced unusually extreme water levels on the east and Gulf coasts of the United States. The eastern Pacific was also subject to extreme water levels associated with several tropical cyclones (see section 4c).

e. *Ocean carbon*—C. L. Sabine,[79] R. A. Feely,[22] and R. Wanninkhof[88]

The paucity of carbon measurements in the ocean currently impedes our ability to generate annual assessments of global anomalies. However, our understanding of the global ocean carbon cycle has greatly improved over the last decade based on accumulated data and modeling activities. Our best estimates of the current distributions of natural and anthropogenic carbon in the ocean stem from the collaborative efforts of two international programs—the World Ocean Circulation Experiment (WOCE) and the Joint Global Ocean Flux Study (JGOFS)—to conduct an extensive survey of the chemical and physical properties of the global ocean in the 1990s (Feely et al. 2001; Wallace 2001). An analysis of more than 70,000 carbon measurements from this survey found that the ocean accumulated approximately 118 Pg of carbon between 1800 and 1994 (Sabine et al. 2004). This accumulation accounts for 48% of the CO_2 released from fossil fuel combustion over this same time period.

Because there were no ocean carbon measurements prior to the mid-1800s, the anthropogenic CO_2 component of the total dissolved inorganic carbon (DIC) concentration was estimated using a back-calculation technique based the on current understanding of the physical and biological contributions to the measured DIC (Gruber et al. 1996; Sabine et al. 2004). As a consequence, it is implicitly assumed that the ocean circulation and biological processes were in steady state over the industrial era. Although this work provided our best assessment of the state of the

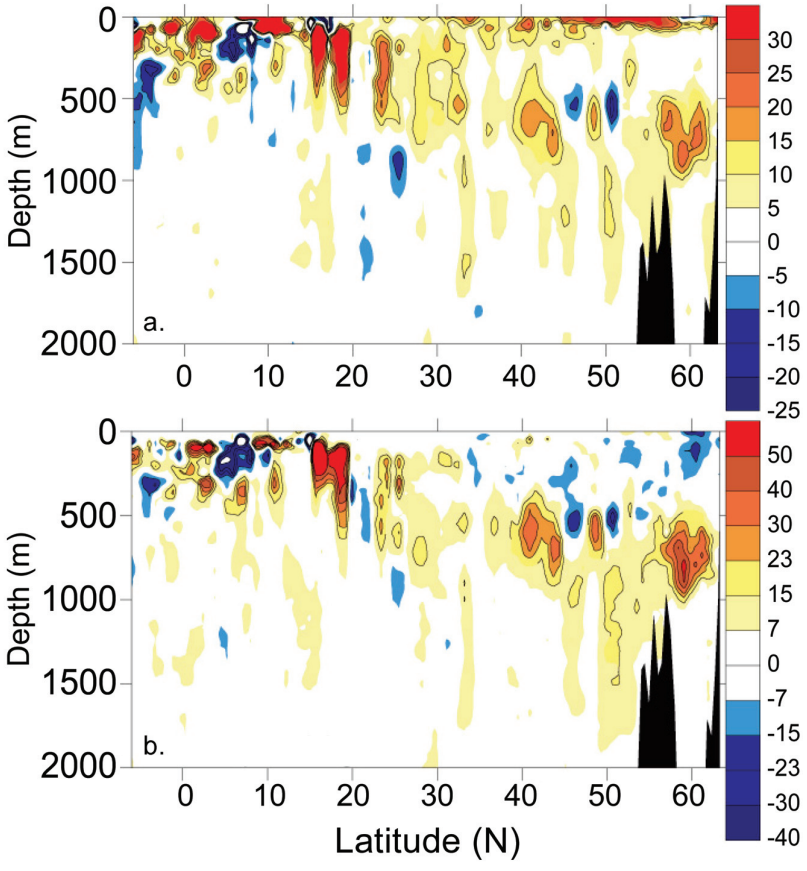

Fig. 3.13. Changes in (a) DIC (μmol kg^{-1}) and (b) AOU (μmol kg^{-1}) in the upper 2000 m between the 2003 and the 1993 occupations of A16N. Positive values are an increase in concentrations between 1993 and 2003 (modified from Feely et al. 2005).

ocean in the mid-1990s, these studies are unable to establish temporal and spatial scales of variability, or the temporal evolution of the ocean carbon cycle.

To address questions of decadal variability and temporal evolution, the U.S. Climate Variability and Predictability (CLIVAR) CO_2 Repeat Hydrography Program has identified 19 hydrographic sections distributed around the global ocean that will be re-occupied every 5–10 years. The program began in 2003 with three cruises in the North Atlantic that were repeats of cruises in the 1990s. Each year one to three cruises are run in different locations with a goal of completing the first global resurvey by 2012. In 2005, cruises were run in the South Atlantic and South Pacific Oceans, but these data will take several years to finalize and thoroughly examine.

Analysis of the initial repeat lines over this past year has indicated that several biogeochemical parameters are changing with time (Feely et al. 2005). For example, changes of –10 to +30 μmol kg^{-1} of DIC have been observed in the upper 1000 m of the water column between the 1993 and 2003 occupations of a track designated as A16N along 25°W in the North Atlantic (Fig. 3.13a). Although the magnitude of the changes is not surprising, the patchiness of the changes was not expected. More surprising is the fact that there have been similar changes in the apparent oxygen utilization (AOU) of the waters (a measure of the decomposition of organic matter in the ocean), indicating significant changes in the organic matter cycling over the last decade that was previously believed to be in steady state (Fig. 3.13b). The complicated patterns of these changes clearly show that carbon is being influenced by more than simple secular increases in atmospheric CO_2. In some cases changes in circulation and organic matter cycling may be masking anthropogenic changes, and in other cases these changes may enhance the apparent ocean carbon uptake.

Another intriguing preliminary finding from a comparison of a 2004 cruise in the North Pacific to the aforementioned North Atlantic results is that anthropogenic carbon inventories may be increasing in the Pacific at about twice the rate of the Atlantic over the last 10 years (Feely et al. 2005). This is in contrast to the long-term anthropogenic CO_2 inventory that shows larger column inventories in the North Atlantic. The interpretation of these recent findings may lie in understanding the effects of climate modes like the NAO or the Pacific Decadal Oscillation (PDO) on the decadal-scale circulation. These results also point to the need for improved approaches for isolating the anthropogenic and natural components of the observed variability.

4. THE TROPICS—H. J. Diamond[19] and K. A. Shein,[82] Eds.

a. Overview—H. J. Diamond[19]

This Tropics section consists of global input on two primary topics: 1) ENSO and the tropical Pacific, including ENSO seasonal variability, and 2) tropical cyclone activity for the 2005 season in the following seven basins: the Atlantic, northeast Pacific, northwest Pacific, North and South Indian,

southwest Pacific, and Australia. The Pacific ITCZ also is discussed.

Persistent anomalous rainfall that characterizes mature warm-phase ENSO conditions failed to develop near the date line, except in February 2005. The relative absence of such convection indicated that the ocean and atmosphere were only weakly coupled during this event. It should be noted that although conditions in the Pacific met the definition for El Niño according to the criterion recently formulated by the NOAA/National Centers for Environmental Prediction (NCEP), namely, five consecutive overlapping 3-month seasons with Niño-3.4 SST anomaly ≥ 0.5°C, this definition is not universally agreed upon, either because it is focused on a single region or defined only in terms of SST. Regarding tropical cyclone activity, while the 2005 season was unprecedented in the Atlantic, setting numerous records, other basins were characterized by near- to below-normal levels of activity. Two sidebars expand upon the record Atlantic basin tropical storm season.

b. El Niño–Southern Oscillation—G. D. Bell,[5] M. S. Halpert,[32] and M. J. McPhaden[53]

i) Overview

Conditions throughout the tropical Pacific during 2005 reflected a weak warm episode that ended in March, followed by the development of below-average SSTs during November and December (Fig. 4.1a). Intraseasonal variability often associated with the MJO also was present. The weak Pacific warm episode early in the year was accompanied by anomalously warm waters at approximately 110–130-m depths across most of the equatorial Pacific (Fig. 4.1b). Subsurface temperatures returned toward normal during April, before cooling during the following months.

The weak warm episode did not show a strong relationship to the 850-hPa zonal wind anomalies, which featured an oscillating pattern indicative of the MJO (Fig. 4.1c). However, a well-defined strengthening of the equatorial easterlies did accompany the transition to below-average SSTs during November and December. These enhanced easterlies also contributed to increased equatorial upwelling and a shoaling of the oceanic thermocline.

There was generally minor reflection of the anomalously warm SSTs in the pattern of deep convection over the central and east-central equatorial Pacific early in the year, as indicated by OLR anomalies (Fig. 4.1d). An El Niño signal was only evident during February, when convection was enhanced over the central equatorial Pacific (negative OLR anomalies) and suppressed across Indonesia early in the year.

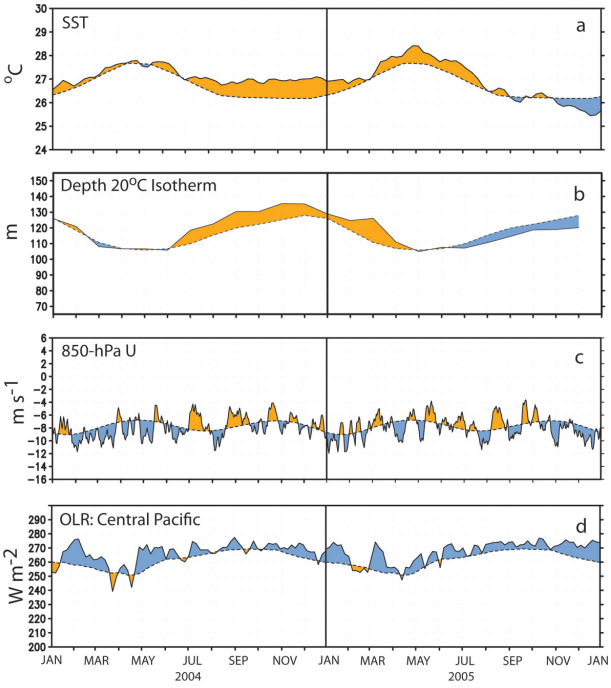

Fig. 4.1. Monthly time series of (a) SST (°C), (b) depth of the 20°C isotherm (m), (c) 850-hPa zonal wind speed (m s^{-1}), and (d) OLR (W m^{-2}) over the central equatorial Pacific. Values were averaged over the region bounded by 5°N–5°S and 180°–100°W. Five-day (solid line) and climatological (1979–95; dashed line) mean values are shown, as are positive (orange) and negative (blue) anomalies (except for OLR, where shading convention is reversed) relative to a 1979–95 base period.

This pattern impacted circulation over the Southern Hemisphere, likely resulting in the observed drop in rainfall across southern Africa during the heart of their rainy season.

Convection was slightly suppressed across the central equatorial Pacific for much of the year, and positive OLR anomalies became increasingly pronounced during November and December as the equatorial easterlies strengthened and SSTs dropped.

ii) The Madden–Julian oscillation, Kelvin wave activity, and atmospheric circulation

Low-frequency variability in the Tropics is strongly influenced by the MJO (Madden and Julian 1971, 1972, 1994), a tropical disturbance that modulates tropical convection and atmospheric circulation patterns with a typical period of 30–60 days. The MJO tends to be most active during ENSO-neutral years, and can produce ENSO-like anomalies (Mo and Kousky 1993; Kousky and Kayano 1994). Low-level (850 hPa) and upper-level (200 hPa) equatorial zonal winds and streamfunction, 200-hPa velocity potential

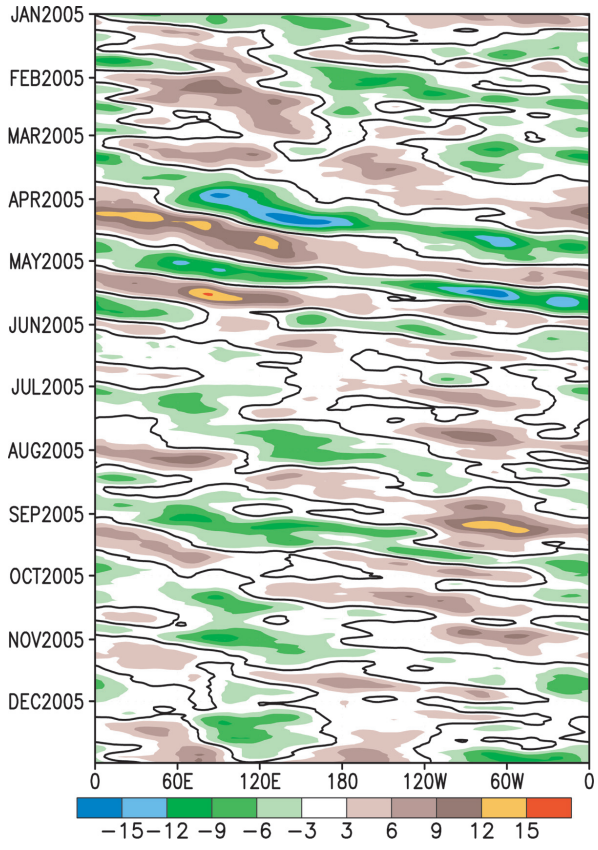

Fig. 4.2. Time–longitude section (5°N–5°S) of daily 200-hPa velocity potential anomalies ($m^2\ s^{-1}$) during 2005. The shading interval is $3 \times 10^6\ m^2\ s^{-1}$, and the thick solid contour is the zero line. Anomalies are departures from the 1971–2000 base period daily means, and plotted using a 5-day running mean smoother.

and tropical convection, and both sea surface and subsurface temperature anomalies exhibited considerable intraseasonal variability during 2005 in association with the MJO.

The MJO is indicated in a time–longitude section by continuous propagation of the 200-hPa velocity potential anomalies around the globe (Fig. 4.2). Periods when the MJO was active include March–May and July–September. This MJO activity contributed to alternating periods of enhanced and suppressed convection from the Indian Ocean to the date line, and to alternating periods of low-level easterly and westerly wind anomalies across the tropical Pacific (Fig. 4.1c).

The low-level wind anomalies associated with the MJO can generate eastward-propagating oceanic Kelvin waves, typically traveling 10° longitude $week^{-1}$, that feature downwelling in the mixed layer at their leading edge and upwelling in their wake (Zhang et al. 2001). Major Kelvin waves occurred during March–May in response to very strong westerly wind bursts over the western equatorial Pacific linked to the MJO (Fig. 4.3). As indicated by a time series of area-averaged SST anomalies in the Niño-3 region, the upwelling phase of one Kelvin wave produced a marked drop in SSTs across the east-central equatorial Pacific during February, followed by a return to near-normal SSTs in March (Fig. 4.4). The downwelling phase of a second Kelvin wave reached the region in early May, causing an abrupt increase in SSTs to 0.9°C above average. These anomalies exceeded earlier values associated with the weak warm episode. Several ENSO forecast models interpreted this anomalous warming as an indication of a possible return to El Niño conditions. However, the upwelling phase of the MJO followed behind, which dissipated the warmth soon thereafter.

An unusual feature of this El Niño was that excess heat content along the equator, typically a precursor to subsequent ENSO SST anomaly development (Jin 1997, Meinen and McPhaden 2000), did not precede but rather developed in phase with Niño-3.4 SST anomalies during 2004/05 (Fig. 4.5). The lack of a subsurface heat content precursor may account for the relative weakness of the 2004/05 El Niño and the difficulty in predicting its onset (Lyon and Barnston 2005). By the end of 2005, the excess equatorial heat

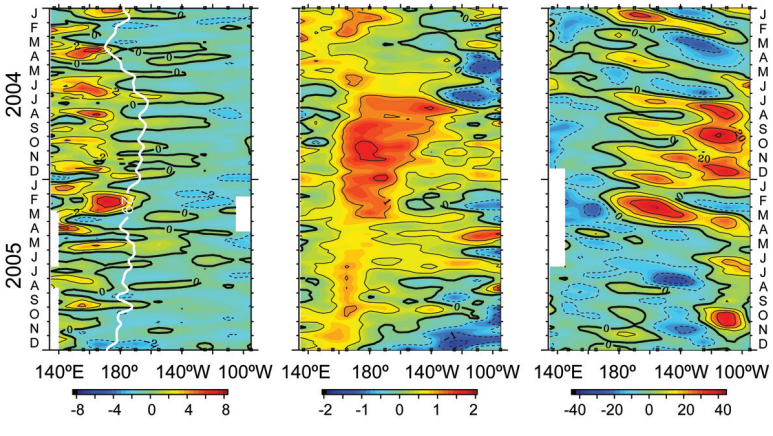

Fig. 4.3. Five-day average anomalies of (left) zonal wind ($m\ s^{-1}$), (center) SST (°C), and (right) 20°C depth (m; an index for the depth of the thermocline) relative to the mean seasonal cycle averaged over 2°N–2°S based on TAO/TRITON moored time series data. The white line on the left panel indicates the 29°C isotherm, which marks the eastern edge of the western Pacific warm pool. Ticks on the horizontal axis indicate longitudes sampled at the start (top) and end (bottom) of record.

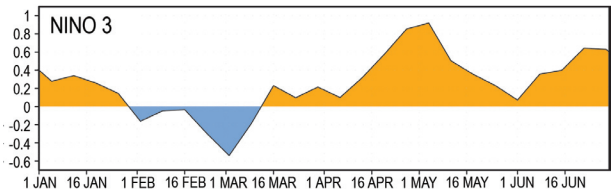

FIG. 4.4. Time series of the Niño-3 region SST anomaly index calculated over the area (5°N–5°S, 90°–150°W).

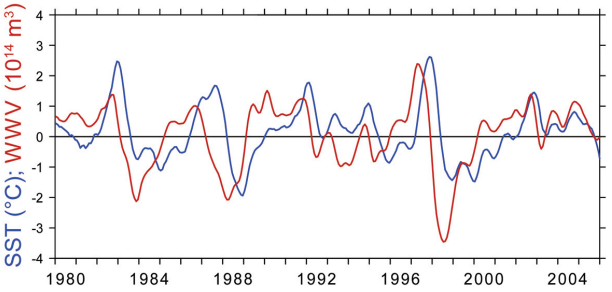

FIG. 4.5. Monthly anomalies of Niño-3.4 SST (°C) and warm water volume (WWV; × 10^{14} m^3) from January 1980 to December 2005. WWV, which is an index of heat content along the equator, is based on a blended thermal field analysis of TAO/TRITON moored time series data and ship-of-opportunity expendable bathythermograph (XBT) data integrated over the region of 5°N–5°S, 80°W–120°E above the 20°C isotherm. Niño-3.4 SST represents an average anomaly over the region of 5°N–5°S, 120°–170°W. Time series have been smoothed with a 5-month running mean filter.

content prevalent during most of 2004/05 had disappeared in association with the onset of cold La Niña conditions (Fig. 4.5).

Anomalous warming associated with the El Niño–like conditions during 2004/05 was centered near the date line. Conversely, near-normal SSTs prevailed in the eastern Pacific and along the west coast of South America. The failure of persistent warm SST anomalies to develop in the eastern equatorial Pacific and along the west coasts of the Americas limited the effects of this El Niño on marine ecosystems and fisheries in those regions.

c. *Tropical cyclones*

i) SEASONAL ACTIVITY OVERVIEW—H. J. Diamond[19] and D. H. Levinson[46]

Averaged across all basins, the tropical storm seasons of 2005 (2004/05 in the Southern Hemisphere) saw an above-normal number of named storms relative to the 1981–2000 mean. Of these, fewer than normal became hurricanes/typhoons/cyclones (HTCs), but the number of major HTCs was slightly above average. Globally, 103 tropical storms (≥ 34 kt) were recorded, with 53 becoming HTCs (≥ 64 kt), and 28 attaining major/intense (≥ 96 kt) status (compared to an average of 97.25, 55, and 25.35 storms, respectively). The 2005 season was unprecedented in the Atlantic, with numerous seasonal and individual storm-related records. The highlights in the Atlantic included the existence of three Saffir–Simpson category 5 storms (e.g., Wilma; Fig. 4.6), which are discussed in a sidebar on the Atlantic season. While the Atlantic had its all-time busiest season ever with 27 total storms (see note in abstract), other basins were characterized by near- to below-normal levels of activity.

ii) ATLANTIC BASIN—G. D. Bell,[5] E. Blake,[8] K. C. Mo,[58] C. W. Landsea,[44] R. Pasch,[65] M. Chelliah,[15] and S. B. Goldenberg[29]

The tropical multidecadal signal incorporates the leading modes of tropical convective rainfall variability occurring on multidecadal time scales. Three important aspects of this signal responsible for the increased hurricane activity since 1995 are 1) a stronger West African monsoon system; 2) suppressed convection in the Amazon Basin; and 3) the warm phase of the Atlantic multidecadal mode (Goldenberg et al. 2001; Bell and Chelliah 2006). This tropical multidecadal signal is very important to Atlantic hurricanes because it affects an entire set of critical conditions across the main development region (MDR) for decades at a time. The MDR consists of the tropical Atlantic and Caribbean Sea south of 21.5°N (Fig. 4.7a, green box). During 2005,

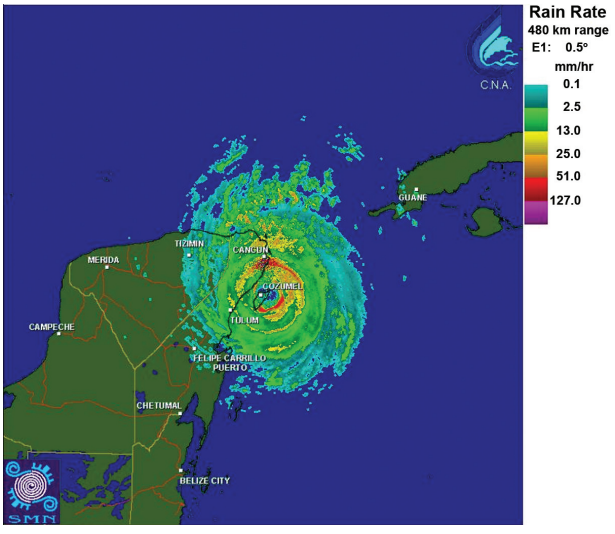

FIG 4.6. Mexican Meteorological Service radar image of category 5 Hurricane Wilma striking the Yucatan Peninsula on 21 Oct 2005. [Source: Servicio Meteorologico Nacional]

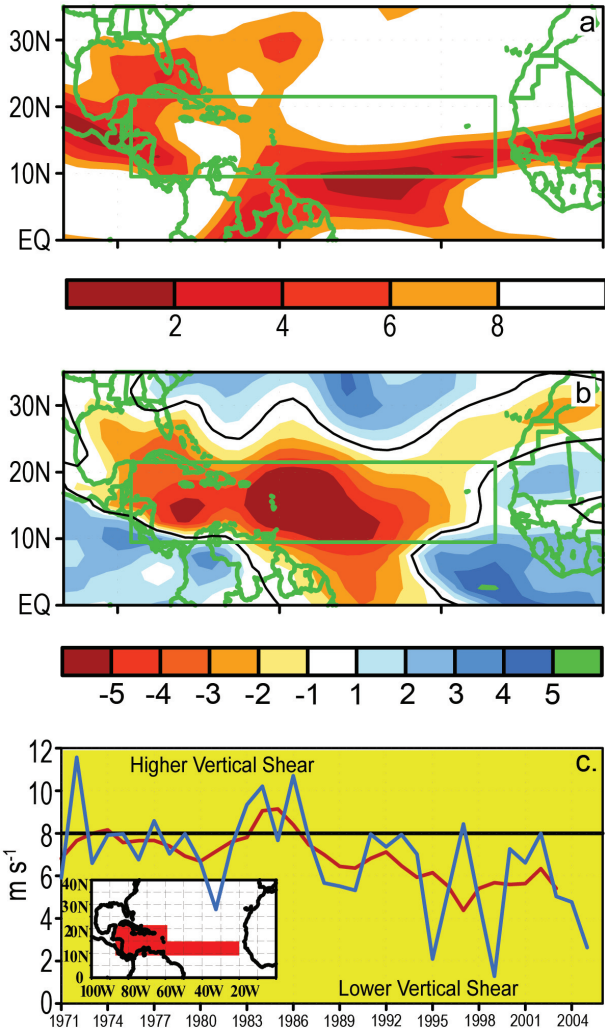

Fig. 4.7. June–October (a) 200–850-hPa vertical wind shear magnitude total (m s^{-1}) and (b) anomalies. In (a) only values less than 8 m s^{-1} are shaded. In (b) red shading indicates below-average strength of the vertical shear. Green box denotes the MDR. Anomalies in (b) are departures from the 1971–2000 base period monthly means. (c) A time series of August–October area-averaged 200–850-hPa vertical shear of the zonal wind (m s^{-1}) across the MDR (inset). Blue curve shows unsmoothed 3-month values, and red curve shows a 5-point running mean applied to the time series.

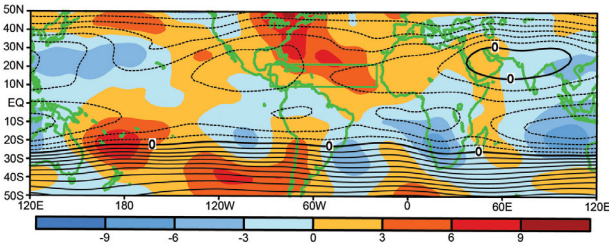

Fig. 4.8. June–October 2005 mean (contours, interval is 10 × 10^6 m^2 s^{-1}) and anomalous (shading) 200-hPa streamfunction. Anticyclonic anomalies are indicated by positive values in the NH and negative values in the SH. Cyclonic anomalies are indicated by negative values in the NH and positive values in the SH. Anomalies are departures from the 1971–2000 base period monthly means. Green box denotes the MDR.

this signal again set the backdrop for many of the observed atmospheric and oceanic anomalies. The 2005 hurricane season featured an extensive area of low vertical wind shear (less than the 8 m s^{-1} threshold for tropical cyclone formation) throughout the MDR and Gulf of Mexico (Fig. 4.7a), with the largest anomalies centered over the central tropical Atlantic and Caribbean Sea (Fig. 4.7b). Since 1995, the area-averaged vertical shear in the heart of the low-shear area has been approximately 5–6 m s^{-1}, with values during individual years such as 2005, 1999, and 1995, dropping to an incredibly low 2 m s^{-1}.

This extensive area of low shear in 2005 resulted in part from a stronger-than-average tropical easterly jet and an expanded area of upper-level easterly winds across the western MDR, both of which were related to an enhanced subtropical ridge at 200 hPa. The 200-hPa streamfunction field (Fig. 4.8) shows that these conditions were part of a larger-scale pattern during 2005, characterized by anticyclonic anomalies (Fig. 4.8; red in NH, blue in SH) and enhanced subtropical ridges in both hemispheres from the eastern Pacific to Africa, and by cyclonic anomalies in both hemispheres over the central tropical Pacific. This Tropics-wide pattern with its pronounced interhemispheric symmetry is a classic signature of very active Atlantic hurricane seasons. Bell and Chelliah (2006) indicate that this pattern signifies a response to anomalous tropical convection, partly related to the ongoing tropical multidecadal signal, and partly related to suppressed convection over the central equatorial Pacific.

During 2005, long periods of anomalous upper-level convergence were evident over the central tropical Pacific, with shorter-period fluctuations sometimes related to the MJO (Fig. 4.9, solid line). Throughout the season, these periods of suppressed convection led to a strengthening of the 200-hPa subtropical ridge over the western North Atlantic (Fig. 4.9, orange shading), which acted to focus periods of TC activity. For example, 10 of the season's 15 hurricanes and all 7 major hurricanes formed during these periods. All seven early season TCs and two mid-November TCs also occurred when convection was suppressed near the date line. This finding is consistent with the study of Mo (2000). Also consistent with that study is the break in activity during the first half of August in association with MJO-related enhanced convection near the date line.

The low vertical shear during 2005 was also associated with westerly wind anomalies in the lower troposphere that reflected a markedly reduced strength of the tropical easterly trade winds from the eastern tropical Pacific to Africa. In combination with the anomalous upper-level easterlies, this wind distribution is consistent with the baroclinic response of the atmospheric circulation to anomalous tropical convection linked in part to the tropical multidecadal signal (Bell and Chelliah 2006). Over the Caribbean Sea, the weaker easterly trade winds corresponded with exceptionally low SLP and 1000-hPa heights in response to a weakening and northeastward shift of the Bermuda high. These conditions were associated with anomalous low-level cyclonic vorticity across the northern half of the MDR, western North Atlantic, and Gulf of Mexico.

These favorable conditions extended up to 700 hPa along the equatorward flank of the African easterly jet (AEJ) (Fig. 4.11). The associated anomaly patterns at this level are also consistent with the ongoing tropical multidecadal signal. Conversely, during the preceding period (1971–94) of below-normal activity, higher vertical shear (Fig. 4.7b), combined with stronger easterly trade winds and reduced cyclonic vorticity south of the AEJ axis, were not conducive to Atlantic hurricane formation in the MDR.

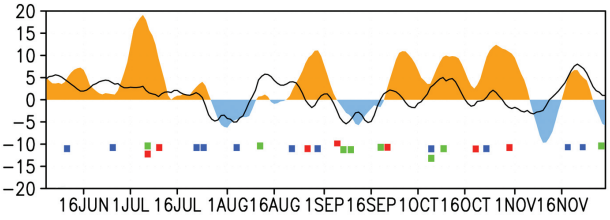

Fig. 4.9. Five-day running mean time series showing area-averaged anomalies of 200-hPa velocity potential (line) and 200-hPa streamfunction (shading) during 10 Jun–30 Nov 2005 ($m^2 s^{-1}$). Velocity potential anomalies are calculated for the central tropical Pacific region bounded by 10°–20°N, 160°E–170°W. Streamfunction anomalies are calculated for the Gulf of Mexico and Caribbean Sea bounded by 10°–30°N, 60°–100°W. Small boxes below time series indicate when tropical storms (blue), Category 1–2 hurricanes (green), and major hurricanes (red) formed in the Atlantic basin. Anomalies are departures from the 1971–2000 period daily means.

Favorable lower-level conditions during 2005 were also associated with record warm SSTs across the tropical Atlantic, Caribbean Sea, and Gulf of Mexico (Fig. 4.12, top). For the entire season SSTs across the western tropical Atlantic and Gulf of Mexico reached an 1870–2005 all-time high of 28.7°C (Fig. 4.12, bottom). The above conditions meant that African easterly waves were embedded within an extended

ATLANTIC MONTHLY AIR–SEA FLUXES AND THE 2005 HURRICANE SEASON—M. A. Bourassa,[9] S. R. Smith,[84] P. Hughes,[33] and J. Rolph[76]

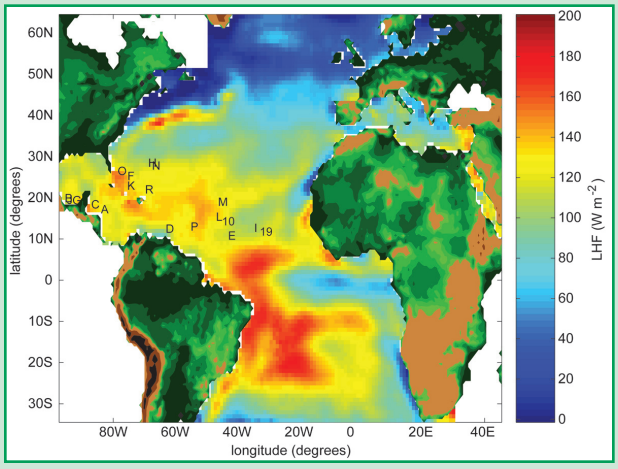

Fig. 4.10. Model-derived latent heat fluxes (W m^{-2}) during June–September 2005. The first letters of named storms are located where the storm was first named. The numbers indicate similar positions for tropical depressions that did not become named storms.

Latent heat flux refers to the rate at which water vapor energy is transferred from the ocean to the atmosphere. The release of this energy occurs at higher altitudes in association with deep convective clouds, and is a critical energy source for developing tropical cyclones. The latent heat flux during 2005 was estimated using a newly completed version of The Florida State University air–sea flux fields (FSU3; Bourassa et al. 2005). The objectively analyzed latent heat fluxes across the tropical Atlantic were generally 100–140 W m^{-2} during June–September, with larger values coinciding with tropical cyclone genesis regions (Fig. 4.10). The area-averaged anomalous latent heat flux during the period was 10 W m^{-2}, which is 20% greater than the largest value in the 1978–2003 time series (not shown). It is suggested that this increased latent heat flux, combined with above average SSTs and a strong cross-equatorial flow of deep tropical moisture into the heart of the MDR, led to a more unstable and deeper boundary layer that favored increased tropical cyclone activity.

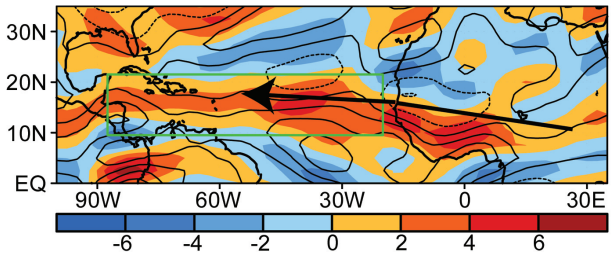

Fig. 4.11. June–October 2005 700-hPa anomalous zonal winds (contour interval is 1.0 m s^{-1}) and relative vorticity (shading, × 10^{-6} s^{-1}). Solid (dashed) contours indicate westerly (easterly) winds. Yellow-red (blue) shading indicates anomalous cyclonic (anticyclonic) relative vorticity. Arrow shows mean position of the African easterly jet axis during August–October. Green box denotes the MDR. Anomalies are departures from the 1971–2000 base period monthly means.

region of anomalous cyclonic vorticity as they moved westward over very warm SSTs into the low-shear, low-SLP, high-vorticity environment of the central and western MDR. This combination is known to favor very active hurricane seasons (Bell et al. 1999, 2000 2004; Lawrimore et al. 2001).

While the combination of the supportive multidecadal signal and suppressed convection near the date line established an environment conducive for a very active season, these factors cannot account for periods when atmospheric anomalies were exceptionally strong. They also cannot account for the propensity of many TCs to develop in and around, or traverse the Gulf of Mexico. Three additional factors likely contributed to these conditions. The first was a northeastward shift and strengthening of the ITCZ over the eastern North Pacific, with a corresponding increase in convection over Central America and southern Mexico. Associated with this pattern, an extensive area of low SLP over the Gulf of Mexico contributed to periods of actual low-level westerly winds across the Caribbean Sea, which further strengthened the low-level cyclonic circulation over the Gulf of Mexico. Second was a persistent ridge of high pressure in the middle and upper troposphere over the southeastern United States and Gulf regions, which can be linked to large-scale extratropical anomaly patterns (Fig. 4.9), and contributed to the low vertical shear across the Gulf of Mexico and western MDR. This ridge was particularly strong in July (Fig. 4.8), when it contributed to a sharp drop in vertical shear across the southern and western MDR. Three hurricanes formed in the MDR during this period, with two becoming major hurricanes. Last, above-average SSTs in an already very warm Gulf of Mexico (Fig. 4.12, top) made the environment over the western Atlantic and Gulf of Mexico even more conducive to tropical cyclogenesis and major hurricane formation. In effect, the environment in these regions during much of the season typified the central MDR during an active season. South of the anomalous upper-level ridge over the eastern United States, enhanced easterly flow also helped to steer many of the developing TCs into the Gulf of Mexico, all of which eventually made landfall.

Finally, the failure of many tropical storms to develop until they reached the western part of the basin is related to a pronounced eastward shift of the mean upper-level trough to the extreme eastern North Atlantic (Fig. 4.8). This shift occurred in association

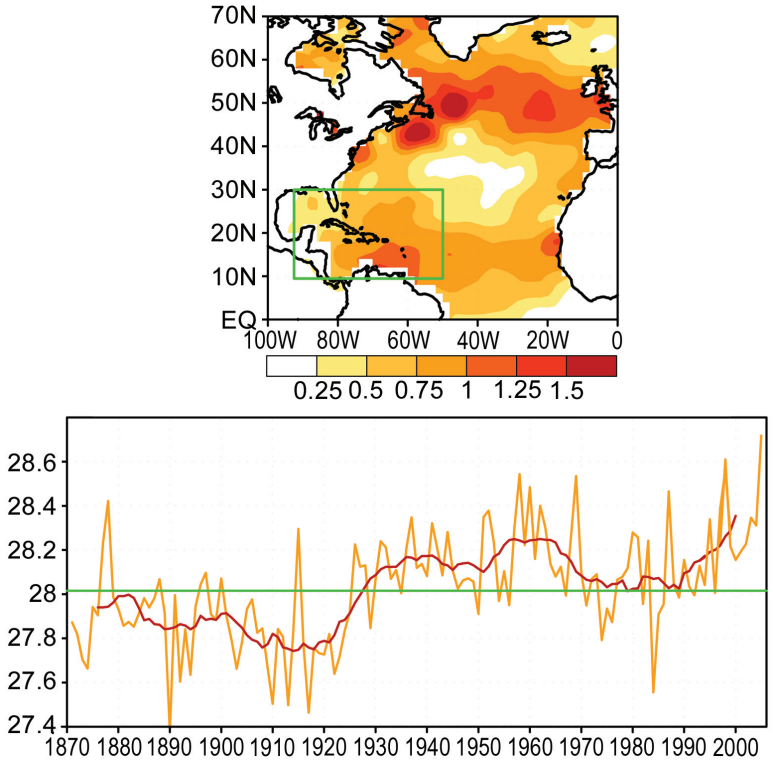

Fig. 4.12. Seasonal June–November (top) SST anomalies (°C) during 2005 and (bottom) time series of area-averaged SSTs (°C) in the (top) green boxed region. (bottom) Red line shows the corresponding 11-yr running mean. Averaging region corresponds to where seasonal activity was heavily focused during 2005.

with the persistent upper-level ridge farther west, and resulted in periods of anomalous upper-level westerlies and increased vertical wind shear that suppressed tropical wave development in the eastern MDR.

iii) East Pacific basin—D. H. Levinson[46]

(i) Overview of the 2005 season

The hurricane season in the eastern North Pacific (ENP) basin typically begins in mid-May and runs through the end of November, with a climatological peak in September. The 2005 hurricane season in the ENP was below normal, with the majority of the activity in the basin occurring during August and September. A total of 15 named storms (NSs), 7 hurricanes (Hs), and 2 major hurricanes (MHs) developed in the ENP basin in 2005, which was less than the NOAA National Hurricane Center (NHC) 1971–2003 seasonal climatology of 15.5 NSs, 9 Hs, and 4.3 MHs. A tropical depression (TD) formed in mid-October (TD 16-E), and was relatively long lived, but did not intensify to tropical storm strength. In addition to the total number of tropical cyclones, the 2005 ENP hurricane season was also below average for landfalling systems along the Pacific coast of Mexico.

(ii) Comparison of the 2005 season with climatology

The variability of ENP tropical cyclone activity is summarized with several widely used parameters and indices (Figs. 4.13a–d). In terms of the number of NSs, which is the total number of tropical cyclones that reach at least minimal tropical storm strength (sustained winds ≥ 34 kt), activity in the ENP basin has been near average since the mid-1990s, fluctuating between slightly above or below the long-term

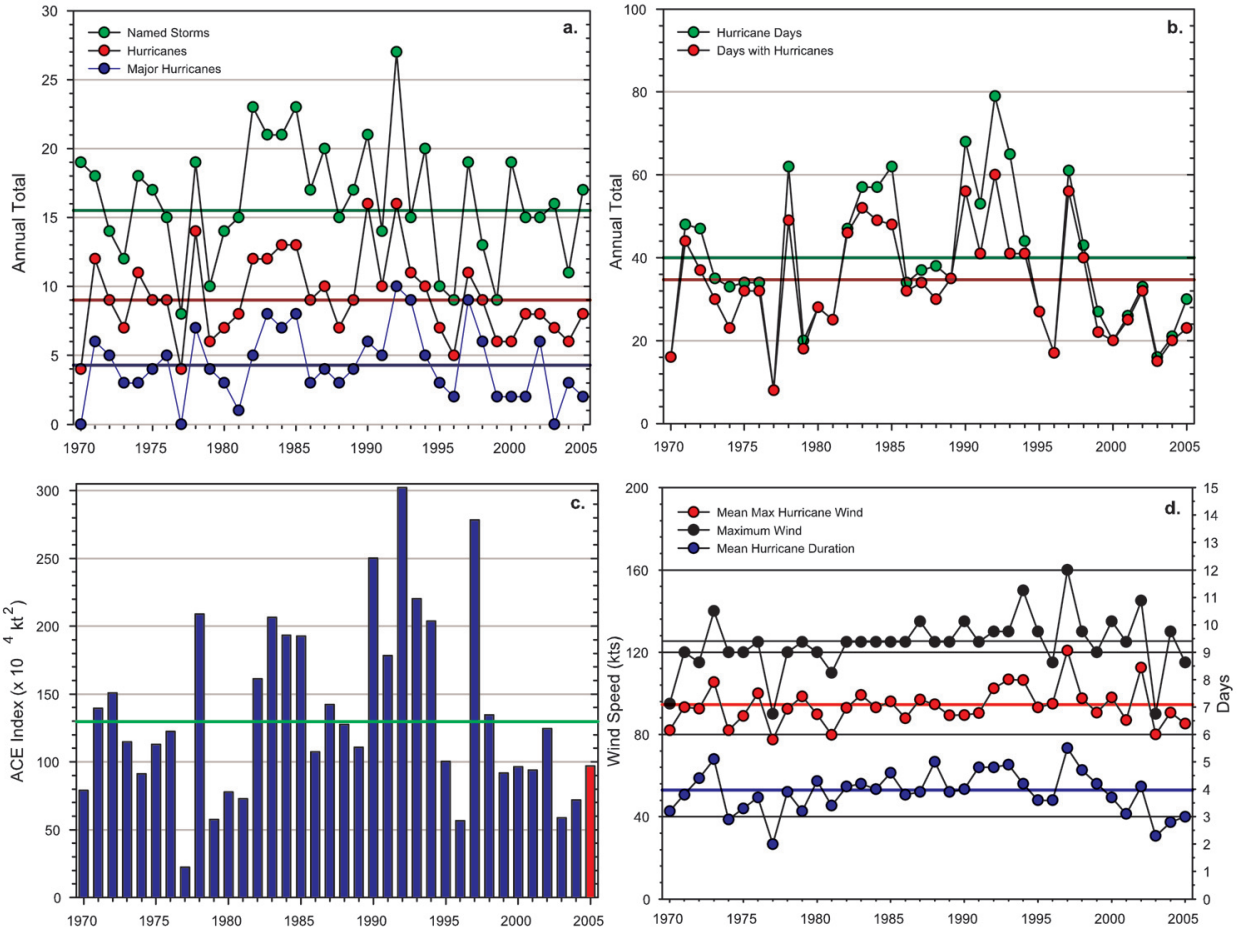

Fig. 4.13. Seasonal tropical cyclone statistics for the east North Pacific Ocean over the period 1970–2005: (a) number of NSs, Hs, and MHs, (b) days with hurricanes (the number of days with winds ≥ 64 kt) and hurricane days (days with winds ≥ 64 kt times the number of storms with winds ≥ 64 kt), c) the Accumulated Cyclone Energy (ACE) Index (× 10^4 kt^2) with 2005 highlighted in red, and d) the maximum and mean maximum wind speed (kt), and mean hurricane duration (days). All time series in (a)–(d) include the corresponding 1971–2003 base period means.

mean of 15.5 yr^{-1} (Fig. 4.13a). However, the annual number of hurricanes and major hurricanes have been below average in most years since 1995, except for the El Niño years of 1997/98. In addition, there were no landfalling named systems during the 2005 ENP season.

Despite the obvious importance of the number of tropical cyclones in any particular year, several other indices are useful in determining the historical significance of an individual hurricane season. Figure 4.13b shows this activity in terms of the annual number of days with hurricanes as well as hurricane days, and both of these statistics have been below average since 1995, again with the exception of the 1997/98 El Niño years.

In recent years, the Accumulated Cyclone Energy (ACE) Index (Bell et al. 2000) has been used as a diagnostic tool for understanding the intensity and duration of tropical cyclone activity. The ACE Index value for the ENP basin in 2005 was approximately 97 $\times 10^4$ kt^2, which was below both the long-term mean and median, and also within NOAA's definition of a "below normal" season. Historically, the ENP basin had a well-defined peak in the ACE Index during the early 1990s, with the highest annual value occurring in 1992. With the exception of 1997, there has been a marked decrease in the ACE Index for the ENP basin beginning in 1995. The below-normal ENP activity since 1995 appears to be inversely related to the increased North Atlantic activity (Lander and Guard 1998; Landsea et al. 1998, 1999; Goldenberg et al. 2001; Bell and Chelliah 2006).

(iii) Impacts

None of the ENP tropical storms or hurricanes that formed in 2005 made landfall along Mexico's Pacific coast, which on average has at least one tropical storm and one hurricane landfall each year (Jauregui 2003). However, remnants of several tropical storms and hurricanes brought heavy precipitation to Mexico and Central America, as well as the Hawaiian Islands.

The first tropical cyclone of the season, Adrian, formed in mid-May from a tropical wave that crossed the Central American isthmus and intensified into a tropical storm on 18 May and to a hurricane the following day. Adrian reached peak intensity on 19 May, about 139 km southwest of El Salvador, with sustained winds of 70 kt. Poststorm reports from ships and reanalysis of satellite-derived intensities using the Dvorak (1984) technique indicate that the storm had weakened to a tropical depression just prior to landfall. Despite this rapid dissipation, heavy rainfall associated with the remnants of Adrian generated flooding and mudslides resulting in one storm-related death in Nicaragua (source: NOAA/NHC).

The other tropical cyclones that impacted Mexico were TS Dora, whose center of circulation did not cross the coast but passed just 65 km off Zihuatanejo, and H Otis that dissipated about 148 km northwest of Cabo San Lazaro. Otis generated tropical storm conditions in some coastal locations and heavy rainfall in the mountains of the southern Baja Peninsula.

The only tropical cyclone to impact the Hawaiian Islands during the 2005 season was MH Kenneth, which had the longest duration and reached the highest intensity of any tropical cyclone in the ENP basin in 2005. Kenneth initially became a tropical depression on 14 September, intensifying to a tropical storm on the 15th, and to a hurricane the following day. It reached its maximum intensity of 115 kt (minimal category 4 on the Saffir–Simpson scale) on 18 September, moved slowly east-northeastward and weakened to a tropical storm. Despite moving into a region of cooler SSTs, Kenneth reintensified into a hurricane and moved northwestward toward the island of Hawaii, finally dissipating just east of the island on 30 September. The remnants of Kenneth produced locally heavy rainfall, but there were no official reports of damages or injuries.

(iv) Environmental influences on the below-normal east North Pacific hurricane season

Tropical cyclone activity (both frequency and intensity) is influenced by several large-scale environmental factors, including SSTs, vertical wind shear in the mid- and upper-troposphere, the phase of the QBO in the tropical lower stratosphere, and the phase of the ENSO in the equatorial Pacific region (Whitney and Hobgood 1997). In 2005, above-normal vertical wind shear in the midtroposphere (850–200 hPa) was observed in the ENP basin during the 3-month (July–September) peak of the hurricane season (Fig. 4.14, top). Vertical wind shear anomalies exceeding 6 m s^{-1} occurred in the ENP basin's MDR, which is defined here between 10°–20°N and 90°–130°W (Fig. 4.14, red box). In addition to increased vertical wind shear, SSTs were below normal in the MDR during the peak of the hurricane season in 2005, with an area of −1° to −1.5°C SST anomalies off the coast of the Baja Peninsula (Fig. 4.14, bottom). These cool SST anomalies were located at the northern edge of the MDR, in a region of normally cooler water due to coastal upwelling and cold advection from the north associated with the California current.

Tropical cyclones in the ENP basin typically attain a higher intensity when the QBO is in its westerly

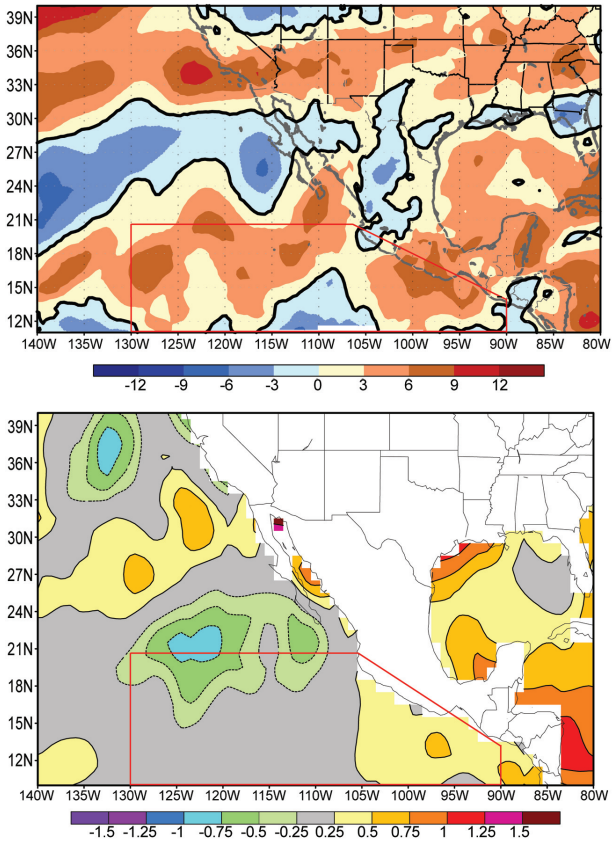

Fig. 4.14. (top) July–September 2005 200–850-hPa vertical wind shear anomaly (m s^{-1}; relative to 1979–2004 means; source: North American Regional Reanalysis dataset). (bottom) July–September 2005 sea surface temperature anomalies (°C) from NOAA's OI dataset (Reynolds and Smith 1994; Reynolds et al. 2002). The main development region for ENP hurricanes is the area delineated by the red box in both panels.

phase at 30 hPa in the tropical lower stratosphere, but there is also a corresponding decrease in the observed seasonal frequency of stroms (Whitney and Hobgood 1997). In 2005, the phase of the QBO anomaly was westerly, but with relatively weak zonal wind anomalies < 10 m s^{-1} at 30 hPa during the majority of the hurricane season (except in October when the phase of the 30-hPa zonal wind became easterly). Therefore, the activity in the ENP basin during 2005 was mixed relative to the phase of the QBO.

iv) Western North Pacific basin—S. J. Camargo[14]

Tropical cyclone [typhoon (TY)] activity in the western North Pacific (WNP) was slightly below average in 2005, with 25 tropical cyclones (TDs, TSs, and TYs), which was below the 1971–2004 climatological median of 31 (Fig. 4.15a). Only one of the tropical cyclones (TD 20W) failed to reach tropical storm intensity or higher. There were 24 NSs in 2005 (8 TSs and 16 TYs), which was below the climatological median of 26. The eight TSs in 2005 were also slightly below the climatological median of nine, and one of these (25W) was not officially named by the Joint Typhoon Warning Center (JTWC). The 16 TYs in 2005 equaled the climatological median, as did the four supertyphoons.

Other indices of tropical cyclone activity indicate a slightly below- to near-normal level of activity in the WNP in 2005. The 2005 ACE Index (Fig. 4.16a) was 298 × 10^4 kt^2 in 2005, which was slightly above the climatological median of 289.8 × 10^4 kt^2 and mainly due to the occurrence of four supertyphoons in 2005, which accounted for 75% of the total.

Monthly ACE values (Fig. 4.16b) were slightly above normal in the early season until September, and below normal during October–December. The June ACE Index value was the eighth highest in the historical record. In contrast, November and December ACE Index values were the 8th and 13th lowest,

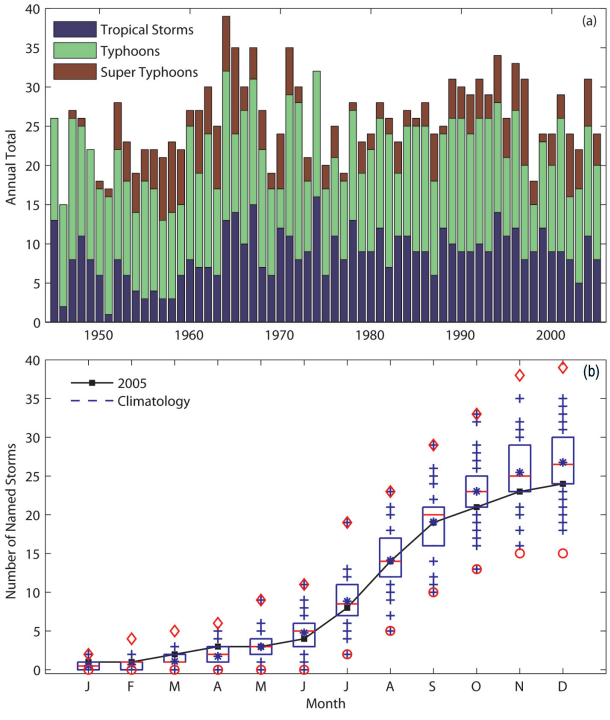

Fig. 4.15. (top) Number of tropical storms, typhoons and supertyphoons per year in the WNP for the period 1945–2005. (bottom) Cumulative number of named storms per month in the WNP: 2005 (black squares and line), and climatology (1971–2004) shown as box plots [box = interquartile range (IQR), red line = median, * = mean, + = values in top or bottom quartile, and diamonds (circles) = high (low) records in the 1945–2005 period]. [Source: JTWC]

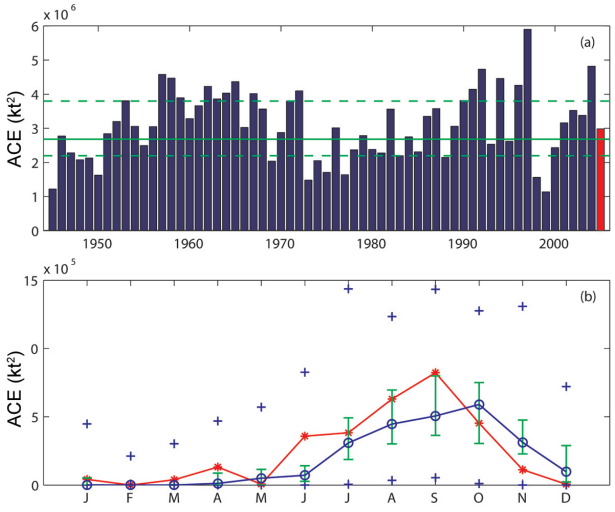

Fig. 4.16. (a) ACE Index (x 104 kt2) per year in the western North Pacific for the years 1945–2005. The solid green line indicates the median for the 1971–2004 base period (climatology), and the dashed green lines show the 25th and 75th percentiles. (b) ACE Index per month in 2005 (red line) and the median in the years 1971–2004 (blue line), where the green error bars indicate the 25th and 75th percentiles. In the cases of no error bars, the upper and/or lower percentiles coincide with the median. The blue plus signs (+) denote the maximum and minimum values during the period 1945–2005. [Source: JTWC]

respectively, in the historical record. The high June ACE value was due to typhoon Nesat, which was in the top 5% of the historical record of ACE per storm. The ACE index values of supertyphoons Longwang and Nabi were both in the top 10% of the historical record of ACE per storm.

The cumulative number of named storms per month (Fig. 4.15b) also shows an active early season (March–May), a slightly above-normal mid-season (August and September), and below-normal activity in the late season (October–December). The 131 NS days (days in which at least one tropical cyclone with tropical storm intensity or higher occurred) in 2005 was below the climatological median of 163.1 days. In contrast, the 29.25 days with intense typhoons (number of days having at least one typhoon with sustained winds ≥ 96 kt) was well above the climatological median of 20 days, and in the top 15% of the historical record.

WNP tropical storms and typhoons in 2005 had an average cyclogenesis position of 14.5°N, 138.4°E, which is slightly northwest of the climatological mean position (12.8°N, 143.5°E; 1.8° lat, 6.6° lon std dev). The average track position of all named storms was 20.4°N, 132.3°E, which is also slightly northwest of the climatological mean (19.0°N, 134.2°E). This shift to the northwest was due to several tropical cyclones that formed at higher latitudes (at or north of 20°N) and the absence of low-latitude (at or south of 15°N) tropical cyclones east of 155°E.

The 2005 WNP typhoon season was responsible for many fatalities and economic losses. Eight named tropical cyclones made landfall in China resulting in around 300 deaths and losses estimated at $3 billion USD (see also section 6f). Four cyclones affected Vietnam in 2005 (Damrey, Haitang, Longwang, and Kai Tak), and three strong typhoons (Talim, Haitang, and Longwang) made landfall in Taiwan. While Japan was struck by 10 tropical cyclones in 2004, only two (Nabi and Mawar) made landfall there in 2005. The high number of landfalls in China, Vietnam, and Taiwan (Fig. 4.17a) and the relative absence thereof in Japan were related to anomalous 500-hPa winds and vertical wind shear (Fig. 4.17b). Also present were anomalous low-level (850 hPa) easterlies, probably responsible for the absence of typhoons east of 150°E at low latitudes.

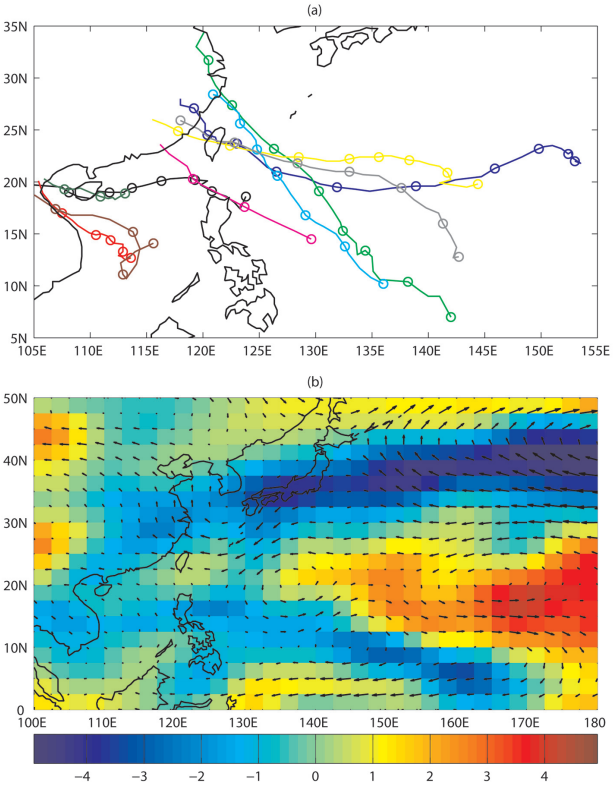

Fig. 4.17. (a) Observed tracks of tropical cyclones that made landfall in China, Taiwan, and Vietnam in 2005. (b) Anomalous 500-hPa winds (vectors) and anomalous vertical wind shear (m s^{-1}, shading) during July–October 2005.

v) Indian Ocean basins—K. L. Gleason[28]

(i) North Indian Ocean

The North Indian Ocean (NIO) tropical cyclone season extends from May to December, with two peaks in activity during May–June and November when the monsoon trough is climatologically positioned over tropical waters in the basin. Tropical cyclones in the NIO basin develop in the Bay of Bengal and the Arabian Sea typically between latitudes of 8° and 15°N and are usually short lived and weak, quickly moving into the subcontinent. However, severe cyclonic storms, with winds > 130 kt, can develop (Neumann et al. 1993).

Using reliable records from 1981 to 2000, a mean of less than one major cyclone (MCYC: sustained winds ≥ 96 kt), 1.6 cyclones (CYC: sustained winds ≥ 64 kt), and 4.75 NSs (sustained winds ≥ 34 kt) form each year in the NIO. The 2005 tropical cyclone season was near normal with one CYC and six NSs forming from January to December (Fig. 4.18, top). The sole CYC lasted at that strength for only 1 day, resulting in a below-average number of NIO cyclone days for 2005.

The estimated 2005 ACE Index for the NIO basin was 7×10^4 kt^2, which is less than half of the 1981–2000 mean of 19×10^4 kt^2 (Fig. 4.18, bottom). In fact, NIO activity has been below normal for the past 6 yr. This period follows four active tropical cyclone seasons with above-average ACE Index values during the late 1990s.

Tropical Cyclone Fanoos was the only hurricane-strength storm of the NIO season. Fanoos developed over the Bay of Bengal west of the Andaman Islands in early December and tracked west toward the southeast Indian coastline. On 9 December, CYC Fanoos briefly became a category 1 tropical cyclone before making landfall on the Tamil Nadu coast near Vedaranyam with 55-kt sustained winds. Two tropical storms also made landfall in 2005. Tropical storm 03B formed in early October along the Indian coastline and came ashore near the West Bengal state with 35-kt sustained winds. Tropical storm 04B formed near the Indian coast and made landfall in the Andhra Pradesh state in late October with sustained winds of 35 kt. Impacts from both of these storms were minimal.

In mid-September, a tropical depression developed over the South China Sea and moved inland over Thailand. Cyclonic Storm Pyarr, identified by the Indian Meteorological Department, moved into the Bay of Bengal and intensified into a tropical storm with estimated sustained winds of between 35 and 45 kt. Pyarr made landfall over the northeast Indian coast and quickly dissipated. This storm was not included in the NIO analyses for 2005 due to a lack of available track data and wind observations.

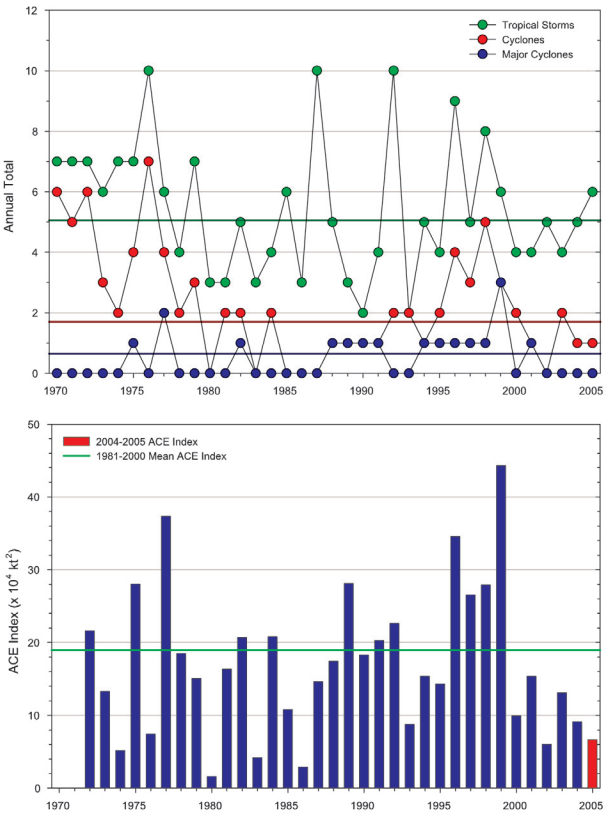

Fig. 4.18. Annual tropical cyclone statistics for the NIO 1970–2005. (top) Number of tropical storms, cyclones, and major cyclones. (bottom) Estimated annual ACE Index (x 10^4 kt^2) for all NIO tropical cyclones during which they were at least tropical storm or greater intensities (Bell et al. 2000). The ACE Index is estimated due to a lack of consistent 6-h sustained winds data for every storm.

(ii) South Indian Ocean

The tropical cyclone season in the South Indian Ocean (SIO) is typically active from December through April and officially extends from July to June, spanning two calendar years. The SIO basin extends south of the equator from the African coastline to 105°E, although most cyclones develop south of 10°S latitude. Cyclones in the SIO that remain east of 105°E are included in the Australian summary (see next section). The vast majority of SIO landfalling cyclones impact Madagascar, Mozambique, and the Mascarene Islands, including Mauritius. Due to a sparse historical observational record, and no centralized monitoring agency, the SIO is probably the least understood of all tropical cyclone basins

(Atkinson 1971; Neumann et al. 1993). As a result, the SIO statistics presented are incomplete, but are based upon verifiable information.

Using reliable data from 1980 to 2000, the SIO averages 2.7 MCYCs, 6.1 CYCs, and 11.95 NSs each year. During the 2004/05 season (from July 2004 to June 2005), the SIO tropical cyclone occurrences were near average with 3 MCYCs, 6 CYCs, and 14 NSs (Fig. 4.19, top). However, the estimated 2004/05 SIO ACE Index was 53×10^4 kt^2, which was less than half of the 1981–2000 average of 112×10^4 kt^2 (Fig. 4.19, bottom). This suggests a decreased intensity of tropical cyclones during this season, because both occurrences and mean cyclone duration (~4 days) were near average.

Three SIO tropical cyclones made landfall during the 2004/05 season. The first of these formed northeast of Madagascar in mid-January and moved west toward the African coastline. This TD became MCYC Ernest after intensifying to 100-kt sustained winds (category 3), while moving south over the warm waters of the Madagascar Channel. Ernest weakened slightly before brushing the southwestern coast of Madagascar on 22 January with 70-kt sustained winds. It then proceeded southeast over the cooler waters of the SIO and dissipated. Later in the month, Tropical Storm Felapi affected the same region. The combined effects from both systems caused widespread flooding across southern Madagascar. Earlier in the season, tropical cyclone 02S formed east-southeast of the Seychelles Islands in late October and moved west toward the African coastline. This storm briefly strengthened into a tropical storm before weakening and made landfall near Dar es Salaam, Tanzania, as a TD.

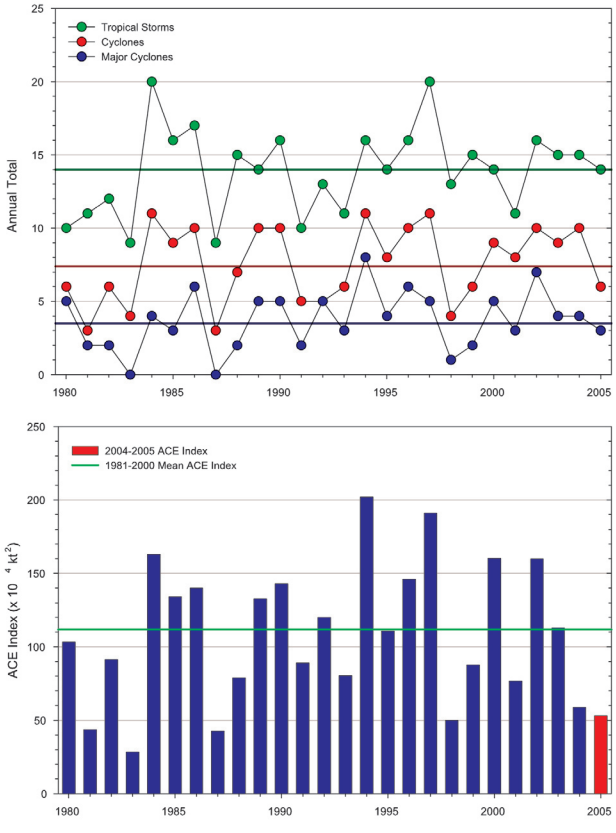

Fig. 4.19. Annual tropical cyclone statistics for the SIO 1980–2005. (top) Number of tropical storms, cyclones, and major cyclones. (bottom) Estimated annual ACE Index (x 10^4 kt^2) for all SIO tropical cyclones during which they were at least tropical storm or greater intensities (Bell et al. 2000). The ACE Index is estimated due to a lack of consistent 6-h sustained winds data for every storm.

The most intense SIO tropical cyclone of the 2004/05 season was MCYC Bento, with sustained winds of 140 kt. Bento developed in late November 2004, east-southeast of Diego Garcia in the central Indian Ocean, and quickly intensified. Fortunately, Bento remained well south of Diego Garcia and there were no significant impacts on the island. Bento was the first tropical cyclone on record in the SIO to reach category 5 intensity equatorward of 10°S latitude.

CYC Adeline-Juliet, formed near the Cocos Islands in the southeast Indian Ocean during early April 2005 and began its westward movement toward the central SIO. Adeline-Juliet reached peak intensity of 120-kt sustained winds (category 4) on 8 April while tracking west-southwest to within 213 km of Rodrigues Island. It then quickly dissipated as it moved southward into an unfavorable environment of strong vertical shear, drier air, and cooler SSTs.

vi) South Pacific basins—M. J. Salinger,[80] A. B. Watkins,[90] and S. M. Burgess[12]

(i) Southwest Pacific

The 2004/05 southwest Pacific tropical cyclone season had a climatological average nine tropical storms east of 150°E (Fig. 4.20), four of which reached MCYC strength. All but one of the nine tropical cyclones originated east of the date line (Fig. 4.21), and all occurred between December and April.

The most devastating tropical cyclones of the 2004/05 season were Meena, Nancy, Olaf, and Percy. These systems all occurred in February in association with an active phase of the Madden–Julian oscillation.

Judy was the first tropical cyclone of the season (25 December) and brought torrential rainfall to parts of

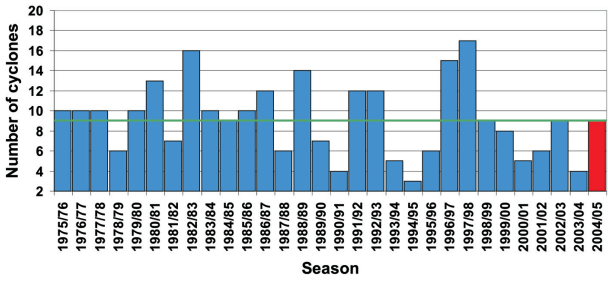

FIG. 4.20. The number of southwest Pacific tropical cyclones for the 2004/05 season (solid red bar) compared to frequencies during the past 30 years. The horizontal green line indicates the 30-yr average (Not including Ingrid, which originated west of 150°E).

the Tuamotu Islands, French Polynesia. CYC Kerry developed northeast of Vanuatu on 6 January, passing over the Pentecost and Malekula Islands the next day, with pressures as low as 987 hPa and maximum sustained wind speeds of 90 kt. Lola affected the region near Tonga from 31 January through 2 February, with strong winds at Fua'amotu Airport.

MCYC Meena formed east of Samoa on 3 February and tracked toward the southern Cook Islands. Estimated maximum sustained wind speeds reached 125 kt, with gusts to 155 kt. Tropical storm–force winds occurred at Mauke on 6 February with pressures as low as 986 hPa. Gale-force winds and gusts to 62 kt occurred in Rarotonga on the same day, preceded by about 100 mm of rain.

MCYC Nancy affected the northern Cook Islands from 13 to 15 February tracking south, forcing Aitutaki residents and tourists into shelters on 15–16 February. Estimated sustained maximum winds in Nancy reached 125 kt, while storm-force winds gusted to 88 kt in Rarotonga with reports of 100 kt elsewhere. Heavy rainfall, pressure as low as 988 hPa, and high seas also accompanied the storm. In Aitutaki, trees were uprooted, roofs damaged, and low-lying areas flooded. Waves caused widespread destruction along the northern and eastern coasts of Rarotonga. The island of Mangaia was also badly hit.

Olaf was named on 13 February, and reached MCYC strength with 145-kt maximum sustained winds. Observed winds exceeded 65 kt in Samoa on 16 February, damaging numerous structures. Gales buffeted the northern and southern Cook Islands on 17 February, with gusts to 51 kt in Rarotonga.

MCYC Percy, with maximum sustained winds reaching 140 kt came next. Gales, storm surge, and high tides affected Tokelau on 26 February, where Percy was reportedly the worst tropical cyclone in living memory. Many homes were damaged and roads washed out, with water up to 1 m deep in some areas.

Rae followed (near the southern Cook Islands) on 6 March, but remained weak. Finally, Shelia formed east of Niue on 22 April and tracked southeast, with maximum sustained winds reaching 35 kt.

(ii) Australian basin

As with the 2003/04 season, the 2004/05 Australian basin TC season saw only six TCs between 105° and 160°E, compared with a long-term average of approximately 10. Three were classified as severe tropical cyclones.

The most severe, TC Ingrid, occurred between 5 and 16 March (Fig. 4.22). Ingrid formed in the Coral Sea south of Papua New Guinea and tracked first east- then westward across Cape York Peninsula and through offshore islands off the Northern Territory coast, before making landfall in the far north of Western Australia. Ingrid is the only TC in Australia's recorded history to impact the coastline of three different states or territories as a severe tropical cyclone (category 3 or above on the Australian tropical cyclone warning scale). Fortunately, some weakening before its coastal crossings resulted in only modest damage.

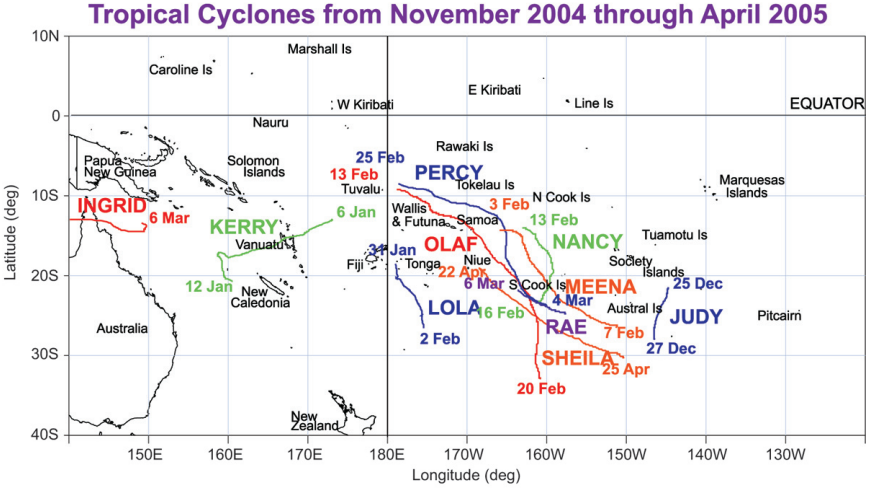

FIG. 4.21. Southwest Pacific tropical cyclone tracks for the 2004/05 season (including Ingrid).

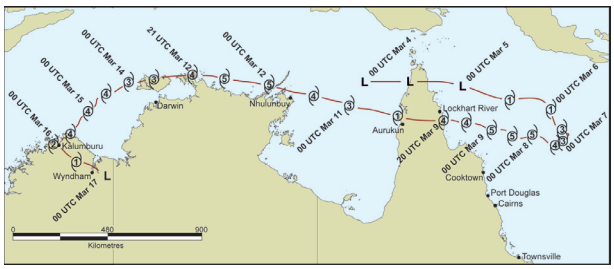

Fig. 4.22. Observed track of Tropical Cyclone Ingrid along the northern coast of Australia. [Courtesy: M. Foley and M. Lesley, Australian Bureau of Meteorology (BOM)]

d. Pacific intertropical convergence zone—A. B. Mullan[59]

Prominent rainfall and cloudiness maxima and OLR minima are associated with the Pacific ITCZ and the SPCZ. The Pacific ITCZ has its main branch in the Northern Hemisphere between 5° and 10°N, where it is strongest during June–August (Fig. 4.25). Between December and February, the ITCZ branches south of the equator, near 5°S, and is associated with the monsoon trough near Australia. Convection frequently extends northward from the monsoon trough across the equator in the region of the Maritime Continent. The southern ITCZ rarely extends

THE RECORD BREAKING 2005 ATLANTIC HURRICANE SEASON—G. D. Bell,[5] E. Blake,[8] K. C. Mo,[58] C. W. Landsea,[44] R. Pasch,[65] M. Chelliah,[15] S. B. Goldenberg,[29] And H. J. Diamond[19]

The 2005 Atlantic hurricane season was unprecedented and broke many tropical cyclone records. The season featured a record 27 tropical storms (previous record of 21 in 1933), a record 15 hurricanes (previously 12 in 1969), a record three category 5 hurricanes (previously two in both 1960 and 1961), a record estimated ACE Index (Bell et al. 2000) of 285% of the median, and a record ACE value of 131% of the median from named storms forming outside the MDR. The MDR is the tropical Atlantic and Caribbean Sea south of 21.5°N (Fig. 4.7, green box). The season also featured a record 15 named storms making landfall in the Atlantic basin. Seven of these made landfall in the United States, including a record four landfalling major hurricanes (categories 3–5 on the Saffir–Simpson scale; Simpson 1974). Also, a record seven named storms occurred during June–July, and a record 10 late-season storms formed after 1 October. Seven storms became major hurricanes during 2005, one shy of the 1950 record.

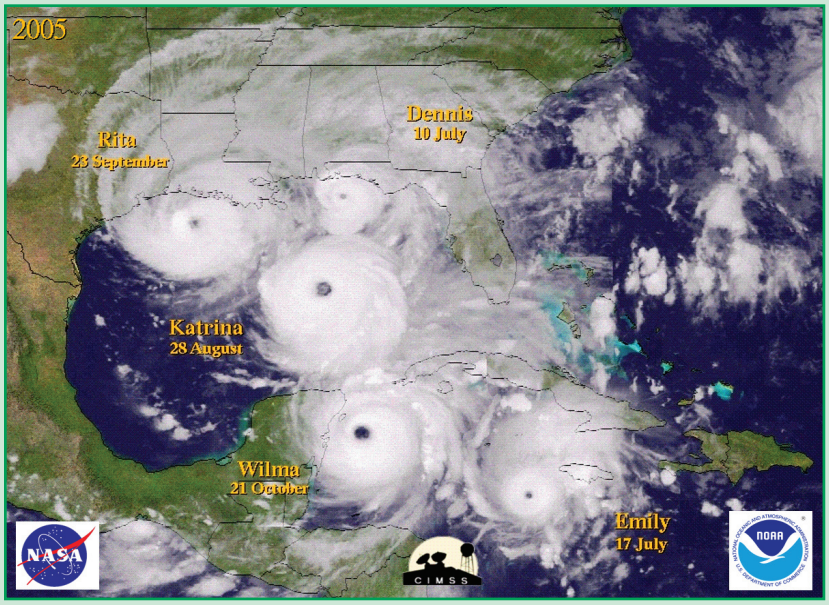

Fig. 4.23. Satellite montage of U.S. landfalling hurricanes. [Courtesy: C. Velden, University of Wisconsin—Madison, Cooperative Institute for Mesoscale Meteorological Studies (CIMMS)]

Two tropical storms, two hurricanes, and four major hurricanes struck the United States during 2005 (Fig. 4.23). These totals reflect the effects of H Ophelia on the Outer Banks of North Carolina.The devastating impacts of H Katrina on the central Gulf Coast in late August, one of the worst natural disasters ever to strike the United States, made the 2005 season the costliest season in the country's history, conservatively estimated at over $100 billion USD. Elsewhere, three tropical storms and three hurricanes (including Wilma) struck Mexico, one tropical storm made landfall in the Dominican Republic, and one hurricane struck Nicaragua. In Guatemala, Stan claimed over 1000 lives in mudslides and flooding. Wilma was the costliest natural disaster in Mexican history with estimated damage at $1–3 billion USD, eight deaths, and a reported 1637 mm (64 in.) of precipitation recorded on Isla de Mujeras. The number of additional monthly and individual records is too numerous to list here, but several are of particular note:

- Since the inception of the current naming system in 1953, this year was the first time the Greek letter naming convention was used.
- Dennis became the most intense hurricane on record before August when a central pressure of 930 hPa was recorded.
- Emily eclipsed the record set by Dennis for the lowest pressure recorded for a hurricane before

eastward of about 160°W, except during March and April when it can reach 90°W. High-resolution Tropical Rainfall Measuring Mission (TRMM) rainfall data show that the southern ITCZ is particularly prominent east of 160°W in La Niña years, such as 1999/2001.

Near the date line, the southern ITCZ merges with the SPCZ, which extends southeastward across the subtropical South Pacific. The SPCZ is most active in austral summer (December–February) and is located in a region of strong SST gradient south of the maximum SSTs. In contrast, the Northern Hemisphere ITCZ is located near the axis of maximum SSTs (Vincent 1998).

The northern ITCZ was continuous across the Pacific from 140°E to 90°W in almost all months except February (Fig. 4.25, top). Also during February, the SPCZ was extremely active from about 160°E to 160°W in association with more extensive equatorial westerlies and several tropical cyclones (see previous section). From May to August the northern ITCZ was positioned slightly equatorward of its normal location, and during June and August it was particularly active in the far eastern tropical Pacific between 120°W and 90°W (Fig. 4.25, bottom).

August when its central pressure reached 929 hPa.

- Vince was the first tropical cyclone in recorded history to strike the Iberian Peninsula. While Alberto (1988) was the most northerly and Ginger (1967) the most easterly, Vince was the most northeasterly, and was also the furthest east when it became a hurricane.
- Wilma's central pressure dropped to 882 hPa, which was the lowest pressure ever measured in the Atlantic basin, eclipsing the old record of 888 hPa set by H Gilbert in 1988.
- Zeta tied Alice (1954) for latest naming (30 December), and was the longest lived into January (6 January).

The activity of the 2005 season is attributed to four main factors: 1) long periods of anomalous upper-level convergence and suppressed convection over the central tropical Pacific, reminiscent of La Niña conditions; 2) record warm sea surface temperatures across the MDR; 3) the ongoing tropical multidecadal signal; and (4) exceptionally conducive upper-level and lower-level wind and air pressure patterns over the western Atlantic and Gulf of Mexico.

NOAA's ACE Index is a measure of seasonal activity that accounts for the combined strength and duration of tropical storms and hurricanes during the season (Fig 4.24; Bell et al. 2000). ACE is calculated by summing the squares of the 6-h maximum sustained wind speed in knots for all periods while the system is a tropical storm, subtropical storm, or hurricane. The 2005 ACE value was a record 249 $\times 10^4$ kt^2 (285% of the 1951–2000 median value). The 2005 season marks a continuation of the current active hurricane era that began in 1995. The historical time series of the ACE Index indicates large multidecadal fluctuations in seasonal activity (Goldenberg et al. 2001; Bell and Chelliah 2006). During the 11-yr period from 1995 to 2005, seasons have averaged 14.7 TSs, 8.4 Hs, and 4.1 MHs, and every season has been classified by NOAA as above normal except for the two El Niño years of 1997 and 2002. In contrast, seasons during the below-normal period 1971–94 averaged only 9 TSs, 5 Hs, and 1.5 MHs, with only three seasons classified as above normal (1980, 1988, 1989). These large differences between the above-normal and below-normal eras result almost entirely from differences in the number of tropical storms that form in the MDR and eventually become hurricanes and major hurricanes (Landsea 1993; Goldenberg et al. 2001).

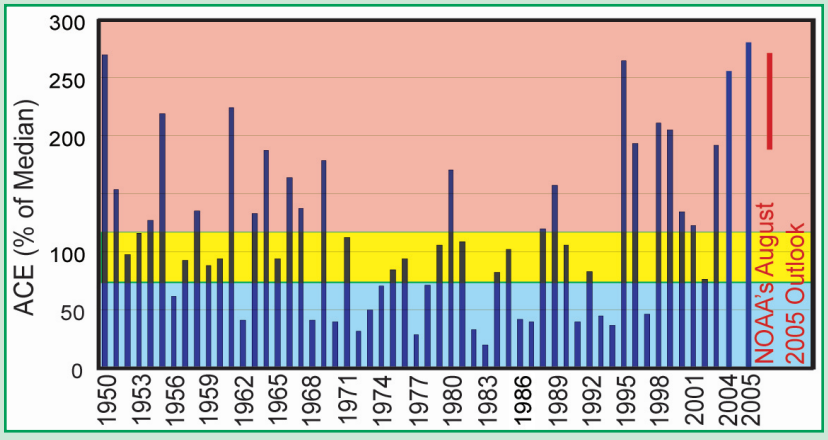

Fig. 4.24. ACE Index expressed as percent of the 1951–2000 median value. Season types are indicated by the background shading, with pink, yellow, and blue approximating above-, near-, and below- normal seasons, respectively.

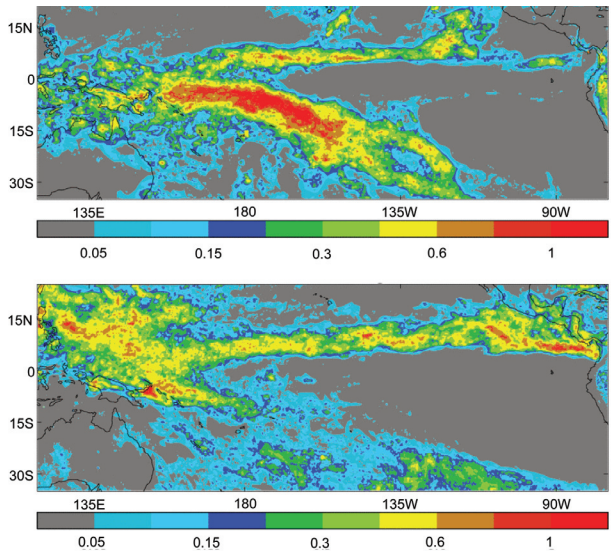

Fig. 4.25. Average rainfall rate (mm h^{-1}) from TRMM 0.25° analysis for (top) February and (bottom) August 2005. Contours are unevenly spaced at 0.05, 0.10, 0.15, 0.20, 0.30, 0.40, 0.60, 0.80, and 1.00 mm h^{-1}.

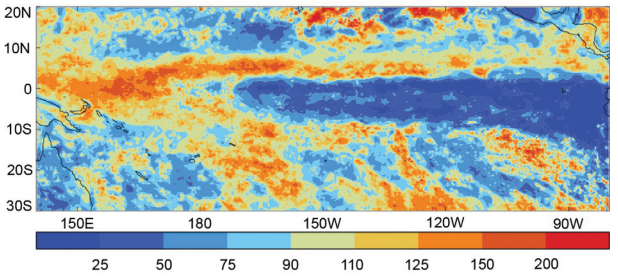

Fig. 4.26. Annual average rainfall rate (mm h^{-1}) from TRMM 0.25° analysis for 2005, as a percentage of the 1998–2004 mean.

For the year as a whole, high-resolution TRMM rainfall data (0.25° latitude × 0.25° longitude grid) suggest that precipitation was slightly above the 1998–2004 average in the northern ITCZ (Fig. 4.26), and also in the southern ITCZ and SPCZ to about 160°W.

5. THE POLES—A. M. Waple[89], Ed.

a. Overview—A. M. Waple[89] and J. Richter-Menge[74]

The permanent presence of sea ice, ice sheets, and continuous permafrost are unique features of the polar regions. The Arctic is further distinguished because it sustains human and wildlife populations in a harsh environment, as documented in the Arctic Climate Impact Assessment published in November 2004 (online at www.acia.uaf.edu). These characteristics amplify the impact of climate change on the region's physical, ecological, and societal systems. Such impacts reach beyond the Arctic region. For instance, studies are underway to determine the extent to which the loss of sea ice cover and the conversion of tundra to larger shrubs and wetlands, observed to have occurred over the last two decades, have impacted multiyear persistence in the surface temperature fields, especially in the Pacific sector.

In this section, observations that indicate continuing trends in the current state of physical components of the Arctic system, including the atmosphere, ocean, sea ice cover, and land, are discussed. The temporal extent of the data provides a multidecadal perspective and confirms the sensitivity of the Arctic to changes in the global climate system. The destabilization of several known relationships between climate indices (e.g., Arctic Oscillation) and Arctic physical system characteristics (e.g., continued reduced sea ice cover and increased greenness of the tundra) presents an intriguing and significant puzzle with respect to the contemporary global climate system.

It was one of the warmest years on record for Greenland, with an especially warm and foggy spring. Surface temperature and ice melt are discussed for Greenland in the context of a warming trend over the nation.

Also, trends and observations in temperature, sea ice, and stratospheric ozone depletion are discussed with respect to Antarctica. As the continent with more than 70% of Earth's freshwater storage, trends in Antarctic climate are of critical importance in determining the long-term impact of climate change.

b. Arctic—J. Richter-Menge,[74] J. Overland,[62] A. Proshutinsky,[68] V. Romanovsky,[77] J. C. Gascard,[25] M. Karcher,[37] J. Maslanik,[52] D. Perovich,[66] A. Shiklomanov,[83] and D. Walker[87]

1) Atmosphere

(i) Circulation regime

The annually averaged AO index in 2005 was slightly negative, continuing the trend of a relatively low and fluctuating index that began in the mid-1990s (Fig. 5.1). This follows a strong positive pattern from 1989 to 1995. Current characteristics of the AO are more consistent with the period from the 1950s to the 1980s, when the AO switched frequently between positive and negative phases.

(ii) Surface temperatures

In 2005, annual average surface temperatures over land areas north of 60°N remained above the mean value for the twentieth century (Fig. 5.2), as they have since the early 1990s. Figure 5.2 also shows warm temperatures in the 1930s and early 1940s, possibly suggesting a longer-term oscillation in climate. However, a detailed analysis shows different proximate

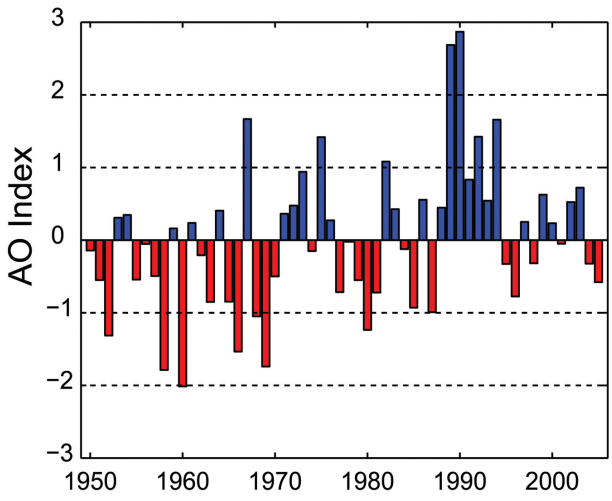

Fig. 5.1. Time series of the annually averaged AO Index for the period 1950–2005, based on data from the following Web site: www.cpc.ncep.noaa.gov. [Courtesy: I. Rigor]

causes and characteristics for the 1930s compared to the 1990s maxima. The early warm anomalies appear to be characterized by large region-to-region differences and are limited to high latitudes (Johannessen et al. 2004; Overland et al. 2004). The warm anomalies since the 1990s tend to be Arctic-wide and reach into the midlatitudes.

Near-surface air temperatures in boreal winter and spring 2005 continued to have the same general spatial pattern of warm anomalies as that of 2000–04 (Fig. 5.3a). The first major feature is positive (warm) anomalies over the entire Arctic, consistent with Fig. 5.2. The second feature is the strong maxima north of eastern Siberia and around the Davis Strait. Spring anomalies (March–June) over the last 6 yr for these coastal areas are near 3°–4°C. The region north of eastern Siberia is also a main location for loss of sea ice cover over the last decade. While the Arctic-wide pattern of positive anomalies was established in the early 1990s, the locations of the 2000–05 temperature anomaly maxima (consistent with the 2005 pattern shown in Fig. 5.3a) contrast with those of the early 1990s (Fig. 5.3b).

The current pattern of near-surface temperature anomalies (2000–05) is distinctly different from the near-surface temperature anomaly patterns associated with the two major atmospheric circulation patterns that characterized the second half of the twentieth century (Quaddrelli and Wallace 2004). The positive phases of these patterns were present during 1989–95 (Fig. 5.3b) and 1977–88 (Fig. 5.3c) and were associated with the AO and Pacific–North American (PNA) indices, respectively. A strong AO climate pattern characterized the late 1980s and early 1990s (Fig. 5.1), with associated temperature anomaly maxima in northern Europe and north-central Asia in winter (Fig. 5.3b), which expanded to northern Alaska in spring. As part of the positive AO pattern, west Greenland was anomalously cold. A positive PNA pattern was dominant from 1977 to 1988, with warm temperature anomalies over northern North America (Fig. 5.3c). The contrast of recent near-surface temperature anomalies, with maxima in west Greenland and northeast Siberia, to the temperature patterns associated with the AO and PNA suggest that the current atmospheric circulation pattern is also different from the main patterns of the second half of the twentieth century (Overland and Wang 2005).

ii) Arctic Ocean

(i) Surface circulation regime

The circulation of the sea ice cover and ocean surface layer are closely coupled and are primarily wind driven. Data from satellites and drifting buoys indicate that the entire period of 2000–05 has been characterized by an anticyclonic circulation regime due to a higher sea level atmospheric pressure over the Beaufort Gyre, relative to the 1948–2005 mean. The dominance of the anticyclonic regime is consistent with the AO index, which has exhibited relatively low and fluctuating values since 1996 (Fig. 5.1).

(ii) Heat and freshwater content

In recent years the heat and freshwater content of the Arctic Ocean have changed dramatically relative

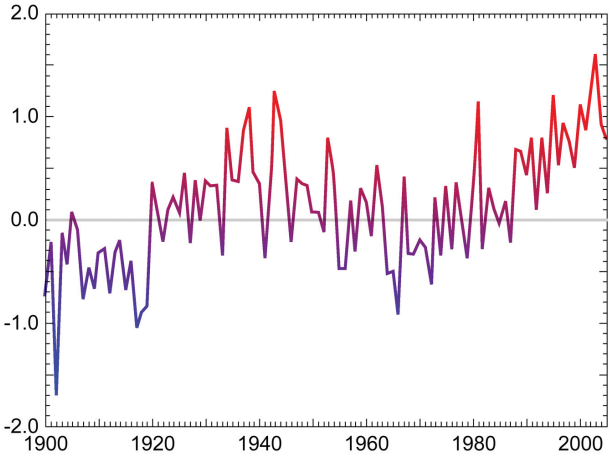

Fig. 5.2. Arctic-wide (60°N–90°) annual average surface air temperature anomalies (°C) over land for the twentieth century based on the Climate Research Unit (CRU) TEM2V monthly dataset.

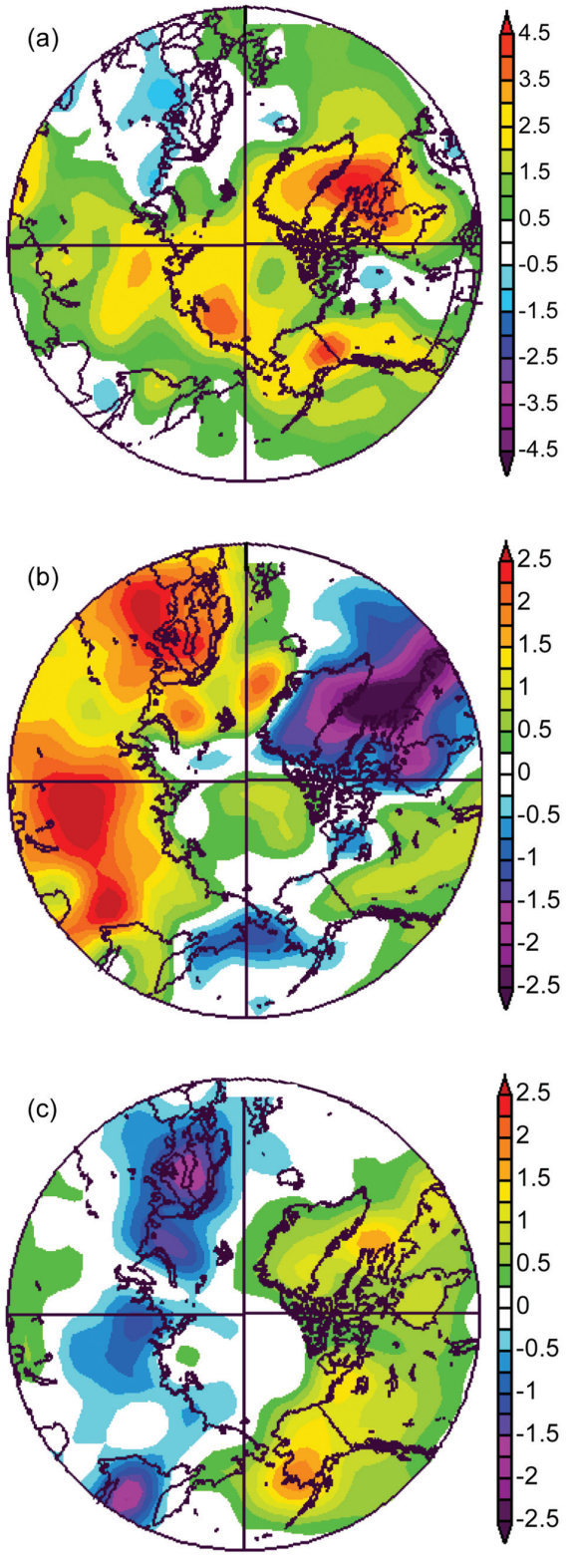

Fig. 5.3. 1000-hPa temperature anomalies (°C) for (a) March–June 2005 (relative to the 1968–98 mean), (b) December–March 1989–95, when the positive AO was strong, and (c) December–March 1977–88, when the positive PNA was strong. [Source: NCEP/NCAR reanalysis; online at www.ncdc.noaa.gov]

to averages established by the Arctic Ocean Atlas of the Arctic Climatology Project (1997), where water temperature and salinity from observations were averaged and gridded for the decades of the 1950s, 1960s, 1970s, and 1980s (Fig. 5.4). From 2000 to 2005, the western Arctic has been the focus of intensive investigation. This region includes the Beaufort Gyre, which is the major reservoir of freshwater in the Arctic Ocean. Although the total freshwater content in the Beaufort Gyre has not changed dramatically, there is a significant change in its distribution (Figs. 5.4c,d). The center of the freshwater maximum has shifted toward Canada and intensified relative to the average. Significant increases were also observed in the heat content of the Beaufort Gyre (Figs. 5.4a,b), primarily because of an approximately twofold increase of the Atlantic layer water temperature (Shimada et al. 2004).

The heat and freshwater content of the Arctic Ocean depends on inputs along open boundaries. The most important are fluxes in the Fram and Bering Straits. An increase of the Atlantic water temperature in the Fram Strait was observed in 2004 (Polyakov et al. 2005). In the Bering Strait region, preliminary observations from a mooring site, established and maintained since 1990, suggest that the annual mean water temperatures have been about a degree warmer since 2002, compared to 1990–2001. Since 2001, there has also been an increase in the annual mean transport. Combined, these changes have resulted in an increased northward heat flux through the Bering Strait in recent years (R. Woodgate, K. Aagaard, and T. Weingartner 2005, personal communication).

(iii)Sea level

There is a positive sea level trend along Arctic coastlines (Fig. 5.5). For 1954–89 the rate of sea level rise was estimated as +0.185 cm yr^{-1} (Proshutinsky et al. 2004). The addition of 1990–2004 data increases the estimated rate to 0.191 cm yr^{-1}. Arctic sea level also correlates relatively well with the AO index ($r = 0.83$). Consistent with the influences of AO-driven processes, Arctic sea level dropped significantly after 1990 and increased after the change from cyclonic to anticyclonic circulation in 1997. In contrast, from 2000 to 2004 the rate of sea level rise has increased in spite of a steady decrease in the AO index. At this point, because of substantial interannual variability, it is difficult to evaluate the significance of this change.

III) Sea ice cover

(i) Extent and thickness

During 2005, every month except May showed a record minimum sea ice extent in the NH relative

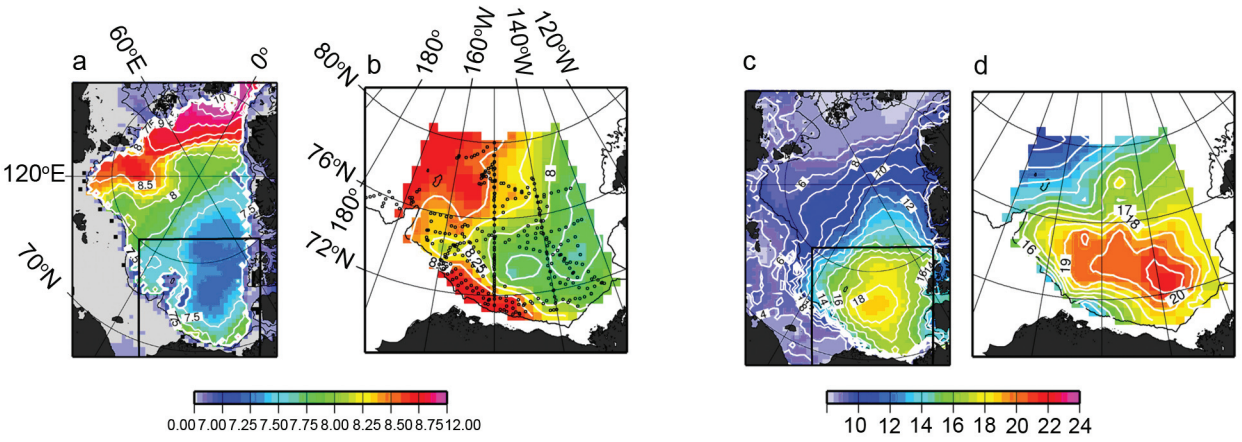

FIG. 5.4. Summer (a), (b) heat (x 10^{10} J m^{-2}) and (c), (d) freshwater (m) content. (a), (c) Heat and freshwater content in the Arctic Ocean based on 1980s averages (Arctic Climatology Project 1997). (b), (d) Heat and freshwater content in the Beaufort Gyre [outlined in black in (a) and (c)] in 2000–05 based on hydrographic surveys (black dots depict locations of hydrographic stations). Heat content is calculated relative to the freezing point in the upper-1000-m ocean layer. Freshwater content is calculated relative to reference salinity of 34.8 psu.

to the period 1979–2005 (J. Stroeve 2006, personal communication). This time period is defined by the availability of passive microwave images of sea ice extent in the NH. The extent of the sea ice cover is at or near its maximum in March and its minimum in September (Fig. 5.6). Ice extent in March 2005 was 14.8 million km^2, decreasing to 5.6 million km^2 in September 2005, compared to the mean (1979–2005) ice extent for March and September of 15.7 million km^2 and 6.9 million km^2, respectively. It is notable that in March 2005, ice extent fell within the mean contour at almost every location. In September 2005, the retreat of the ice cover was particularly pronounced along the Eurasian and North American coastlines.

To put the 2005 minimum and maximum ice extent into context, the variability of ice extent in March and September for the period of 1979–2005 is presented in Fig. 5.7. In both cases, a negative trend is apparent, with a rate of 2% $decade^{-1}$ for March and 7% $decade^{-1}$ for September. Furthermore, the summers of 2002–05 have experienced an unprecedented series of extreme ice extent minima (Stroeve et al. 2005).

Ice thickness is intrinsically more difficult to monitor. With satellite-based techniques only recently introduced, observations have been spatially and temporally limited (Laxon et al. 2003; Kwok et al. 2004). Data from submarine-based observations indicate that at the end of the melt season the permanent ice cover thinned by an average of 1.3 m between the period 1956–78 and the 1990s, from 3.1 to 1.8 m (Rothrock et al. 1999). On the other hand, measurements of the seasonal ice cover do not indicate any statistically significant change in thickness in recent decades (Melling et al. 2005; Haas 2004; Polyakov et al. 2003).

Trends in the extent and thickness of ice cover are consistent with observations of a significant loss of older, thicker ice out of the Arctic via the Fram Strait (e.g., Rigor and Wallace 2004; Pfirman et al. 2004; Yu et al. 2004) in the late 1980s and early 1990s. This event coincides with the strong, positive AO period from 1989 to 1995 (Fig. 5.1). When the AO is positive, atmospheric and oceanic conditions favor a thinner ice cover. A relatively younger, thinner ice cover, like the one left behind from this event, is intrinsically more susceptible to atmospheric or oceanic warming.

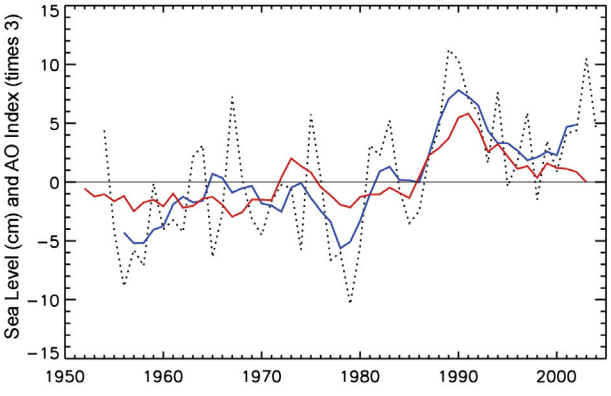

FIG. 5.5. Annual mean relative sea level (cm) from nine coastal tide gauge stations in the Siberian Seas (dotted line). The blue line is the 5-yr running mean sea level. The red line is the 5-yr running mean AO index (multiplied by 3 for comparison).

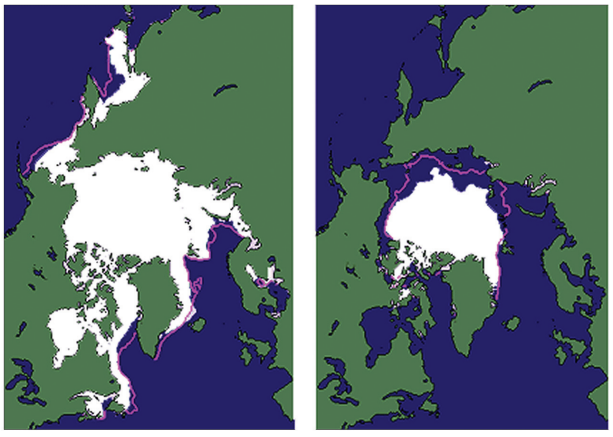

FIG. 5.6. Sea ice extent in (left) March and (right) September 2005, when the ice cover was at or near its maximum and minimum extent, respectively. The magenta line indicates the median maximum and minimum extent of the ice cover, for the period 1979–2000. [Source: NOAA/National Snow and Ice Data Center (NSIDC)]

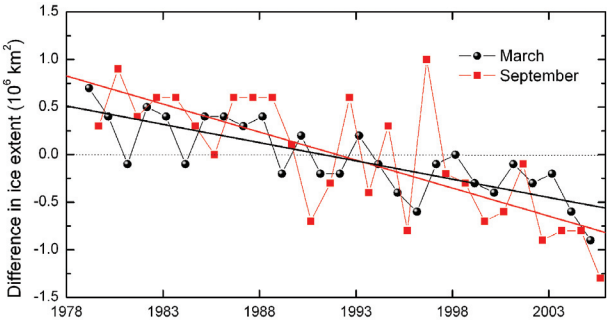

FIG. 5.7. Time series of the variability of ice extent in March (maximum) and September (minimum) for the period 1979–2005, normalized by the respective monthly mean ice extent for the period 1979–2005. Based on a least-squares linear regression, the rate of decrease in March and September was 2% decade^{-1} and 7% decade^{-1}, respectively.

(ii) Sea ice surface conditions

Data from 1982 to 2004, derived from AVHRR Polar Pathfinder extended (APP-x) products (updated from Wang and Key 2005a,b), indicate an overall negative trend for boreal summer (June–August) mean albedo of –0.4% yr^{-1} (Fig. 5.8a). The trend increases slightly to –0.5% yr^{-1} for the period from April through September (Fig. 5.8b), suggesting a possible increase in the duration of the melt season. In both cases, the surface albedo is relatively low from 2001 to 2004 and is consistent with observations of an earlier, more spatially extensive onset of melt and decrease in ice concentration (Belchansky et al. 2004, Stroeve et al. 2005).

The time series of APP-x annual mean skin temperatures (Fig. 5.8c) over the same period shows less consistent change over time, with a general increase in annual mean temperatures through the early 1990s and a decrease from 1995 onward. When the time series is limited to boreal spring (March–May) temperatures, the 23-yr linear trend is positive (0.14°C yr^{-1}), with greater interannual variability (Fig. 5.8d), indicative of the seasonal dependence of warming trends.

Large regional variability, typical of Arctic conditions, is observed in albedo, skin temperature, and ice concentration (Cavalieri et al. 1996). From 1996 to 2004, the largest decreases in surface albedo correspond to a reduction in ice extent in the Beaufort and Chukchi Seas. Lower albedos over the central ice pack appear consistent with the lower total ice concentrations over this same period.

IV) LAND

(i) Vegetation

The most convincing evidence of widespread change in Arctic vegetation comes from the historic

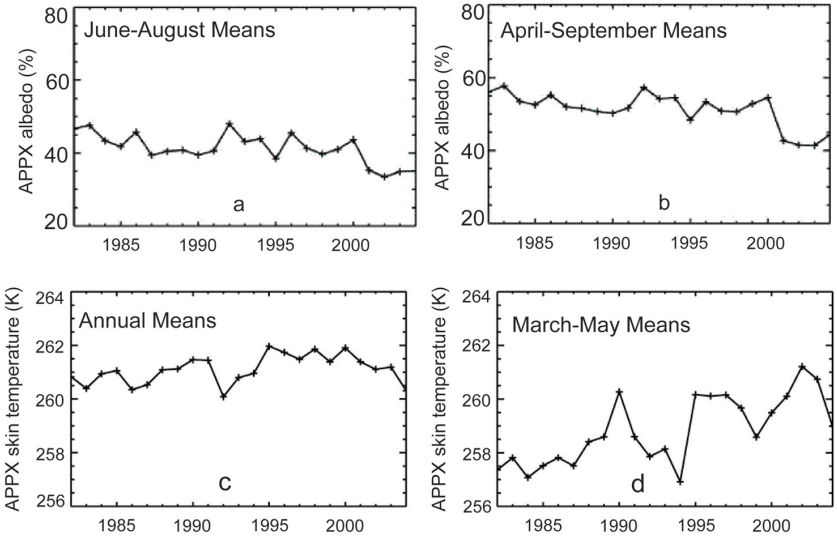

FIG. 5.8. APP-x (a), (b) surface albedo and (c), (d) skin temperature for areas between 60°N and 90° and ice concentrations of 15%–100% averaged over (a) June–August, (b) April–September, (c) January–December, and (d) March–May through 2004.

trends of tundra greenness as detected from satellites. The NDVI is a measure of vegetation greenness derived from surface reflectance in the red and near-infrared wavelengths. Higher-latitude NDVI values might be expected to increase under a warmed climate. Earlier global studies of NDVI changes indicated a general pattern of increased NDVI in the region between 40° and 70°N during the period of 1981–99 (Myneni et al. 1997, 1998; Zhou et al. 2001; Lucht et al. 2002). Studies of the NDVI indicate an increase of 17% in NDVI values in the tundra area of northern Alaska where the summer warmth index (SWI) values at meteorological stations have been increasing by 0.16° to 0.34°C yr^{-1} (Fig. 5.9) during the same period (Jia et al. 2003).

A more recent analysis covering the boreal forest and tundra region of North America indicates that different patterns of greening have occurred in the boreal forest and tundra areas (Goetz et al. 2005). The NDVI has increased in tundra regions by an average of about 10% for all of North America, whereas the NDVI has declined in the boreal forest regions particularly during the past 10 years.

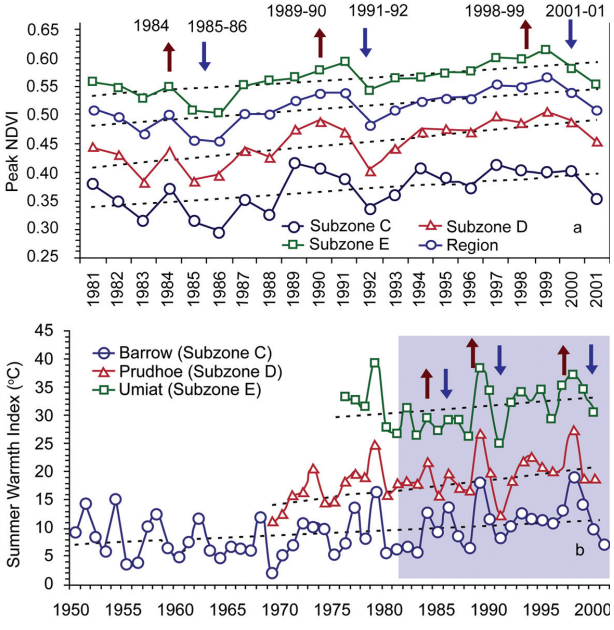

Fig. 5.9. (a) Peak NDVI derived from 8-km-resolution AVHRR data from 1981 to 2001 among the bioclimate subzones and for the whole Arctic slope. (b) Summer warmth index (SWI; °C) over the past 22–50 years at meteorological stations in each bioclimate subzone. Dashed lines are linear regressions. The shaded area in (b) highlights the period of SWI covered by the NDVI data in (a). The arrows show years of corresponding increases (red) and decreases (blue) in NDVI and SWI (from Jia et al. 2003).

(ii) Water

The R-ArticNet river discharge database (available online at www.R-Arcticnet.sr.unh.edu) was extended up to 2004 for 48 downstream river gauges. The last 5 years were characterized by an increase of total discharge to the Arctic Ocean mainly due to a contribution from Asian rivers. Mean 2000–04 discharge from Asia was 110 km^3 (5%) higher than over the previous 20 years. The mean discharge to the ocean from North America and Europe for 2000–04 was practically unchanged relative to 1980–99. A consistent increase in river discharge is observed from Eurasia for a longer time interval as well. The maximum total discharge of the six largest Eurasian rivers over 1936–2004 was observed in 2002, at 2080 km^3 yr^{-1} (Fig. 5.10). Mean discharge over 2000–04 for the large Eurasian rivers was 3%–9% higher than the discharge over 1936–2004. Thus, the contemporary data further confirm the presence of a significant increasing trend in the freshwater discharge to the Arctic Ocean from Eurasia documented earlier by Peterson et al. 2002 (Fig. 5.10).

(iii)Permafrost

Observations show a general increase in permafrost temperatures during the last several decades in Alaska (Osterkamp and Romanovsky 1999; Romanovsky et al. 2002; Osterkamp 2003), northwest Canada (Couture et al. 2003; Smith et al. 2003), Siberia (Pavlov 1994; Oberman and Mazhitova 2001; Romanovsky et al. 2002; Pavlov and Moskalenko 2002), and Northern Europe (Isaksen et al. 2000; Harris and Haeberli 2003). Uninterrupted permafrost temperature records over more than 20 years have been obtained by the University of Alaska–Fairbanks along the International Geosphere–Biosphere Pro-

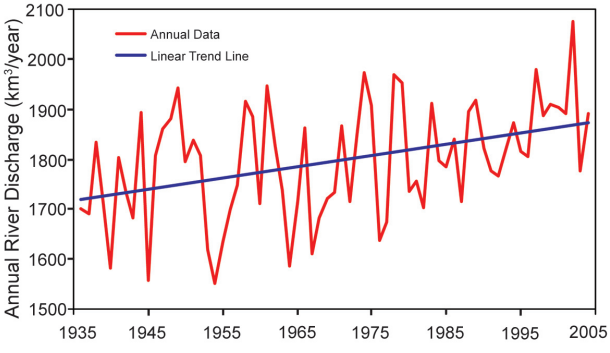

Fig. 5.10. Total annual discharge (km^3 yr^{-1}; red) to the Arctic Ocean from the six largest rivers in the Eurasian pan-Arctic for the observational period 1936–2004 (updated from Peterson et al. 2002). The least squares linear increase (blue) was 2.3 (km^3 yr^{-1}) yr^{-1}.

gramme (IGBP) Alaskan transect, which spans the entire continuous permafrost zone in the Alaskan Arctic. All observatories show a substantial warming during the last 20 years. This warming varied by location, but ranged typically from 0.5° to 2°C at the depth of zero seasonal permafrost temperature variations (Fig. 5.11).

These data also indicate that the increase in permafrost temperatures is not monotonic. During the observational period, relative cooling has occurred in the mid-1980s, in the early 1990s, and then again in the early 2000s. As a result, permafrost temperatures at 20-m depth experienced stabilization and even a slight cooling during these periods. An even more significant cooling of permafrost was observed during the very late 1990s and the early 2000s in interior Alaska. A significant portion of this cooling is related to a shallower-than-normal winter snow cover during this period. During the last three years, there was a sign of recovery in mean annual temperatures at shallow depths. Soil temperatures in interior Alaska during 2005 reached the temperatures of the early to mid-1990s, which were the warmest from during the last 70 years.

Data on changes in active layer thickness (ALT) in the Arctic lowlands are less conclusive. In the North American Arctic, ALT experiences substantial interannual variability, with no discernible trends; this is likely due to the short length of historical data records (Brown et al. 2000). A noticeable increase in the active layer thickness was reported for the Mackenzie Valley (Nixon et al. 2003). However, this positive trend became negative at most of these sites after 1998 (Tarnocai et al. 2004). An increase of more than 20 cm in thickness between the mid-1950s and 1990, derived from the historical data collected at Russian meteorological stations, was reported for the continuous permafrost regions of the Russian Arctic (Frauenfeld et al. 2004; Zhang et al. 2005). At the same time, reports from several specialized permafrost research sites in central Yakutia show no significant changes in the ALT (Varlamov et al. 2001; Varlamov 2003). The active layer was especially deep in 2005 in interior Alaska. Around Fairbanks, the 2005 active layer depth was the deepest observed in the past 10 years. Data from many of these sites show that the active layer that developed during the summer of 2004 (one of the warmest summers in Fairbanks on record) did not completely freeze during the 2004/05 winter. A thin layer just above the permafrost table remained unfrozen during the entire winter.

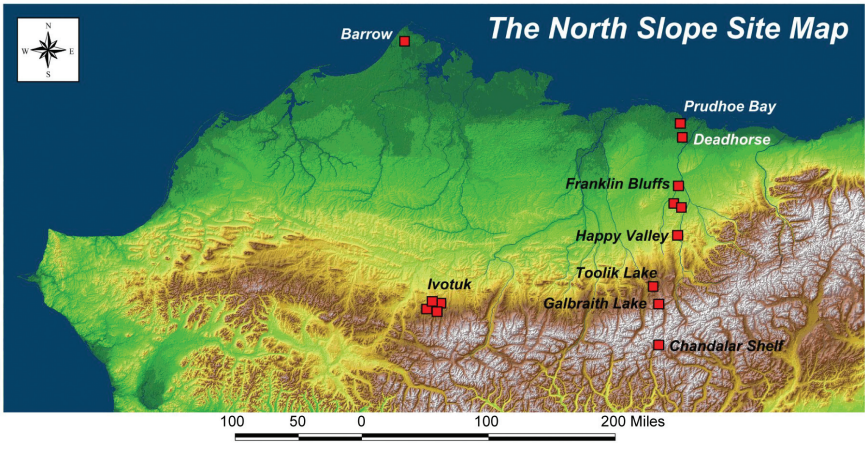

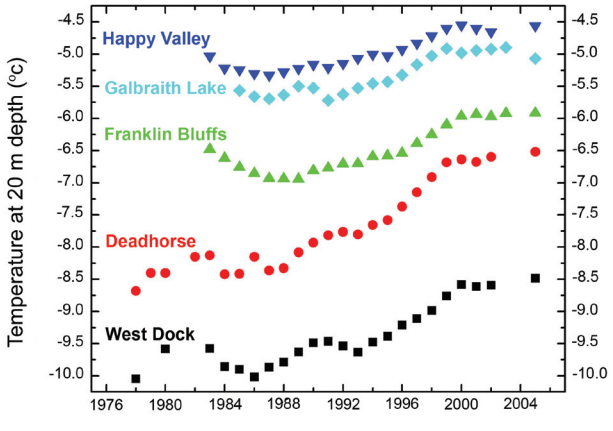

Fig. 5.11. (top) Location of the long-term University of Alaska permafrost observatories in northern Alaska 1978–2005. (right) Changes in permafrost temperatures (°C) at 20-m depth during the last 20–25 years (updated from Osterkamp 2003).

v) Greenland—J. E. Box[10]

(i) Overview

Temperatures in 2005 around Greenland were anomalously warm, particularly in boreal spring. In the period of record that includes three stations that began observations in the late 1800s, mean 2005 temperatures are rivaled only by recent years (e.g., 2003) and by warm conditions during the 1930s/40s. Unprecedented spring coastal fog caused flight delays along western Greenland that made European headlines. Widespread positive sea surface temperature anomalies surrounded Greenland for all seasons of 2005, according to the NOAA

SST OI version 2 (OIV2) dataset (1982–2005; available online at www.cdc.noaa.gov/cdc/data.noaa.oisst.v2.html). Upper-air temperature soundings available from the NCDC Integrated Global Radiosonde Archive (IGRA; Durre et al. 2006) indicate a pattern of tropospheric warm and stratospheric cool anomalies over Greenland, particularly in boreal winter.

(ii) Coastal temperature records

Although the coastal location of most meteorological stations makes it difficult to construct a representative climatology of temperature for Greenland, the existing 55-yr (1951–2005) record allows the annual mean temperatures of 2005 to be placed into historical context being as among the warmest, if not the warmest, on record (Table 5.1; see also Fig. 6.30). In northeast Greenland (Danmarkshavn) winter temperatures were among the warmest on record (99th percentile). Boreal spring was also unusually warm. Annual mean temperatures at all stations fell within the warmest decile (10%) of a normal distribution.

(iii)Greenland Ice Cap

Due to the paucity of regular observations of the Greenland Ice Cap, analysis of its behavior must necessarily be estimated by numerical modeling. Polar fifth-generation Pennsylvania State University (PSU)–National Center for Atmospheric Research (NCAR) Mesoscale Model (MM5) calculations (Box et al. 2006) indicate that increases in ice sheet melting exceeded increased snow accumulation in 2005, yielding a large (76%) negative surface mass balance anomaly (Table 5.2). In addition to precipitation increases, more of the precipitation was solid, despite a 1°C overall warm anomaly, suggesting that the upper elevations of the ice sheet received more snowfall than usual. Evaporation rates were 30% greater than normal, driven by warmer-than-normal average air temperatures. Blowing snow sublimation was slightly below normal due to decreased snow entrainment by the wind as a result of increasing melt duration (i.e., 10 days on average for the area below equilibrium line altitude). Meltwater production was 40% above normal owing to elevated summer temperatures and low-albedo positive feedback, which was particularly strong in August. Runoff rates were 45% above normal. Because of an apparent expansion of the ablation zone in this simulation, the accumulation area ratio was 7% below that of the most recent 17 years.

Previous observations have demonstrated accelerated ice sheet dynamic flow during surface melt water production (Zwally et al. 2002). Remote sensing measurements indicated widespread increases in glacier velocity south of 70°N (Rignot and Kanagaratnam 2006), confirming that flow rates did in fact increase in 2005. This suggests a Greenland Ice Sheet contribution to sea level that explains at least one-third of the observed recent accelerating global sea level rise (Leuliette et al. 2004).

c. Antarctic

1) ATMOSPHERIC CIRCULATION—A. Arguez[3]

The Southern Hemisphere annular mode (SAM; also known as the Antarctic Oscillation) is the Arc-

TABLE 5.1. Greenland station temperature statistics: 2005 versus 1951–2005.

Station Region	Location	Statistic	Winter	Spring	Summer	Autumn	Annual
Egedesminde	68.7 N	Rank	13	1	2	13	3
Central-west	52.8 W	*Z* score	–1.5	2.2	0.8	–0.1	1.9
Nuuk	64.2 N	Rank	N/A	1	10	19	N/A
Southwest	51.8 W	*Z* score	N/A	2.3	–1.4	0	N/A
Prins Christian Sund	60.0 N	Rank	7	1	1	17	1
South	43.2 W	*Z* score	–0.7	3.3	2.6	–0.3	2.4
Tasiilaq	65.6 N	Rank	7	2	2	34	3
Southeast	37.6 W	*Z* score	0.6	2.1	0.9	–1.1	3.2
Danmarkshavn	76.8 N	Rank	1	4	6	26	1
Northeast	18.7 W	*Z* score	2.8	–0.1	–0.8	0	2.6

Table 5.2. Greenland ice sheet surface mass balance parameters: 2005 departures from 1988 through 2004 average.

	% of 1988–2004 average	2005 minus 1988–2004 average [$km^3\ y^{-1}$]*
Total precipitation	110%	73
Liquid precipitation	107%	2
Evaporation	130%	21
Blowing snow sublimation	98%	–1
Snow accumulation	108%	52
Meltwater production	140%	238
Meltwater runoff	145%	206
Surface mass balance	24%	–153
Mean temperature	—	1.0°C
Accumulation area ratio	93%	–0.06

* Unless otherwise indicated.

tic Oscillation's (or Northern Hemisphere annular mode's) counterpart in the Southern Hemisphere. It is defined as the leading mode of 700-hPa height anomalies south of 20°S. Since early 2003, SAM positive and negative phase events have been uncharacteristically weak and ephemeral. During 2005, SAM values were fairly small except for a value of +1.2 in February and a considerably negative reading (–2.0) in December. However, weak values prevailed during the austral winter (Fig. 5.12).

ii) Temperature—A. M. Waple[89]

Surface air temperatures across the majority of stations on the Antarctic continent were near to above average in 2005, with the largest warming trends over the last several decades measured along the Antarctic Peninsula, for example, at the Rothera meteorological station (Fig. 5.13). Observed trends across the rest of the continent have been mixed, with interior stations such as Amundsen–Scott South Pole Station and Vostok showing small, significant trends in surface temperature. Not surprisingly, many stations in Antarctica are located near the more accessible coast and, therefore, deriving a representative continental temperature is virtually impossible. From the available temperature data, it is, perhaps, Antarctica's apparent continentwide temperature stability that is remarkable in the context of global warming. Only the Antarctic Peninsula (4% of the continental area)

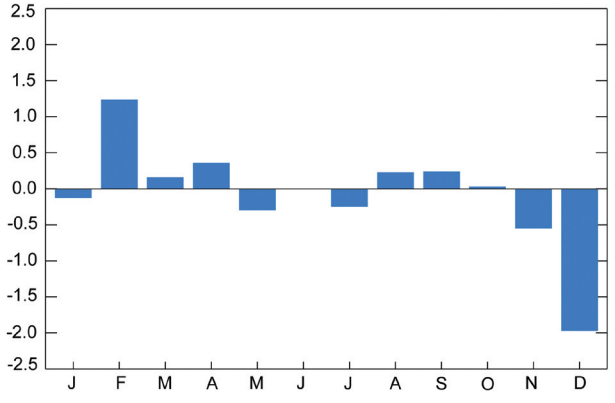

Fig. 5.12. Monthly values of the Southern Hemisphere annual mode index for 2005 (June value is missing).

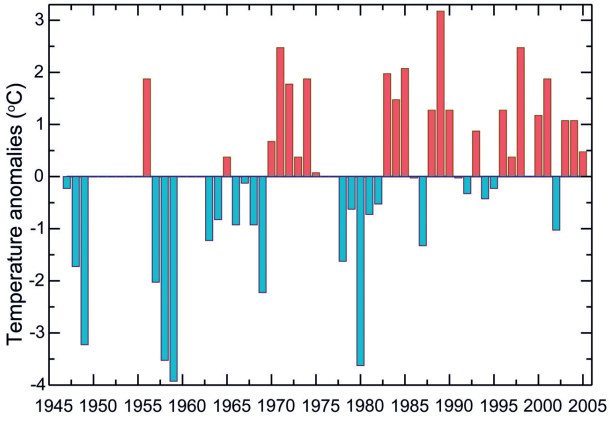

Fig. 5.13. Annual temperature anomalies from Rothera Meteorological Station on the Antarctic Peninsula. Base period is 1947–2005 and years without bars indicate unavailable data.

shows a significant warming trend. The peninsula is also the warmest area of the continent on average, rising above freezing for 2 months a year on its warmest coast (see information online at www.antarctica.ac.uk/About_Antarctica/Above_Antarctica/Weather/Temperature/index.php). Due to the paucity of stations on Antarctica, the lack of long-term records, and the high interannual temperature variability, it is impossible to state with certainty whether the Antarctic continent is warming or cooling overall. However, despite the lack of any clear warming signal in most coastal stations, there are indications that ice sheet thinning is occurring in west Antarctica and is considered a likely result of reduced buttressing by coastal ice shelves, which are melting or disintegrating, perhaps in response to coastal warming (e.g., Levinson 2005).

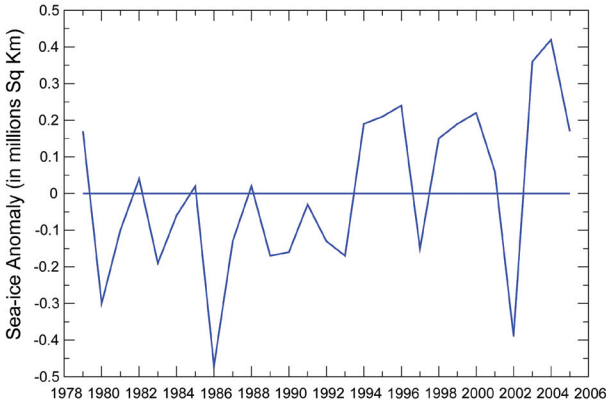

Fig. 5.14. Annual anomalies of Southern Hemisphere sea ice. Base period is 1979–2005. [Source: NOAA/NSIDC]

iii) Sea ice—A. M. Waple[89]

Southern Hemisphere sea ice extent has been increasing since the late 1970s (Fig. 5.14), with above-average extent in 2005. However, seasonal and spatial variability has been extreme in the Southern Hemisphere, with ice shelf and sea ice retreat occurring in those areas that have shown a warming trend over the last 50 years, such as the Antarctic Peninsula and Bellingshausen Sea (e.g., Vaughan and Doake 1996). The collapse of the Larsen A and Larsen B ice shelves in 1995 and 2002, respectively, indicate that pronounced regional warming can lead to ice shelf collapse and to glacial acceleration (Waple and Rignot 2005).

iv) Stratospheric Ozone—R. C. Schnell[81]

This year, 2005, was the 20th consecutive year of NOAA ozonesonde measurements at the Admunsen–Scott South Pole Station, and the NOAA/ESRL/Global Monitoring Division launched 68 balloon-borne ozonesondes in 2005. Figure 5.15a shows the total column ozone (blue line) in Dobson units and 20–24-km stratospheric temperature (red line), illustrating the development of the ozone hole over South Pole Station in 2005. The severity of ozone depletion depends on wintertime stratospheric temperatures, the stability of the polar vortex, and active chlorine levels. July and August profiles showed typical cold temperatures throughout the lower stratosphere, reaching a minimum of –92.3°C (180.9 K) on 10 July. The cold temperatures provided favorable conditions for the formation of polar stratospheric clouds that enable the transformation of Cl and Br compounds into species that destroy O_3 when sunlight returns to the Antarctic stratosphere. Total column O_3 remained stable until mid-August (Fig. 5.15b). Stratospheric O_3 declined to a minimum of 110 DU on 29 September, and was nearly completely destroyed in the 15–21-km layer (Fig. 5.15c). Compared to the years since 1986, 2005 was the 10th lowest for O_3 levels on record, with the record being 89 DU on 6 October 1993. Ozone abruptly increased to 333 DU on 13 November 2005 (Fig. 5.15d), due to midlatitude ozone-enriched air transported over the continent after the polar vortex began to break up.

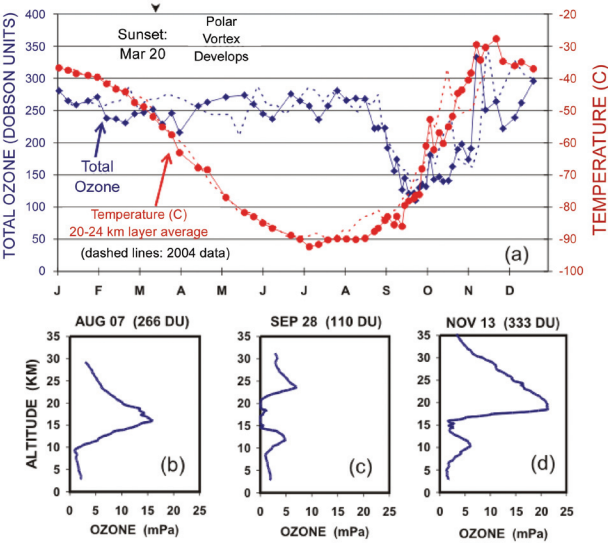

Fig. 5.15. (a) Summary of South Pole total ozone in Dobson units and stratospheric temperatures measured by ozonesondes during 2005. Three selected profiles of altitude vs ozone partial pressure (mPa) are shown (b) prior to the 2005 ozone hole, (c) at minimum total ozone, and (d) postozone hole. [Source: B. Johnson and S. Oltmans, NOAA/ESRL/GMD]

6. REGIONAL CLIMATES—K. A. Shein,[82] Ed.

a. *Overview*—K. A. Shein[82]

While the anomalous global warmth of 2005 is generally reflected in regional temperatures, various regions of the planet respond differently to climate forcings at many scales, both spatial and temporal. An analysis of globally averaged climate may mask a number of important climatic conditions that have impacted some areas more than others. This section chronicles regional climatic conditions relative to their historical context, and highlights notable atmospheric events of 2005. In fact, most regions experienced some form of record-breaking weather or climate conditions in 2005.

This section is distributed by continent or major land region, and each regional subsection is further divided into logical climatic divisions, either geographic or political. The use of national names in no way implies political preference or precedence. Also, it should be noted that while the large-scale temperature and precipitation anomaly maps (i.e., Figs. 6.1, 6.7, 6.16, 6.17, 6.24, 6.29, and 6.39) all use a 1971–2000 base period for temperature and a 1979–2000 base period for precipitation, discussions of anomalies in individual regions may refer to alternate base periods.

b. *Africa*

1) Eastern Africa—C. Oludhe,[61] P. Ambenje,[2] and L. Ogallo[60]

The rainy seasons in the Greater Horn of Africa (GHA) are influenced by the intra-annual north–south migration of the ITCZ. In the GHA region, rainfall exhibits strong variability both in space and time. Much of the variability is strongly accounted for by the existence of complex topographic features, including the East African lakes, and is also partly influenced by the movement of the ITCZ. The subregion can, however, be divided into three sectors (Southern, Equatorial, and Northern) based on rainfall onsets and withdrawals. The Southern sector (central and southern Tanzania) experiences a unimodal precipitation regime, with rain occurring between December and April. The Equatorial sector (northern Tanzania, Kenya, southern and extreme eastern Ethiopia, southern Sudan, and the southern half of Somalia) generally exhibits a bimodal rainfall regime, with the "Long Rains" season from March to May and the "Short Rains" extending from October to December. However, both the western and coastal areas also receive substantial rainfall during July and August. In the Northern sector (central and northern Ethiopia, Eritrea, Djibouti, and the northern half of Sudan), the major rainy season is between June and September, but a few areas receive a secondary peak from March to May.

The climate over the GHA is largely regulated by sea surface temperatures in the Indian and Atlantic

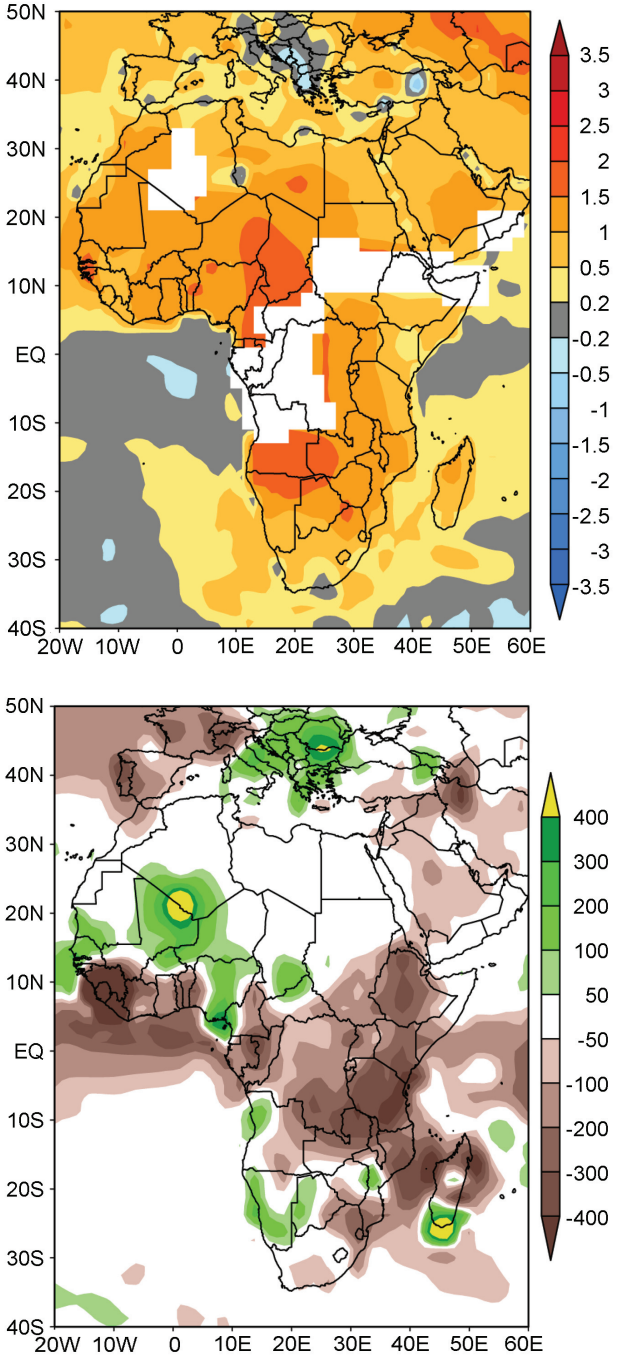

Fig. 6.1. African 2005 annual (top) temperature anomalies (°C; 1971–2000 base), and (bottom) precipitation anomalies (mm; 1979–2000 base) from the CAMS–OPI dataset (Janowiak and Xie 1999). [Source: NOAA/NCDC]

Oceans, general atmospheric circulation and large-scale anomalies (e.g., ENSO, Indian Ocean dipole), Indian Ocean tropical cyclone activity, and the variability of the monsoon.

(i) Climate patterns in the GHA in 2005

Parts of the GHA were under persistent drought throughout the year with most stations recording rainfall much below their long-term mean (Fig. 6.1). In some of the arid and semiarid lands (ASALs), no significant rainfall was recorded for the year. Erratic rainfall and poor temporal distribution was common during the rainy seasons, even in areas that recorded normal to above-normal precipitation.

Most socioeconomic and subsistence activities in the GHA depend directly or indirectly on rainfall. Below-average rainfall during the year had far-reaching socioeconomic impacts, including the loss of life, livestock, and property.

The Southern sector experienced abundant rainfall between December 2004 and February 2005, providing relief, especially in areas such as central and southern Tanzania that had experienced extremely dry conditions during the 2003/04 rainfall season.

From March to May 2005 (Long Rains), most locations over the Equatorial sector received near-normal to below-normal rainfall amounts. There was a general late onset and early withdrawal as well as poor temporal and spatial distribution of the seasonal rainfall in most areas of the sector, especially the ASALs.

The month-by-month evolution of the Drought Severity Index for the Long Rains season indicates that although near-normal to wet conditions were observed at some locations during March and May, long dry spells were predominant, especially during the peak rainfall month of April, which was relatively dry at many locations within the Equatorial sector. Occasional short-lived heavy rainfall events, some exceeding 50 mm in 24 h, significantly contributed to seasonal rainfall totals in some areas. Unfortunately, these events generated flash flooding in some parts of the GHA, displacing thousands of people.

Western and coastal areas of the Equatorial sector recorded significant rainfall from June to August, although totals were slightly below the seasonal average in some areas (Fig. 6.2).

From October to December (Short Rains), most parts of the Equatorial sector received between 25% and 75% of long-term seasonal mean precipitation (Fig. 6.2). Like the Long Rains, the Short Rains were also characterized by poor temporal distribution, and were devoid of the heavy rainfall events common during tropical rainy seasons. The rains ceased in the second half of November instead of the usual mid-December. Performance was extremely poor in the ASALs, enhancing the cumulative rainfall deficiencies these areas had been experiencing for several consecutive seasons. As a result, an estimated five million people in Kenya and Tanzania were affected by famine.

The Northern sector had one major rainfall peak concentrated in June–September, with few areas receiving the usual secondary rainfall peak between March and May. Near- to above-normal rainfall was observed in parts of western and northern areas of the subregion during June–August 2005 (Fig. 6.2). Most locations recorded June–September rainfall totals of 75%–125% of the long-term average. Much of the eastern and central parts of the Northern sector experienced dry conditions, with most locations recording rainfall below 75% of the long-term average.

ii) Northern Africa—M. A. Bell[6] and K. Kabidi[36]

(i) Temperature

For 2005, mean temperature anomalies were generally between 0.25° and 1.5°C above normal throughout most of North Africa (Fig. 6.1). The year started with below-normal monthly mean tempera-

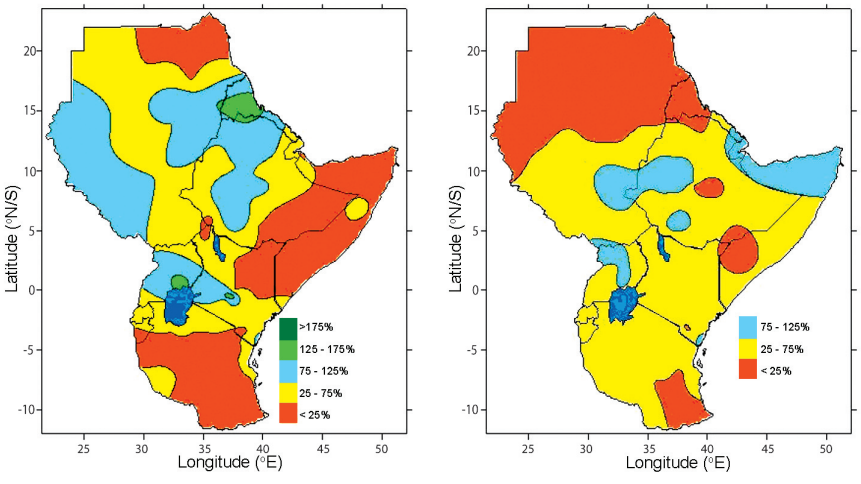

Fig 6.2. East African rainfall anomaly percentages for (left) June to August and (right) October to December 2005. [Source: Kenya Meteorological Service]

tures in January, and particularly in February. Chefchaouen, Morocco, recorded 18 below-freezing days in January. Subfreezing temperatures were recorded in many other areas and broke numerous records. A low of –14°C was recorded in a mountainous area of Morocco. By April, positive temperature anomalies had begun to dominate, and a heat wave in mid-July resulted in at least 13 deaths in Algeria due to sunstroke, according to the British Broadcasting Corporation (BBC). In Algeria, the heat wave pushed July temperatures as high as 50°C.

(ii) Precipitation

The Mediterranean coast of North Africa receives the majority of its rainfall during October–April, largely from midlatitude cyclones and associated cold fronts. In the Atlas Mountains of northern Morocco, Algeria, and Tunisia, cold-frontal passages can bring subfreezing temperatures and heavy rain or snow, occasionally causing floods and landslides.

Accumulated precipitation anomalies for the October 2004–April 2005 rainy season indicate below-normal precipitation totals in most of Morocco (particularly in the north), northwestern Algeria, the southern half of Tunisia, and much of northern Libya, and above-normal precipitation in northeastern Algeria and northern Tunisia (Fig. 6.3).

The precipitation deficits in Morocco developed in November 2004, in concert with the genesis of the severe drought that would plague the Iberian Peninsula and other sections of southwestern Europe for much of the year. Although rain in mid- to late-February provided some relief, dry conditions persisted throughout most of the remainder of the 2004/05 boreal winter rainy season in Morocco. October–December 2005 began the winter rainy season with near-normal precipitation throughout North Africa.

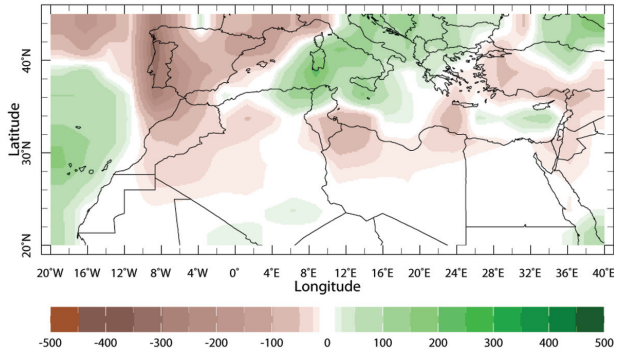

Fig. 6.3. October 2004–April 2005 precipitation anomalies (mm; 1979–2000 monthly means base) for northern Africa from CAMS–OPI.

As discussed in the CPC/Famine Early Warning System Network (FEWS NET) Africa Weekly Weather Hazards Assessments in 2005, although the cooler-than-normal temperatures early in the year may have temporarily reduced moisture demand and partially mitigated precipitation deficits in the major wheat-growing areas of North Africa, the persistence of below-normal rainfall and the development of positive temperature anomalies had a detrimental effect on the region's winter wheat crop, with grain production (including wheat) in 2005 was well below the previous year's record levels in Morocco, Algeria, and Tunisia, and also below the average of the past 5 yr in Morocco and Algeria [Source: U.S. Department of Agriculture (USDA) and United Nations (UN) Food and Agriculture Organization (FAO).]

(iii) Notable events

A winter storm in late January 2005 produced the heaviest snowfall seen in Algiers in "more than 50 years," according to the BBC, and was responsible for at least 10 deaths, primarily due to traffic accidents.

During February, a synoptic low pressure system brought heavy rainfall to the region, with a record of 193 mm falling in less than 24 h at Tetuan, Morocco. This system also brought high wind speeds exceeding 31 m s^{-1} in some places, and waves up to 10 m were recorded along the northwestern Atlantic coast (Fig. 6.4).

The most unusual climatic event recorded during 2005 was the landfall of Tropical Storm Delta. On 29 November, Delta passed to the north of the Canary Islands, where widespread damage and seven fatalities were reported. Soon after, Delta crossed over the southern coast of Morocco in the area of Tantan and Layoune Ports, where it quickly dissipated, but not before delivering much-needed rain to the area.

iii) Southern Africa—W. M. Thiaw,[85] T. Gill,[27] and W. A. Landman[43]

(i) Temperature

Annual mean temperatures across southern Africa for 2005 were generally 0.5°–1.5°C above the 1971–2000 mean (Fig. 6.1). Most of Madagascar was 0.5°–1.0°C above normal. Temperatures were up to 2°C above normal in an area including northern Namibia, southern Angola, northwestern Botswana, and western Zambia. In South Africa, June–August mean temperatures were 2°–3°C above normal over the northeastern parts of the country, 1°–2°C above normal over central regions, and near normal in southern and western sections.

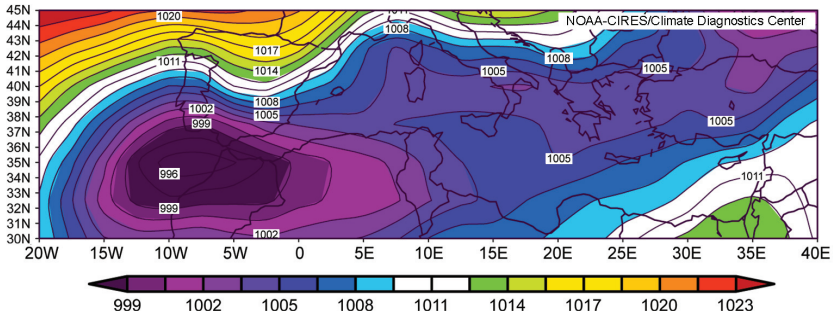

Fig. 6.4. Mean sea level pressure (hPa) over North Africa on 28 February. [Source: NOAA/Cooperative Institute for Research in Environmental Science (CIRES)/Climate Diagnostics Center (CDC)]

iv) Western Africa—W. M. Thiaw[85] and M. A. Bell[6]

(i) West African Monsoon

West African rainfall can be divided into two quasi-homogeneous regions: the Sahel and the Gulf of Guinea. Rainfall in both areas is controlled by the annual progression of the ITCZ over the region. The African Sahel, defined here as the region between 12°–20°N, 18°W–20°E (Fig. 6.6, boxed region), receives

(ii) Precipitation

The rainy season in southern Africa extends from October to April, with the greatest amounts typically observed between December and March. In general, ENSO conditions play an important role in the variability of southern Africa rainfall, which tends to be drier than average during El Niño and wetter than average during La Niña.

Overall, the 2004/05 southern Africa rainy season was characterized by near-average rainfall (Fig. 6.1), although delayed onset of the rains in October 2004 and inconsistent rainfall led to deficits in January and February. Rainfall anomalies were quite variable in the wet zone (east of 25°E; Fig. 6.5 boxed region). In this area, 200–400 mm of rain fell during the period of November 2004–April 2005, ranking in the 10th–30th percentile across northeastern Botswana, the eastern half of Zimbabwe, and northeastern South Africa. Rainfall was also below normal in pockets along the east coast of Madagascar. In contrast, central Mozambique and southern Madagascar received from 700 to over 900 mm of rainfall, which ranked in the 70th–90th percentile. Average conditions prevailed in most of interior South Africa, eastern Zimbabwe, and southern Mozambique. Climatologically dry areas of the region registered near- to above-normal rainfall, with amounts in the 70th–90th percentile across southern Namibia.

The low-level atmospheric circulation for the 2004/05 rainy season featured near normal easterly winds (~4 m s^{-1}) along the equatorward flank of the Mascarene high. A significant reduction in low-level easterlies associated with the presence of an anomalous anticyclonic flow in the southwestern Indian Ocean contributed to rainfall deficits in November 2004 and February 2005. In addition, an elongated ridge extending from high latitudes into the continent contributed to strong subsidence in southern Africa.

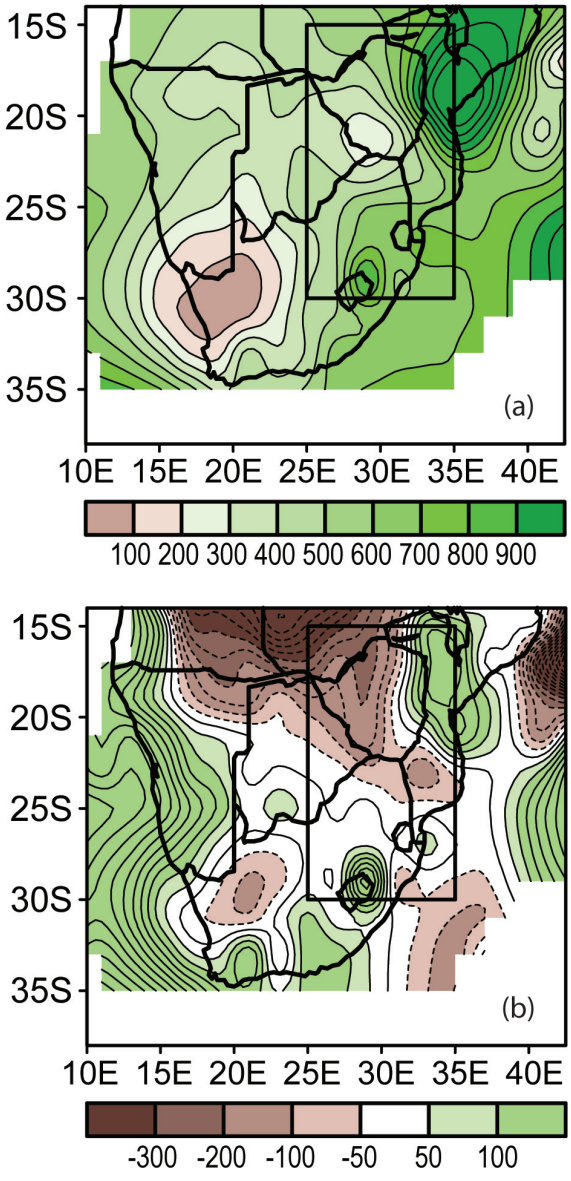

Fig. 6.5. November 2004–April 2005 (a) total rain and (b) precipitation anomaly (mm; 1971–2000 base) for southern Africa. Boxed region is considered the "wet zone."

approximately 90% of its mean annual rainfall during June–September. The rainfall is monsoonal and its penetration into the region is closely related to the position of the mid- and upper-level jets, and to the ITCZ, which starts its northward progression in March and reaches its northernmost position in August. Seasonal precipitation exhibits a strong meridional gradient, with average totals exceeding 600 mm in the south, and 100–300 mm in the north. These larger-scale circulation features are fairly sensitive to changes in the global monsoon circulation on both interannual and interdecadal time scales.

Further south, along the central Gulf of Guinea coast, the rainy season is bimodal and runs from about April to October, typically with a "little dry season" in July–August. This configuration produces an extremely marked north-to-south gradient in annual precipitation totals across the region.

(ii) Precipitation

The 2005 rainy season featured above-normal rainfall across most of the Sahel (Fig. 6.6). Rainfall totals exceeded 100 mm above average across most of the central and western areas of the Sahel. Overall, the 2005 rainy season was the second wettest since 1994.

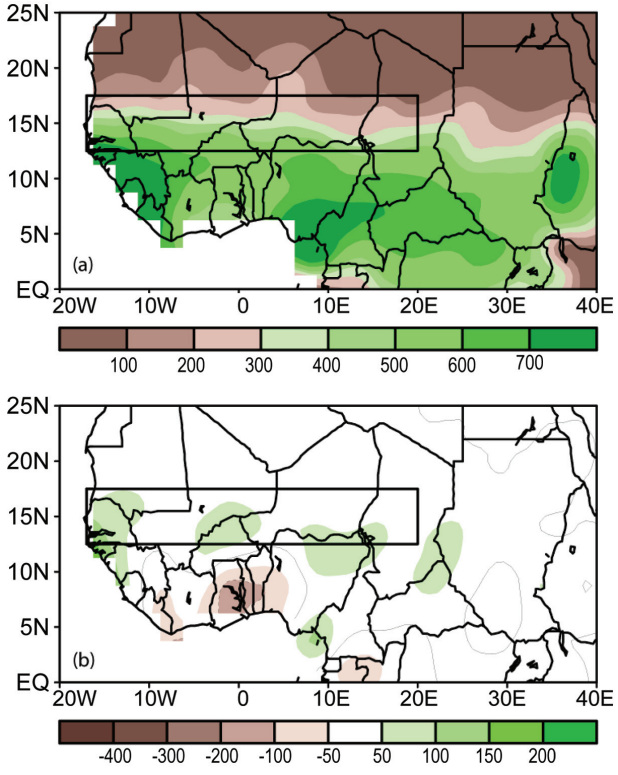

Fig. 6.6. June–September 2005 (a) total rainfall and (b) anomalies (mm; 1971–2000 base) for western Africa. Boxed region is the Sahel.

In particular, most of Senegal and southern areas of Mauritania, northern Burkina Faso, eastern Mali, southern and western Niger, and southeastern Nigeria received above-normal rainfall throughout most of the rainy season, with the exception of July precipitation in southeastern Nigeria. Rainfall anomalies were extremely strong over western Senegal, which received around 700 mm of rainfall between July and September (Fig. 6.6). That is about 300 mm above the long-term mean, making 2005 the rainiest season in this area since 1970. Seasonal totals along most of the Gulf of Guinea coast, from Côte d'Ivoire to western Nigeria were below normal, particularly in central Benin and Côte d'Ivoire. Rainfall deficits ranged between 50 and 200 mm below the climatological mean in the central areas of Ghana, Togo, and Benin.

Heavy rainfall in June, near the start of the rainy season in Guinea and Guinea-Bissau, reportedly sparked a severe cholera epidemic that would eventually spread to at least nine countries in West Africa over the course of the last half of the year, according to the World Health Organization (WHO). Initially, cases were largely confined to the capital city of Bissau, but it spread quickly. Heavy rainfall in Dakar, Senegal, from mid-August through early September not only flooded areas of the city's outer suburbs and forced the evacuation of approximately 60,000 people, but it also triggered a sharp increase in the number of local cholera cases. According to WHO statistics available in late September 2005, at least 43,638 cases of the disease and 759 deaths had been reported throughout West Africa. The end of the rainy season and a lack of new reported cases by the end of December allowed the Ministry of Health in Guinea-Bissau to declare an end to the epidemic in that country, according to the UN Integrated Regional Information Networks (IRIN).

c. North America

1) Canada—C. Kocot,[39] D. Phillips,[67] and R. Whitewood[92]

The climate of Canada in 2005 was characterized by warmer and wetter conditions than normal (relative to the 1951–80 base period). Although Canada was spared much of the extreme weather that impacted other regions of Earth, it was not totally immune. Anomalous winter warmth adversely impacted snowpack in British Columbia (BC). Several tornadoes and heavy flooding in three provinces contributed to 2005 being the costliest year to date, weatherwise, for insurers.

(i) Temperature

Above-normal temperatures were observed throughout the country, with most areas at least 1°C

above normal (Fig. 6.7). Departures of 3°C above normal were experienced in the southwest corner of the Yukon Territory. The 1.7°C above-normal (1951–80 mean) average national temperature experienced by Canada in 2005 marked it as the ninth consecutive year of above-normal temperatures (Fig. 6.8). Overall, 2005 tied 2001 and 1999 as the third warmest year since reliable nationwide records began in 1948. The year's national average is exceeded only by 1998 (+2.5°C) and 1981 (+2.0°C).

Ten of the 11 Canadian climate regions had temperatures that ranked among the 10 warmest years in their records. However, of those, only the north BC mountains/Yukon region tied 1981 for its warmest year (+2.8°C). The remaining nine regions were the following: Arctic mountains and fjords (second warmest, +2.0°C); Pacific coast (fifth warmest, +1.2°C); northwestern forest (sixth warmest, +2.0°C); Arctic tundra (sixth warmest, +1.7°C); northeastern forest (sixth warmest, +1.4°C); Mackenzie district (seventh warmest, +2.1°C); Atlantic Canada (seventh warmest, +0.9°C); south BC mountains (eighth warmest, +1.1°C); and Great Lakes/St. Lawrence (ninth warmest, +1.1°C). The lowest-ranked region, the prairies, experienced its 11th warmest year (+1.2°C). Over the 58-yr period of record (1948–2005), all 11 regions show a positive annual temperature trend, with the greatest increase (+2.2°C) in the north BC mountains/Yukon and the smallest (+0.1°C) in Atlantic Canada.

(ii) Precipitation

In 2005, Canada experienced its wettest year in the 58 years since reliable nationwide records commenced (Fig. 6.7). The 13.4% above the 1951–80 mean displaced the previous record of +9.1% (1996). Areas with precipitation values over 20% above normal in 2005 were most of Yukon, some of the southern Northwest Territories, most of Nunavut, the southwest coast of BC, southern Alberta, most of Saskatchewan and Manitoba, the extreme north of Quebec, and the western part of Nova Scotia. Areas with precipitation amounts at least 20% below normal were along the west coast of BC, the eastern edge of BC, and the western edge of Alberta. The remainder of the country was close to normal.

Regionally, six climate regions experienced conditions in 2005 that would rank them among the 10 wettest years: Arctic tundra (second wettest, +23.1%); northwestern forest (second wettest, +12.8%); Arctic mountains and fjords (fifth wettest, +32.0%); Mackenzie district (fifth wettest, +19.9%); north BC mountains/Yukon (fifth wettest; +19.1%); prairies (seventh wettest, +18.2%). While no region ranked 2005 as the record wettest, a sufficient portion of the country was enough above normal to collectively produce Canada's wettest year on record. The three driest regions of the country were south BC mountains (−3.8%), Pacific coast (−5.5%), and Great Lakes/St. Lawrence (−3.5%). These three regions recorded only slightly drier-than-normal conditions.

(iii) Notable events

Although 2005 started out dry across the province, a series of June storms drenched portions of southern Alberta, resulting in widespread flooding as rain-swollen rivers escaped their banks. Extensive damage was reported to dwellings and infrastructure in over 40 municipalities. At 247.6 mm, Calgary recorded its wettest June on record (79.8 mm is normal). Outside

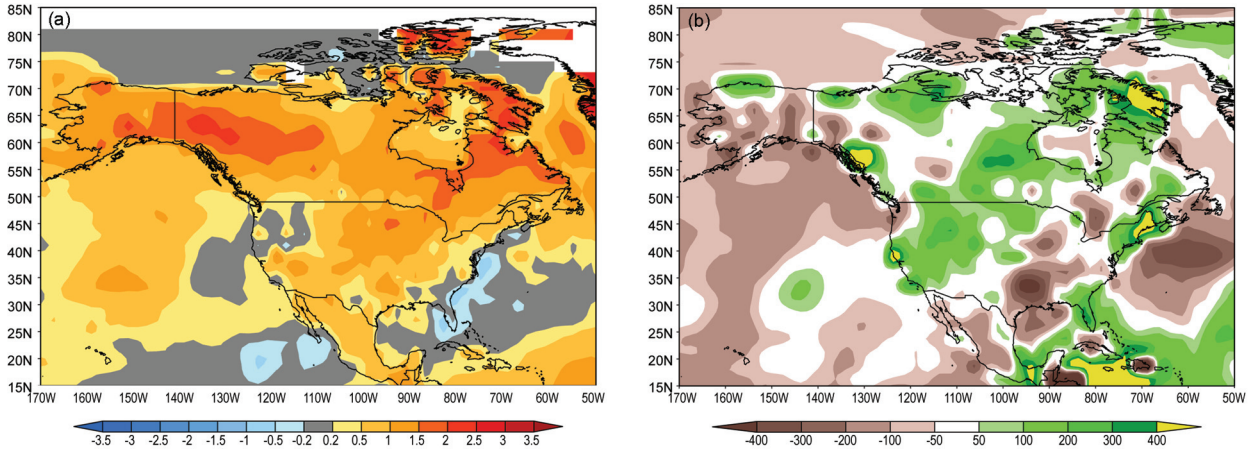

Fig. 6.7. North American 2005 annual (left) temperature anomalies (°C; 1971–2000 base), and (right) precipitation anomalies (mm; 1979–2000 base) from CAMS–OPI.

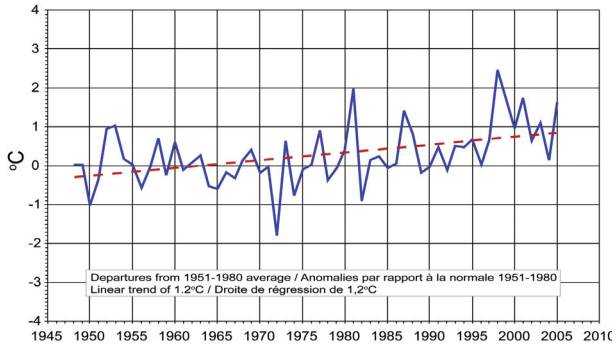

Fig. 6.8. Annual average air temperature anomalies (°C; blue) and 1948–2004 trend (red) for Canada. [Source: Environment Canada]

the city, monthly rainfall approached 400 mm. Total losses are estimated at $400M (million) Canadian dollars (CAD; $344M USD) of which $275M CAD ($232M USD) was insured, making this weather event one of the costliest in Alberta's history.

Manitoba was treated to rare and record widespread flooding as the result of frequent and intense June and July thunderstorms. The Churchill River crested at its highest levels ever recorded and Manitoba Agriculture estimated more than a quarter of the province's farmland was inundated during the flooding.

A line of severe thunderstorms tracked across southern Ontario on 19 August, leaving record damage estimated at over $500M CAD ($430M USD). The storms spawned two F2 tornadoes and a rare tornado warning was issued for Toronto. In and around Toronto, ~45 mm diameter hail, straight line winds with gusts reaching 72 km h^{-1}, and rainfall rates exceeding 100 mm h^{-1} generated the most damage.

The 2005 sea ice extent in Canadian Arctic waters dropped to its lowest level on record, 5.3 million km^2; down 20% from 1978 when satellite observations began. The previous record minimum of slightly less than 6 million km^2, was set in 2002. Since the 1970s the geographical extent has been decreasing by around 8% $decade^{-1}$.

The Canadian International Forest Fire Centre (CIFFC) reported a near average fire year in Canada in terms of the number of fires (7438; –1.3% of normal), but with significantly fewer hectares (ha) of forest consumed, 1.7 million ha, or ~68% of the 1995–2004 mean. The total number of fires in 2005 was down in most provinces and territories, with notable exceptions in Ontario (1961 fires; +51% of normal) and Quebec (1374 fires, +57% of normal). In contrast, and with respect to the total area affected, all provinces and territories, with the exception of Quebec, reported lower than average area burned. The total area burned within the province of Quebec in 2005 (831,022 ha) however, accounted for ~49% of the national total.

ii) United States of America—K. L. Gleason[28]

(i) Overview

Reliable weather records for the United States exist from 1895 to the present, enabling the climate of 2005 to be placed in a 111-yr context for the contiguous United States. The nationally averaged temperature in 2005 was the seventh (105 of 111 years) warmest on record, with an annual mean of 12.3°C (+0.8°C relative to the period of record). The linear temperature trend for the 111-yr record over the contiguous United States is 0.056°C $decade^{-1}$, with an increase to 0.32°C $decade^{-1}$ since 1976. Seven of the ten warmest years on record for the United States have occurred since 1986.

Precipitation in the United States in 2005 was variable throughout much of the country, with periods of excessive rainfall in the Southwest and Northeast, persistent drought in portions of the Northwest, and developing drought from the Southern Plains to the Great Lakes. Nationally, it was the 43rd wettest year on record, which is near the long-term mean. Maine and New Hampshire had their wettest year on record, surpassing 1909 and 1954, respectively. Conversely, Arkansas had its second driest year since 1895.

Temperature and precipitation anomalies for the United States are based upon the 1895–2005 data record, rather than on any particular 30-yr normal statistics (e.g., 1971–2000 mean). With respect to the United States, temperature or precipitation is described as "much above" or "much below" normal when the value falls within the top or bottom 10% (decile) of the historical record distribution. Temperatures are simply "above" ("below") normal if they fall within the upper (lower) third, or tercile, of the distribution, but are not in the top (bottom) decile. Values falling within the middle tercile are considered near normal.

(ii) Temperature

Temperatures were above average across most of the contiguous United States from December 2004 to February 2005, with no state ranking below average. Colorado, Wyoming, and Utah were much above normal for the season. From March to May (spring) was exceptionally cool from Texas to Florida and along the entire eastern seaboard. Eleven states had below-average seasonal temperatures. Three additional states reported much-below-average temperatures for the

season (Fig. 6.9, left). Extremely cool May temperatures covered the Northeast and Mid-Atlantic coast, with seven states (Connecticut, Rhode Island, Massachusetts, Pennsylvania, Delaware, Maryland, and South Carolina) experiencing one of their 10 coldest Mays on record.

In contrast, record to near-record summer (June–August) heat occurred from the Great Lakes into the Northeast with record seasonal heat in New Hampshire and New Jersey. Much-above-average temperatures in the southwestern United States during July resulted from an upper-level ridge situated over the region for most of the month. Temperatures exceeded 38°C (100°F) and broke more than 200 daily records in six western states. A new record of seven consecutive days at or above 52°C (125°F) was observed in July at Death Valley, California (previous record of five days). A persistent upper-level cyclonic circulation positioned over the central United States into August contributed to above-average summer temperatures across the eastern United States, where August temperature records were set in New Jersey and Rhode Island. No state in the contiguous United States reported below-average temperatures during the season.

An uncharacteristic blocking ridge over Alaska fostered an exceptionally warm and dry summer throughout the state. Statewide June–August 2005 temperatures were third warmest since reliable records began in 1918. Overall, 2005 was Alaska's sixth warmest year on record, and was the sixth consecutive above-average year for the state (Fig. 6.10).

Autumn (September–November) temperatures were much above average across large parts of the southern and central United States and portions of the Northeast and Mid-Atlantic, with warmer-than-average temperatures present throughout all but three states in the Pacific Northwest (Fig. 6.9, right). The contiguous United States recorded its fourth warmest autumn in the last 111 years. This near-record heat resulted from a quasi-stationary 500-hPa ridge situated across eastern North America. No state in the contiguous United States was cooler than average during this season.

(iii)Precipitation and drought

Average precipitation for the contiguous United States in 2005 was 755 mm, slightly above the long-term (1895–2005) mean of 740 mm. Precipitation across the United States in 2005 was characterized by persistent moderate wetness in the Northeast and Southwest, below-average precipitation in some parts of the Northwest, and developing dryness from the Southern Plains into the Great Lakes (Fig. 6.9). An area from Texas to parts of the Midwest and Ohio Valley was drier than normal. Also, despite the significant rainfall associated with Hurricanes Katrina and Rita, Arkansas and Louisiana reported much-below-normal precipitation for the year. Conversely, Maine and New Hampshire had their wettest year on record, and most states had above- or much-above-normal precipitation.

December 2004 through February 2005 was very wet from the California coast, through the Plains, and into the Great Lakes and Northeast. There also was much-above-normal precipitation around the Great Lakes. A strong blocking high over the Gulf of Alaska in conjunction with an amplified trough over the southwestern United States generated an active storm season along the West Coast. However, March marked the beginning of a very dry period across the central United States, extending from

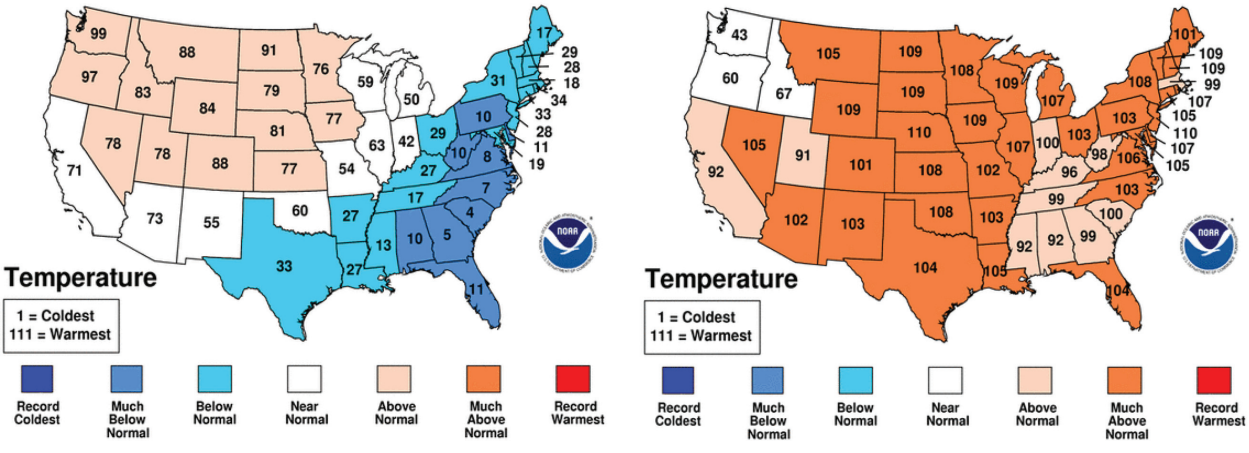

Fig. 6.9. Statewide rankings of temperature as measured across the contiguous United States in 2005: (left) March–May and (right) September–November. A rank of 111 (1) in the U.S. Historical Climatology Network (USHCN) record represents the warmest (coldest) season since 1895.

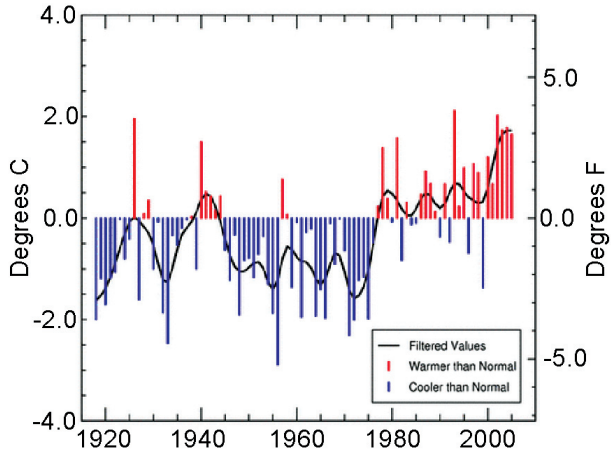

Fig. 6.10. Alaska statewide average annual temperature anomalies (°C), 1919–2005. [Source: NOAA/NCDC]

Texas to the Great Lakes (Fig. 6.11). An active storm track across the western United States led to above to much-above-normal precipitation in the West, the Northern Plains, the Southeast, and the far Northeast.

Boreal summer (June–August) brought much-above-normal rainfall to the Southeast and parts of the central and northern Great Plains. Only nine states experienced below-normal precipitation, and just one state (New Mexico) much-below-normal summer precipitation. Stormy conditions contributed to a record wet October and fall season across much of the region. Six states (Maine, Vermont, New Hampshire, Connecticut, Rhode Island, and Massachsetts) reported their wettest fall on record, and nine states set a record for the wettest October, with two additional states reaching their second wettest. Mt. Washington, New Hampshire, set a record for the greatest October snowfall on record (200 cm), exceeding the previous record set back in 2000 by 102 cm.

The year ended with a very dry December from the Southwest, across the Southern Plains, to the Ohio Valley and eastern Great Lakes. Several states from the Southwest to the Lower Mississippi Delta had one of their 10 driest Decembers; Arizona and Arkansas had their driest December on record. December capped a three-month period of much-drier-than-normal weather in the Southern Plains, with Arkansas and the Arklatex region (nexus of Arkansas, Texas, Louisiana, and Oklahoma) all experiencing the driest October–December on record.

At the beginning of the year, approximately 8% of the contiguous United States was in moderate to extreme drought, as defined by the Palmer Hydrological Drought Index (PHDI; Palmer 1965; Heim 2002). The areal extent of moderate to extreme drought grew to reach a peak of 21% of the contiguous United States in December 2005 (Fig. 6.12). Precipitation deficiencies from March to June and again from September to December resulted in the emergence and intensification of drought conditions from the Texas Gulf Coast to the Great Lakes. Northeastern Illinois and the Arklatex region were significantly impacted by the emerging drought.

The development of drought conditions in parts of the Midwest and Southern Plains can be attributed to a pronounced shift in synoptic circulation in March–June and October–December. During both periods, the northern branch of the polar jet was active across the western United States, while the southern branch was active over the United States. Southeast and Atlantic coast. The resulting absence of storms from the Deep South to the Great Lakes created substantial precipitation deficits. The lack of precipitation from October to December left Arkansas with its driest of such periods on record and Louisiana with its third driest.

The same synoptic conditions brought above to much-above-normal rainfall to the northwestern United States during the spring and the last two months of 2005, contributing to a significant reduction in total drought area across parts of the Northwest by the end of the year. The western United States drought of 1999–2004 was one of the most severe droughts in this region over the last 100 years. More than five years of precipitation deficits lowered streamflows and depleted reservoirs. Some reservoirs recovered during 2005, but aggregated reservoir levels were still below average at the end of the year.

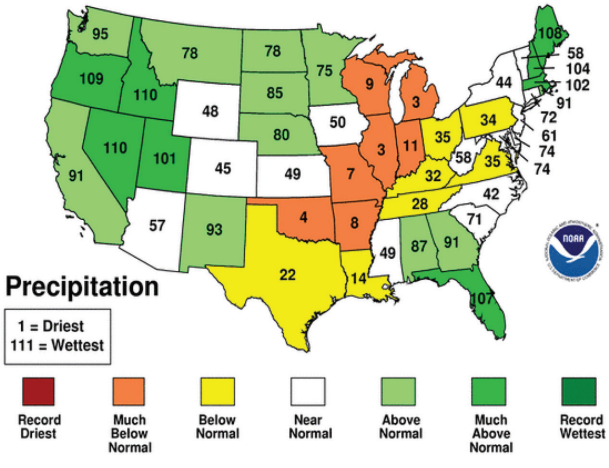

Fig. 6.11. March–May 2005 statewide ranks of precipitation for the contiguous United States. A rank of 111 (1) in the USHCN record represents the wettest (driest) year since 1895.

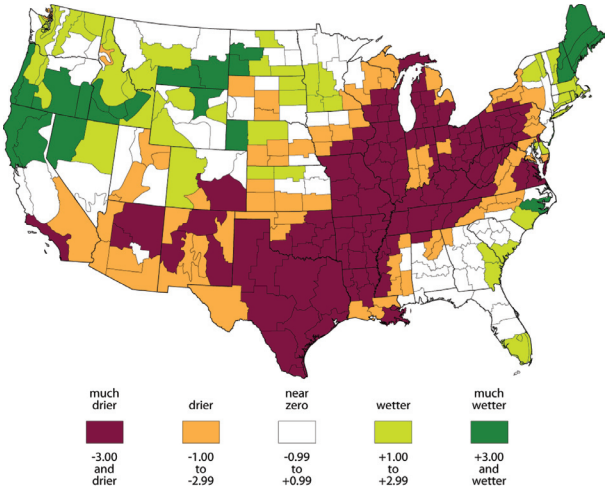

Fig. 6.12. Change in the PHDI between 1 January–31 December shown by U.S. Climate Division. [Source: NOAA/NCDC]

(iv) Snowpack and wildfires

(a) Snow

The 2004/05 snow season and snowpack was generally above average across the Southwest and much below average across the northern Rockies and Pacific Northwest. By the end of the 2004/05 winter, the Northwest snowpack was just 50% of normal. Snow cover was slightly below average for the North American continent as a whole over the winter, and much below average for the spring. This is consistent with a trend toward reduced spring snow cover over North America (Mote et al. 2005). Snow cover has been below average in all but four years since the mid-1980s.

Notable snow storms in 2005 include a major winter storm, referred to as the "Blizzard of 2005," which deposited well over 30 cm of snow across much of southern New England in January. Boston, Massachusetts, had its snowiest January on record partly as a result of that storm. NOAA's operational Northeast Snowfall Impact Scale (NESIS), developed by Kocin and Uccellini (2004) to characterize and rank high-impact northeastern U.S. snowstorms, ranked this January snow storm as the seventh most intense on record for the region. In other regions, a late-season (April) snow event produced over 61 cm of accumulation in the mountains west of Denver, Colorado, and a significant snow storm on 27–28 November generated blizzard conditions across the northern High Plains, accumulating up to 61 cm of snow in parts of Nebraska and the Dakotas.

In contrast to the above-average snowfall season in 2004/05, the beginning of the 2005/06 snow season in the Southwest was nearly nonexistent. An examination of USDA snowcourse/snow telemetry (snotel) station data in Arizona revealed that 31 of 33 sites (94%) were snow free at the end of 2005—the most snow-free locations in at least the past 40 years.

(b) Wildfires

Preliminary estimates from the National Interagency Fire Center suggest that 2005 will break the record set in 2000 with over 3.45 million ha (8.53 million acres) burned. During the 2000 fire season, roughly 3.41 million ha were consumed across the entire United States, with over 2.83 million ha burned in the contiguous United States. Despite the record area burned, the total number of fires across the country continued to decline in 2005, suggesting the average size of individual fires has increased over the past 20 years.

In Alaska, over 1.78 million ha burned in 2005, compared to nearly 2.43 million ha consumed in 2004, which was the worst fire season on record for the state. Above-average temperatures coupled with below-normal precipitation during the summer months contributed to the above-average wildfire season across Alaska in 2005.

Atypical wildfire activity erupted across parts of the central United States during December 2005. Numerous large fires, enhanced by extreme drought conditions, developed across parts of Oklahoma, Texas, and the Southern Plains. Many of these fires continued to burn into early January 2006. Over 162,000 ha had burned across the Southern Plains during the first week of the New Year, normally a time of very low fire activity.

(v) Severe extratropical storms

Preliminary estimates indicate there were only nine very strong to violent tornadoes (F3–F5 on the Fujita scale) during the 2005 official tornado season (March–August), all of F3 intensity. This was significantly below the 1971–2000 mean of 37, contributing to a slight negative trend in very strong to violent tornadoes observed since 1950. However, two late-year (out of season) tornado outbreaks increased the annual total.

A severe weather outbreak accompanied by over 30 reported tornadoes occurred across Mississippi and Louisiana in April. In June, tornadoes ripped through the town of Hammond, Wisconsin, causing over $3 million USD in damage. Severe thunderstorms in August generated tornadoes that killed at least three people in Wisconsin and Wyoming. Tornadoes also touched down in September across parts of the central United States between Oklahoma and Wisconsin. On

6 November, a deadly Midwestern tornado outbreak claimed 24 lives in and around Evansville, Indiana. This was the deadliest United States outbreak since 1998. Additional severe weather impacted the same region on 15 November, with over 30 tornadoes reported. Among these was the strongest tornado of the year, an F4 twister that reached a higher intensity than any of the tornadoes that developed during the official season.

iii) Mexico—M. Cortez Vázquez[18]

(i) Temperature

In 2005, the areally averaged annual mean temperature for Mexico was 21.4°C, which is 0.7°C warmer than normal (based on the period of record, 1980–2004). The year, 2005, was ranked as the second warmest, behind 1998, since the start of the national temperature dataset in 1980 (Fig. 6.14). The warmth in 2005 continued the trend of above normal temperatures in Mexico since the mid-1980s. Nationally, the lowest minimum temperature for the year was –17°C, reported in the mountains of Durango in northwest Mexico, the same area that holds the long-term historical record minimum temperature of –25°C reported in December 1997 (based on 1980–2005 data). In 2005, maximum temperatures of 49.5°C were reported in Chihuahua and Michoacán, and these temperatures were only 0.5°C less than the national all-time historical record temperature of 50°C.

(ii) Precipitation

Nationwide, the areally averaged rainfall was 778 mm, which was 14.5 mm (2%) above the long-

U.S. CLIMATE EXTREMES INDEX (CEI)—K. L. Gleason[28]

How has the climate changed over the past century? In what ways is it changing and by how much? Many people, including climatologists, have been struggling with these questions for some time now, not only for scientific interest, but also to aid in policy decisions (Houghton et al. 2001) and to inform the general public. In order to answer these questions, it is important to obtain comprehensive and intuitive information that allows interested parties to understand the scientific basis for confidence, or lack thereof, in the present understanding of the climate system. One tool, first developed as a framework for quantifying observed changes in climate within the contiguous Unites States, is the United States Climate Extremes Index (CEI).

The CEI was first introduced in early 1996 (Karl et al. 1996), with the goal of summarizing and presenting a complex set of climate changes in the United States so that the results could be easily understood and used to aid decision making by policy makers. The CEI initially consisted of a combination of five separate climate change indicators. Recent revisions include a sixth indicator related to extremes in landfalling tropical system wind speed. The CEI is also now evaluated for nine standard periods or seasons including: spring (MAM), summer (JJA), autumn (SON), winter [December–February (DJF)], warm (April–September), cold (October–March), hurricane (June–November), year to date, and annual (January–December). The CEI conveys the percentage area of the United States that has been affected by climate extremes as they relate to monthly maximum and minimum temperatures, daily precipitation, and the Palmer Drought Severity Index (PDSI) within a given period.

The annual CEI for 2005 was about 41%, which is much above the expected value of 20% and is the second largest value since reliable records began in 1910 (Fig. 6.13). This high 2005 CEI was due to the combined impacts from a record active Atlantic hurricane season, extremes in monthly maximum and minimum temperature, much-above-normal wet PDSI, and extremes in daily precipitation. In addition, the 2005 hurricane and cold seasons had record CEI percentages. Approximately 44% of the United States was affected by climate extremes during the hurricane season and nearly 38% during the cold season. All six indicators were well above the expected percentage during the hurricane season. Extremes in much-above-average mean minimum temperature were more than five times the expected value. Much-above-average mean maximum and minimum temperatures, a wet PDSI, and the large number of days with precipitation all contributed significantly to the record extreme 2005 cold season. A more detailed explanation of the CEI and graphs of the most current CEI and the individual indicators that comprise the CEI may be viewed at the NCDC CEI Web site at www.ncdc.noaa.gov/oa/climate/research/cei/cei.html.

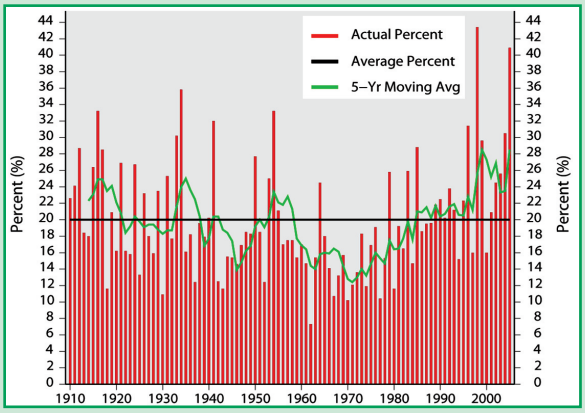

Fig. 6.13. Annual U.S. Climate Extremes Index values (1910–2005). [Source: NOAA/NCDC]

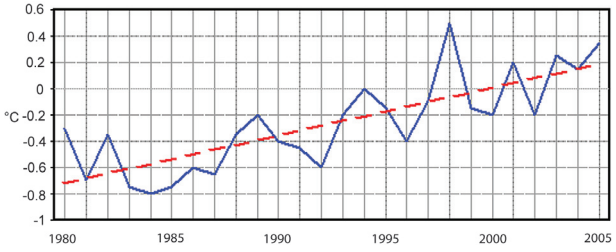

Fig. 6.14. Annual temperature anomalies (°C) over Mexico (1980–2005).

term climatological mean defined by the period of 1941–2004. The year ranks as the 25th wettest on record. Although the annual rainfall total was slightly above average, rainfall distribution was very irregular throughout the year. The rainy season (June–October) was characterized by short events of heavy rainfall, which were mainly associated with tropical cyclones that approached Mexico from the Atlantic side of the continent. Wet conditions were observed in February, followed by a dry trend from March to May. The onset of the summer rainy season started 3–4 weeks later than normal in southern Mexico, and this delay influenced the northward progression of the monsoon during the early summer. The 2005 rainy season was finally established after mid-June, with exceptionally wet conditions being recorded in July and again in October. Large rainfall deficits developed in September, which is normally the wettest month on average for Mexico. Although the total amount of rainfall was slightly above normal, precipitation was localized over small areas in the south and southeast, around the tracks of landfalling tropical cyclones. Portions of northern Mexico also received significant amounts of rain during February, associated with midlatitude systems. However, an early withdrawal of the summer monsoon in northern Mexico, along with a persistent meteorological drought in the western part of the country during the entire summer, resulted in limited water storage at all dams and hydrological drought declarations by year-end along the Lerma–Chapala and Cutzamala Basins.

(iii)Notable events

Climatologically, the annual rainfall distribution in Mexico clearly reflects the influence of tropical cyclone activity on both sides of the country (Fig. 6.15). The southwest coast and western Mexico typically receive appreciable rainfall from Pacific tropical storms, but during the 2005 season the storms developed and tracked farther offshore than normal (see section 4c). This helped to depress rainfall totals in western and northwest Mexico, with only two systems (Dora and Otis) approaching the Pacific coast states. In contrast, a very active season was observed in the Atlantic and Caribbean basins, with seven systems making landfall in Mexico: Hurricanes Emily, Stan and Wilma; Tropical Storms Bret, Gert, and Jose; and Tropical Depression Cindy. The number of landfalling tropical cyclones in Mexico in 2005 represented a new record since the start of the satellite era. In southeast Mexico, Stan produced abundant rainfall across the Yucatan Peninsula on 2–3 October before moving into the states of Veracruz and Oaxaca. Pentad and monthly rainfall totals exceeded 200% of normal along and to the right of Stan's track into mainland Mexico, with heavy flooding in portions of northern Veracruz and Oaxaca. Stan developed a large moisture tap across the Pacific slope of Chiapas and this promoted widespread flooding along the Pacific slope of Chiapas, and sections of Central America. By far the most destructive tropical cyclone during the 2005 season was Wilma, which moved slowly across the Yucatan Peninsula on 20–23 October causing severe economic loss and several fatalities in the Cozumel and Cancun areas. Based upon wind speeds and sea level pressure readings, Wilma was the most powerful hurricane on record to make landfall in Mexico.

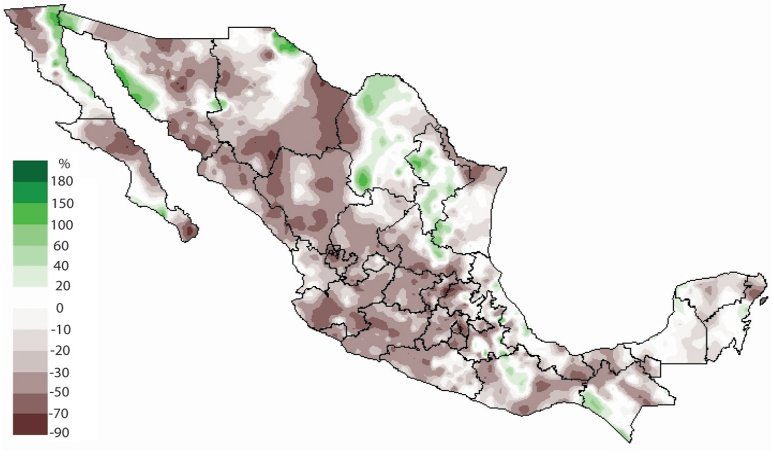

Fig. 6.15. Percent of normal precipitation across Mexico during the 2005 rainy season (May–October) relative to the 1941–2005 mean.

d. Central America and the Caribbean—E. K. Grover-Kopec[31]

i) Temperature

Annual mean surface temperatures were slightly above average across Central America and the Caribbean during 2005 (Fig. 6.16). Temperatures were at least 0.5°C above normal for the year over the entire region except for western Cuba and the Pacific coastal regions of Costa Rica and Panama. The warmest conditions, relative to climatology, were observed in Guatemala and Belize, where annual departures from the 1971–2000 mean exceeded 1°C.

ii) Precipitation

Most of the Central American isthmus experienced drier-than-normal conditions in 2005, though precipitation deficits were not as severe and widespread as those seen in recent years. The most significant standardized 12-month precipitation anomalies occurred across Honduras, Nicaragua, central Costa Rica, and southern Panama (Fig. 6.16). The largest absolute annual precipitation deficits compared to the 1979–2000 base period were observed in this same region. Negative anomalies exceeding 1000 mm were observed in eastern Honduras and Nicaragua, accounting for approximately half of the climatological mean annual precipitation in these areas, typically among the wettest regions in Central America.

The largest contrast between the precipitation regime of 2005 and that of recent years was observed in the Caribbean, particularly in Jamaica, eastern Cuba, and western Haiti. Drought conditions, which have had a large impact on water resources and agriculture over the past few years in Cuba (Levinson 2005), eased a bit as the eastern portion of the island received 25% more precipitation than normal during the year. Much of this excess precipitation came during May, June, and October, which are among the wettest months of the year in that area. The climatological precipitation distribution across most of the Caribbean and Central American region is bimodal, with relative maxima occurring in May–June and September–October.

iii) Notable events

The record-breaking 2005 Atlantic hurricane season (see section 4 sidebar) caused devastating losses across the region from July to November. Most damage came from Hurricanes Dennis, Emily, Stan and Beta, and Tropical Storm Gamma, which primarily affected the countries of Cuba, Grenada, Guatemala, Nicaragua, and Honduras, respectively.

While all of these storms had tremendous localized impacts, Stan was arguably the most destructive and certainly the deadliest in the region, affecting eight countries in early October. The storm brought 150–400 mm of precipitation to western Guatemala. One-third of the population of Guatemala was affected by Stan and more than 1000 deaths were reported. Agence France-Presse and Reuters reported that most of these deaths occurred when mudslides buried the villages of Panabaj and Tzanchal in the southwestern department of San Marcos, where some of the largest precipitation accumulations were reported.

e. South America

i) Overview—M. Rusticucci[78] and J. L. Camacho[13]

South America experienced below-normal precipitation anomalies across a majority of the conti-

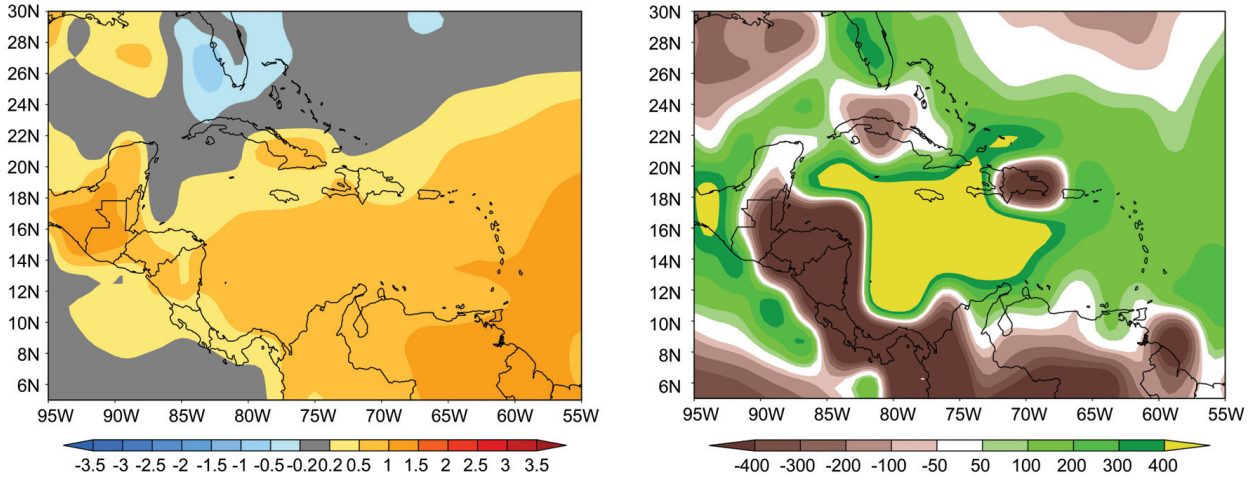

Fig. 6.16. Central American and Caribbean 2005 annual (left) temperature anomalies (°C; 1971–2000 base), and (right) precipitation anomalies (mm; 1979–2000 base) from CAMS–OPI.

nent in 2005, with some excesses in the northwest and southwest (Fig. 6.17). However, despite overall deficits, extreme but inconsistent and widely scattered precipitation events over most of the continent adversely impacted the population. Additionally, anomalously frequent cold air advection from higher latitudes was experienced by both the north and south sides of the continent.

Most of northern and eastern South America experienced temperatures above the 1961–90 normal, while western parts were below average. This is generally reflected in Fig. 6.17.

One important recent improvement in the climatic analysis of South America has been the addition of annual or monthly averages from up to 516 individual stations, as provided by the National Meteorological and Hydrometeorological Services of Argentina, Bolivia, Chile, Colombia, Ecuador, Uruguay, Paraguay, Peru, and Venezuela, and also from the Brazilian Centre de Provisão de Tempo Estudos Climáticos (CPTEC). Attention has been given to minimizing excessive local-scale influence to better establish the regional behavior of extreme climatic events. These data are the primary source for subsequent precipitation analyses, and they have been blended with the NCDC/GHCN database for temperatures; the reference period is 1961–90.

ii) Northern South America and the Southern Caribbean—J. D. Pabón[63]

Typical responses to equatorial Pacific cold conditions were observed in northern and northwestern South America in 2005, with precipitation generally above normal except in the Colombian–Venezuelan Amazonia region, where precipitation deficits occurred. Intense rainfall, particularly from March to May and during the second half of the year caused flash flooding and landslides that resulted in death and considerable damage. Around 1 million people were affected during intense October–December rainfall events in Colombia, which caused more than 500 deaths, destroyed over 1,000 houses, and heavily damaged infrastructure.

Although average temperatures for several months were below normal over several regions of Colombia, northeastern parts of Columbia and Venezuela experienced annual average air temperature up to 1.0°C above normal, while western regions were slightly below normal. Northern Hemisphere midlatitude synoptic activity penetrated further south than normal, generating perturbations in the ITCZ and producing considerable precipitation over the Caribbean and northern South America. The Caribbean also was affected by the increased tropical cyclone activity in the Atlantic basin in 2005 (see section 4c).

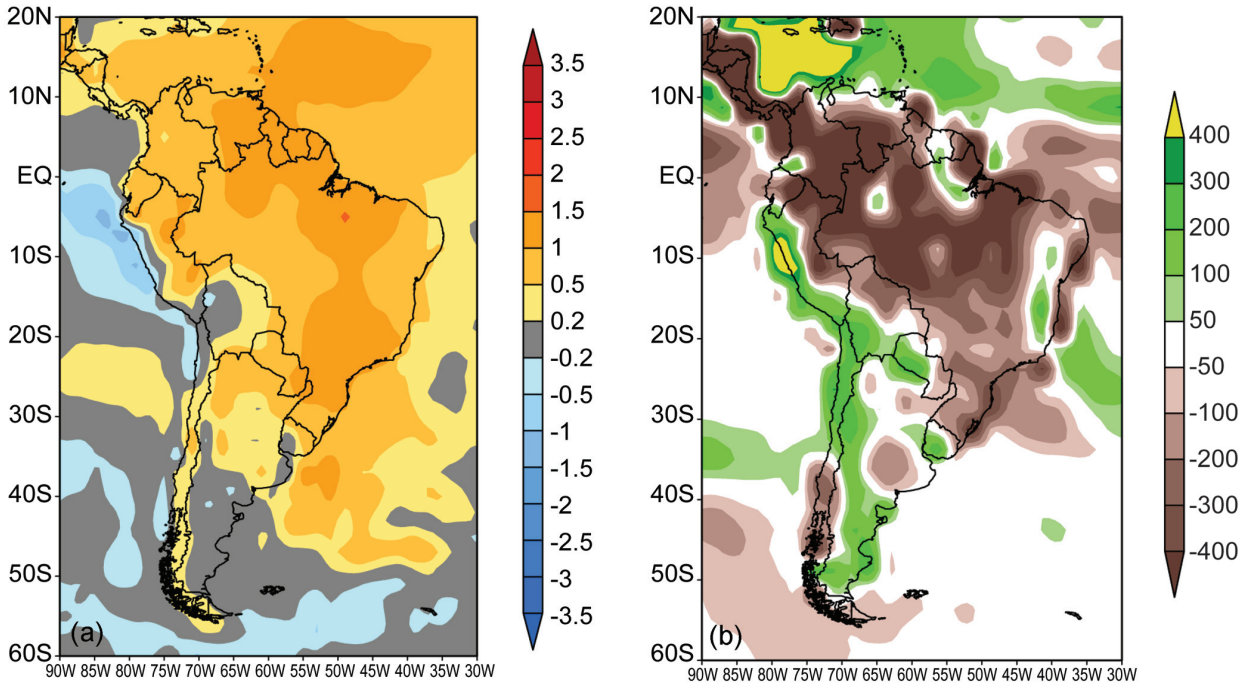

Fig. 6.17. South American 2005 annual (left) temperature anomalies (°C; 1971–2000 base), and (right) precipitation anomalies (mm; 1979–2000 base) from CAMS–OPI.

iii) Tropical South America East of the Andes—J. A. Marengo[50]

Heavy rain in January caused flooding in Georgetown, Guyana, and surrounding areas, affecting an estimated 290,000 people. Conversely, large negative rainfall anomalies were measured east of the Andes in the Amazon, northeast and southern Brazil, and in the South American monsoon–Pantanal regions. The rainy season in northeast Brazil during February–May was below normal, reaching drought levels in some semiarid interior regions, and severely impacting over two million inhabitants. Amazonia also experienced intense drought during most of 2005, especially in southern and western sections of the basin (see sidebar). More than 167,000 people have been affected by the drought, both directly and indirectly. Low river levels impacted the region's main source of transport and contributed to the deaths of large numbers of already endangered manatees and river dolphins.

In west-central and southeastern Brazil, the rainy season was from below to slightly below the normal. Drought conditions were present in the Chaco region of Bolivia and Paraguay during January and February 2005. Low water levels on the Paraguay River significantly reduced barge traffic in 2005.

Rainfall in southeastern Brazil was primarily in the form of intense events that lasted several days. Several of Brazil's large cities were flooded by these events, leaving much of the population without power or shelter. In and around São Paulo and Rio de Janeiro, dozens of people died due to landslides and flooding.

Annual air temperature anomalies reached almost 3°C above normal in eastern Brazil, with every month above normal and the warmest months being April, August and October. In October, typically the onset of the rainy season in the southern areas, temperature anomalies were up to 5°C above normal. From Octo-

DROUGHT IN AMAZONIA—J. Marengo[50]

In 2005, large sections of the western part of the Amazon Basin endured the worst drought in 40 years and also one of the most intense since the beginning of the twentieth century. While the Amazon normally rises and falls in conjunction with seasonal precipitation, 2005 rainfall was well below normal (Fig. 6.18), which allowed rivers to drop to record low levels. Levels of the Madeira and Solimões Rivers, two of the Amazon's major tributaries, dropped to record and 38-yr lows, respectively. In the Brazilian states of Rio Branco, Rondonia, southern Para, and southern Amazonas, rainfall was 30%–50% below normal in January–April 2005, 33% below normal in June and August, and 65% below normal in July. According to the meteorological service of Peru, the hydrological year of 2004/05 exhibited rainfall well below normal in Peruvian Amazonia, with mean rainfall for the hydrological year September 2004–August 2005 up to 39% below normal. Rainfall on the basins of the Bolivian Beni and Mamoré Rivers was about 20%–30% below normal for January–April. Drought conditions favored the occurrence of forest fires, and in September the number of fires was about 300% more than those detected in September 2004.

Levels of the Amazonas River at Iquitos, Peru, and Leticia, Colombia; the Solimões River at Tabatinga and Fonte Boa, Brazil; the Acre River at Rio Branco, Brazil; the Mamoré at Puerto Varador, Bolivia; and the Ibaré River at Puerto Almacén, Bolivia all were well below the normal during most of 2005 until September, in some cases as much as 2 m below normal monthly means. At daily time scales, the situation was even more dramatic. The level of the Solimões River at Tabatinga and Fonte Boa decreased from 11.5 and 21 m (respectively) in May to near 1 and 11 m (respectively) in September. Rainfall started by the end of October 2005, reached a November mean of almost 107% above normal, and recharged the Rio Amazonas in Iquitos to a normal level by November. By January 2006 the Acre and Madeiras Rivers achieved anomalously high levels (11.08 and 12.34 m, respectively) due to the intense rains. In contrast to the intense drought of the 1982/83 and 1997/98 El Niño years, the 2005 drought was concentrated in western and southern Amazonia and was not related to El Niño, which brings drought to central and eastern Amazonia, but rather to a warming of the tropical North Atlantic during most of 2004 and 2005.

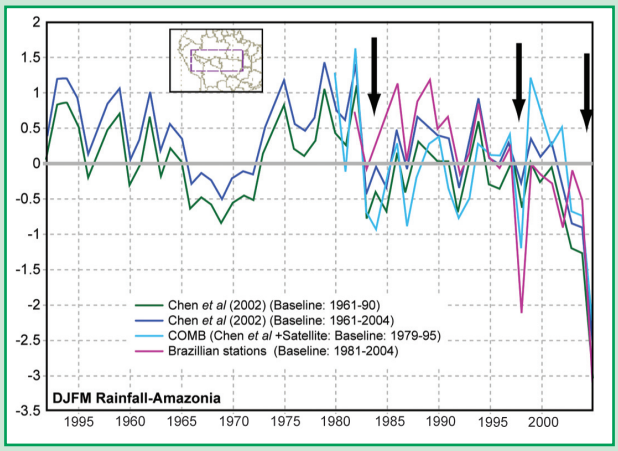

Fig. 6.18. Rainfall anomalies (mm day^{-1}) in central Amazonia during the peak season (December–May) 1951–2005. Black arrows represent drought years 1983, 1998, and 2005.

ber to December, temperatures were over 3°C above normal in far western Amazonia. Air temperatures in Bolivia and northern Paraguay were 1°–4°C below normal from September to November.

iv) Tropical South America West of the Andes—R. Martínez[51]

As in northern South America, rainfall in Ecuador and Peru was strongly influenced by SST over the Niño-1+2 region during 2005. Despite weak warming in the tropical Pacific, cold coastal SST anomalies led to negative rainfall anomalies along the Ecuadorian coast. Mean temperature also was below normal during 2005. In November 2005, a strong frost caused significant damage in the central and southern highland of Ecuador. In Peru, rainfall was below normal along the central and southern highlands, continuing several years of drought in this region. Bolivia also experienced drier-than-normal conditions in 2005, except for October and November when intense rains generated flooding and damage. The mean temperature in Bolivia was above normal across most of the country.

v) Southern South America—M. Bidegain[7] and M. Rusticucci[78]

Annual precipitation anomalies over southern South America show light deficits over the east and surplus over central Chile and western and southern Argentina. Above-normal precipitation for several months contributed to the positive anomalies in these regions. A series of intense summer (June–August) precipitation events also contributed, with some local anomalies exceeding 700% of the normal. On 26 June, 162.4 mm of rain fell over Concepción, Chile, generating landslides that killed 5 and injured 4,800. Between 26 and 28 August, 120 mm of rain fell in 48 h in Santiago, Chile, resulting in 1,153 injured, 755 houses damaged, and an estimated economic cost of $10 million USD.

The regional core of negative precipitation anomalies was in the Chaco region and southern Paraguay, where intense drought prevailed to spring 2005. Precipitation deficits produced livestock losses and reduced water levels on the Uruguay River, impacting hydroelectric generation. Strong negative October–December rainfall anomalies dominated the southern part of the region, affecting agriculture in this productive region. In southern Brazil, seasonal (December 2004–March 2005) rainfall 100–500 mm below normal produced intense drought and heavy agricultural losses. The southern state of Rio Grande do Sul was the most affected, and while May rainfall alleviated the drought, it produced flooding in some cities. Damage attributed to the drought of 2005 in southern Brazil was considerable: 2 million people were affected by water shortages, 13 million tons of agricultural products were lost, and economic losses were on the order of $3 billion USD.

Annual air temperature anomalies were generally near normal, with eastern regions above normal and central and western region slightly below normal. Uruguay experienced temperatures above the normal (up to +1.2°C), especially near the Brazilian border. From January to August most monthly temperatures were above normal, with May–August having the largest anomalies. June temperature broke records (for the 1961–2004 period) over northeastern Argentina, and winter was 2°C warmer than normal in Uruguay. In contrast, cold air advection in September affected the eastern part of the region. October–December temperature anomalies were up to 3°C below normal, with early December frosts, including a few intense frosts in the Andes that killed thousands of sheep. Annual air temperatures in Chile were slightly above normal in the central region, and slightly below normal in the south. April, May, and June temperatures were below normal, especially in southern Chile. The week of 26 June, a severe cold air outbreak between 34° and 36°S left 30,000 injured and affected 12,000 homes.

On 23–24 August 2005, an exceptionally strong midlatitude cyclone occurred over Rio de la Plata and southern Uruguay. The gale was characterized by unforced rapid deepening to a near–record (locally) low mean sea level pressure, very high winds, and anomalous cold surface temperatures. High winds contributed to extensive damage and 10 deaths along the Uruguayan riverside.

f. Asia

i) Russia—O. N. Bulygina,[11] N. N. Korshunova,[40] and V. N. Razuvaev[72]

(i) Temperature

Russia experienced very warm conditions in 2005. The mean annual air temperature anomaly relative to the period of record (1936–2005) was +1.6°C, which is the second highest value since 1936 (Fig. 6.19).

The year began with January temperatures above normal across all of Russia, although very cold weather was observed in places. Northeast European Russia experienced particularly warm conditions, with mean monthly temperature anomalies exceeding +8°C. Anomalies reached +7°C over central regions. Moscow's January 2005 temperature ranked third highest on record, with record maximum daily

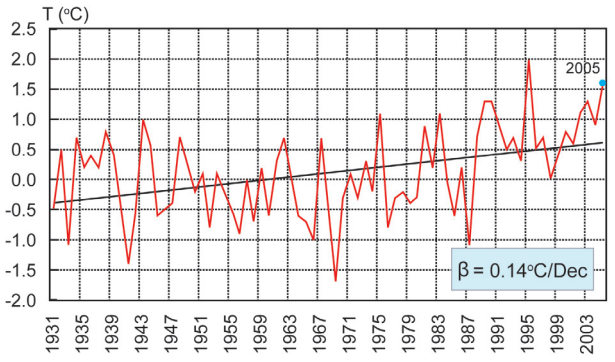

Fig. 6.19. Departures of mean annual air temperatures (red) over the Russian territory for the period 1931–2005. A linear trend of +0.14°C decade^{-1} (black) is also shown.

air temperatures observed on five days (e.g., 5.2°C on the 9th). February temperatures in north European Russia and western Siberia were up to 10°C above normal.

Interestingly, January and February air temperatures in the north of Asian Russia were often higher than those to the south. At Turukhansk, the 12 January mean air temperature was –5.5°C, which is 21.5°C above normal. In contrast, at the end of January the Novosibirsk and Kemerovo regions experienced temperatures as low as –38°C, and temperatures in the Republic of Altai reached –47°C. Particularly strong February frosts occurred between the 15th and 18th in Altai (–40° to –43°C), and from the 1st to the 10th in Trans-Baikal (–38° to –44°C), while true "Siberian" frosts (–35° to –40°C) were recorded during 14–19 February in the Krasnoyarsk Territory and Khakasia (south-central Siberia). The Republic of Tuva experienced its most severe and persistent frosts in the past 20 yr, as temperatures fell to –48°C in the Tuva hollow.

March brought bitter cold across much of European Russia, with record cold mean monthly temperature anomalies (–5° to –6°C) set in several northeastern areas, and colder-than-normal (–3° to –4°C anomaly) conditions in central and western regions. However, April countered with positive temperature anomalies over most of Russia. Western parts of the Sakha Republic (northeast Siberia) were particularly warm, with mean monthly anomalies from +7° to +8°C. Anomalous warmth continued into May, with the mean May temperature for Russia tying the record set in 1943. May 2005 was the hottest May in the 105-yr temperature record for the Ural Federal District.

During the first 20 days of June, central and southern regions of European Russia recorded anomalously cold air temperatures (0° to –2°C) as a result of frequent cold air intrusion. Concurrently, temperatures ran 1° to 2°C above normal across most of the Russian Far East. In early July, western and southern-central regions of Siberia experienced a heat wave, with diurnal temperatures climbing to 39°C in places.

A strong anticyclone centered over European Russia caused very dry and hot weather in August. The Novosibirsk region and Altai in western Siberia experienced mid-August diurnal temperatures between 28° and 38°C. At 40°C, Zmeinogorsk exceeded the previous August maximum temperature record by 2°C. For the whole of Russia, summer 2005 was one of the warmest on record.

With a temperature anomaly of +2.7°C, autumn 2005 was the hottest autumn on record for Russia (Fig. 6.20). While September was warm, eastern Siberia experienced its warmest October in the past 65 yr, with October temperatures 2°–5°C above normal. Record November temperatures were also reported at several meteorological stations in northeastern European Russia and in the southeast of the Sakha Republic as two large heat domes formed over those regions (Fig. 6.20). Temperatures near the centers of these areas of heat were 9° and 11°C above normal, respectively.

The warm weather over European Russia and the Sakha Republic persisted into December, with monthly temperatures being 1°–4°C above normal. However, December temperatures were 4°–5°C below normal in southern Siberia (Krasnoyarsk Territory and Irkutsk region) as a cold pool formed in the Siberian anticyclone zone following the warm autumn.

(ii) Precipitation

The warm winter temperatures also led to above-normal January precipitation in places. Moscow reported a new record January precipitation total of 98 mm (232% of monthly average). Heavy March precipitation was recorded in the eastern regions of European Russia and in the Urals, in some regions exceeding normal values threefold. Frequent March snowstorms with heavy snow were observed across European Russia (from the Nenets Autonomous District to northern Caucasia). The Taimyr Peninsula experienced strong winter blizzards with heavy snow and winds exceeding 25 m s^{-1}. In the east, Trans-Baikal, Sakhalin, and Kamchatka were repeatedly attacked by strong cyclones that brought heavy snow and blizzard conditions. March precipitation in these regions was more than double that of normal amounts.

Heavy April precipitation (200% to > 300% of normal) was recorded in central and southern regions of

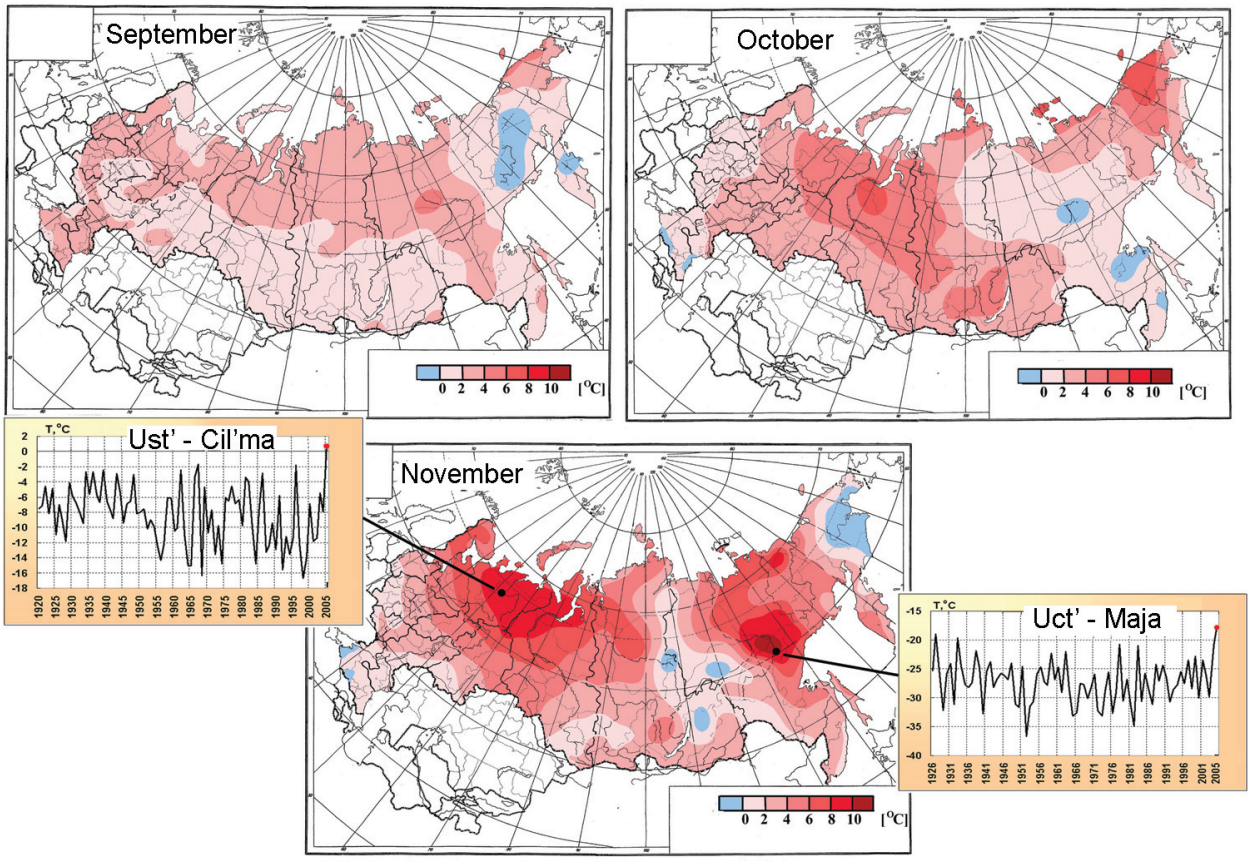

Fig. 6.20. Russian air temperature anomalies (°C) in autumn 2005. Insets show November mean monthly air temperatures at meteorological stations Ust'-Cil'ma (1920–2005) and Uct'-Maja (1926–2005).

Siberia (Krasnoyarsk Territory, Khakasia, Cis-Baikal, and Trans-Baikal). From 12 to 16 days of precipitation fell in Khabarovsk Territory and the Amur region, more than double the normal frequency and totaling over 200% of the normal precipitation for the month. Wet conditions continued into May in Khabarovsk, Maritime Territories, and Sakhalin, resulting in high river levels.

Summer precipitation across Russia was often accompanied by severe thunderstorms with hail and wind squalls. Hail to 35 mm was recorded in the Krasnodar Territory. In early June, the Arkhara River (Amur region) flooded to a record June level of 4.1 m after a 2-day, 100-mm rainfall. However, the hot June was accompanied by precipitation deficits over western Siberia (20%–30% of monthly normals). July precipitation in European Russia was inconsistent, with heavy thunderstorms in places and precipitation deficits in others. August precipitation was just 8%–30% of normal across European Russia, although the Kaliningrad region in the far west received over 300% of normal monthly precipitation.

Precipitation deficits continued into September. Moscow experienced one of its driest Septembers on record (12.2 mm, 18% of normal). With the high temperatures, fire hazard increased over much of European Russia, and several peat bogs caught fire. Near-normal precipitation returned to Russia by December, with the exception of the south of the Central Federal District, where around 200% of monthly normal snow fell.

ii) China—F. Ren[73] and G. Gao[23]

(i) Temperature

In 2005, the annual mean temperature of China was 0.6°C above the 1971–2000 mean (Fig. 6.21). It was the ninth consecutive year of warmer-than-normal temperature since 1997. Regionally, temperatures were above or near normal across most of China, with 1°–2°C above normal in the middle Tibetan Plateau and eastern Xinjiang.

The 2004/05 winter (December–February) mean temperature was near normal for China, but it ranked the third lowest since the 1986/87 winter. In mid-February, rare icing events occurred in some provinces

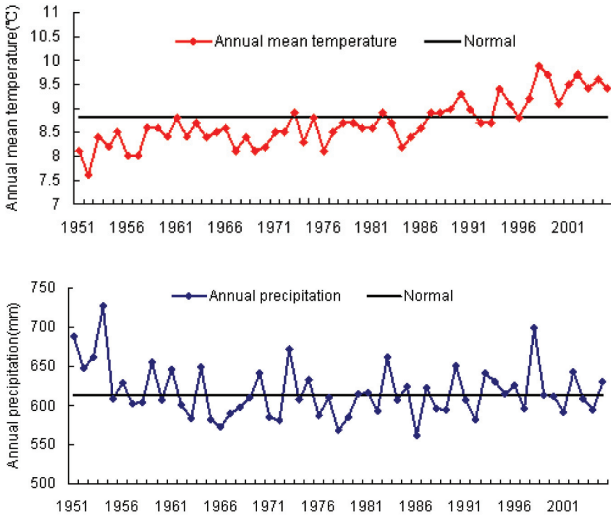

Fig. 6.21. Mean annual (top) temperature (°C) and (bottom) precipitation (mm) averaged over China relative to the 1971–2000 mean.

in southern China (e.g., Hunan, Hubei, Guizhou). In Hunan Province, the power grid was the most heavily affected by icing since 1954.

Summer seasonal mean temperature tied 2000 and 2001 as the highest ranked since 1951. Heat waves occurred frequently in central-eastern China and Xinjiang. Southeastern China experienced 5–15 days more than normal (20–40 days) with maximum temperatures at or above 35°C. Seasonal extreme daily maximum temperatures were 38°–42°C in North China, western Huanghuai Region, and South China, while records (1951–2005) of seasonal extreme daily maximum temperature were broken in parts of Hebei, Shanxi, Shandong, Zhejiang, and Inner Mongolia.

China also experienced a warm autumn, and the seasonal mean temperature ranks second in the historical record (1951–2005). In southeastern China, heat waves returned during the middle of September, and daily maximum temperatures soared to 35°–39°C.

(ii) Precipitation

In 2005, annual precipitation was 17.7 mm above the 1971–2000 mean across China (Fig. 6.21). Regionally, precipitation was 30%–100% above normal in the Huanghuai region, southern and northern Xinjiang, Qinghai, northwestern Tibet, and the southeast coast, and 30%–80% below normal in northern Heilongjiang, the middle of Inner Mongolia, and northern Ningxia (Fig. 6.22).

Regional and short-term drought was a major characteristic in 2005. In southern South China, precipitation was only 300–600 mm from September 2004 to May 2005, or about 30%–80% below normal, resulting in severe persistent drought. From April to May, rare spring drought occurred in Yunnan Province as a result of long-term rainfall deficiency. Early summer drought occurred in middle and lower reaches of the Yangtze River due to a delay in the onset and shortened duration of the plum rain season generating below-normal precipitation. Summer–autumn drought occurred in northeast part of northwest China and Inner Mongolia, and autumn drought affected Hunan and western South China.

(iii)Notable events

An above-normal eight tropical storms or typhoons made landfall in China, of which six (Haitang, Matsa, Talim, Khanun, Damrey, and Longwang) were severe, with winds over 162 km h^{-1} (see section 4c). Heavy rain and high winds generated mudflows and widespread flooding. About 92 million people were affected (386 dead), and economic losses of over 82 billion yuan Renminbi (RMB; $10 billion USD) were exceeded only by losses in the 1996 typhoon season.

From 17 to 25 June, consecutive heavy rainstorms impacted South China with 300–600 mm of rain falling in parts of Fujian, Guangdong and Guangxi Provinces. The Xijiang River in Guangxi and the Minjiang River in Fujian exceeded flood stage. About 21 million people were affected by the floods—171 people lost their lives and direct economic loss was over 18 billion RMB ($2.2 billion USD).

During early and middle July, heavy rain and flooding occurred in the upper reaches of the Huaihe River Basin. Between late September and early October heavy flooding occurred in the Hanjiang River and the Weihe River as the result of frequent and

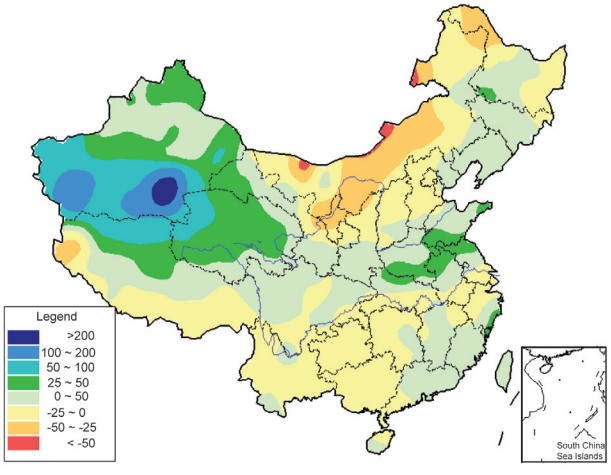

Fig. 6.22. Precipitation anomalies (%) across China (1971–2000 base).

widespread rainfall in the southeast part of northwest China and the Huanghuai region. About 5.52 million people were affected, with 14 dead in Shanxi, Hubei, and Gansu Provinces and 2.5 billion RMB ($311 million USD) of direct economic loss.

Although fewer dust storms affected China than in 2004, and 2005 had the lowest number since 1954, 13 storms occurred. The most widespread occurred from 16 to 21 April, affecting 12 provinces in northern China, while the most intense storm occurred on 27–28 April, impacting nine northern provinces or regions, including Beijing.

III) Southeast Asia—F. Ren[73] and G. Gao[23]

(i) East Asian monsoon

Onset commenced over the South China Sea (SCS) in the sixth pentad of May, about two pentads later than normal. Stronger-than-normal southwesterly flow advanced to and persisted over South China until the fourth pentad of June. In the last 10 days of June, the monsoon advanced to the region between the Yellow and Huaihe Rivers. In mid-August, rapid retreat occurred to around 30°N where it remained until mid-September. In the sixth pentad of September the warm and humid air had withdrawn from East Asia, and wind direction in the SCS shifted from the southwest to northeast, signifying a near-normal closing date to the East Asian summer monsoon.

The SCS summer monsoon index (–1.42) was weaker than normal. Intensity of the SCS monsoon also was weaker than normal during summer except for the periods from the sixth pentad of May to the third pentad of June and from the second pentad of August to the third pentad of August (Fig. 6.23). Precipitation was above normal in most of South China in June and in the Upper Huaihe River from July to September.

(ii) Temperature

Annual air temperature anomalies were generally 0.5°–1°C above the 1971–2000 mean. However, annual temperatures over the SCS were near to slightly below normal (Fig. 6.24). Seasonal mean surface air temperatures were above average in most of southeast Asia during December 2004–February 2005, with anomalies exceeding 1°C in the northern and southeastern Indo–China Peninsula. Generally, temperatures were close to normal across southeast Asia through the remainder of the year.

(iii)Precipitation

Precipitation was generally below normal across most of continental Southeast Asia in 2005. Northern and western Myanmar, southern Vietnam, and portions of Malaysia observed annual anomalies more than 400 mm below normal. The Philippines, western Thailand, and the northern Malay Peninsula received above-normal precipitation, with northeastern Malaysia, central Vietnam, and Mindanao all receiving over 400 mm above normal for the year (Fig. 6.24).

December 2004–February 2005 rainfall was below average over most of Southeast Asia, and more than 80% below normal in the western Indo–China Peninsula. March–May rainfall totals were well below normal in the northern Indo–China Peninsula and close to normal over the remainder of Southeast Asia. In April, Thailand experienced its worst drought in seven years. June–August precipitation was close to normal, though heavy rainfall caused flooding in northern Thailand. In Myanmar, heavy monsoon-related rainfall affected the southern coastal areas during the second week of September. Otherwise, September–November rainfall was near normal.

(iv)Notable events

In Indonesia, heavy January rains hampered tsunami (December 2004) relief efforts, and continued heavy rain in February generated landsides that left 61 dead and 90 missing. On 9 June, continuous heavy rain brought mudslides with 12 deaths and 11 missing in northern Vietnam. In West Sumatra, Indonesia, heavy rainfall produced landslides near Padang on 2 September. There were 16 fatalities and at least 10 injuries. Heavy October rains across central Vietnam produced flooding with at least 67 fatalities. The most severely affected area was Binh Dinh Province, where 3,200 houses were damaged and most of the fatalities occurred.

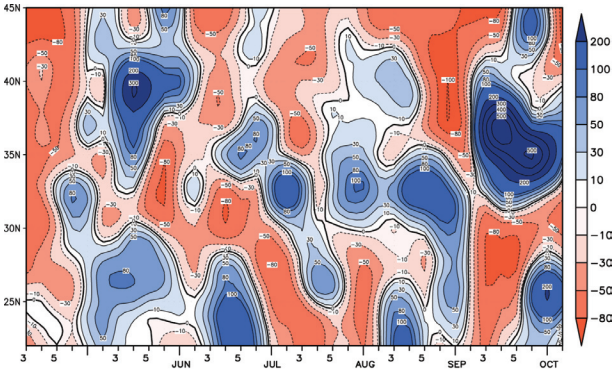

Fig. 6.23. Time–latitude cross section of pentad precipitation anomalies (%) for 110°–120°E. [Source: National Climate Center (NCC) China Meteorological Administration (CMA)]

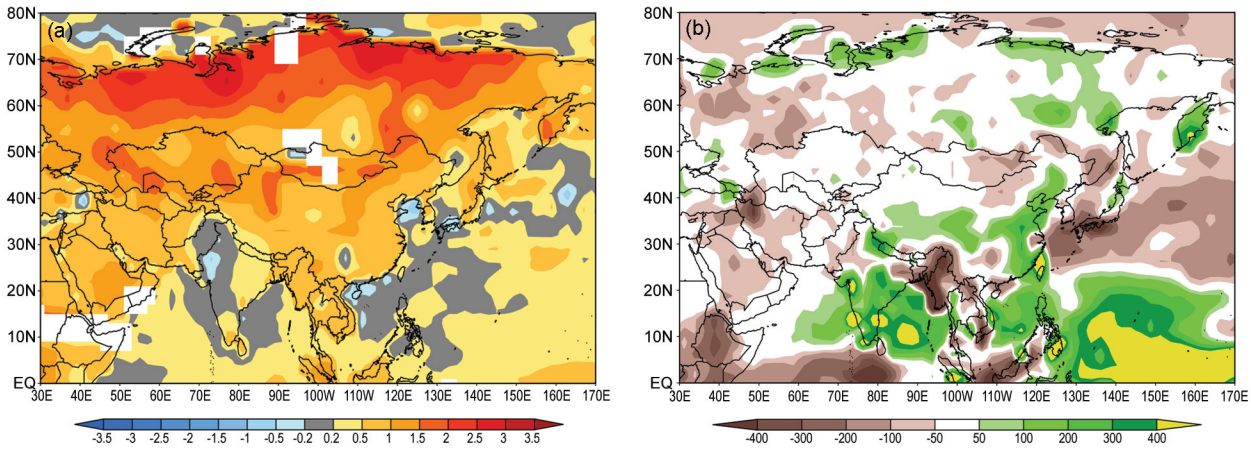

Fig. 6.24. Asian 2005 annual (left) temperature anomalies (°C; 1971–2000 base), and (right) precipitation anomalies (mm; 1979–2000 base) from CAMS–OPI.

iv) India and Southern Asia—M. Rajeevan[71] and K. R. Kumar[42]

(i) Temperature

This year was marked by extreme weather all across South Asia, both in terms of temperature and precipitation. At the beginning of the year, parts of Afghanistan and adjoining Pakistan experienced extreme cold weather, with temperatures more than 5°C below normal in February. Severe cold also prevailed over northern India and adjoining regions in late February. During the postmonsoon season and toward the end of the year, heavy snow and extreme low temperatures occurred over northern parts of South Asia, causing several casualties and seriously affecting the rescue and rehabilitation work in Pakistan following the destructive earthquake of 8 October.

On the other extreme, May and June brought scorching heat waves, with maximum temperatures around 45°–50°C in India, Pakistan, and Bangladesh. Delayed southwest monsoon rains allowed the heat to persist into June, claiming at least 400 lives in India. An anomalous anticyclone and northwesterly winds created a severe heat wave over central and northeastern India, with maximum temperatures 6°–8°C above normal.

(ii) Precipitation

During the third week of February, sections of northern Pakistan and neighboring areas of northern India received heavy snowfall, described as the worst in two decades. Snowfall accumulations reached almost 2 m in some parts of Jammu and Kashmir in India. In Pakistan, heavy rains in the south and snow in the north triggered flooding and avalanches, causing the extensive loss of life and property. Heavy rains in March also caused flooding in parts of western Pakistan and Afghanistan; Balochistan Province was the worst affected. Over Pakistan, the 2005 January–March seasonal rainfall was 121% of its long-term average.

(a) *South Asian Summer monsoon*

The summer monsoon this year was marked by unprecedented heavy rains and extensive flooding in parts of western and southern India, affecting more than 20 million people and resulting in more than 1,800 deaths. Rainfall activity in Nepal and Bangladesh was, however, below normal. Central and southern parts of India received excess rainfall during the season (Fig. 6.25). While northwest India received normal rainfall, seasonal rainfall over

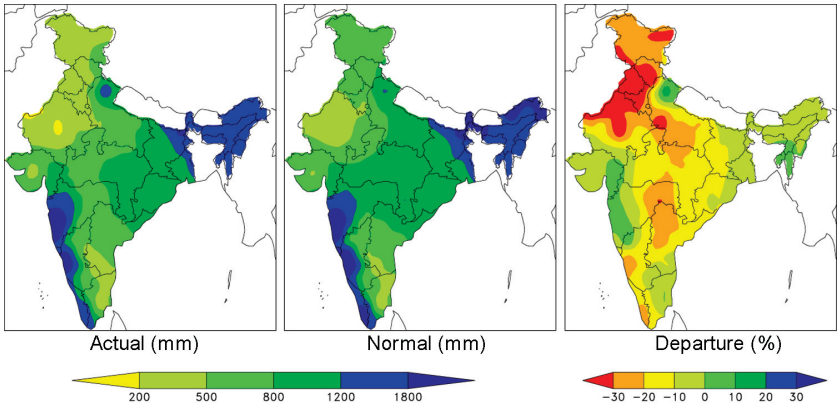

Fig. 6.25. June–September precipitation (mm) over India in 2005: (left) actual; (center) normal; and (right) percentage anomaly.

northeastern parts of India was below normal by more than 20%.

Onset of the 2005 southwest monsoon was delayed to 5 June, when it arrived over the south peninsula and northeastern parts of India. Despite unfavorable synoptic conditions, the monsoon advanced more quickly over northwestern India and Pakistan, covering the entire subcontinent by 30 June, 15 days ahead of the normal.

Countering declining trends of recent years, 12 low pressure systems formed (the most since 1998), of which five developed into monsoon depressions and one into a cyclonic storm (the first in September since 1997). The storm tracked from the Bay of Bengal across central India and the Gangetic Plains, resulting in widespread flooding.

While the spatial distribution of rainfall this season was normal, it was intermittent. There were prolonged dry spells in June and August, though excess rainfall in July and September ultimately helped the season end with near-normal rainfall. Due to the late onset and sluggish advance of the monsoon, rainfall during much of June was limited. In August, monsoonal rainfall was 27% below normal over India. Precipitation deficits lead to moderate drought for 25% of India's meteorological districts (2% severe drought). For the season, average rainfall over India was near normal (–1%).

(b)*Northeast monsoon*

Heavy rainfall continued unabated in southeastern parts of India and Sri Lanka during the northeast monsoon season of October–December. Five low pressure systems (four depressions and one cyclonic storm) affected southern parts of India and Sri Lanka. In India, Tamil Nadu and Andhra Pradesh were the most affected states. The northeast monsoon seasonal rainfall over south India was 165% of normal, the highest since 1901. Associated flooding affected more than 3 million people, with at least 300 fatalities and considerable socioeconomic impact. In Sri Lanka, approximately 29,000 families in 10 districts were affected and at least six deaths were reported.

(iii)Notable events

The most notable event of 2005 occurred on 27 July, when Mumbai (Bombay) received its greatest-ever recorded 24-h rainfall of 944.2 mm (most of it in just 6 h, between 1430 and 2030 local time) at Santacruz, an observatory at the airport (Fig. 6.26). The previous record of 575.6 mm was set at Colaba on 5 July 1974. Interestingly, in the 2005 event Colaba, just 20 km from Santacruz, recorded only 73.4 mm of rain. This localized event was confined to a region of a 20–30 km radius. Although a warning for regionally heavy rainfall had been issued, torrential rain severely disrupted life in the city, with numerous fatalities, heavy damage, and large economic losses.

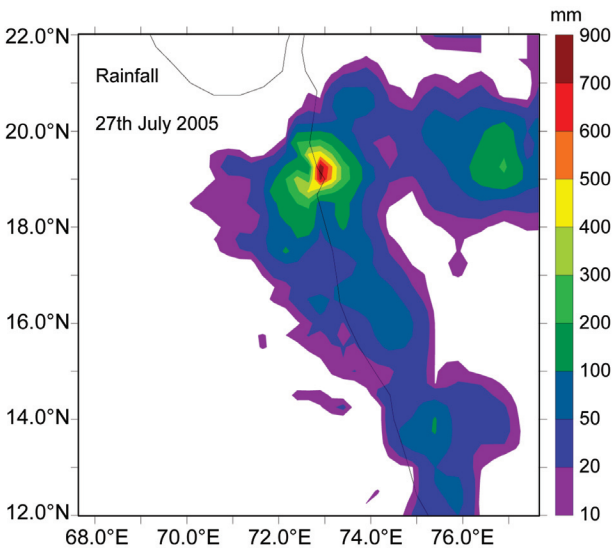

Fig. 6.26. Rainfall totals (mm) on 27 July around Mumbai, India.

v) Southwestern Asia—F. Rahimzadeh,[70] M. Khoshkam,[41] and E. K. Grover-Kopec[31]

(i) Temperature

All of southwest Asia experienced above-normal temperature in 2005, with annual temperature anomalies of 0.5°–2°C. North and northeastern Iran were 3°C warmer than normal for the year. Despite these positive 12-month departures, the northern half of the region experienced cooler-than-normal conditions during February, when mean temperatures ranged from 5°C in western Turkmenistan to –18°C in the highlands of Tajikistan and Kyrgyzstan. Temperatures were 1°–6°C below normal in these areas. Northern Iran experienced winter temperatures 3°C below normal. Northern Afghanistan, where hypothermia and other cold-related illnesses claimed more than 100 deaths, recorded temperatures of 1°–2°C below normal during February.

In contrast, temperatures were above the 90th percentile across the central portion of Southwest Asia during March (2°–7°C above the long-term average; Fig. 6.27). Afghanistan, Kyrgyzstan, Tajikistan, and Pakistan experienced temperatures 1°–2°C above normal in June. Spring temperatures in Iran were split between cooler-than-average conditions in areas of the east, center, and northeast of the country, and warmer-than-normal conditions elsewhere.

Seasonal mean temperatures in southern Iran were 10°–35°C.

Most of Iran saw positive summer temperature anomalies exceeding 2°C. A heat wave that affected Iran in July produced monthly anomalies up to 4°C above normal. Autumn remained on average 2°C above normal across Iran, although cooler-than-normal conditions were observed over the Persian Gulf.

(ii) Precipitation

Southwest Asia generally receives most of its annual precipitation from extratropical disturbances traveling eastward from the Mediterranean Sea between November and April. From July through August, the South Asian monsoon generally brings precipitation to southeastern Afghanistan, but tends to suppress summer precipitation in areas farther north and west.

Annual precipitation accumulations were slightly below normal across the majority of the region during 2005, and most of these negative annual anomalies were 25–75 mm below normal (Fig. 6.27). These departures were modest, however, and generally accounted for less than 25% of normal annual precipitation (i.e., 2005 annual totals were about 75%–100% of normal). A few areas received above-average precipitation during 2005, including portions of southern Afghanistan, western and northern Pakistan, and south-central Kazakhstan. However, these departures were also relatively small (10–50 mm) compared to long-term mean accumulations.

Despite the relative precipitation deficits across Southwest Asia, portions of the region experienced record snow amounts during January and February. As much as 200 cm of snow fell in just 2 weeks in parts of Tajikistan, contributing to more than 475 avalanches in the mountainous country. Similar impacts were reported in northeastern Afghanistan where avalanches claimed approximately 160 lives. The heavy snowfall in January and February, and above-average precipitation in late 2004 (Levinson 2005), contributed to a healthy snowpack in the highland areas of Southwest Asia, which is responsible for providing most of the region's water supply later in the year.

The 2004/05 winter was also wetter than normal across most of Iran, averaging 154.1 mm, or 14% above 2004 levels and 24% above the long-term mean. The largest anomalies were in southeast Iran, where some locations received up to 3.5 times the normal seasonal amounts. Also, early winter snow alleviated a 7-yr drought in the region. Tehran experienced record February snowfall, and in northern Iran, heavy late-February snow damaged or destroyed over 7,000 homes.

Unfortunately, abnormally warm conditions in March hastened the melting of the highland snowpack and swelled rivers across the region. Heavy rainfall in central and western Afghanistan during March exacerbated conditions and caused extensive flooding in those areas. The June heat wave melted remaining snowpacks in Afghanistan, Kyrgyzstan, Tajikistan, and Pakistan. Pakistan's northern provinces in were extremely hard hit by the resulting flooding. More than 460,000 people were affected and nearly 1 million ha of crops suffered damage.

Although spring is generally the rainy season for Iran, and wetter-than-average (100%–200%) spring conditions prevailed over northern Iran, it was much drier than normal (0%–10%) across southern areas,

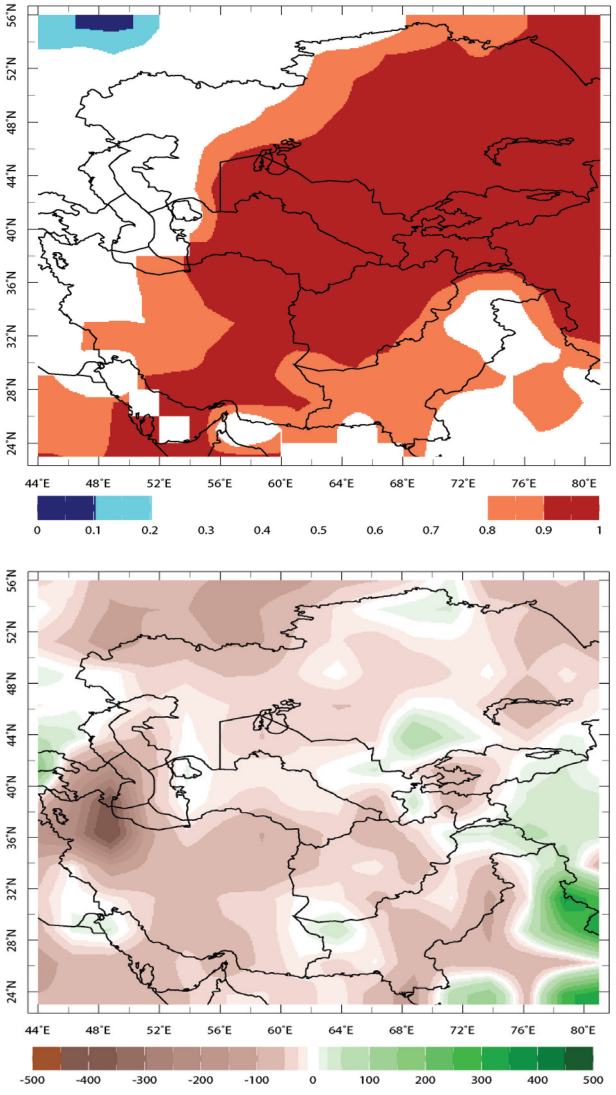

Fig. 6.27. Annual average (top) temperature deciles and (bottom) precipitation anomalies (mm; 1971–2000 base) for southwest Asia.

and also (50% of normal) in central regions. Overall, spring precipitation in Iran was just 42% of the normal. Summer precipitation in Iran was 20% below normal, with especially dry conditions in the west half of the country. However, heavy rains in the east did result in flooding. Below-normal precipitation continued into the autumn across much of Iran. Autumn precipitation in Iran was 37% below the long-term mean, and some parts in the east received just 0%–25% of the normal seasonal precipitation due to the delayed onset of late-season precipitation.

g. *Europe*

i) Overview—J. J. Kennedy[38]

The annual surface temperature anomaly (Brohan et al. 2006) averaged over Europe in 2005 was 0.71 ±0.07°C above the 1961–90 average (Fig. 6.28). Only a small area extending north from Greece had annual temperatures below average (Fig. 6.29), and that was only by around 0.1°C. Annual average temperatures in the United Kingdom and northern Norway and Finland were above the 90th percentile of occurrence according to statistics based on the period 1961–90 (all European temperature and precipitation percentiles herein refer to this period).

Temperatures during the first three months of 2005 were significantly (meaning in the upper or lower decile of the distribution) below average in southern Europe, through Spain and the Mediterranean and into Italy. In the same period, above-average temperatures observed in the north and east exceeded the 90th percentile only over Scotland. Between April and June, temperatures were above average in all areas and significantly above normal over much of Europe west of 15°E and south of 55°N.

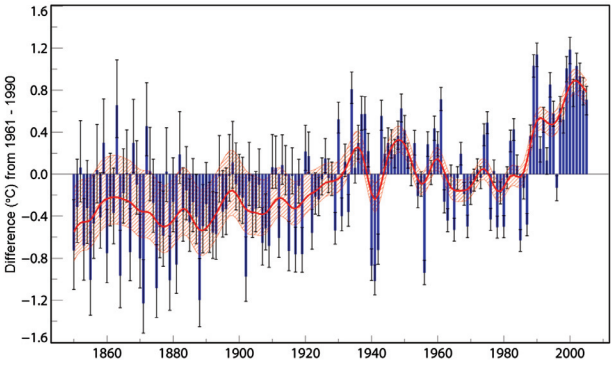

Fig. 6.28. European average temperature anomalies (°C; relative to 1961–90 mean) 1850–2005. Blue bars show the annual values with uncertainties represented by the black bars. The red curves show the annual anomalies and uncertainties after smoothing with a 21-term binomial filter. [Source: Brohan et al. 2006]

Temperatures in Spain and France exceeded the 98th percentile. From July to September temperatures once again were above average in most areas, although temperatures were close to average in southeastern Europe. Scandinavia and Eastern Europe were significantly above normal. Cooler conditions in southeastern and central Europe coincided with the largest regional rainfall totals for the season. October–December brought a north–south split, with much of the Mediterranean and southern Europe experiencing below-average temperatures, while in the north temperatures were generally above average with areas of the United Kingdom and Scandinavia significantly above average.

Total precipitation (Rudolf et al. 1994, 2005; Rudolf and Schneider 2005; Beck et al. 2005) between January and November 2005 (Fig. 6.29) was below

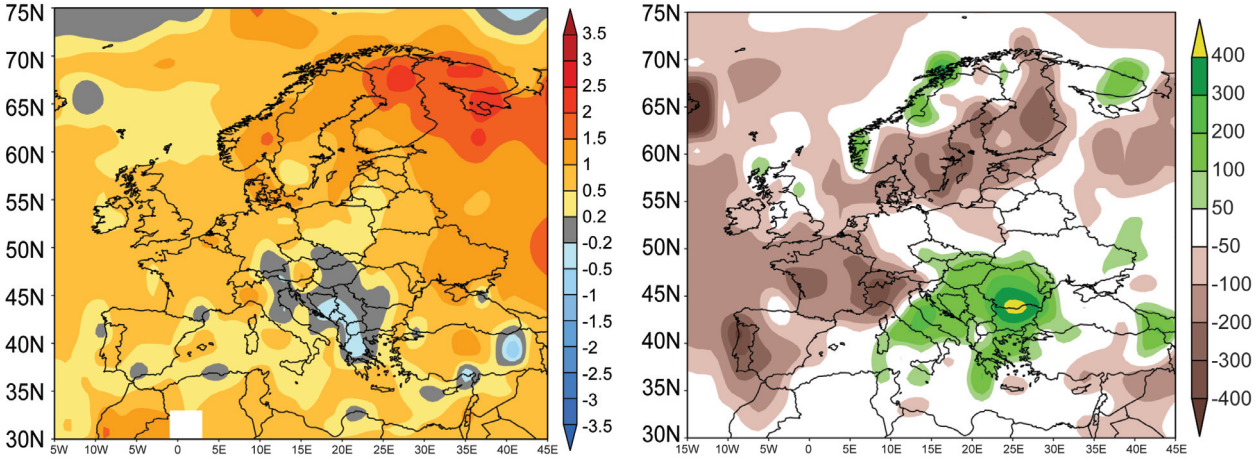

Fig. 6.29. European 2005 annual (left) temperature anomalies (°C; 1971–2000 base), and (right) precipitation anomalies (mm; 1979–2000 base) from CAMS–OPI.

average in southwestern Europe, with parts of France and the Iberian Peninsula receiving less than 40% of the 11-month 1961–90 average. Precipitation in southeastern Europe was above the 1961–90 average. Romania and Bulgaria received significant rainfall excesses during the year, with August totals in some areas approaching 500% of the monthly average.

ii) Central and Eastern Europe—J. J. Kennedy[38]

Annual average temperatures in the region ranged from near average in Hungary and neighboring countries to over 2°C above average in eastern Ukraine (Fig. 6.29). January–November rainfall was significantly above average in Romania (Fig. 6.29).

A warm January, with areas of eastern Ukraine more than 5°C above average, gave way to colder conditions in February and March. Precipitation was generally below average in the southwest, but further north and east exceeded the average, with the largest excesses occurring in January and February. March rainfall was below average in most areas.

April–June temperatures in parts of Austria and the Czech Republic were significantly above average, and in Switzerland some western areas experienced temperatures above the 98th percentile. Further east, however, temperatures were nearer the average. Rainfall anomalies were generally higher in the east than the west, with the highest anomalies in Romania and Moldova.

In June, temperatures were significantly above normal in Austria and Switzerland and, in the far west, were high enough to exceed the 98th percentile. At the same time, temperatures in Ukraine and Romania fell below average. With only eastern Ukraine experiencing below-average rainfall, April precipitation was above average in most areas and the excess rainfall led to flooding in Romania. May precipitation was close to average in many areas, but Romania again experienced above-average totals. Most areas were drier than usual in June, with only eastern Romania and Ukraine experiencing wetter-than-normal conditions.

Temperatures were above average between July and September everywhere. The largest anomalies were in the east where temperatures were significantly above average. Smaller positive temperature anomalies further to the west coincided with the largest rainfall anomalies. Some areas of southern Romania received more than three times the seasonal average, generating widespread flooding in July and August. July temperatures were above average in all areas, but above-average precipitation contributed to depressed temperature anomalies in central Europe. Only Ukraine, where precipitation levels were below normal, showed significant warmth. August brought above-average rainfall to all but the most easterly areas, and temperatures fell below average in the west. Ukraine showed the highest temperature anomalies, with temperatures significantly above normal in parts.

October and November were mainly drier than usual in western areas, with wetter-than-average conditions confined to eastern Romania and Ukraine. Cold anomalies spread from the southeast in October to cover the central and western states in November. In December, cold anomalies were confined to the westernmost regions, with some parts of Austria significantly below normal.

iii) Fennoscandinavia, Iceland, and Greenland—C. Achberger[1] and D. Chen[16]

Fennoscandinavia's (here Norway, Sweden, Finland, and Denmark) climate is to a large extent controlled by the atmospheric circulation over the European and North Atlantic region. Objective synoptic classification based on the Lamb scheme (Lamb 1950) has been extensively used in Sweden to quantify impacts of atmospheric circulation (e.g., Chen 2000). In 2005, occurrences of the four dominant weather types—anticyclonic (A), cyclonic (C), westerly (W), and southwesterly (SW)—were all above the 1961–90 mean. The generally warmer than normal conditions over Fennoscandinavia in 2005 correspond well to increased frequencies of W and SW types.

(i) Temperature

Annual mean temperatures for 2005 in the Nordic countries (including Greenland and Iceland) were around 0.5° to 4.5°C above the 1961–90 mean (Fig. 6.30), depending on geographical location. At Svalbard on Spitsbergen, annual mean temperatures reached –3.0°C, which is 3.6°C above normal, ranking 2005 as the warmest year since 1912. Danmarkshavn, in northeastern Greenland, reported an annual mean temperature of –9.5°C, placing 2005 as the warmest year since reliable measurements started in 1949. Parts of Finland were also unusually warm, at around 2.3°C above the long-term mean. Sweden, Denmark, and Norway, however, experienced more moderate temperature deviations, ranging between 1.1° and 1.7°C above normal, while the annual mean temperature for Iceland was about 1°C warmer than the 1961–90 mean. The warmer-than-normal temperatures were most profound at the highest latitudes.

Autumn (September–November) was extraordinarily warm at many Nordic locations, several of

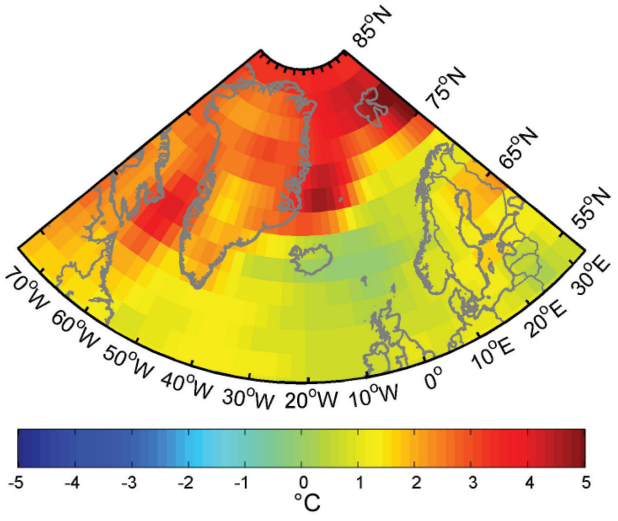

Fig. 6.30. Annual temperature anomalies (°C) across Fennoscandinavia, the North Atlantic, and Greenland in 2005 (1961–90 base). [Source: NCAR–NCEP Reanalysis]

which broke existing records. For example, on 11 October 2005 several Norwegian stations reported daytime temperatures well above 20°C. Of these, Molde Airport recorded the highest temperature (25.6°C), which is a new Norwegian record for October. Finland also experienced two unusually warm spells in autumn, making November 2005 the warmest November since 1900 in the central regions. For Denmark, 2005 was the fourth sunniest year on record and Reykjavik, Iceland, experienced 280 more sunshine hours compared to the 1961–90 mean. In all, 2005 is ranked as the fifth to eight warmest year since the second half of the eighteenth century, when regular measurements commenced in many Nordic countries.

(ii) Precipitation

Annual precipitation amounts across the region were both above and below the 1961–90 average (Fig. 6.31). Across much of Finland, northern regions of Norway and Sweden, the Färö Islands, and along the southern half of the Norwegian west coast, annual precipitation was above average (Fig. 6.31, right), where positive departures reached up to 40% of the long-term mean. Greenland also experienced remarkable precipitation deviations from the long-term mean (Fig. 6.31, left). However, while large regions of southernmost, western, and northern Greenland received from 50% to over 100% more precipitation than the 1961–90 mean, parts of eastern and southern Greenland were considerably drier than normal (Fig. 6.31, left).

Southern Sweden, Denmark, and Iceland received annual precipitation amounts either somewhat below or close to the long-term average. Many locations across Fennoscandinavia, though, reported record or near-record precipitation in 2005: Nuuk, Greenland, received 1219 mm, ranking 2005 as the wettest year there since 1958. For Norway, 2005 was among the second to third wettest year since measurements began. Parts of Finland experienced a very wet May, with precipitation 200%–300% above normal. Severe flooding occurred along several rivers in northern Finland as a result of snowmelt. Also, Sweden experienced heavy rainfall in July and August.

(iii)Notable events

For much of the region, 2005 started with an extremely severe storm. On 8–9 January an intense low pressure system formed west of the British Isles and intensified on its way toward Fennoscandinavia. Mean sea level pressure dropped as low as 960 hPa when the system, named Gudrun, reached Sweden, causing major damage. Mean wind speeds and maximum gusts reached 33 and 42 m s^{-1}, respectively. In addition to widespread power failure and infrastructure damage, Gudrun was responsible for several fatalities, and became the worst tree-felling storm in Sweden since 1930, when statistics on storm-related forest damage started. In addition, record sea levels and coastal flooding occurred along parts of

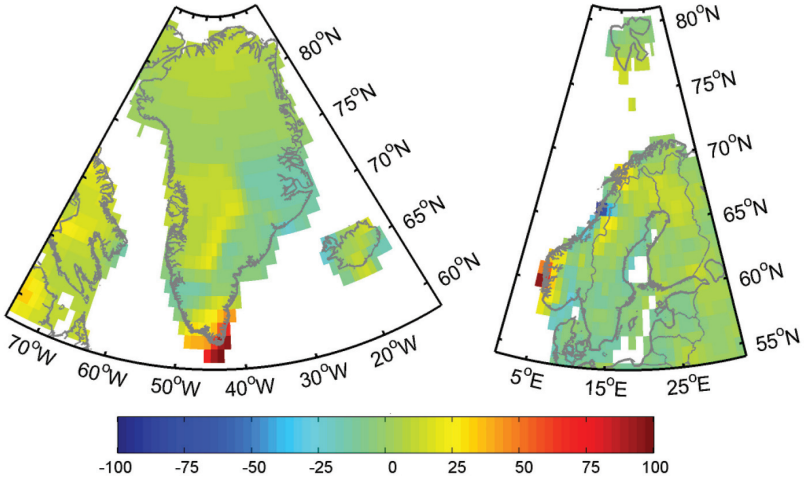

Fig. 6.31. Annual precipitation departures from normal (mm yr^{-1}) across (left) Greenland and (right) Fennoscandinavia (1961–90 base). [Source: Global Precipitation Climatology Center (GPCC)]

the Swedish, Norwegian, and Finnish west coasts. Swedish insurance companies rank Gudrun as the costliest natural event in their history.

Remnants of Hurricane Katrina reached Greenland as an extratropical low pressure system in early September. The low brought several thunderstorms and frequent lightning to southwest Greenland.

On 14 November, an exceptionally strong low pressure system named Loke reached Norway and brought over 200 mm of precipitation over 24 h to several locations. In addition to one fatality, the storm generated landslides across Norway, closing many roads and the train line between Oslo and Bergen. Loke produced the country's second highest daily precipitation amount (223 mm) on record, measured near Bergen.

iv) Central northern Europe—J. J. Kennedy[38]

Annually averaged temperatures in 2005 were above average throughout the region (Fig. 6.29). Precipitation totals for January–November were near average in the west and east, but somewhat drier than average in Poland (Fig. 6.29).

January temperatures and precipitation were above average everywhere, with the largest temperature anomalies (more than 5.3°C) in the east. February temperatures fell to below average everywhere except the far northeast. These northeastern areas were also drier than normal, but most areas experienced above-average rainfall in February. March temperatures were more than 3°C below average in Estonia and Latvia, and only western Germany experienced warmer-than-average temperatures. Rainfall totals in March were anomalously large in Belarus, Lithuania, and eastern Poland, but were lower than average in other areas.

April–June temperatures in some areas of Poland and Germany were significantly above average. Temperatures were above average everywhere in April, with significant warmth (> 2°C) in parts of Germany and Poland. May anomalies were generally lower than those in April, with below-average temperatures in the east. After a dry April, May rainfall was above average. Precipitation was particularly heavy in the east with many areas receiving more than twice the usual monthly amount. One area in Belarus received nearly three times its average monthly total. In June, temperature anomalies fell again in the east, with temperatures dropping below average everywhere east of central Poland. Temperature anomalies in southwestern Germany, however, rose above 2.8°C (98th percentile).

July–September was another warm period. Temperature anomalies were highest in the east, exceeding the 90th percentile in large parts of Poland, Belarus, and Estonia. Precipitation was below average except in Germany. July saw above-average temperatures in all areas, although significant positive anomalies were found in only a few areas of Poland, Belarus and Lithuania. Above average rainfall in Germany and Poland may have acted to reduce temperature anomalies in those regions. Below-average August temperatures occurred in Germany and much of Poland, and wetter-than-average conditions existed in the east. September was drier and warmer than average in most areas, with Belarus, northern Germany, and western Poland experiencing significant warmth. Only central parts of Germany received above-average rainfall.

Temperatures between October and December were above average and precipitation totals were below average in all regions. October temperature anomalies were highest in Germany, where temperatures were significantly above normal over much of the country, and even rose above the 98th percentile in the west (+2.5°C anomaly). Some areas of Poland received less than 20% of the average October precipitation. In November southern Germany and Poland had below-average temperatures, but anomalies increased to the north. November was another dry month, and no area experienced above-average rainfall. In December, temperatures were above average in most areas, although southern Germany had temperatures that were more than 1.6°C below the average.

v) Northwestern Europe—J. J. Kennedy[38]

Annually averaged temperatures in northwestern Europe in 2005 were above average in all areas. The United Kingdom and Netherlands experienced significantly above-normal temperatures, and anomalies in Scotland exceeded the 98th percentile for the year. France and the south of the United Kingdom were drier than average between January and November 2005 and some areas of France received less than 60% of the average rainfall.

January saw significantly above-average temperatures in the United Kingdom. Most areas were dry, but the north of the United Kingdom received above-average rainfall, which led to flooding in a number of areas. Temperatures fell below average in most areas in February. In the south of France both temperatures and rainfall were significantly below average, with some areas receiving less than 20% of normal precipitation. Drier-than-average conditions continued in March across France and the United Kingdom. March temperatures were above average in most areas, and significantly so in Scotland and Ireland.

April–June average temperatures were significantly above normal everywhere except Scotland and Ireland. Temperatures in France exceeded the 98th percentile. April was warmer than average in all regions, but significant warmth was confined to the Low Countries, southeast England, and western Scotland. Precipitation was above average in most areas. Temperatures in May were below average only in Ireland and Scotland, while the south of France experienced significantly high temperatures. Rainfall was below average in England, Wales, and France, but above average in Scotland and Ireland. Significantly high June temperatures covered all areas except central England, where subzero temperatures were experienced near the start of the month and the central England minimum temperature index (Parker and Horton 2005) dropped below the 5th percentile of occurrence (3.6°C on 7 June). Contrastingly, temperatures in the southeast of France exceeded the 98th percentile. Precipitation totals were below average over continental regions.

July was warmer than average in all areas, with the highest anomalies over continental areas. Rainfall deficits were observed in the south of France and Scotland, but other areas experienced above-average rainfall. August was warmer and drier than usual in the west, but cooler and wetter than normal in the east. Anomalies increased in September with above-average temperatures in all areas. Southern France had the lowest temperature anomalies and highest rainfall anomalies, but other areas were predominantly dry.

In October temperatures in central areas exceeded the 98th percentile. On 12 October the highest ever October minimum central England temperature (15.2°C) was recorded. October precipitation was above average in the United Kingdom and northwest France, but below average in other areas. November temperatures in France and England were below average, and it was drier than average over most of the region. Temperatures in December were below average in France, particularly in the south of the country, where it was significantly below normal (< –2°C anomaly).

vi) Iberia—R. Trigo,[86] R. Garcia-Herrera,[24] and D. Paredes[64]

(i) Temperature

The average 850-hPa temperature across Iberia in 2005 was 0.3°C above normal (1961–90 base period mean). However, this relatively moderate annual anomaly conceals considerably larger cold and warm temperature anomalies observed in winter (-1.6°C) and summer (+1.7°C).

Wintertime upper-level 500-hPa geopotential height anomaly fields confirm the overall structure observed at surface, with intense positive anomalies centered between the Azores and Iceland (Fig. 6.32, left). As a consequence of this strong northwest–southeast geopotential height gradient, Western Europe was under the influence of strong cold air advection from higher latitudes. Several consecutive cold wave outbreaks were observed between the end of January and early March affecting all of Iberia as well as France and central Europe (Garcia-Herrera et al. 2006, manuscript submitted to *J. Hydrometeor.*). Daily maximum and minimum temperatures for Lisbon, Portugal, reveal that these cold waves reached the western coast of Iberia, producing a number of days with temperatures in the coldest decile (lowest 10%) of daily long-term records (Fig. 6.33). Interestingly, soon after the last cold wave, a circulation shift to North African air penetration resulted in late-March/early April daily temperatures within the highest decile (hottest 10%) of long-term temperature records for those days (Fig. 6.33).

Spring and summer months were characterized by warmer-than-normal temperature values, particularly between late May and August, with most of Iberia impacted by two intense heat waves in June and August (Fig. 6.33). Positive SLP anomalies over Europe, due to the extended Azores anticyclone, contributed to the anomalous warmth in these months. The summer 500-hPa geopotential height anomaly field was dominated by a positive anomaly maximum centered between Iberia and the United Kingdom (Fig. 6.32, right). This large-scale feature not only impeded the natural eastward progression of low pressure systems that frequently cross northern Europe in the summer, but contributed to the advec-

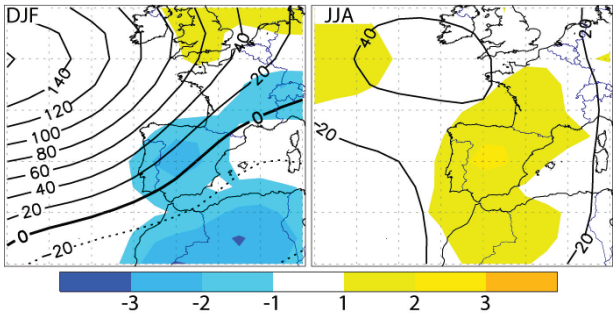

Fig. 6.32. (left) Winter (DJF) and (right) summer (JJA) anomalies of 500-hPa geopotential height (contours; gpm) and corresponding 850-hPa temperature anomaly field (color; °C) over southwest Europe and North Africa. [Source: NCAR NCEP reanalyses; 1961–90 base]

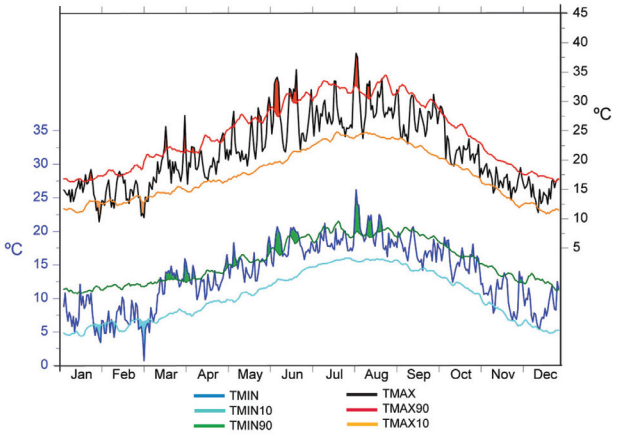

Fig. 6.33. Daily Tmax (black) and Tmin (dark blue) temperature (°C) in Lisbon during 2005. Red (green) and orange (light blue) lines correspond to the 90th and 10th percentiles, respectively, of the Tmax (Tmin) for each day of the year (10-day moving window), and were computed using the period 1941–2000.

tion of warm air masses in the south as well as enhanced adiabatic heating through subsidence (Trigo et al. 2004). Furthermore, extended periods of clear skies associated with anticyclonic conditions contributed to increased solar radiative heating over the region.

(ii) Precipitation

The Iberian Peninsula experienced drier-than-normal conditions during 2005 relative to the 1961–90 base period mean (Fig. 6.29). The hydrological year of 2004/05 (October 2004–September 2005) was among the driest since regular precipitation records started in both Portugal and Spain (see sidebar). In fact, based on the monthly Global Precipitation Climatology Center (GPCC)-gridded dataset (Rudolf and Schneider 2005), drought conditions prevailed in 2005 over a large area of Western Europe, including the southern United Kingdom, France, and Northern Italy (Fig. 6.29). During winter and spring, usually the wettest seasons, dry conditions prevailed over much of Iberia, with precipitation less than 50% (and in places < 25%) of 1961–90 mean values. Winter months were characterized by the presence of intense anticyclonic circulation, located northward of its usual latitude (Azores). Drought conditions continued through the spring months, although with less intensity than in winter. However, unlike winter, several storm tracks progressed from the Atlantic toward Iberia and France, but were stopped from penetrating the European continent by the development of extensive blocking events.

The summer season of 2005 was also characterized by reduced precipitation over Western Europe and northern Africa, with the maximum amplitude over Iberia. Precipitation totals rebounded across the northeastern sector of the Iberian Peninsula during autumn 2005, but normal precipitation fell in the remaining areas, particularly in the southern sector.

Major climatic anomalies are often driven by enhanced values of large-scale atmospheric circulation indices [e.g., ENSO, PNA, NAO, east Atlantic (EA)]. Interestingly, this record-breaking drought is only partially associated with extreme values of teleconnection indices, particularly those that are known to have a significant impact upon winter Iberian precipitation (NAO and EA). Moderately positive (negative) values of NAO (EA) recorded between November and February are clearly associated with the scarce precipitation observed over Iberia. However, the similarly dry conditions observed in March are more difficult to associate with the intense negative NAO (–1.8) and moderately positive EA (+1.1) indices. Instead, an extremely intense blocking event positioned over unusually southern latitudes contributed to the widespread March precipitation anomaly over Europe.

vii) Mediterranean and southern Europe—J. J. Kennedy[38]

Temperatures in the Mediterranean were above average in most areas in 2005. Greece was one of the few countries that experienced below-average temperatures for the year as a whole. Precipitation was generally below average in the west, but above average further east.

January–March temperatures were below average in all regions and significantly below average in Italy. In the western Mediterranean, temperatures fell below the 2nd percentile of occurrence. The north of Italy and the western Mediterranean were drier than average, while southern Italy and Greece were wetter. January temperatures were above average only in Greece, and in the western Mediterranean temperatures were below the 2nd percentile. Cold conditions continued into February and the whole of the Mediterranean area west of 25°E experienced significant cold. The south and west were the coolest areas, with temperature anomalies of –3.7°C in the Balearic Islands falling below the 2nd percentile. January was drier than average in the west, but above-average January precipitation in Greece and Italy spread westward in February, when only northern Italy experienced below-average rainfall. March was much drier, with most areas experiencing below-average rainfall.

In April–June, average temperatures were significantly above normal in all areas except Greece. West of Sardinia, temperatures exceeded the 98th percentile. Precipitation was below average in most regions,

with the exception of southern Italy and Sicily. April temperatures were near average in most regions. May was warmer with large areas in the west showing significant warmth. Heating continued through June, with significantly above-normal temperatures in all areas except Greece. Parts of northern Italy exceeded the 98th percentile. Anomalous rainfall occurred in southern Italy and Sicily, where totals were above average in all three months.

Significant heat continued into July over large areas of the region. Above-normal precipitation fell over Greece, with eastern areas receiving more than twice the monthly average. Temperature anomalies were somewhat lower in August, dropping below average in northeastern areas, but high temperatures in the western Mediterranean brought large numbers of jellyfish to Spanish beaches. Most areas saw above-average rainfall, and northern Greece again received significant excesses of precipitation. Temperature anomalies in the west fell in September, and most areas experienced above-average rainfall.

Average October–December temperatures were below average in most areas. October temperatures were below average in the east, and above average in the west. In November, cold anomalies spread over much of the Mediterranean and by December temperatures had dropped significantly below normal in central areas. In December, Greece was the only country in the region to experience above-average temperatures. October was mainly a dry month, with northern Italy the only place to receive above-average precipitation. November in contrast was wetter than average in most areas.

viii) Southeastern Europe—J. J. Kennedy[38]

Temperatures in southeastern Europe in 2005 were within 0.2°C of the 1961–90 average. Eastern areas, particularly Bulgaria, received significantly

THE EXTREME IBERIAN DROUGHT OF 2004/05—R. Trigo,[86] R. Garcia-Herrera,[24] and D. Paredes[64]

The year 2005 was characterized by one of the worst droughts ever recorded in the Iberian Peninsula, particularly in its southern half. The hydrological year that spans between October 2004 and September 2005 was the driest on record for several locations throughout Iberia, namely in the capital cities of Lisbon, Portugal, and Madrid, Spain, where reliable precipitation records have been kept since 1865 and 1859, respectively (Fig. 6.34). In particular, in Lisbon the 2004/05 event surpassed the previous record drought of the 1944/45 hydrological year (Fig. 6.35).

The precipitation regime over Iberia is characterized by strong seasonal behavior, with a unimodal rainy season concentrated between October and March and relatively arid conditions at other times. Therefore, all major droughts in this region are characterized by lack of rainfall during several months of the winter half of the year (Trigo et al. 2004). Using data from the GPCC (Rudolf and Schneider 2005) the spatially averaged precipitation over Iberia, between October 2004 and September 2005, was roughly 45% less than the 1961–90 climatological average (Garcia-Herrera et al. 2006, manuscript submitted to *J. Hydrometeor.*). However, regionally, the drought was most intense in the southern and southwestern sectors of the Iberian Peninsula, where rainfall was as little as 40% of normal during that period (Fig. 6.34)

The 2004/05 drought had major socioeconomic impacts in both Iberian countries, particularly for hydroelectricity and cereals production, which decreased to 40% and 60%, respectively, of their long-term average values. Agricultural losses due to scarce water resources and diminished pasture land during this season have been estimated to be on the order of $2 billion USD.

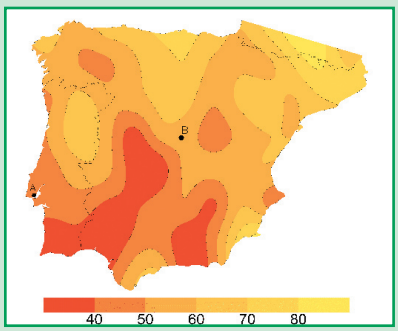

Fig. 6.34. Percentage of normal (1961–90 base) precipitation accumulated between October 2004 and September 2005. [Source: GPCC] Lisbon (A) and Madrid (B) are shown.

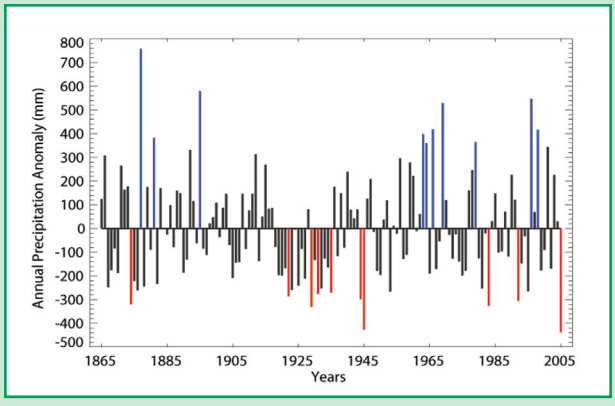

Fig. 6.35. Annual precipitation anomaly (mm) for Lisbon from 1865 to 2005 (1865–2005 mean). Anomalies correspond to the hydrological year that spans between October of year *n*-1 and September of year *n*.

above-average precipitation totals for the year, causing flooding in many areas.

The January–March period was colder than average in all but eastern Bulgaria. January was generally warmer than average, but February saw significant cold in most areas, with temperatures in Serbia more than 3°C below average. Temperatures in March were also below average, but not significantly so. The greatest precipitation anomalies occurred in Bulgaria in all three months, which led to flooding there in February.

April saw the end of the anomalously cold weather, with above-average temperatures in all areas. May and June temperatures were above average in most areas, significantly warmer than normal in Croatia and Bosnia-Herzegovina, but below average for June in Bulgaria. Rainfall totals in April and June were close to average in most parts, but in Bulgaria significant May rainfall once again brought flooding.

Although July temperature anomalies in southeastern Europe were positive, they were lower than in most areas of Europe. Even so, temperatures along the Adriatic coast were significantly above normal. Temperatures in August were below average except in eastern Bulgaria, which experienced significant warmth. September was warmer than average. July, August, and September rainfall totals were far above average, with Bulgaria receiving more than twice the seasonal average, and large areas recording more than three times the average. In August, 500% above-normal monthly rainfall in Bulgaria produced flooding that continued into September and left more than 30 dead.

Excessive rains continued in the east into October, but November totals were close to average in all areas. October and November temperatures were below average in the south and east, but December saw the colder weather shifting to the west. Temperatures in the north were above average in October, but fell below average for the last two months of the year.

h. Oceania

1) Australia—A. B. Watkins[90]

Despite the notable absence of an active basin-wide El Niño event, 2005 was the hottest year on meteorological record for Australia.[2] Neutral to slightly warm conditions in the equatorial Indian and Pacific Oceans at the start of 2005 persisted until June, returning to near normal in the latter half of the year. Correspondingly, pressure over Australia was higher than normal during the first half of the year, and from normal to below normal during the remainder of 2005. The anomalously high pressure over the country during early 2005 greatly reduced rainfall over the interior and inhibited the northward penetration of frontal systems from the Southern Ocean. High pressure also contributed to a sporadic Australian monsoon, which failed to extend far inland, resulting in anomalously warm and dry conditions in the north.

(i) Temperature

Due in part to the inconsistent Australian monsoon, the tropical wet season (October 2004–April 2005) was relatively warm. Northern Australia experienced a +1.5°C maximum temperature (Tmax) anomaly (0.6°C above the previous wet season record). Additionally, April, ordinarily the start of the main winter cropping season, was climatologically one of the most remarkable months on record for Australia. Australia-wide, April mean Tmax was 3.11°C above normal (Fig. 6.36). Not only was this 0.7°C above the previous April record, but it was the largest anomaly recorded for any month since Australia-wide temperature records began in 1950, which is substantially higher than the previous record (+2.68°C) set in October 1988. Combined with record high minimum temperatures (Tmin), the April mean temperature anomaly of +2.58°C was 0.85°C above the previous April record set in 2002 and 0.26°C above the previous record for any month (June 1996). Notably, the April mean temperature was the highest on record over 66% of the continent, with 86% of the continent experiencing mean temperatures for the month in the highest 10% the of recorded totals.

June–December Tmax and Tmin remained above average across virtually the entire country (+0.75° and +0.94°C anomalies, respectively). When combined with the hot start to the year, temperatures for 2005 were exceptional. The Australia-wide Tmax anomaly for 2005 was +1.21°C, equal to the record set in 2002, while the Australia-wide Tmin anomaly

[2] For Australia-wide, as well as large-scale regional averages, high-quality monthly temperature data is available from 1950, with high-quality annual temperature data starting 1910. For rainfall, high-quality area-averaged data commences in 1900. All records and percentile values are calculated with respect to these years. Anomalies are calculated with respect to the 1961 to 1990 average, in accordance with World Meteorological Organization guidelines (WMO Publication No. 100: www.wmo.ch/web/wcp/ccl/ GuideHome/html/wmo100.html).

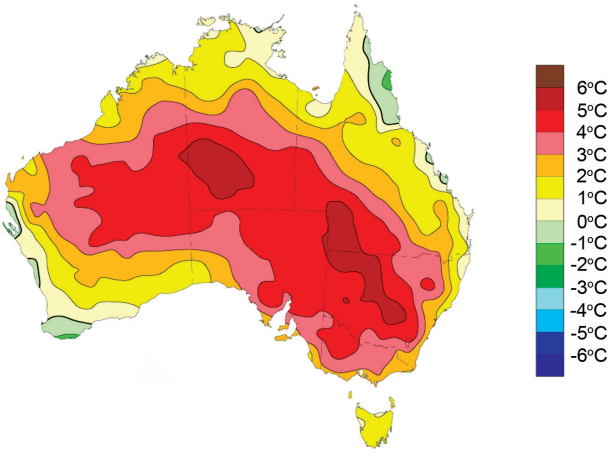

Fig. 6.36. Australian maximum April temperature (Tmax) anomalies (°C) for 2005 (1961–90 base).

of +0.91°C was the third warmest on record behind 1998 (+1.12°C).

Overall, the mean temperature anomaly for 2005 of +1.06°C was 0.23°C above the previous hottest year (1998). Consequently, Australia experienced its hottest mean temperature since annual mean records commenced in 1910. In total, 95% of the continent experienced above-average mean temperatures during 2005 (Fig. 6.37). With the absence of a decaying El Niño event, the record Australian heat of 2005 clearly highlights the impact of the long-term warming trend of the global and Australian climate upon the natural variability of year-to-year fluctuations.

(ii) Precipitation

High pressure over the continent and the weak Australian monsoon contributed to extremely dry conditions during the first five months of the year (Watkins 2005), with 44% of the country experiencing rainfall in the lowest 10% of recorded totals (decile 1). Australia-wide, April was the eighth driest April on record, with only 10.7 mm for the month (average of 31.1 mm). The Australia-wide average rainfall of 168 mm was the second lowest January–May total (after 1965) since Australia-wide monthly records began in 1900. While short-term dry spells are not unusual for Australia, it hindered the limited recovery from the devastating 2002/03 El Niño–related Australian drought (Coughlan et al. 2003), one of the worst droughts in Australia's recorded meteorological history (Nicholls 2004).

In a remarkable turnaround, 80% of the country experienced above-average rainfall between June and December, which corresponded to a change in ocean conditions in the equatorial Pacific. June–December precipitation over many previously drought-affected parts of New South Wales was in the top 10% (decile 10) of recorded totals. Australia-wide, 23% of the country experienced decile-10 precipitation between June and December, compared to only 0.6% for the January–May period.

Despite the average to above-average rainfall totals in the second half of the year, the extremely dry conditions during the first five months contributed to a generally below-average rainfall year for Australia (Fig. 6.37). The 2005 Australia-wide average rainfall of 407.2 mm was the 33rd driest such period since all-Australian records commenced in 1910, which is 65 mm below the 1961–90 mean of 472 mm. Overall, 63% of Australia experienced below-average rainfall during 2005.

(iii)Notable events

In January, Nyang Station, in the Gascoyne region of inland Western Australia, measured Australia's

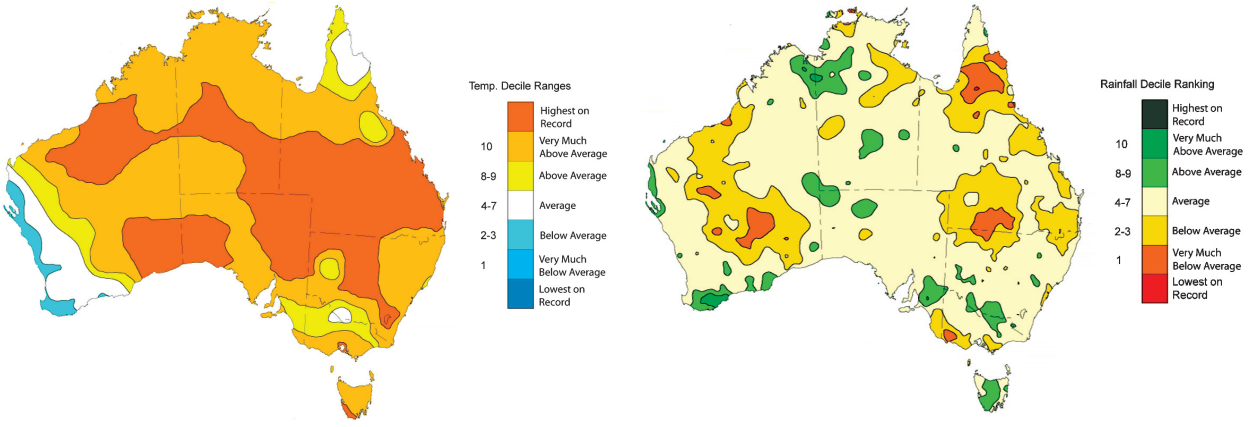

Fig. 6.37. Australian mean (left) temperature and (right) precipitation accumulation deciles for 2005 (relative to 1950–2005 for temperature and 1900–2005 for precipitation). [Source: Australian BOM]

hottest month on record, when its average maximum temperature of 44.8°C equaled the previous record, also set at Nyang, from February 1998.

An intense low pressure system developed over Eastern Bass Strait on 2 February, resulting in substantial rainfall and low temperatures for Victoria, southern New South Wales, South Australia, and Tasmania. The event made February 2005 Victoria's wettest February since 1973. Despite the 2-day event supplying 22% of Melbourne's annual mean rainfall (638.8 mm), the city's 2005 total precipitation of 589.8 mm was below average for the ninth year in succession.

Tropical Cyclone Ingrid, which occurred between 5 and 16 March (see section 4c), reached category 5 (Australian scale; information online at www.bom.gov.au/catalogue/warnings/WarningsInformation_TC_Ed.shtml) on at least two occasions, and is the only TC in Australia's recorded history to impact three different states or territories (Queensland, Northern Territory, Western Australia) as a severe tropical cyclone (category 3 or above).

Despite the generally mild winter, three major low-elevation snow events occurred during the season. These affected the Northern Tablelands of New South Wales and adjoining southern Queensland (22–23 June), the Monaro district of New South Wales (8–9 July), and southern Victoria and Tasmania (10 August). The August event brought snow to sea level in Victoria for the first time since 9 August 1951.

A notable heat wave affected large parts of central and eastern Australia during late December 2005 and early January 2006. The most abnormal conditions occurred in the period from 30 December 2005 to 1 January 2006, when northwesterly winds brought extreme heat to southeastern Australia. Arguably, the most exceptional record occurred at Montague Island (New South Wales), where a reading of 41.0°C broke its previous all-time record by 3.8°C. Sydney reached 44.2°C on 1 January 2006, second only to the 45.3°C reached there on 14 January 1939.

ii) New Zealand—M. J. Salinger[80]

New Zealand's climate of 2005 was influenced by more frequent anticyclonic activity in the Tasman Sea and to the east of the South Island, resulting in less wind, warmer temperatures, and generally decreased precipitation for much of New Zealand. However, more cyclonic activity was present in February, March, May, and December, and the northeast of the North Island experienced more frequent easterlies at times (Fig. 6.38). Notable climate features in various parts of the country included heat waves, low soil moisture, localized flooding, the Greymouth tornado, an unseasonable snowstorm, and damaging hailstorms.

(i) Temperature

The national average temperature in 2005 was 13.1°C, 0.5°C above the 1971–2000 normal. It was the fourth warmest year nationally since reliable records commenced in the 1860s. Only 1971, 1998, and 1999 have been warmer with temperatures of 13.2°, 13.3°, and 13.3°C, respectively. For New Zealand as a whole, there were seven warmer-than-normal months (February, March, May, July through September, and December), two cooler months (January and April), and three months with mean temperatures close to the climatological average (June, October, and November).

A combination of anticyclones and northeasterlies brought one of the warmest Februaries on record, with maximum temperatures of 30°C or more in many locations throughout New Zealand, and temperatures of 35°C or more in sheltered inland areas of the South Island during the first 10 days. The highest recorded extreme air temperature for the year was 38.7°C at Alexandra on 5 February (the highest temperature there for any month, in records back to 1929). Overall, February was the eighth warmest on record, with a mean temperature of 18.6°C (+1.3°C anomaly).

Halfway through the year, more frequent anticyclones over the North Island and northwesterlies over the South Island produced the sixth warmest winter (June–August) on record, even though June

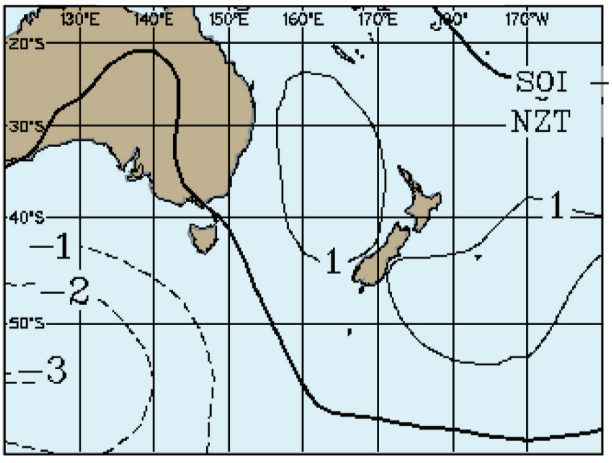

Fig. 6.38. 2005 mean sea level pressure anomaly map for the New Zealand region showing departures from average (hPa). Anticyclones were more frequent than normal east of the South Island and in the Tasman Sea.

was the coldest in a decade. With a mean temperature of 9.1°C (+1.2°C), July was the third warmest on record. Record high August maximum temperatures were recorded at Hanmer Forest (25.1°C on the 30th) and Amberley (25.4°C on the 31st). August's 9.8°C (+1.1°C) made it the fourth warmest on record. Mild conditions accompanied continued anticyclonic activity into spring (September–November). A changing atmospheric pattern to warm northerlies produced the third warmest December on record, with 17.5°C (+1.9°C).

Mean temperatures in 2005 were at least 0.3°C above average in most regions, and 0.5°–0.9°C above average in parts of Auckland, Coromandel, western Bay of Plenty, and western North Island from Wanganui to Wellington, as well as Wairarapa and much of the South Island. Temperatures were near average in coastal Wairarapa, along the Kaikoura Coast, and in coastal areas of south Canterbury. The warmest locales were Cape Reinga and Whangarei Airport, both with a mean temperature for the year of 16.1°C (0.2° and 0.5 °C above normal, respectively). Several locations observed record warmest annual average temperature in 2005.

(ii) Precipitation

New Zealand's climate for 2005 was marked by too little rain in some places, and too much in others. Annual rainfall during the year was less than 75% of normal over much of the South Island, and 75%–90% of normal in the north and west of the North Island (excluding Wanganui) and southern Wairarapa (Fig. 6.39). Clyde recorded the least annual precipitation at 348 mm (76% of normal). Near-record to record low precipitation was observed at numerous locations. Conversely, well-above-average precipitation (> 125%) fell in the western Bay of Plenty, Hawke's Bay, and the far southwest of the South Island. Precipitation was near normal elsewhere. The wettest location was Cropp River in Westland, with an annual total of 9290 mm.

Anticyclones in January commenced the trend of low rainfall and severe or significant soil moisture deficits in the northern half of the North Island and Canterbury; these conditions persisting into April. March was wetter in the North Island, but more anticyclones in April kept conditions dry. However, weather patterns changed abruptly in May, resulting in widespread flooding in the Bay of Plenty.

Frequent winter anticyclones over the North Island and northwesterlies over the South Island produced extremely dry conditions in the east of the South Island between June and September. Winter snowfall was much less frequent than normal. However, an early spring snow (19 September) down to sea level in Canterbury was unusual for the month.

Below-average spring rainfall resulted in significant soil moisture deficits developing much earlier than usual from Southland to Marlborough. Deficits spread to Nelson and the southwest of the North Island in November, and developed in Hawke's Bay, Auckland, and parts of Northland in December. However, southeasterlies in both October and November produced significant flooding in Gisborne.

(iii)Notable events

For the year, there were at least 26 heavy rainfall events, half of which produced floods. There were also 7 damaging hailstorms and 12 damaging tornadoes (or events attributed to tornadoes) in 2005. The Greymouth tornado of 10 March was particularly

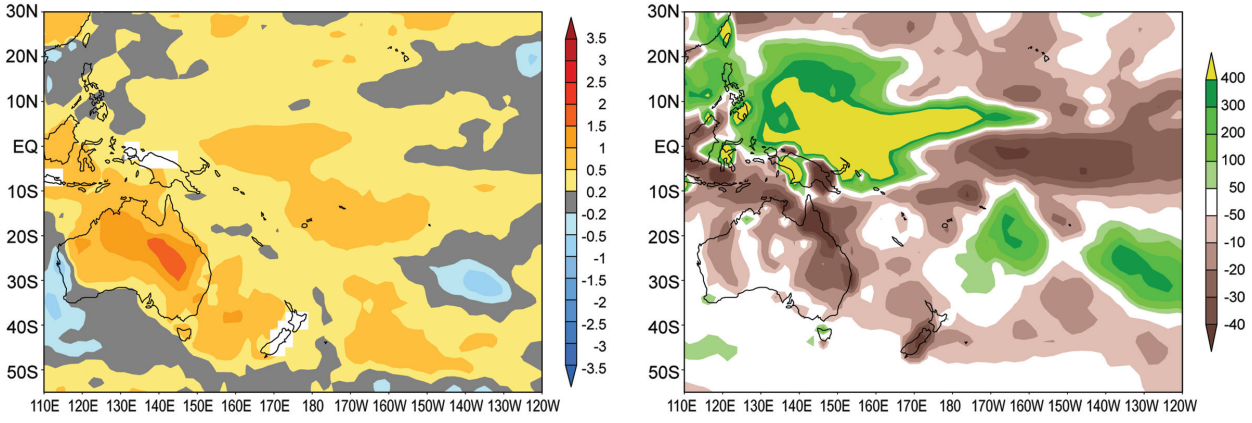

Fig. 6.39. South Pacific 2005 annual (left) temperature anomalies (°C; 1971–2000 base) and (right) precipitation anomalies (mm; 1979–2000 base) from CAMS–OPI.

destructive, leaving 30 people homeless and resulting in damage worth at least $10 million New Zealand dollars (NZD; $6.3 million USD). Wellington Airport was closed for many more hours than usual in 2005. There were 52 h with fog there, the highest for any year in 45 years of measurement.

The Bay of Plenty floods of 3–4 May and 17–18 May were most disastrous, with the earlier of the two causing widespread damage in parts of Tauranga, and the later being phenomenal, with unprecedented high rainfall for the district and a state of emergency declaration from Tauranga to Matata. Hundreds of people were evacuated. Homes were destroyed by mudslides and flooding, and rising waters threatened hundreds of others, especially in Matata.

The extremely high temperatures during the first 10 days of February are notable because there are very few instances prior to this event where temperatures anywhere in New Zealand have exceeded 38°C (100°F).

In Canterbury, the Christchurch airport, schools, and universities were closed due to an unusual early spring snow (19 September) in Canterbury. Snow depths of 5–10 cm were recorded in the region.

iii) South Pacific Islands—M. J. Salinger[80] and S. M. Burgess[12]

A high frequency of surface equatorial westerlies occurred near the date line in February (the most since the last El Niño in 2002). Trade winds generally were near normal in strength at other times of the year. There was also some ENSO influence on the location of the SPCZ during the year. West of the date line, the SPCZ was further north than usual from January through August, and further south than usual from November through December. East of the date line, the SPCZ was very weak from March through August. It was further south than usual from October through December (see section 4d). Above-average equatorial SSTs occurred with the weakly negative El Niño; however, the region of positive SST anomalies drifted west as the El Niño faded. From August through December OLR anomalies showed enhanced convection over Papua New Guinea, and suppressed convection over Western and Eastern Kiribati, Tokelau, Tuvalu, and the North Cook Islands. For much of the year, mean sea level pressures were above average west of the date line, and below average in the east.

(i) Temperature

Overall, 2005 was warmer than normal (1971–2000 mean) across much of the region (Fig. 6.39). Above-average SSTs occurred throughout much of the tropical Southwest Pacific during 2005 (Fig. 6.40). Notably, SSTs were about +1.0°C above average around western Kiribati, and at least +0.5°C above average in many other island nations, especially those north of 20°S. New Caledonia, the Southern Cook Islands, the Austral Islands, and Pitcairn Island were surrounded by near-average SSTs. Southwest Pacific island surface air temperature anomalies for 2005 were consistent with the SST anomalies throughout the region. It was an extremely warm year in Tahiti-Faa'a, central French Polynesia, where the annual mean temperature was 27.0°C (+0.8°C above the 1971–2000 normal), and equal the highest since measurements commenced in 1957.

Locally, a heat wave occurred from 4 to 7 January in La Tontouta, New Caledonia, with maximum temperatures between 36° and 37°C. New Caledonia's mean temperatures were 1.3°C above normal for the month. In general, southern locations such as Vanuatu, Fiji, New Caledonia, and southern French Polynesia experienced a cooler-than-normal July and August. Tahiti-Faa'a recorded its hottest November and December maximum temperatures in 2005 (33.9° and 28.1°C, respectively).

(ii) Precipitation

Southwest Pacific 2005 OLR anomalies showed a region of enhanced convection over Papua New Guinea extending toward the Solomon Islands (Fig. 6.41). There was also an area of weakly enhanced convection over Niue and the Southern Cook Islands, as well as Pitcairn Island. Convection was suppressed in 2005 over western and eastern Kiribati, Tokelau,

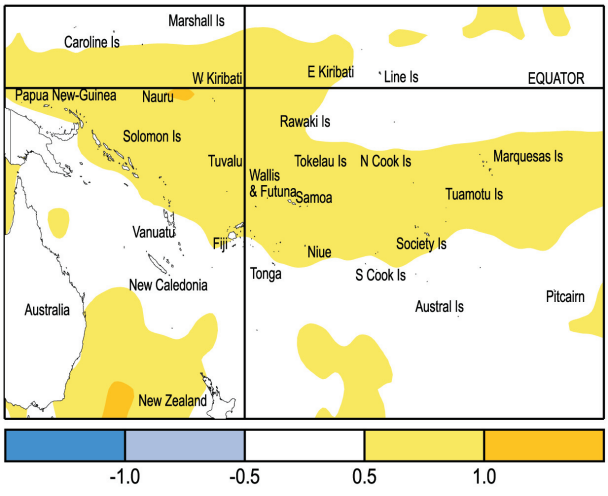

Fig. 6.40. South Pacific annual SST anomalies (relative to 1971–2000 mean; °C). Yellow or orange areas represent above-average temperatures.

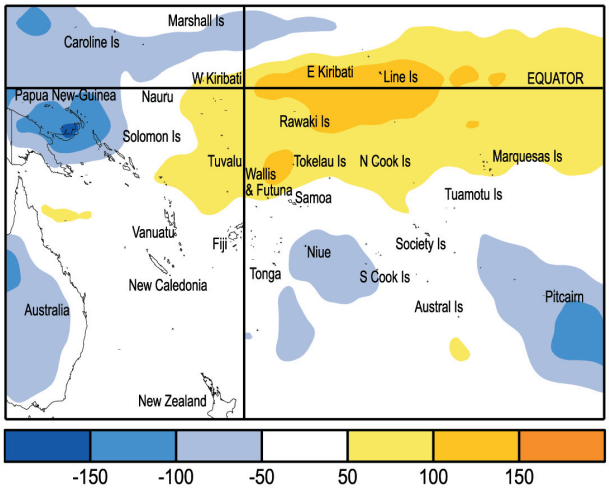

Fig. 6.41. Annual South Pacific outgoing longwave radiation anomalies (W m^{-2}). High radiation levels (yellow or orange) are typically associated with clearer skies and lower rainfall, while low values (blue) often indicate cloudy conditions and more rain for the region.

Tuvalu, Wallis and Futuna, the North Cook Islands, and the Marquesas Islands. The year's rainfall distribution shows similarities to the OLR pattern. However, for rainfall there were not many significant anomalies. Annual rainfall was at least 110% of normal in an area affecting a region extending from Niue to the north and east of Fiji, and also parts of Southern French Polynesia. In contrast, 2005 rainfall was less than 90% of the average throughout much of New Caledonia.

One location, Gambier, Rikitea, French Polynesia, recorded an extremely high 2005 precipitation anomaly of 127% of normal (2505 mm). Several locations received record monthly rainfall amounts: Vunisea, Fiji (786 mm, April), Viwa (205 mm, June), Monasavu (640 mm, June), Navua (587 mm, June), Nausori Airport (474 mm, September), Vatukoula (353 mm, November), and at Lupepau'u, Tonga (440 mm, June). On 4 March, Vunisea set a record for daily rainfall of 251 mm, and on 18 November, Vatukoula received a record 119 mm of precipitation. Record low monthly precipitation was also recorded at Udu Point, Fiji (84 mm), and Tuamotu, Takaroa, French Polynesia (25 mm), in March, Nadi Airport and Penang Mill, Fiji (1 and 7.8 mm, respectively), in May, and Bora Bora, French Polynesia (23 mm) in October.

Rainfall occurred almost every day from 6 to 20 April in Fiji's Western Division. Extensive flooding occurred in the Northern and Western Divisions over 16–20 April, closing almost 50 roads. There was one fatality. Vanuatu, Pekoa, recorded 950 mm for April, including 5 days exceeding 100 mm. Torrential rainfall occurred in Fiji's Central Division during the last week of September, leading to flooding in parts of Suva, Nausori, and Tailevu. A large number of villages were evacuated and there was one fatality. Nausori Airport recorded 187 mm of rain on the 28th.

(iii)Notable events

In February, a record four intense tropical cyclones (Meena, Nancy, Olaf, and Percy) impacted the South Pacific Islands (see section 4c). All four occurred east of the date line, with most being triggered during an active phase of the Madden–Julian oscillation. On the Saffir–Simpson scale, Meena and Nancy reached category 4 status, while Olaf and Percy were category 5 at their height.

The first of the cyclones, Meena, passed close to Rarotonga on 6 February, with wind gusts exceeding 115 km h^{-1}. Cyclone Nancy tracked through the Northern Cook Islands from 13 to 15 February with winds gusting to 163 km h^{-1} in Rarotonga and to 185 km h^{-1} elsewhere. In Aitutaki, trees were uprooted, roofs damaged, and low-lying areas flooded. Wind and storm surge caused widespread damage along the northern and eastern coasts of Rarotonga. On 16 February, Olaf's storm surge destroyed numerous coastal structures and high winds lifted many roofs in both Samoa and American Samoa. Rarotonga's west coast received substantial damage. Late in the month, Percy, with maximum sustained winds reaching 260 km h^{-1}, caused widespread damage and destruction on Pukapuka, Nassau, Swain, and Tokelau Islands. In Tokelau, Percy destroyed most of the island's agriculture and was reportedly the worst tropical cyclone in living memory. Fortunately, despite the intense nature of these four cyclones, and reconstruction estimates exceeding $25 million USD, there were no confirmed fatalities from these storms (two listed as missing at sea following Olaf).

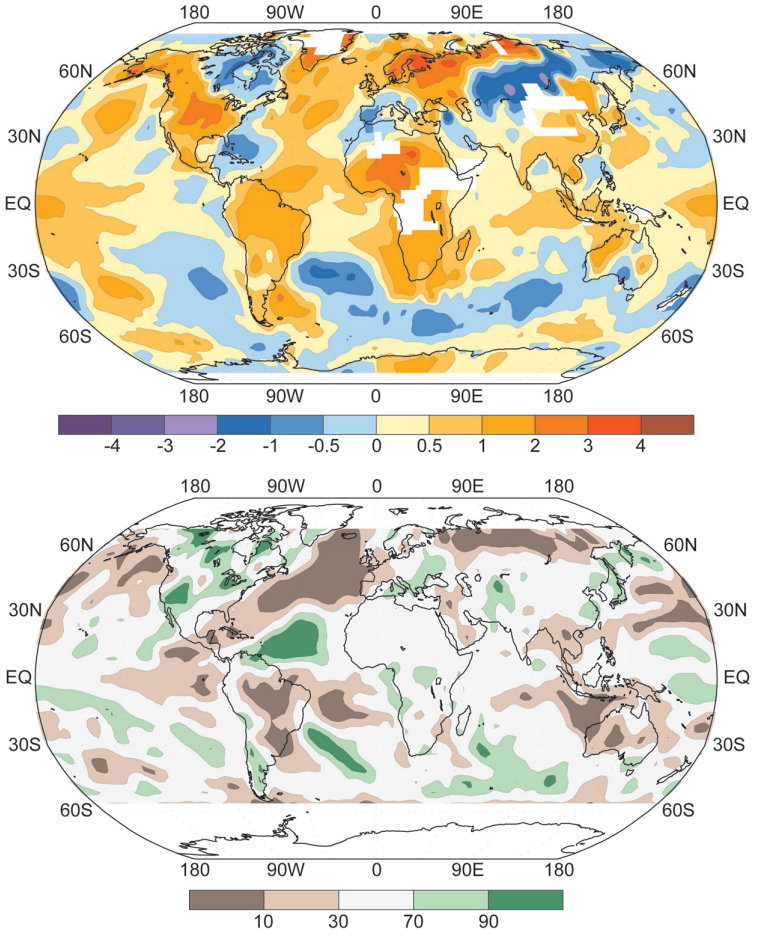

Fig. 7.1. December 2004–February 2005 (top) surface temperature anomalies (°C) and (bottom) precipitation percentiles based on a gamma distribution fit to the 1979–2000 base period. Temperature anomalies (1971–2000 base period) are based on station data over land and sea surface temperature over water. Precipitation data were obtained from a combination of rain gauge observations and satellite-derived estimates (Janowiak and Xie 1999). Analysis was omitted in data-sparse regions (white areas).

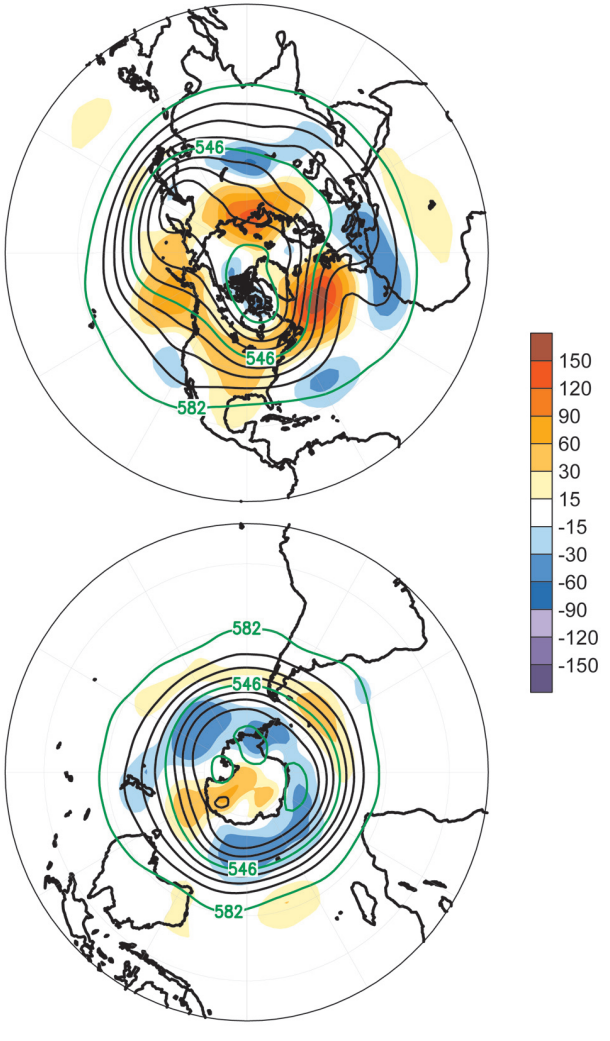

Fig. 7.2. December 2004–February 2005 (top) Northern Hemisphere and (bottom) Southern Hemisphere 500-hPa geopotential heights (9-dam contour interval) and anomalies (shading, m) from the 1979–2000 base period mean.

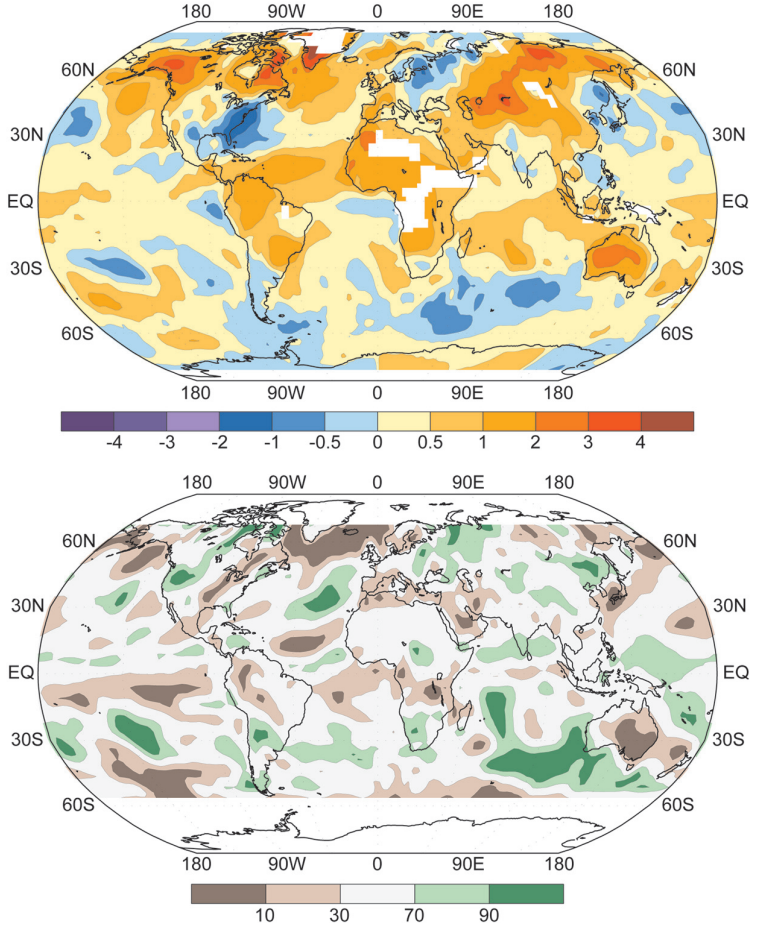

FIG. 7.3. March–May 2005 (top) surface temperature anomalies (°C) and (bottom) precipitation percentiles based on a gamma distribution fit to the 1979–2000 base period. Temperature anomalies (1971–2000 base period) are based on station data over land and sea surface temperature over water. Precipitation data were obtained from a combination of rain gauge observations and satellite-derived estimates (Janowiak and Xie 1999). Analysis was omitted in data-sparse regions (white areas).

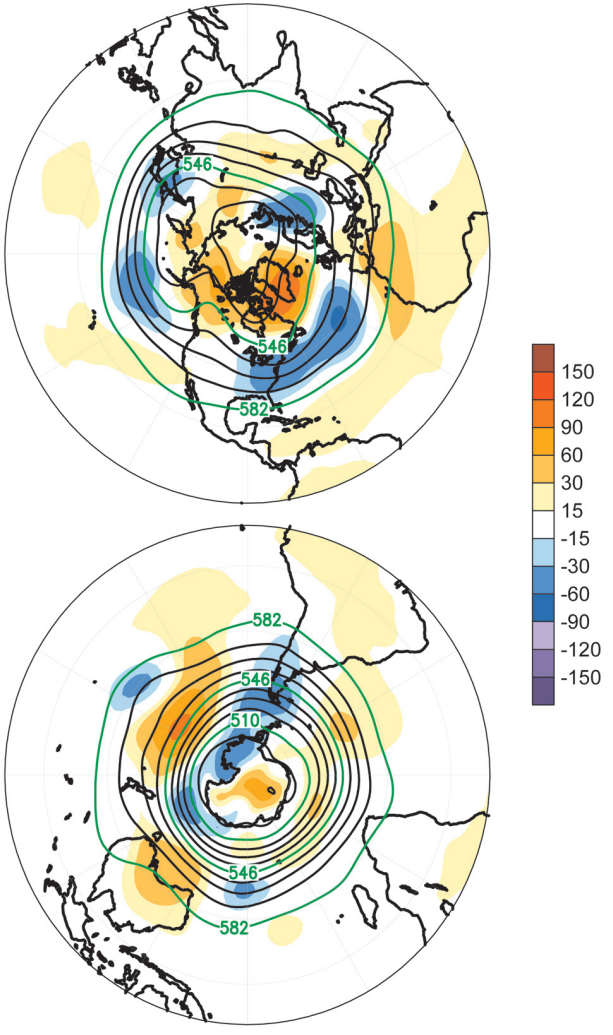

FIG. 7.4. March–May 2005 (top) Northern Hemisphere and (bottom) Southern Hemisphere 500-hPa geopotential heights (9-dam contour interval) and anomalies (shading, m) from the 1979–2000 base period mean.

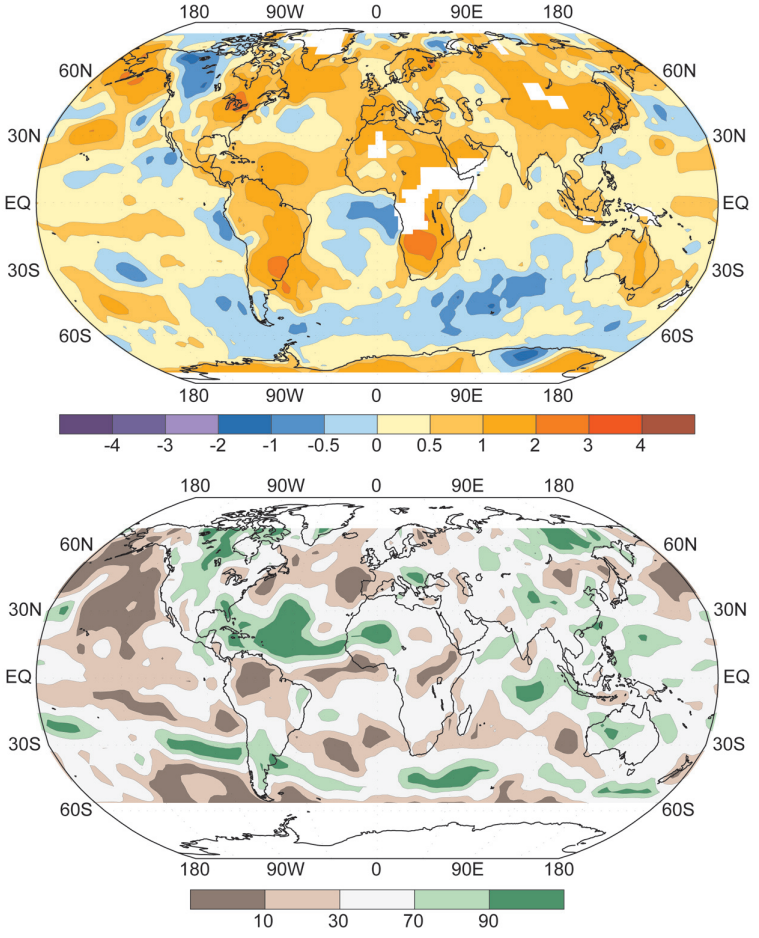

Fig. 7.5. June–August 2005 (top) surface temperature anomalies (°C) and (bottom) precipitation percentiles based on a gamma distribution fit to the 1979–2000 base period. Temperature anomalies (1971–2000 base period) are based on station data over land and sea surface temperature over water. Precipitation data were obtained from a combination of rain gauge observations and satellite-derived estimates (Janowiak and Xie 1999). Analysis was omitted in data-sparse regions (white areas).

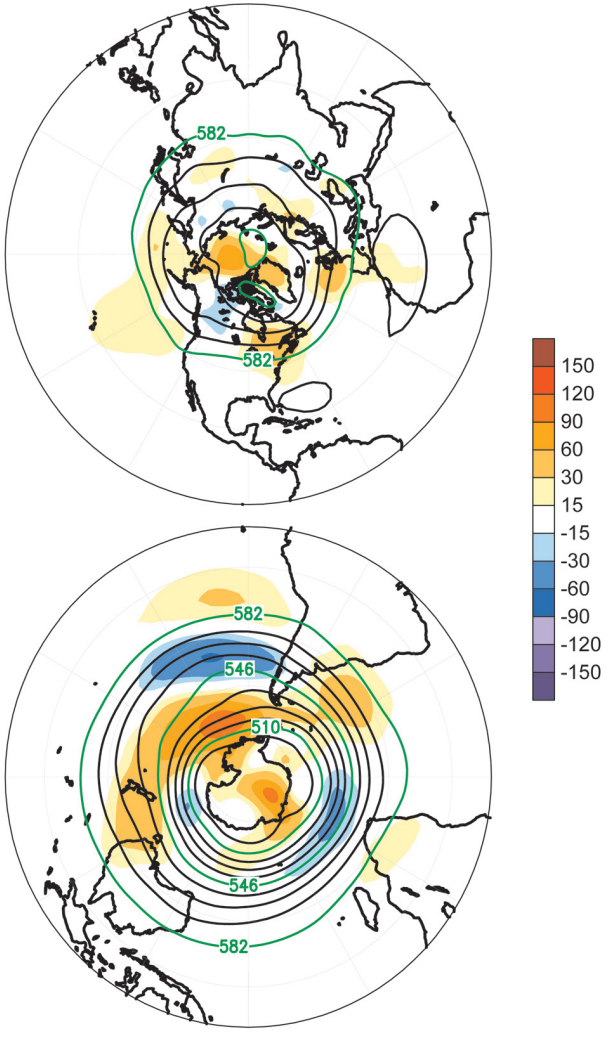

Fig. 7.6. June–August 2005 (top) Northern Hemisphere and (bottom) Southern Hemisphere 500-hPa geopotential heights (9-dam contour interval) and anomalies (shading, m) from the 1979–2000 base period mean.

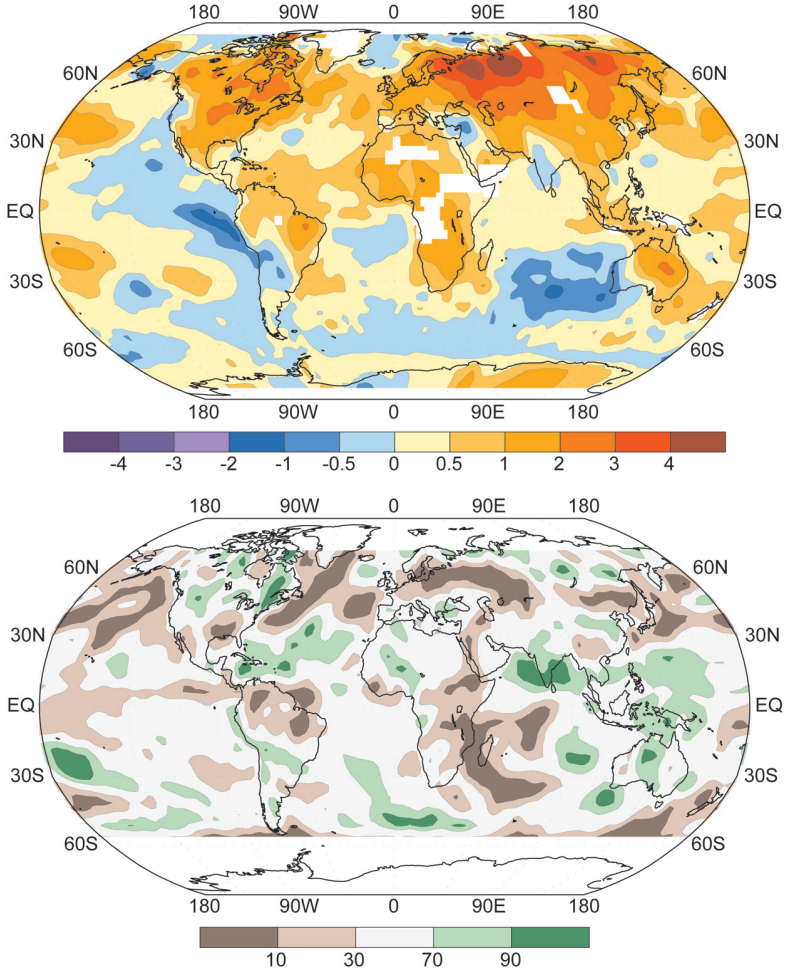

Fig. 7.7. September–November 2005 (top) surface temperature anomalies (°C) and (bottom) precipitation percentiles based on a gamma distribution fit to the 1979–2000 base period. Temperature anomalies (1971–2000 base period) are based on station data over land and sea surface temperature over water. Precipitation data were obtained from a combination of rain gauge observations and satellite-derived estimates (Janowiak and Xie 1999). Analysis was omitted in data-sparse regions (white areas).

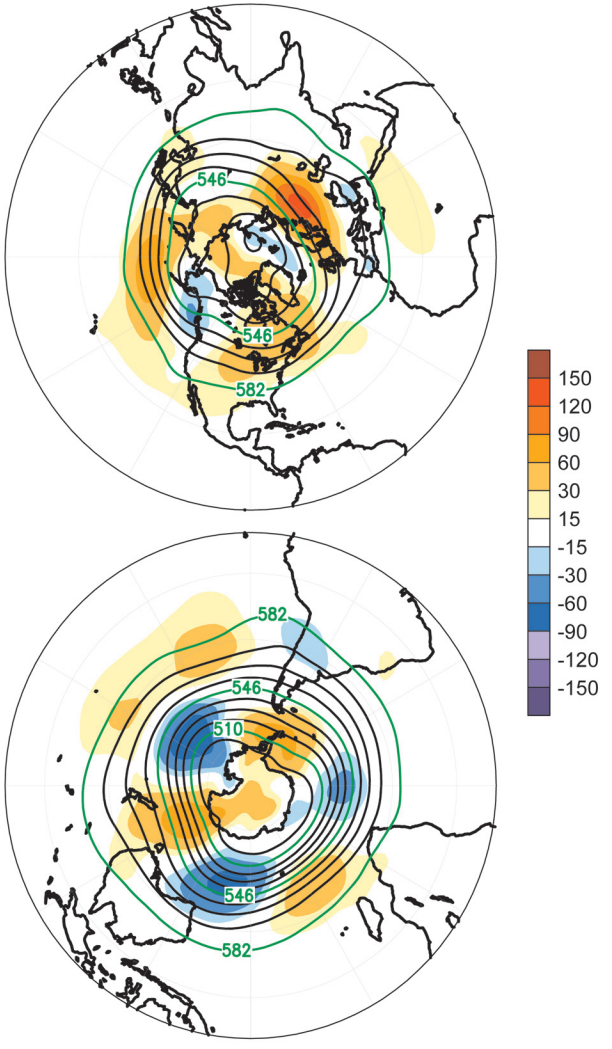

Fig. 7.8. September–November 2005 (top) Northern Hemisphere and (bottom) Southern Hemisphere 500-hPa geopotential heights (9-dam contour interval) and anomalies (shading, m) from the 1979–2000 base period mean.

ACKNOWLEDGMENTS

This assessment would not have been possible without the talents, assistance, and contribution of many scientists and technical experts from around the world. In addition to the cited authors, a number of additional contributors and reviewers provided valuable information, guidance, figures, and expertise. Where known, we gratefully acknowledge these contributors in the appendix below.

The editors also wish to acknowledge Omar Baddour of the World Meteorological Organization (WMO) for his help in identifying and soliciting additional authors and contributors. J. Kennedy is supported by the U.K. Department of the Environment, Food and Rural Affairs under Contract Number PECD 7/12/37.

Special acknowledgement and thanks must be given to Glenn Hyatt, Sara Veasey, and Deborah Riddle at NOAA/NCDC for the extensive time and graphical expertise they devoted to preparing this document for publication. The editors also wish to thank last year's editor, David Levinson, for his advice and guidance. This assessment was partially supported by a grant from the NOAA Climate Program Office Climate Change Data and Detection Program.

APPENDIX: CONTRIBUTORS AND REVIEWERS

Alfred Wegener Institute, Bremerhaven, Germany
- V. Rachold

Danish Meteorological Institute, Copenhagen, Denmark
- J. Cappelen

Finnish Meteorological Institute, Helsinki, Finland
- R. Heino
- S. Saku

Hadley Centre for Climate Prediction and Research, Devon, United Kingdom
- D. Parker

Icelandic Meteorological Office, Reykjavic, Iceland
- T. Jonsson

International Arctic Research Center, Fairbanks, Alaska
- J. Walsh

Max-Planck Institute for Meteorology, Hamburg, Germany
- L. Bengtsson

Naval Postgraduate School, Monterey, California
- W. Maslowski

Nicolaus Copernicus University, Toruń, Poland
- R. Przybylak

Norwegian Meteorological Office, Oslo, Norway
- E. Førland
- K. A. Iden

NOAA National Climatic Data Center, Asheville, North Carolina
- P. Groisman
- H.-M. Zhang
- W.E. Angel
- N. Guttman
- T. Whitehurst
- W. Brown
- S. Stephens
- B. Gleason
- S. LeDuc
- D. Easterling

Swedish Meteorological and Hydrometeorological Institute, Norrköpking, Sweden
- H. Alexandersson

REFERENCES

Arctic Climatology Project, 1997: *Environmental Working Group joint U.S.–Russian Atlas of the Arctic Ocean—Winter Period*. L. Timokhov and F. Tanis, Eds., Environmental Research Institute of Michigan in association with the National Snow and Ice Data Center. Ann Arbor, MI, CD-ROM.

Atkinson, G. D., 1971: Forecasters' guide to tropical meteorology. U.S. Air Force Tech. Rep. 240, 360 pp.

Beck, C., J. Grieser, and B. Rudolf, 2005: *A New Monthly Precipitation Climatology for the Global Land Areas for the Period 1951 to 2000*. DWD, Klimastatusbericht KSB 2004, ISSN 1437-7691, ISSN 1616-5063 (Internet), ISBN 3-88148-402-7, 181–190.

Bell, G. D., and M. Chelliah, 2006: Leading tropical modes associated with interannual and multidecadal fluctuations in North Atlantic hurricane activity. *J. Climate*, **19**, 590–612.

——, and Coauthors, 1999: Climate Assessment for 1998. *Bull. Amer. Meteor. Soc*., **80**, S1–S48.

——, and Coauthors, 2000: Climate Assessment for 1999. *Bull. Amer. Meteor. Soc*., **81**, S1–S50.

——, S. Goldenberg, C. Landsea, E. Blake, R. Pasch, M. Chelliah, and K. Mo, 2004: Atlantic Hurricane Season. *State of the Climate in 2003*. A. M. Waple and J. H. Lawrimore, Eds., *Bull. Amer. Meteor. Soc*., **85**, S1–S68.

Belchansky, G. I., D. C. Douglas, and N. G. Platonov, 2004: Duration of the Arctic sea ice melt season: Regional and interannual variability. *J. Climate*, **17**, 67–80.

Bourassa, M. A., R. Romero, S. R. Smith, and J. J. O'Brien, 2005: A new FSU winds climatology. *J. Climate*, **18**, 3692–3704.

Box, J. E., and Coauthors, 2005: Greenland ice sheet surface mass balance variability (1988–2004) from calibrated Polar MM5 output. *J. Climate*, in press.

Brohan, P., J. J. Kennedy, I. Harris, S. F. B. Tett, and P.D. Jones, 2006: Uncertainty estimates in regional and global observed temperature changes: a new dataset from 1850. *J. Geophys. Res*., in press.

Brown, J., K. M. Hinkel, and F. E. Nelson, 2000: The Circumpolar Active Layer Monitoring (CALM) program: Research Designs and Initial Results. *Polar Geog.*, **24**, 163–258.

Bryden, H. L., H. R. Longworth, and S. A. Cunningham, 2005: Slowing of the Atlantic meridional overturning circulation at 25°N. *Nature*, **438**, 655–657.

Cavalieri, D., C. Parkinson, P. Gloerson, and H. J. Zwally, 1996: Sea ice concentrations from Nimbus-7 SMMR and DMSP SSM/I passive microwave data, June to September 2001. National Snow and Ice Data Center. Boulder, CO. [Available online at http://arcss.colorado.edu/data/docs/daac/nsidc0051_gsfc_seaice.gd.html; updated 2005.]

Cazenave, A., and R. S. Nerem, 2004: Present-day sea level change: Observations and causes. *Rev. Geophys.*, **42**, RG3001, doi:10.1029/2003RG000139.

Chen, D., 2000: A monthly circulation climatology for Sweden and its application to a winter temperature case study. *Int. J. Climatol.*, **20**, 1067–1076.

Christy, J. R., R. W. Spencer, W. B. Norris, W. D. Braswell, and D. E. Parker, 2003: Error estimates of Version 5.0 of MSU/AMSU bulk atmospheric temperatures. *J.Atmos Oceanic Technol.,* **20,** 613–629.

Climate Prediction Center, 2005: Climate Diagnostics Bulletin: January 2005. U.S. Dept. of Commerce, NOAA/NWS/CPC. [Available online at www.cpc.ncep.noaa.gov/products/analysis_monitoring/bulletin_0105.]

Conway, T. J., P. P. Tans, L. S. Waterman, K. W. Thoning, D. R. Kitzis, K. A. Masarie, and N. Zhang, 1994: Evidence for interannual variability of the carbon cycle from the NOAA CMDL global air sampling network. *J. Geophys. Res.*, **99**, 22831–22855.

Coughlan, M., D. Jones, N. Plummer, A. Watkins, B. Trewin, and S. Dawkins, 2003: Impacts of 2002–03 El Niño on Australian climate. Extended Abstracts, *DroughtCom: Improving the Communication of Climate Information*, N. Plummer, M. Flannery, C. Mullen, B. Trewin, A. Watkins, W. Wright, T. Powell, S. Power, Eds., Vol. 2, Melbourne, Autralia, Bureau of Meteorology, 7–12.

Couture, R., S. Smith, S. D. Robinson, M. M. Burgess, and S. Solomon, 2003: On the hazards to infrastructure in the Canadian North associated with thawing of permafrost. *Proc. Geohazards 2003, 3rd Canadian Conf. on Geotechnique and Natural Hazards*. Edmonton, AB, Canada, Can. Geotech. Soc., 97–104.

Cummins, P. F., G. S. E. Lagerloef, and G. Mitchum, 2005: A regional index of northeast Pacific variability based on satellite altimeter data. *Geophys. Res. Lett.*, **32**, L17607, doi:10.1029/2005GL023642.

Curry, R. G., and M. S. McCartney, 2001: Ocean gyre circulation changes associated with the North Atlantic oscillation. *J. Phys. Oceanog.*, **31**, 3374–3400.

——, and C. Mauritzen, 2005: Dilution of the northern North Atlantic in recent decades. *Science*, **308**, 1772–1774.

Daniel, J. S., and S. Solomon, 1998: On the climate forcing of carbon monoxide. *J. Geophys. Res.*, **103**, 13,249–13,260.

Dlugokencky, E. J., S. Houweling, L. Bruhwiler, K. A. Masarie, P. M. Lang, J. B. Miller, and P. P. Tans, 2003: Atmospheric methane levels off: Temporary pause or new steady state? *Geophys. Res. Lett.*, **30**, 19, doi:10.1029/2003GL018126.

Durre, I., R. S. Vose, and D. B. Wuertz, 2006: Overview of the Integrated Global Radiosonde Archive. *J. Climate*, **19**, 53–68.

Dvorak, V. F., 1984: Tropical Cyclone Intensity Analysis Using Satellite Data. NOAA Technical Rep. NESDIS 11, 47 pp.

Eisenman, I., L. Yu, and E. Tziperman, 2005: Westerly wind bursts: ENSO's tail rather than the dog? *J. Climate*, **18**, 5224–5238.

Emanuel, K. A., 2005: Increasing destructiveness of tropical cyclones over the past 30 years. *Nature*, **436**, 686–688.

Feely, R. A., C. L. Sabine, T. Takahashi, and R. Wanninkhof, 2001: Uptake and storage of carbon dioxide in the oceans: The global CO_2 survey. *Oceanography*, **14**, 18–32.

——, L. D. Talley, G. C. Johnson, C. L. Sabine, and R. Wanninkhof, 2005: Repeat hydrography cruises reveal chemical changes in the North Atlantic. *Eos Trans. Amer. Geophys. Union*, **86**, 399, 404–405.

Frauenfeld, O. W., T. Zhang, R. G. Barry, and D. Gilichinsky, 2004: Interdecadal changes in seasonal freeze and thaw depths in Russia. *J. Geophys. Res.*, **109**, D05101, doi:10.1029/2003JD004245.

Free, M., D. J. Seidel, J. K. Angell, J. Lanzante, I. Durre, and T. C. Peterson, 2005: Radiosonde Atmospheric Temperature Products for Assessing Climate (RATPAC): A new dataset of large-area anomaly time series. *J. Geophys. Res.,* **110,** D22101, doi:10.1029/2005JD006169.

Ganachaud, A., and C. Wunsch, 2003: Large-Scale Ocean Heat and Freshwater Transports during the World Ocean Circulation Experiment. *J. Climate*, **16**, 696–705.

Goetz, S. J., A. G. Bunn, G. J. Friske, and R. A. Houghton, 2005: Satellite-observed photosynthetic trends across boreal North America associated with climate and fire disturbance. *Proc. Nation. Acad. Sci.*, **102**, 13,521–13,525.

Goldenberg, S. B., C. W. Landsea, A. M. Mestas-Nuñez, and W. M. Gray, 2001: The recent increase in Atlantic hurricane activity: Causes and implications. *Science*, **293**, 474–479.

Gruber, N., J. L. Sarmiento, T. F. Stocker, 1996: An improved method for detecting anthropogenic CO_2 in the oceans. *Global Biogeochem. Cyc.*, **10**, 809–837.

Haas, C., 2004: Late-summer sea ice thickness variability in the Arctic Transpolar Drift 1991–2001 derived from ground-based electromagnetic sounding. *Geophys. Res. Let.*, **31**, L09402, doi:10.1029/2003GL019394.

Hansen, J., and Coauthors, 2005: Earth's energy imbalance: Confirmation and implications. *Science*, **308**, 1431–1435.

Harris, C., and W. Haeberli, 2003: Warming permafrost in European mountains. *Global Planet. Change*, **39**, 215–225.

Heim, R. R., Jr., 2002: A review of twentieth century drought indices used in the United States. *Bull. Amer. Meteor. Soc.*, **83**, 1149–1165.

Horton E. B., C. K. Folland, and D. E. Parker, 2001: The changing incidence of extremes in worldwide and central England temperatures to the end of the twentieth century. *Climatic Change,* **50,** 267–295.

IPCC, 2001: *Climate Change 2001: The Scientific Basis. Contribution of Working Group I to the Third Assessment Report of the Intergovermental Panel on Climate Change*. World Meteor. Org./U. N. Environment Programme, J. T. Houghton, Y. Ding, D. J. Griggs, M. Noguer, P. J. van der Linden, X. Dai, K. Maskell, and C. A. Johnson, Eds., Cambridge University Press, 881 pp.

Isaksen, K., D. Vonder Mühll, H. Gubler, T. Kohl, and J.L. Sollid, 2000: Ground surface temperature reconstruction based on data from a deep borehole in permafrost at Janssonhaugen, Svalbard. *Ann. Glaciol.*, **31**, 287–294.

Janowiak, J. E., and P. Xie, 1999: CAMS-OPI: A global satellite-rain gauge merged product for real-time precipitation monitoring applications. *J. Climate*, **12**, 3335–3342.

Jauregui, E., 2003: Climatology of landfalling hurricanes and tropical storms in Mexico. *Atmosfera*, **16**, 193–204.

Jia, G. J., H. E. Epstein, and D. A. Walker, 2003: Greening of arctic Alaska, 1981–2001. *Geophys. Res. Lett.*, **30**, 2067, doi:10.1029/2003GL018268.

Jin, F. F., 1997: An equatorial recharge paradigm for ENSO. Part I: Conceptual model. *J. Atmos. Sci.*, **54**, 811–829.

Johannessen, O. M., and Coauthors, 2004: Arctic climate change: Observed and modeled temperature and sea ice variability. *Tellus*, **56A**, 328–341.

Karl, T. R., R. W. Knight, D. R. Easterling, and R. G. Quayle. 1996: Indices of Climate Change for the United States. *Bull. Amer. Meteor. Soc.*, **77**, 2, 279–292.

Kasischke, E. S., and Coauthors, 2000: Contributions of 1998 fires in the boreal forest to atmospheric concentrations of carbon monoxide and methane. *Eos Trans. Amer. Geophys. Union*, **81**, 260.

Kocin, P. J., and L. W. Uccellini, 2004: A snowfall impact scale derived from northeast storm snowfall distributions. *Bull. Amer. Meteor. Soc.*, **85**, 177–194.

Koltermann, K. P., A. V. Sokov, V. P. Tereschenkov, S. A. Dobroliubov, K. Lorbacher, and A. Sy, 1999: Decadal changes on the thermohaline circulation of the North Atlantic. *Deep-Sea Res. II*, **46**, 109–138.

Kousky, V. E. and M. T. Kayano, 1994: Principal modes of outgoing longwave radiation and 250-mb circulation for the South American sector. *J. Climate*, **7**, 1131–1143.

Kwok, R., H. J. Zwally, and D. Yi, 2004: ICESat observations of Arctic sea ice: A first look. *Geophys. Res. Lett.*, **31**, L16401, doi:10.1029/2004GL020309.

Lamb, H.H., 1950: Types and spells of weather around the year in the British Isles. *Quart. J. Roy. Meteor. Soc.*, **76**, 393–438.

Lander, M. A., and C. P. Guard, 1998: A look at global tropical cyclone activity during 1995: Contrasting high Atlantic activity with low activity in other basins. *Mon. Wea. Rev.*, **126**, 1163–1173.

Landsea, C. W., 1993: The climatology of intense (or major) Atlantic hurricanes. *Mon. Wea. Rev.*, **121**, 1703–1713.

——, G. D. Bell, W. M. Gray, and S. B. Goldenberg, 1998: The extremely active 1995 Atlantic hurricane season: Environmental conditions and verification of seasonal forecasts. *Mon. Wea. Rev.*, **126**, 1174–1193.

——, R. A. Pielke Jr., A. M. Mestas-Nuñez, and J. A. Knaff, 1999: Atlantic basin hurricanes: Indices of climatic changes. *Climatic Change*, **42**, 89–129.

Langenfelds, R. L., R. J. Francey, B. C. Pak, L. P. Steele, J. Lloyd, C. M. Trudinger, and C. E. Allison, 2002: Interannual growth rate variations of atmospheric CO2 and its δ13C, H2, CH4, and CO between 1992 and 1999 linked to biomass burning. *Global Biogeochem. Cyc.*, **16**, 1048, doi:10.1029/2001GB001466.

Lawrimore, J., and Coauthors, 2001: Climate Assessment for 2000. *Bull. Amer. Meteor. Soc.*, **82**(6), S1–S55.

Laxon, S., N. Peacock, and D. Smith, 2003: High interannual variability of sea ice thickness in the Arctic Region. *Nature*, **425**, 947–950.

Leuliette, E. W, R. S. Nerem, and G. T. Mitchum, 2004: Calibration of TOPEX/Poseidon and Jason altimeter data to construct a continuous record of mean sea level change. *Mar. Geodesy.*, **27**, 79–94.

Levinson, D. H., Ed., 2005: State of the Climate in 2004. *Bull. Amer. Meteor. Soc.*, **86**(6), S1–S86.

Levitus, S., J. I. Antonov, and T. P. Boyer, 2005: Warming of the World Ocean, 1955–2003. *Geophys. Res. Lett.*, **32**, L02604, doi:10.1029/2004GL021592.

Lucht, W., and Coauthors, 2002: Climate control of the high-latitude vegetation greening trend and Pinatubo effect. *Science*, **296**, 1687–1689, doi:10.1126/science.1071828.

Lumpkin, R., and Z. Garraffo, 2005: Evaluating the decomposition of tropical atlantic drifter observations. *J. Atmos. Oceanic Technol.*, **22**, 1403—1415.

Lyon, B., and A. G. Barnston, 2005: The evolution of the weak 2004–2005 El Nino. *U.S. CLIVAR Variations*, Vol. 3, US CLIVAR Office, Washington, DC, 1–4.

Madden, R. A., and P. R. Julian, 1971: Detection of a 40–50 day oscillation in the zonal wind in the tropical Pacific. *J. Atmos. Sci.*, **28,** 702–708.

——, and ——, 1972: Description of global-scale circulation cells in the Tropics with 40–50 day period. *J. Atmos. Sci.*, **29**, 1109–1123.

——, and ——, 1994: Observations of the 40–50 day tropical oscillation—A review. *Mon. Wea. Rev.*, **122**, 814–837.

Mantua, N. J., S. R. Hare, Y. Zhang, J. M. Wallace, and R. C. Francis, 1997: A Pacific interdecadal climate oscillation with impacts on salmon production. *Bull. Amer. Meteor. Soc.*, **78**, 1069–1079.

Mears, C.A., M. C. Schabel, and F. J.Wentz, 2003: A reanalysis of the MSU channel 2 tropospheric temperature record. *J. Climate,* **16,** 3650–3664.

Meinen, C. S., and M. J. McPhaden, 2000: Observations of warm water volume changes in the equatorial Pacific and their relationship to El Niño and La Niña. *J. Climate,* **13,** 3551–3559.

Melling, H., D. A. Riedel, and Z. Gedalof, 2005: Trends in the draft and extent of seasonal pack ice, Canadian Beaufort Sea. *Geophys. Res. Lett.*, **32**, L24501, doi:10.1029/2005GL024483.

Mo, K. C., 2000: The association between intraseasonal oscillations and tropical storms in the Atlantic Basin. *Mon. Wea. Rev.*, **128**, 4097–4107.

——, and V. E. Kousky, 1993: Further analysis of the relationship between circulation anomaly patterns and tropical convection. *J. Geophys. Res.*, **98**, 5103–5113.

Montzka, S. A, J. H. Butler, B. D. Hall, J. W. Elkins, and D. J. Mondeel, 2003a: A decline in tropospheric organic bromine. *Geophy. Res. Lett.*, **30**, 1826, doi:10.1029/2003GL017745.

——, and Coauthors, 2003b: Controlled substances and other source gases. *Scientific Assessment of Ozone Depletion: 2002*, Global Ozone Research and Monitoring Project—Report No. 47.

Mote, P. W., A. F. Hamlet, M. P. Clark, and D. P. Lettenmaier, 2005: Declining mountain snowpack in western North America. *Bull. Amer. Meteor. Soc.*, **86**, 39–49.

Moyer, K. A., and R. A. Weller, 1997: Observations of surface forcing from the Subduction Experiment: a comparison with global model products and climatological datasets. *J. Climate*, **10**, 2725–2742.

Munich Re, 2006: Annual Review: Natural catastrophes 2005. Knowledge Series, Topics Geo. [Available online at www.munichre.com/.]

Myneni, R. B., C. D. Keeling, C. J. Tucker, G. Asrar, and R. R. Menani, 1997: Increased plant growth in the northern high latitudes from 1981 to 1991. *Nature*, **386**, 698–702.

——, C. J. Tucker, G. Asrar, and C. D. Keeling, 1998: Interannual variations in satellite-sensed vegetation index data from 1981 to 1991. *J. Geophys. Res.*, **103**, 6145–6160.

Neumann, C. J., B. R. Jarvinen, C. J. McAdie, and J. D. Elms, 1993: *Tropical Cyclones of the North Atlantic Ocean, 1871–1992*, NOAA National Climatic Data Center, in cooperation with the National Hurricane Center, Coral Gables, FL, 193 pp.

Nicholls, N., 2004: The changing nature of Australian droughts. *Climatic Change*, **63**, 323–336.

Nixon, F. M., C. Tarnocai, and L. Kutny, 2003: Long-term active layer monitoring: Mackenzie Valley, northwest Canada. *Proc. Eighth Int. Conf. on Permafrost,* Vol. 2, Zurch, Switzerland, International Permafrost Association, 821–826.

NOAA OCO, 2006: The State of the Ocean Observing System for Climate. FY 2005 Annual Report: Office of Climate Observation, J. M. Levy, D. M. Stanitsky, and P. Arkin, eds., U.S. Dept. of Commerce, National Oceanic and Atmospheric Administration, Office of Climate Observation, Silver Spring, MD, 337 pp.

Novelli, P. C., K. A. Masarie, P. M. Lang, B. D. Hall, R. C. Myers, and J. C. Elkins, 2003: Reanalysis of tropospheric CO trends: Effects of the 1997–1998 wildfires, *J. Geophys. Res.*, **108**, D15, 4464, doi:10.1029/2002JD003031.

Oberman, N. G., and G. G. Mazhitova, 2001: Permafrost dynamics in the northeast of European Russia at the end of the 20th century. *Norweg. J. Geog.*, **55**, 241–244.

Osterkamp, T. E., 2003: A thermal history of permafrost in Alaska. *Proc. Eighth Int. Conf. on Permafrost*, M. Phillips, S. M. Springman, and L. U. Arenson, Eds., Zurich, CH, A. A. Balkema, Vol. 2, 863–868.

——, and V. E. Romanovsky, 1999: Evidence for warming and thawing of discontinuous permafrost in Alaska. *Permafrost Periglacial Process.*, **10**, 17–37.

Overland, J. E., and M. Wang, 2005: The third Arctic climate pattern: 1930s and early 2000s. *Geophys. Res. Lett.*, **32**, L23808, doi:10.1029/2005GL024254.

——, M. C. Spillane, D. B. Percival, M. Wang, and H. O. Mofjeld, 2004: Seasonal and regional variation of pan-Arctic surface air temperature over the instrumental record. *J. Climate*, **17**, 3263–3282.

Palmer, W. C., 1965: Meteorological Drought. U.S. Weather Bureau Research Paper 45, 58 pp. [Available from NOAA Library and Information Services Division, Washington, DC 20852.]

Parker, D. E., and E. B. Horton, 2005: Uncertainties in the Central England Temperature series 1878–2003 and some improvements to the maximum and minimum series. *Int. J. Climatol.*, **25**, 1173–1188.

Pavlov, A. V., 1994: Current changes of climate and permafrost in the Arctic and Sub-Arctic of Russia. *Permafrost Periglacial Process.*, **5**, 101–110.

——, and N. G. Moskalenko, 2002: The thermal regime of soils in the north of Western Siberia. *Permafrost Periglacial Process.*, **13**, 43–51.

Peterson, B. J., R. M. Holmes, J. W. McClelland, C. J. Vörösmarty, R. B. Lammers, A. I. Shiklomanov, I. A. Shiklomanov, and S. Rahmstorf, 2002: Increasing river discharge to the Arctic Ocean. *Science*, **298**, 2171–2173.

Peterson, T. C., and R. S. Vose, 1997: An overview of the Global Historical Climatology Network temperature database. *Bull. Amer. Meteor. Soc.*, **78**, 2837–2849.

Pfirman, S., W. F. Haxby, R. Colony, and I. Rigor, 2004: Variability in Arctic sea ice drift. *Geophys. Res. Lett.*, **31**, L16402, doi:10.1029/2004GL020063.

Polyakov, I., and Coauthors, 2003: Long-term ice variability in arctic marginal seas. *J. Climate*, **16**, 2078–2085.

——, and Coauthors, 2005: One more step toward a warmer Arctic. *Geophys. Res. Lett.*, **32**, L17605, doi:10.1029/2005GL023740.

Prather, M. J., 1996: Natural modes and time scales in atmospheric chemistry: Theory, GWPs for CH4 and CO, and runaway growth. *Geophys. Res. Lett.*, **23**, 2597–2600.

Prentice, I. C. and Coauthors, 2001: The carbon cycle and atmospheric carbon dioxide. *Climate Change 2001: The Scientific Basis*, Cambridge University Press, 190 pp.

Proshutinsky, A., I. M. Ashik, E. N. Dvorkin, S. Häkkinen, R. A. Krishfield, and W. R. Peltier, 2004: Secular sea level change in the Russian sector of the Arctic Ocean. *J. Geophys. Res.*, **109**, C03042, doi:10.1029/2003JC002007.

Quadrelli, R., and J. M. Wallace, 2004: A simplified linear framework for interpreting patterns of northern hemisphere wintertime climate variability. *J. Climate*, **17**, 3728–3744.

Quayle, R. G., T. C. Peterson, A. N. Basist, and C. S. Godfrey, 1999: An operational near real time global temperature index. *Geophys. Res. Lett.,* **26,** 333–336.

Reynolds, R. W., and T. M. Smith, 1994: Improved global sea surface temperature analyses using optimum interpolation. *J. Climate*, **7**, 929–948.

——, N. A. Rayner, T. M. Smith, D. C. Stokes, and W. Wang, 2002: An improved in situ and satellite SST analysis for climate. *J. Climate*, **15**, 1609–1625.

Rignot, E., and P. Kanagaratnam, 2006: Changes in the velocity structure of the Greenland Ice Sheet. *Science*, **311**, 986–990.

Rigor, I., and J. M. Wallace, 2004: Variations in the age of Arctic sea-ice and summer sea-ice extent. *Geophys. Res. Lett.*, **31**, L09401, doi:10,1029/2004GL019492.

Roemmich, D., S. Riser, R. Davis, and Y. Desaubies, 2004: Autonomous profiling floats: Workhorse for broadscale ocean observations. *J. Mar. Technol. Soc.*, **38**, 31–39.

Romanovsky, V. E., M. Burgess, S. Smith, K. Yoshikawa, and J. Brown, 2002: Permafrost temperature records: Indicator of climate change. *Eos Trans. Amer. Geophys. Union*, **83**, 589, 593–594.

Ropelewski, C. F., and M. S. Halpert, 1987: Global and regional scale precipitation patterns associated with the El Niño/Southern Oscillation. *Mon. Wea. Rev.*, **115**, 1606–1626.

——, and ——, 1989: Precipitation patterns associated with the high index phase of the Southern Oscillation. *J. Climate*, **2**, 268–284.

——, J. E. Janowiak, and M. S. Halpert, 1985: The analysis and display of real time surface climate data. *Mon. Wea. Rev.*, **113**, 1101–1106.

Rothrock, D. A., Y. Yu, and G. A. Maykut, 1999: Thinning of the Arctic sea-ice cover. *Geophys. Res. Lett.*, **26**, 3469–3472.

Rudolf, B., and U. Schneider, 2005: Calculation of gridded precipitation data for the global land-surface using in-situ gauge observations. *Proc. Second Workshop of the Int. Precipitation Working Group*, Monterey, CA, EUMETSAT, ISBN 92-9110-070-6, ISSN 1727-432X, 231–247.

——, H. Hauschild, W. Rueth, and U. Schneider, 1994: Terrestrial Precipitation Analysis: Operational Method and required density of point measurements. *Global Precipitations and Climate Change*, NATO ASI Series I, Vol. 26, M. Desbois, and F. Desalmond, Eds., Springer-Verlag, 173–186.

——, C. Beck, J. Grieser, and U. Schneider, 2005: Global precipitation analysis products. global precipitation

Climatology Centre (GPCC), DWD, 8 pp. [Available online at www.dwd.de/en/FundE/Klima/KLIS/int/GPCC/Reports_Publications/QR/GPCC-intro-products-2005.pdf.]

Sabine, C. L., and Coauthors, 2004: The oceanic sink for anthropogenic CO_2. *Science*, **305**, 367–371.

Schmittner, A., M. Latif, and B. Schneider, 2005: Model projections of the North Atlantic thermohaline circulation for the 21st century assessed by observations. *Geophys. Res. Lett.*, **32**, L23710, doi:10,1029/2005GL024368.

Shimada, K., F. McLaughlin, E. Carmack, A. Proshutinsky, S. Nishino, and M. Itoh, 2004: Penetration of the 1990s warm temperature anomaly of Atlantic Water in the Canada Basin. *Geophys. Res. Lett.*, **31**, L20301, doi:10.1029/2004GL020860.

Simpson, R. H., 1974: The hurricane disaster potential scale. *Weatherwise*, **27**, 169–186.

Smith, S. L., M. M. Burgess, and A. E. Taylor, 2003: High Arctic permafrost observatory at Alert, Nunavut—Analysis of 23 year data set. *Proc. 8th Int. Conf. on Permafrost*, M. Phillips, S. M. Springman, and L. U. Arenson, Eds., Zurich, CH, A. A. Balkema, Vol. 2, 1073–1078.

Smith, T. M., and R. W. Reynolds, 2005: A global merged land air and sea surface temperature reconstruction based on historical observations (1880–1997). *J. Climate*, **18**, 2021–2036.

Stroeve, J. C., M. C. Serreze, F. Fetterer, T. Arbetter, W. Meier, J. Maslanik, K. Knowles, 2005: Tracking the Arctic's shrinking ice cover: Another extreme September minimum in 2004. *Geophys. Res. Lett.*, **32**, L04501, doi:10.1029/2004GL021810.

Talley, L. D., 2003: Shallow, intermediate, and deep overturning components of the global heat budget. *J. Phys. Oceanog.*, **33**, 530–560.

Tarnocai, C., F. M. Nixon, and L. Kutny, 2004: Circumpolar-Active-Layer-Monitoring (CALM) sites in the Mackenzie Valley, Northwestern Canada. *Permafrost Periglacial Process.*, **15**, 141–153.

Thorne, P. W., D. E. Parker, S. F. B. Tett, P. D. Jones, M. McCarthy, H. Coleman, and P. Brohan, 2005: Revisiting radiosonde upper-air temperatures from 1958 to 2002. *J. Geophys. Res.,* **110,** D18105, doi:10.1029/2004JD005753.

Trenberth, K., 2005: Uncertainty in hurricanes and global warming. *Science*, **308**, 1753–1754.

Trigo, R. M., D. Pozo-Vazquez, T. J. Osborn, Y. Castro-Diez, S. Gámis-Fortis, and M. J. Esteban-Parra, 2004: North Atlantic Oscillation influence on precipitation, river flow and water resources in the Iberian Peninsula. *Int. J. Climatol.*, **24**, 925–944.

Varlamov, S. P., 2003: Variations in the thermal state of the lithogenic base of landscapes in Central Yakutia. *Proc. Second Int. Conf. "The Role of Permafrost Ecosystems in Global Climate Change,"* Yakutsk, Russia, Permafrost Institute for Biological Problems of Cryolithozone Siberian Division of the Russian Academy of Sciences, 52–56.

——, Y. B. Skachkov, P. N. Skryabin, and N. I. Shender, 2001: Thermal response of the lithogenic base of permafrost landscapes to recent climate change in Central Yakutia. *Proc. Int. Conf. "The Role of Permafrost Ecosystems in Global Climate Change,"* Yakutsk, Russia, Permafrost Institute for Biological Problems of Cryolithozone Siberian Division of the Russian Academy of Sciences, 44–45.

Vaughan, D. G., and C. S. M. Doake, 1996: Recent atmospheric warming and retreat of ice shelves on the Antarctic Peninsula. *Nature,* **379,** 328–331.

Vincent, D. G., 1998: Pacific Ocean. *Meteorology of the Southern Hemisphere*, *Meteor. Monogr.*, No. 49, Amer. Meteor. Soc., 410 p.

Vose, R. S., R. L. Schmoyer, P. M. Steurer, T. C. Peterson, R. Heim, T. R. Karl, and J. Eischeid, 1992: The Global Historical Climatology Network: Long-term monthly temperature, precipitation, sea level pressure, and station pressure data. ORNL/CDIAC-53, NDP-041, Carbon Dioxide Information Analysis Center (CDIAC), Oak Ridge National Laboratory, Oak Ridge, Tennessee, 324 pp.

Wallace, D. W. R., 2001: Storage and transport of excess CO_2 in the oceans: The JGOFS/WOCE Global CO_2 Survey. *Ocean Circulation and Climate: Observing and Modelling the Global Ocean*, G. Siedler, J. Church, and J. Gould, Eds., Academic Press, 489–521.

Wang, X., and J. R. Key, 2005a: Arctic surface, cloud, and radiation properties based on the AVHRR Polar Pathfinder dataset. Part I: Spatial and temporal characteristics. *J. Climate*, **18**, 2558–2574.

——, and ——, 2005b: Arctic surface, cloud, and radiation properties based on the AVHRR Polar Pathfinder dataset. Part II: Recent trends. *J. Climate*, **18**, 2575–2593.

Waple, A. M., and E. Rignot, 2005: Antarctic. *State of the Climate in 2004,* D. H. Levinson, Ed., *Bull. Amer. Meteor. Soc.,* **86**(6), S42–S44.

Watkins, A. B., 2005: The Australian Drought of 2005. *WMO Bull.*, **54**, 156–162.

Webster, P. J., G. J. Holland, J. A. Curry, and H.-R. Chang, 2005: Changes in tropical cyclone number, duration, and intensity in a warming environment. *Science*, **309**, 1844–1846.

Whitney, L. D., and J. S. Hobgood, 1997: The relationship between sea surface temperatures and maximum intensities of tropical cyclones in the Eastern North Pacific Ocean. *J. Climate*, **10**, 2921–2930.

Willis, J. K., D. Roemmich, and B. Cornuelle, 2004: Interannual variability in upper ocean heat content, temperature, and thermosteric expansion on global scales. *J. Geophys. Res.*, **109**, C12036, doi: 10.1029/2003JC002260.

Xie, P., and P. A. Arkin, 1997: Global precipitation: A 17-year monthly analysis based on gauge observations, satellite estimates, and numerical model outputs. *Bull. Amer. Meteor. Soc.*, **78**, 2539–2558.

——, and ——, 1998: Global monthly precipitation estimates from satellite-observed outgoing longwave radiation. *J. Climate*, **11**, 137–164.

——, J. E. Janowiak, P. A. Arkin, R. Adler, A. Gruber, R. Ferraro, G. J. Huffman, and S. Curtis, 2003: GPCP pentad precipitation analyses: An experimental dataset based on gauge observations and satellite estimates. *J. Climate*, **16**, 2197–2214.

Xue, Y., T. M. Smith, and R. W. Reynolds, 2003: A new SST climatology for the 1971–2000 base period and interdecadal changes of 30-year SST normal. *J. Climate*, **16**, 1601–1612.

Yu, L., R. A. Weller, and B. Sun, 2004: Mean and variability of the WHOI daily latent and sensible heat fluxes at in situ flux measurement sites in the Atlantic Ocean. *J. Climate*, **17**, 2096–2118.

Yu, Y., G. A. Maykut and D. A. Rothrock, 2004: Changes in the thickness distribution of Arctic sea ice between 1958–1970 and 1993–1997. *J. Geophys. Res.*, **109**, C08004, doi:10.1029/2003JC001982.

Zervas, C., S. Gill, and A. Stolz, 2005: Relative Sea Level Trends from Tide Stations: How are they determined and what do they tell us? *Climate Change Science Program Workshop, Climate Science in Support of Decision Making*, Arlington, VA, U.S. Climate Change Science Program, P-GC1.6. [Available online at www.climatescience.gov/workshop2005/posters/P-GC1.6_Zervas.pdf.]

Zhang, C., H. Hendon, W. Kessler, and A. Rosati, 2001: A workshop on the MJO and ENSO. *Bull. Amer. Meteor. Soc.*, **82**, 971–976.

Zhang, T., and Coauthors, 2005: Spatial and temporal variability of active layer thickness over the Russian Arctic drainage basin. *J. Geophys. Res.*, **110**, D16101, doi:10.1029/2004JD005642.

Zhou, L., C. J. Tucker, R. K. Kaufmann, and D. Slayback, 2001: Variations in northern vegetation activity inferred from satellite data of vegetation index during 1981 to 1999. *J. Geophys. Res.*, **106**, 20 069–20 083.

Zwally, H. J., W. Abdalati, T. Herring, K. Larson, J. Saba, and K. Steffen, 2002: Surface melt-induced acceleration of Greenland ice-sheet flow. *Science*, **297**, 218–222.